

# Driven Phase Space Structures In A 1D Vlasov-Poisson Plasma

*By*

PALLAVI TRIVEDI

(PHYS06201304003)

Institute for Plasma Research, Gandhinagar

*A thesis submitted to the  
Board of Studies in Physical Sciences  
In partial fulfillment of requirements*

*for the Degree of  
DOCTOR OF PHILOSOPHY*

*of*

HOMI BHABHA NATIONAL INSTITUTE

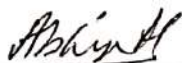


April 2019

# Homi Bhabha National Institute

## Recommendations of the Viva Voce Committee

As members of the Viva Voice Committee, we certify that we have read the dissertation prepared by **Pallavi Trivedi** entitled "DRIVEN PHASE SPACE STRUCTURES IN A 1D VLASOV-POISSON PLASMA" and recommend that it may be accepted as fulfilling the dissertation requirement for the award of Degree of Doctor of Philosophy.



Date : 11/07/2019

Chairman - Prof. A. Sen



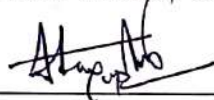
Date : 11/07/2019

Guide/Convener - Prof. R. Ganesh



Date : 11/07/2019

Examiner - Prof. Avinash Khare



Date : 11/07/2019

Member - Prof. S. Sengupta



Date : 11/07/2019

Member - Dr. R. Srinivasan



Date : 11/07/2019

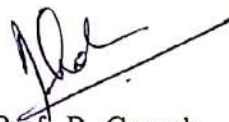
Member - Dr. D. Raju

Final approval and acceptance of this dissertation is contingent upon the candidate's submission of the final copies of the thesis to HBNI.

I hereby certify that I have read this dissertation prepared under my direction and recommend that it may be accepted as fulfilling the thesis requirement.

Date : 11/07/2019

Place : IPR, Gandhinagar

  
Prof. R. Ganesh

Guide

## STATEMENT BY AUTHOR

This dissertation has been submitted in partial fulfillment of requirements for an advanced degree at Homi Bhabha National Institute (HBNI) and is deposited in the Library to be made available to borrowers under rules of the HBNI.

Brief quotations from this dissertation are allowable without special permission, provided that accurate acknowledgment of source is made. Requests for permission for extended quotation from or reproduction of this manuscript in whole or in part may be granted by the Competent Authority of HBNI when in his or her judgment the proposed use of the material is in the interests of scholarship. In all other instances, however, permission must be obtained from the author.

Pallavi Trivedi  
<Signature>

Pallavi Trivedi

## DECLARATION

I, hereby declare that the investigation presented in the thesis has been carried out by me. The work is original and has not been submitted earlier as a whole or in part for a degree / diploma at this or any other Institution / University.

Pallavi Trivedi

<Signature>

Pallavi Trivedi

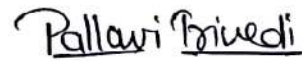
## List of Publications arising from the thesis

1. *Chirp-driven giant phase space vortices*, Pallavi Trivedi and Rajaraman Ganesh, [Physics of Plasmas 23, 062112 \(2016\)](#)
2. *Driven phase space vortices in plasmas with nonextensive velocity distribution*, Pallavi Trivedi and Rajaraman Ganesh, [Physics of Plasmas 24, 032107 \(2017\)](#)
3. *Symmetry in electron and ion dispersion in 1D Vlasov-Poisson plasma*, Pallavi Trivedi and Rajaraman Ganesh, [Physics of Plasmas 25, 112102 \(2018\)](#)
4. *Formation and Dynamics of Electrostatic Phase space Vortices: The Role of Kinetic Ions*, Pallavi Trivedi and Rajaraman Ganesh, [Manuscript Under Preparation \(2019\)](#)
5. *Eulerian Simulations of Collisional Effects on Driven Electrostatic Phase Space Vortices*, Pallavi Trivedi and Rajaraman Ganesh, [Manuscript Under Preparation \(2019\)](#)

## Conferences and Symposium Presentations

1. Pallavi Trivedi and Rajaraman Ganesh  
“A New Unified Understanding Of Electron And Ion Normal Modes In A 1D Electrostatic Vlasov-Poisson Plasma”  
60<sup>th</sup> Annual Meeting of the APS Division of Plasma Physics, Portland, Oregon, 5-9 November, 2018.
2. Pallavi Trivedi and Rajaraman Ganesh  
“Kinetic Eulerian simulations of Driven Electrostatic Phase Space Vortices in a 1D Vlasov-Yukawa System”  
6<sup>th</sup> PSSI-PLASMA SCHOLARS COLLOQUIUM (PSC-2018), Sikkim Manipal Institute of Technology, Majitar, Sikkim, 24-26 August 2018.
3. Pallavi Trivedi and Rajaraman Ganesh  
“Effects of Kinetic Ions On the Driven Phase Space Structures in a 1-D Vlasov Plasma”  
32<sup>nd</sup> National Symposium on Plasma Science & Technology (PSSI), Gandhinagar, India November, 7-10 November, 2017.
4. Pallavi Trivedi and Rajaraman Ganesh  
“Vlasov simulations of Driven Electrostatic Phase Space Vortices in a 1-D electron-ion plasma”  
Conference on “Collisionless Boltzmann (Vlasov) equation and modelling of self-gravitating systems and plasmas”, CIRM, Luminy, Marseille, France, October 30 - November 03, 2017.

5. Pallavi Trivedi and Rajaraman Ganesh  
"Chirp Driven Electron And Ion Phase Space Structures in a 1-D Vlasov Plasma"  
44<sup>th</sup> European Physical Society Conference on Plasma Physics - EPS, Belfast,  
Northern Ireland, 26-30 June, 2017.
6. Pallavi Trivedi and Rajaraman Ganesh  
"Study of Chirp Driven Vlasov-Poisson Systems"  
5<sup>th</sup> International Workshop on the Theory and Applications of the Vlasov Equation-  
Vlasovia, Copanello, Italy, May 30 - June 2, 2016.
7. Pallavi Trivedi and Rajaraman Ganesh  
"Study Of Phase Space Structures In Driven 1D Vlasov Poisson Model"  
10<sup>th</sup> Asia Plasma and Fusion Association Conference, 14-18 December, 2015.
8. Pallavi Trivedi and Rajaraman Ganesh  
"Vlasov-Poisson Systems and Collisionless Plasmas Towards Langmuir Turbulence"  
29<sup>th</sup> National Symposium on Plasma Science & Technology (PSSI), Kottayam, Kerala,  
India, 8-11 December, 2014.

  
Pallavi Trivedi

## DEDICATIONS

To My Grandfather

My Parents

&

My Brother

*the hidden strength behind my every success...*

## ACKNOWLEDGEMENTS

This thesis is the culmination of my journey of Ph.D. which was just like climbing a high peak step by step accompanied with encouragement, hardship, trust, support and frustration. When I found myself at top experiencing the feeling of fulfillment, I realized though only my name appears on the cover of this dissertation, a great many people including my family members, my friends, colleagues and well-wishers have contributed to accomplish this huge task.

At this moment of accomplishment, I convey my hearty gratitude to my thesis supervisor *Prof. Rajaraman Ganesh*. His diligent, friendly and spirited support and guidance through this long journey has been the source of inspiration for me. His enthusiasm, endless patience, understanding and availability for discussion made the journey much easier. Under his guidance I successfully overcame many difficulties and learnt a lot. His own zeal for perfection, passion, unflinching courage and conviction has always inspired me to do more. For all these, I sincerely thank him from bottom of my heart and will be truly indebted to him throughout my life time.

My earnest thanks to *Prof. A. Sen*, my Doctoral Committee Chairman, for his valuable advice, positive appreciation and counsel throughout the course of the investigations which led to the successful completion of the research work. I am obliged to Prof. S. Sengupta, Dr. R. Srinivasan, Dr. D. Raju for consenting to be my Doctoral Committee members. I am grateful for their unstinting support and also listening to their advice through the years have been a pleasant experience. It was a privilege to have them on my committee.

I would like to thank Prof. S. Mukherjee, Dr. Mainak Chattopadhyay for their continuous support and advice in Academic affairs. I would also like to thank Prof. S. K. Mattoo, Prof. Y.C. Saxena, Prof. A. Sen and Prof. A. Das for their special lectures. These lectures have introduced me to the advances of plasma physics covering the domains of theoretical, simulation and experimental realization of plasma physics. I am also grateful to other faculty members Prof. R. Ganesh, Prof. S. Sengupta, Dr. M. Ramasubramanian, Dr. R. Goswami, Dr. M. Kundu, Dr. A. K. Chattopadhyay, Dr. V. P. Anitha and others, who have taught me basic plasma physics, experimental, computational techniques and other disciplines of plasma physics during the PhD course work.

I am thankful to all in Library, Computer centre and IPR Administration for their timely help and support in the time of my need.

The long stay in IPR Hostel was made eventful and pleasant by the welcoming team of seniors Vikrant, Vikram, Kshitish, Ujjawal, Gurudatt, Prabal, Sita, Ashwin, Sharad, Pravesh, Shekar, Jugal, Sanat, Sushil, Sayak, Manjit, Aditya, Soumen, Vikram Dharodi, Vedaprakash, Neeraj, Samir, Meghraj, Mangilal, Bibhu, Harish, Vara, Chandrasekhar, Vidhi, Deepa, Akansha, Arghya, Surbahi, Bhumika, Narayan, Ratan, Modhu, Amit, Debraj, Umesh. I am thankful to my batchmates Sagar, Atul, Jervis, Prabhakar, Meenakshi, Alamgir, Sandeep, Harshita for making my first year course work enjoyable. I am going to miss tea time with Prabhakar, Meenakshee and Roopendra. The hostel life was only made better by the juniors Shivam, Sanjeev and others.

I would like to specially mention my friends Meenakshee, Prabhakar, Hirel, Roopendra, Akansha, Anjali for their constant support during good and hard times of my PhD tenure. They were always beside me during the happy and hard moments to push me and motivate me. I have been fortunate to have them as my friends who cherish me despite my eccentricities. I will miss our adventures, our anytime “Tea-time”, from our silly chats to hardcore intellectual discussions.

As always it is impossible to mention everybody who had an impact to this work however there are those whose spiritual support is even more important. I feel a deep sense of gratitude for my grand father *Mr. Kuber Dutt Trivedi*, who formed part of my vision and taught me good things that really matter in life. I would like to acknowledge the people who mean a lot to me, my parents, *Mr. Sunil Dutt Trivedi and Mrs. Lata Trivedi*, for showing faith in me and giving me liberty to choose what I desired. They have been a continuous source of impeccable support and motivation, to say the least. Their unconditional love, patience and sacrifice will remain my inspiration throughout my life. Without them, I would not have been able to complete much of what I have done and become who I am.

I owe thanks to a very special person, my younger brother *Paresh* for his eternal support and understanding of my goals and aspirations. His selfless love, care and dedicated efforts which contributed a lot for completion of my thesis. Words would never say how grateful I am to you. I consider myself the luckiest sister in the world to have such an adventurous, humorous, intellectual and loving brother to stand beside me with all his love and unconditional support and for the excellent example he sets for daring to follow our dreams.

Finally, I would like to thank the Almighty, the One who has always guided me to work on the right path of life.



---

---

# Contents

Synopsis . . . . .	iii
List of Figures . . . . .	xv
List of Tables . . . . .	xix
<b>1 Electrostatic Modes and Driven Phase Space Vortices (PSV) In the back-ground of Immobile Ions</b>	<b>1</b>
1.1 Introduction . . . . .	2
1.2 Governing Equations & Simulation Setup . . . . .	6
1.2.1 Plasma Dispersion Relation . . . . .	7
1.3 Simulation . . . . .	9
1.3.1 Driven Electrostatic Modes :- Constant Frequency Drive . . . . .	9
1.3.2 Chrip Driven Phase Space Vortices . . . . .	15
1.3.2.1 Chrip Driven Giant PSVs . . . . .	16
1.3.2.2 Transient Honeycomb Structures . . . . .	20
1.3.2.3 Response of the system to the different chrip intervals . . . . .	22
1.4 Discussion . . . . .	24
1.5 Summary and Conclusions . . . . .	28
<b>2 Driven phase space vortices in plasmas with nonextensive velocity distribution</b>	<b>33</b>
2.1 Introduction . . . . .	34
2.2 Mathematical Model And Numerical Scheme . . . . .	36

2.3	Simulation Results . . . . .	38
2.3.1	Case $q=1$ . . . . .	39
2.3.2	Case $q<1$ . . . . .	42
2.3.3	Case $q>1$ . . . . .	44
2.3.4	Transient Honeycomb Structures . . . . .	46
2.4	Discussion . . . . .	49
2.5	Summary and Conclusions . . . . .	51
<b>Appendix A Plasma Dispersion Relation:- Kinetic Electrons and Immobile Ions</b>		<b>53</b>
A.1	Pseudo Potential Method . . . . .	54
A.2	Landau Method . . . . .	58
<b>Appendix B Electron Gas Model</b>		<b>61</b>

# Synopsis

## I. INTRODUCTION

Plasma is a quasi-neutral ionized medium consisting of, in general, charged and neutral particles, that exhibits collective behavior due to Coulomb forces. Each particle in plasma feels all the other particles, but mainly the collective fields. Collisionless plasmas, by definition, are characterized by charged particles undergoing several small angle Coulomb collisions leading to a rare large angle collision. Rarity of such large angle collisions renders these plasmas “collisionless” and such plasmas are well described by kinetic models in the limit of weak particle-particle correlations. Collision-less plasmas are often found in natural conditions such as space plasmas as well as in laboratory conditions such as Tokamaks, for example.

In a warm quasi neutral plasma, when a bunch of electrons are displaced from their mean (equilibrium) position, the resulting electrostatic interaction, causes electrons to oscillate about their equilibrium position, thus, sustaining a steady plasma oscillations in the electric field with a characteristic electron plasma frequency. In 1946, Landau [1] discovered that in the limit of small amplitude perturbations in a warm collisionless plasma, these plasma oscillations can be exponentially damped, due to interaction with particles streaming with velocities close to the wave phase speed  $v_\phi$ . For warm unmagnetized uniform plasmas, the damping/growth rate of wave is generally proportional to the slope of the equilibrium particle velocity distribution at wave phase velocity of the distribution. Therefore, for monotonically falling equilibrium velocity distribution functions (such as the usual Maxwellian, for example), plasma waves are damped exponentially in time. However, when the amplitude of the perturbation is increased, the process of particle trapping in the wave potential well can inhibit Landau damping, by flattening the velocity distribution near the wave phase speed due to contributions from the non-linear or finite amplitude effects on the propagation of plasma waves, as was analyzed first by O’Neil [2].

In collisionless plasmas, the trapped particles oscillate in the trough of the wave approximately with the time period,  $\tau_r = 2\pi/\sqrt{\alpha}$ , where  $\alpha$  is the amplitude of density perturbation. The plasma wave thus formed is dissipated by Landau damping (LD) before particles are trapped i.e., unless  $\gamma_L\tau_r < 1$ , where  $\gamma_L$  is the linear Landau damping rate. Hence, when the amplitude of electric field is large enough to overcome LD, particles may get trapped in electric field pockets, which in turn flattens the distribution locally near the phase velocity of the wave, thus rendering the Landau damping ineffective as LD is proportional to  $|\partial f/\partial v|_{v_\phi}$ . This wave-particle interaction leads to formation of coherent structures in phase-space. A well known class of such coherent phase space structures are Bernstein-Greene-Kruskal (BGK) structures. These are exact stationary solutions for electrostatic, collisionless plasmas described by the Vlasov-Poisson model [3]. These BGK modes are in general, spatially inhomogeneous and therefore exhibit a finite amplitude self-consistent electric potential and field structures. These structures have continued to attract attention as they may represent the final saturated state of instabilities which are stabilized by particle trapping in the potential well formed by the finite amplitude waves.

The seminal work of BGK[3] opened a new window which described ways to construct a large class of nonlinear states. Since then, there has been an enormous body of work that speculates about which of these states might occur in nature,[4, 5, 6] in experiments,[7, 8, 9] and in numerical simulations,[10] in a variety of situations. In the past, in a series of papers, [11]-[12] nonlinear solutions and nonlinear dispersion relation have been obtained to describe a large class of coherent phase space structures such as electron-ion holes, cnoidal holes, double layers and more. The stability of these structures has also been of great interest[10, 13].

Scope of this Thesis is focused on the study of phase space dynamics of a collisionless plasma starting from a homogeneous Maxwellian distribution, for example electrostatic plasma waves and BGK modes or Phase Space Vortices (PSV), using an external electric field drive which is currently a subject of great interest in both interplanetary environments

and for laboratory plasma systems. Several investigations aim to understand the features of the dynamics at ion scales and electron scales in space plasmas by analyzing both spacecraft data [14, 15, 16] as well as numerical results from kinetic or phase space simulations [17, 18, 19, 20, 21, 22, 23]. For example, quasiregular packets of Langmuir waves (LAN) are frequently observed in the solar wind and magnetospheric plasmas [24, 25, 26]. The high frequency regions of the energy spectra, obtained by analyzing solar-wind measurements from the Helios spacecraft are dominated by longitudinal electrostatic modes, identified as ion-acoustic (IA) waves [27, 28, 29]. Recent observations and studies [30, 31, 32, 33, 34] point out that besides these LAN and IA branches, in agreement with spacecraft and solar-wind observations, two other novel branches of electrostatic waves exists. These waves have been dubbed as electron acoustic waves (EAW) and ion-bulk (IBk) waves [19, 35], as their phase velocities are nearly constant and are comparable to the electron thermal velocity ( $v_{the}$ ) and ion thermal ( $v_{thi}$ ) velocity, respectively. Generally, these electrostatic modes at finite amplitude lead to nonlinear BGK mode with charged particles trapped in the wave troughs. As described earlier, because of the trapped particles, the charged particle distribution becomes effectively flat at the wave phase velocity which in turn minimize Landau damping (LD) as it is proportional to  $|\partial f / \partial v|_{v_\phi}$ .

A natural way to achieve a PSV or BGK state (both are used interchangeably throughout) is to increase the amplitude of initial density perturbation “ $\alpha$ ” decribed earlier, without directly perturbing the distribution in velocity space. The amplitude should be large enough to trap particle and to overcome Landau damping[2, 10]. More recently, external drives with time dependent frequency  $\omega(t)$  or chirp, have been used to obtain BGK modes in bounded systems[36, 37, 38, 39, 40, 41]. For example, in a pure electron plasma confined in a Penning-Malmberg trap, it was shown that phase space holes can be created by choosing the frequency chirp window to be around axial electron bounce frequency[36, 37, 38]. Similarly, a downward frequency sweeping has been performed in a pure ion plasma experiment where extreme modification of initial distribution has been observed (for eg. splitting of an initial Maxwellian distribution into two counterpropagating distributions)[42].

The above said studies were performed for the bounded systems. However, in many cases, such as fusion experiments, solar wind and magnetospheric plasmas etc, various plasma modes and various frequency bursts has been seen over the spatial and temporal scales. Associated nonlinear wave-particle interactions can generate significantly enhance the levels of energetic particle transport which can happen both along and across the magnetic field lines[43]. In such cases, along the magnetic field lines in a Tokamak or for periodically bounded systems, the presence of energetic heavy ions and the associated wave-particle interaction (like formation and dynamics of coherent structures) are known to play an important role in the transfer of energy from the external drive the bulk plasma. For unbounded or periodic system, the study of PSVs generated from an external drive has not been addressed in the past.

As discussed earlier, in the limit of zero correlations and weak collisions, plasmas in the electrostatic limit, are well described in their electrostatic limit by Vlasov-Poisson system of equations. We begin our investigation by studying the excitation of electrostatic plasma waves in a 1D unbounded Vlasov-Poisson system modelled using Periodic Boundary Conditions (PBC)[21]. The plasma is subjected to an infinitesimal external drive. As is well known[30, 33, 42, 44], both abrupt as well as adiabatic (or continuously changing) external drive of constant frequency, say  $\omega = \omega_0$ , wavenumber  $k$  and linear amplitude (i.e. infinitesimal) are expected to generate plasma modes over a range of frequencies along with its harmonics. The following questions have been addressed in the Thesis: what would happen in an unbounded plasma modelled using PBC, if a Maxwellian, homogeneous plasma is driven externally with a drive frequency  $\omega = \omega_0$ . Furthermore, what would happen if external drive frequency  $\omega(t)$  is chirped up/down (frequency sweeping) in time interval  $\Delta t$ , say from  $\omega_1$  to  $\omega_2$ . How does the frequency sweeping affect the formation and dynamics of phase space vortices, particle trapping and generation of untrapped non-Maxwellian component. It has been found that the frequency chirping allow “continuous” flattening in the velocity space leading to large coherent structures in phase space with embedded holes and clumps resulting in Phase Space Vortices (PSV) with multiple extrema and phase velocities. The drive increases both kinetic energy and potential energy of the

system. Meaning both untrapped and trapped particle fraction is seen to increase, leading to flattening of the distribution function. As the external drive is switched off, the above said large coherent phase space structure is found to attain a steady state leading to large amplitude steady multiple extrema PSV [P. Trivedi and R. Ganesh, Physics of Plasmas 23, 062112 (2016)].

The above said studies were for the initial velocity distributions which were Maxwellian. As is well known, for systems with short range interactions, the energy of the system is extensive. Thus the “canonical” distribution is a “Maxwellian” and may be obtained by extremizing Boltzmann-Gibbs-Shannon (BGS) entropy subject to energy constraint. However, for a variety of interesting physical problems such as thermodynamics of self gravitating systems with long range interactions, energy is non-extensive [45, 46]. Recently, there have been several attempts to define a BGS-like entropy for nonextensive systems. For example, Tsalli’s definition [47] of  $q$ -nonextensive entropy where “ $q$ ” is the strength of nonextensivity and the corresponding “canonical” distribution function has been derived using nonextensive statistical mechanics framework. This formalism has found many applications in systems with the non-Maxwellian particle distribution functions observed in space and laboratory. These include the solar wind and the long-range interacting systems containing plentiful superthermal particles[48, 49], the peculiar velocity distributions of galaxy clusters[50], and the solar neutrino problem[51]. The  $q$  distribution lend themselves to applications in vast number of problems in areas of ion acoustic waves, electron acoustic solitons and other areas of plasmas[52, 53, 54, 49, 55]. On the theoretical front, a comprehensive discussion of plasma oscillations, Landau damping and dispersion relation for electrostatic waves, which can be found and solved for an equilibrium distribution function, in a collisionless thermal plasma has been provided based on  $q$ -statistics[56]. The dispersion relation is found to fit experimental data better than a Maxwellian. This formalism has also been extended to study non-linear Landau damping and formation of Bernstein-Greene-Kruskal structures for plasmas with  $q$ -nonextensive velocity distributions[57, 58]. In this Thesis, a numerical study has been performed to study the formation and dynamics of phase space vortices as the effect of the frequency chirp on the  $q$ -nonextensive distribution as ini-

tial distribution function [P. Trivedi and R. Ganesh, *Physics of Plasmas* 24, 032107 (2017)].

The role of ions on the phase space dynamics of electrons is a related and important question. The above said electrostatic waves have been studied either in the background of immobile ions resulting in a “thumb curve” dispersion (for LAN and EAW waves) with kinetic electrons or in the frame of Boltzmann electrons resulting in a “teardrop” curve (for IA and IBk waves)[17, 19, 34] with kinetic ions. Thus, the electron scale physics and ion scale physics have been separately studied and applied whereas the actual physical picture would emerge only when both ion and electron scale dynamics are included self consistently and simultaneously in a model or symmetric framework where both high frequency (“thumb curve”) and low frequency (“teardrop”) solutions can be obtained simultaneously. From this symmetrical framework, both electron scale dispersion (“thumb curve”-LAN and EAW) and ion scale dispersion (“teardrop”-IA and IBk) can be obtained in appropriate limits of where each of them again consists of a high frequency branch (LAN/IA) and a low frequency branch(EAW/IBk). Therefore, an attempt has been made by means of numerical simulations, considering both kinetic electrons and kinetic ions on the same physics footing, wherein the Vlasov equations are integrated for both electron and ion species without any approximations in length scale or time scales. First, the weakly driven fully nonlinear Vlasov-Poisson (VP) equations has been solved which facilitates weak flattening of distribution function or weak trapping. The eigenvalue values ( $\omega_r$ ) thus obtained for various wavenumbers are compared with frequencies obtained from solving the linearized eigenvalue equations considering weak trapping which allows us to neglect the contribution from the imaginary part of the dielectric function. The numerical results obtained show that both electron and ion waves can be excited simultaneously in phase space. In appropriate limits, it is shown that the “thumb” and “teardrop” curves are different parts of a general symmetric dispersion relation and are recovered in appropriate limits of that dispersion relation [P. Trivedi and R. Ganesh, *Physics of Plasmas* 25, 112102 (2018), P. Trivedi and R. Ganesh, Manuscript under preparation (2019)].

Moreover, in systems governed by kinetic processes, limit of low collisionality (or nearly collisionless regimes) is not the same as the limit of zero collisionality. This is mainly because, kinetic processes in a plasma is determined by the details of the particle distribution function in velocity space and on the nature of subtle trapping-detrapping processes. For example a slight departure from a Maxwellian can produce significant modifications in the dispersion of electrostatic waves. Since particle collisions work to restore thermal equilibrium, it is clear that their effect can eventually change the features of the kinetic dynamics of a plasma, even in situations where collisionality can be considered very weak. In these conditions, kinetic processes and collisionality are in competition between each other: while the first works to produce deformations of the particle distribution function away from a Maxwellian, the latter tends to restore the Maxwellian configuration. The evolution of the plasma is, therefore, a result of nontrivial combination of these two effects. Therefore, an attempt has been made by means of numerical simulations, to study effect of weak collisionality on the electrostatic driven phase space vortices. In the Thesis, two types of collision operators has been used: (1) Boltzmann collision operator, where the colliding particles can be treated as isolated pairs and, (2) Fokker-Planck (FP) collision type operator, where many weak collisions lead to particle diffusion in velocity space. Depending on the collision models used, it is shown that the giant PSVs smoothen out, yet retain large excess density fractions [P. Trivedi and R. Ganesh, Manuscript under preparation (2019)].

In this Thesis, by performing analytical calculations and computer experiment, we present investigations of a variety of electrostatic modes driven phase space vortices starting with a homogeneous plasma in periodic boundary conditions. A more systematic chapter-wise presentation of driven phase space vortices is presented below.

## **II. Contents Of Thesis**

### **Chapter 2: One Dimensional Vlasov-Poisson System - The Numerical Scheme**

In this Chapter, the details of the development and upgradation of numerical techniques used to simulate driven homogeneous plasma . For purpose of suitable code, an Eulerian approach is applied with a 1D Vlasov-Poisson (VP) numerical solver that simulates 1D collisionless dynamics of plasmas and can self-consistently solve both the Vlasov and Poisson equations and advances the solution in time[58]. The well known “time-splitting” method[59] which rests on splitting the Vlasov solver into separate spatial and velocity space updates and has the advantage that each of these updates can then be treated as simple advections at constant speed. In order to solve these advection equations the third-order-accurate, positivity and monotonicity preserving “piecewise parabolic method” (PPM) [60] has been applied to simulate the evolution of phase space distributions of both electrons and ions governed by the 1D Vlasov equations. In this Chapter, all the basic components of the numerical solver have been explained. In addition to these, a number of additions made in the solver. All phenomena considered in this Thesis have been studied by upgrading an inhouse 1D electrostatic Vlasov-Poisson Solver VPPM-1.0 code to VPPM-2.0 with various additions/modifications such as (1) Inclusion of external drive, (2) Study of Vlasov-Yukawa (VY) system - Kinetic Ions and Boltzmann Electrons, (3) Inclusion of Ion dynamics- facilitates the study of both Kinetic Ions and Kinetic Electrons, (4) Inclusion of Collisions which are modeled through one dimensional operators of the Bhatnagar-Gross-Krook (BGK)/Zakharov-Karpman (ZK) operator type etc, which will be described in detail in this Chapter [21, 22, 23, 61, 62].

### **Chapter 3: Driven Phase Space Vortices (PSV) In the background of Immobile Ions**

In this Chapter, excitation of electrostatic modes and formation of steady state phase space coherent structures or phase space vortices (PSV), sometimes also called Bernstein-Greene-Kruskal (BGK) modes, is investigated in a collisionless, unbounded, one-dimensional plasma, modelled using Periodic Boundary Conditions (PBC). Using a high resolution

one-dimensional Vlasov-Poisson solver (VPPM 2.0), the excitation of Electron Acoustic wave (EAW) along with Langmuir wave (LAN) and formation of giant PSV is addressed numerically. An EAW wave is heavily Landau damped within the linear theory as its wave phase velocity is comparable to the electron thermal velocity.

However, it has been shown that this nonlinear EAW wave can be successfully excited when a relatively low amplitude external electric field driver is applied for a sufficiently long time (i.e. several trapping periods). This drive excites both EAWs as well as LAN along with some harmonics and create particle trapping (BGK/PSV) in both regions, which survives at a nearly constant amplitude long after the drive is turned off. Also, for an infinitesimal external drive amplitude and wavenumber  $k$ , the existence of a window of chirped external drive frequency is demonstrated which leads to formation of giant PSV. The linear, small amplitude, external drive, when chirped, is shown to couple effectively to the plasma and increase both streaming of “untrapped” and “trapped” particle fraction. The steady state attained after the external drive is turned off is shown to lead to a giant PSV with multiple extrema and phase velocities, with excess density fraction, defined as the deviation from the Maxwellian background. It is shown that the process depends on the chirp time duration  $\Delta t$  and chirp frequency range in  $\omega$ . Novel features such as “shark”-like structures and transient “honeycomb”-like structures in phase space are discussed. Both undamped electrostatic modes (EAW and LAN) and steady state giant PSV, with multiple extrema due to embedded holes and clumps, are shown to survive long after the external drive is turned off[21].

#### **Chapter 4: A $q$ -Nonextensive Statistics Approach for Driven Phase Space Vortices**

In this Chapter, the evolution of driven phase space vortices in an unmagnetized plasmas is numerically investigated in the context of the  $q$ -nonextensive statistics proposed by Tsallis[47]. For an infinitesimal amplitude of external drive, the effects of chirp driven dynamics has been investigated that leads to the formation of giant phase space vortices

(PSV) for both Maxwellian ( $q = 1$ ) and non-Maxwellian ( $q \neq 1$ ) plasmas. For non-Maxwellian plasmas, the formation of giant PSV with multiple extrema and phase velocities is shown to be dependent on the strength of “ $q$ ” i.e. the chirp dynamics and trapping phenomenon is shown to be strongly affected by the deviations from the Maxwellian distribution. Novel features such as “shark”-like and transient “honeycomb”-like structures in phase space are also discussed for  $q$ -nonextensive velocity distributions [*P. Trivedi and R. Ganesh, Physics of Plasmas 24, 032107 (2017)*].

## **Chapter 5: Formation and Dynamics of Electrostatic Phase space Vortices: The Role of Kinetic Ions**

In the previous Chapters, ions have been assumed to be immobile. However, ion motion may significantly change the evolution of high and low frequency motions which in turn may affect the trapping and formation of PSVs. In the first part of this Chapter, we bring out several interesting features of ion modes (Ion Acoustic waves (IA), Ion Bulk waves (IBk)) and driven phase space structures, in Maxwellian plasma, analyzed by means of kinetic Eulerian simulations, composed of kinetic warm ions and Boltzmannian electrons. The details of which will be presented.

Moreover, while understanding the phase space dynamics of a collisionless plasma, one usually deals with the various time scales, from electron to ion response times. The novel branches of electrostatic waves [Langmuir waves (LAN), Electron Acoustic waves (EAW), Ion Acoustic waves (IA), Ion Bulk waves (IBk)] have been studied either in the background of immobile ions with kinetic electrons or in the frame of Boltzmann electrons with kinetic ions. However, the actual physical picture would emerge only when both ion and electron scale dynamics are included self consistently and simultaneously in a model or framework. Hence, in the second part of this Chapter, a unified picture of electrostatic waves, considering both kinetic electrons and kinetic ions on the same physics footing, has been presented, wherein the Vlasov equations are integrated for both electron and ion species without any approximations in length scales or time scales [*P. Trivedi and R. Ganesh, Physics of Plasmas 25, 112102 (2018)*]. It has been demonstrated that the hitherto separate normal mode branches of electrons and ions are in fact “continuously”

connected branches and can be excited simultaneously in phase space for a range of electron to ion temperature ratios and mass ratios, the details of which will be presented.

## **Chapter 6: Eulerian Simulations of Collisional Effects on Driven Electrostatic Phase Space Vortices**

In the major part of this Thesis, the plasma is considered to be collisionless. However, from the kinetic point of view, the range of low collisionality can be significantly different from that of null collisionality. This is mainly due to the fact that the kinetic dynamics of a plasma is determined by the details of the particle velocity distribution function where a slight departures from a Maxwellian can produce significant modifications in the dispersion relation of electrostatic waves and particle collisions work to restore thermal equilibrium. The effect of such collisions can eventually change completely the features of the kinetic dynamics of a plasma, even in situations where collisionality can be considered weak. Nearly collisionless regimes are important to a number of physical processes, including runaway electrons in magnetically confined fusion plasmas, magnetic reconnection in weakly collisional regime, low density edge in a tokamak plasma, solar plasma near sunspots, and non-neutral plasmas etc. For such kind of plasma phenomena, kinetic dynamics along the magnetic field lines can only be explained if a collision term is added to the model described here. In this Chapter, the inclusion of collisional effects in Eulerian time-splitting algorithm has been done to the study the effect of weakly dissipative/collisional effects on driven electrostatic phase space vortices (PSV). Collisions are modeled through one dimensional operators of the Bhatnagar- Gross-Krook (BGK)/Fokker-Plank type[61, 62, 63]. The accuracy of the numerical code is discussed by comparing the numerical results to the analytical predictions obtained in some limiting cases to evaluate the effects of collisions on linearly stable (Landau damping) distributions and in the dissipation of Bernstein-Greene-Kruskal waves. Particular attention is devoted to the study of collisional effects on the formation and dynamics of driven PSVs which have been studied previously for an unbounded collisionless plasma with both Maxwellian and non-Maxwellian distributions [*P. Trivedi and R. Ganesh, Physics of Plasmas 23, 062112 (2016), P. Trivedi and R. Ganesh, Physics of Plasmas 24,*

*032107 (2017)*]. In this Chapter, using VPPM-2.0 solver with inclusion of collisional models, we bring out several interesting features of driven phase space structures in the presence of weakly collisional environment, in Maxwellian plasma, the details of which will be presented.

## **Chapter 7: Conclusion and Future Work**

In this Chapter, we summarize our results and discuss future possibilities for extending the present work in various limits.

---



---

## List of Figures

- 1.1 Dispersion curves or “*Thumb*” curves for the electrostatic waves (LAN, EAW) in  $k - \omega$  plane, obtained by assuming zero damping:- (a) The “*Thumb*” curve represents the solutions or the roots of Eq.(1.4). (b) The same “*thumb*” curve plotted in the  $k - v_\phi$  plane. (c) The gradient of the real part of the complex plasma dispersion function  $-\frac{1}{2}Z'(v)$  is plotted for real arguments for immobile ions. . . . . 7
- 1.2 A cartoon figure of  $(E_{ext}, t)$  showing frequency turn on-off of external drive. Constant frequency drive is applied for  $(0 \leq t \leq t_1)$ . . . . . 10
- 1.3 (a) Plot of electron velocity distribution function  $\hat{f}_e(v)$  at different times. Two small “seed” flattening can be seen at  $v_\phi^{EAW} \simeq 1.572$  and  $v_\phi^{LAN} \simeq 3.162$ . (b) Contour plot of  $\log_{10}f(x, v)$  at  $t=2000$  indicating both EAW and LAN regions. . . . . 11
- 1.4 (a) Plot of time evolution of excess density fraction  $\delta n(x, t)/n_0 = \int f(x, v, t)dv - \int f_0(v)dv$  at  $x = L/2$ . (b) Plot of relative energy with time, when plasma is driven with a constant frequency for  $\Delta t = 1000$  for the following parameters:-  $k = 0.4$ ,  $\omega_d = 0.6241$ .(c) Plot of evolution of electric field  $E(x, t)$  with  $x$  at different times. (d) Plot of evolution of excess density fraction  $\delta n(x, t)/n_0 = \int f(x, v, t)dv - \int f_0(v)dv$  with  $x$  at different times. The vertical line in Fig. (a) and (b) represents the time at which drive is turned off. . . . . 12
- 1.5 Plot of electron velocity distribution function  $\hat{f}_e(v)$  indicating flattening in EAW region for two different values of  $E_0 = 0.01$  and  $E_0 = 0.025$  after one  $\tau_r$  for each case, respectively. . . . . 13
- 1.6 Frequency spectrum of perturbed electric field after switching off the constant frequency drive given in EAW region (both adiabatic and abrupt drive) obtained by Fourier transform of electric field during off time i.e. time  $t_1 < t < t_2$ . The abrupt drive is same as given in Eq.(2.4) and the adiabatic drive is given by  $E_{adiabatic} = E_{ext}[1 + (t - \tau)^n/\Delta\tau^n]^{-1}$  [17] where I choose  $\tau = 1000$ ,  $\Delta\tau = 700$  and  $n = 20$ . [33] For  $k = 0.4$ , the circle indicates the LAN plasma frequency for our parameters where the other peaks indicate weakly nonlinear EAW and its harmonics. . . . . 14

1.7	Excitation of EAW by driving the homogeneous Maxwellian plasma for nearly one trapping period $\tau_r$ (a) Different Adiabatic profile for which plasma is driven with $E_{adiabatic} = E_{ext}g(t)$ where $g(t) = [1 + (t - \tau)^n / \Delta\tau^n]^{-1}$ [17]. Here, I choose $\tau = 150, \Delta\tau = 70$ for different $n$ values indicating different profiles from adiabatic to nearly abrupt. (b) Plot of electron velocity distribution function $\hat{f}_e(v)$ indicating flattening in EAW region for corresponding adiabatic profiles. Profiles with the higher values of $n$ also produce the similar results and are equivalents to abrupt drive cases. In the present work, the external drive is always turned on abruptly. . . . .	14
1.8	A cartoon figure of $(\omega, t)$ showing frequency turn on-off of external drive. A downward chirp $\omega = \alpha t + \beta$ is applied for $(0 \leq t \leq t_1)$ . . . . .	15
1.9	Plots of (a) Electron velocity distribution function $\hat{f}_e(v)$ at different times in log scale, and (b) Relative energy $\delta E$ with time, when plasma is driven with a downward frequency chirp from $\omega_{high} = 2$ to $\omega_{low} = 1$ for $\Delta t_d = 200$ after which the drive is turned off. . . . .	16
1.10	Phase space plot of $f(x, v)$ at $t=2000$ , when plasma is driven with a downward frequency chirp for $\delta t_d = 200$ . The large PSV structure contains peaked spikes and holes embedded in it along with a “shark”-like structure, i.e., a bunch of particles moving together within the giant phase space vortices. . . . .	16
1.11	Plots for the case where plasma is driven with a downward frequency chirp for $\delta t_d = 200$ for $k = 0.4$ :- (a) Plot of excess density fraction (defined in Eq.2.12) evolution at $x = L/2$ with time. (b) Plot of excess density fraction (defined in Eq.2.12) evolution with $x$ at different time. (c) Plot of relative entropy $S_{rel}$ with time. The vertical line represents time at which drive is turned off. (d) Plot of electric field $E(x, t)$ with $x$ at different times. The vertical line represents time at which drive is turned off. . . . .	19
1.12	Plots of (a) “Thumb” curve indicating chirp frequency ranges used for different $k$ values, and (b) Electron velocity distribution function $\hat{f}_e(v)$ for different $k$ values in log scale, when plasma is driven with a downward frequency chirp for chirp interval $\Delta t_d = 200$ from LAN to EAW region [see Table1.1]. . . . .	20
1.13	Phase-space portrait of the electron distribution $f(x, v)$ , when plasma is driven in subharmonic region from $\omega_{high}=0.8$ to $\omega_{low} = 0.4$ for $\Delta t_d = 250$ . Contour plots (a) $t = 250$ , when drive is turned off, and (b) at $t = 2000$ , at the end of simulation. These portraits show dynamic activity in subharmonic region leading to transient multi-extrema phase structures in sub-harmonic region or “honeycomb”-like structures. (c) Plot of excess density fraction evolution with $x$ at different time. (d) Plot of electric field $E(x, t)$ with $x$ at different times. . . . .	22
1.14	(a) Plot of velocity distribution function $\hat{f}_e(v)$ , when external downward chirp is given from the start ( $t = 0$ ) for different time intervals. (b) Plot of relative entropy $S_{rel}$ with time when external downward chirp is given from the start ( $t = 0$ ) for different time intervals. The vertical lines represent time $t$ at which chirp is turned off. . . . .	23

1.15	Phase space plots of $f(x, v)$ at $t = 2000$ when external downward chirp is given from the start for different time intervals. (a) Plot of $f(x, v)$ at time $t = 2000$ for chirp interval $\Delta t = 50$ . (b) Cross-section of $f(x, v)$ at time $t = 2000$ for chirp interval $\Delta t = 50$ . (c) Plot of $f(x, v)$ at time $t = 2000$ for chirp interval $\Delta t = 250$ . (d) Cross-section of $f(x, v)$ at time $t = 2000$ for chirp interval $\Delta t = 250$ . (e) Plot of $f(x, v)$ at time $t = 2000$ for chirp interval $\Delta t = 400$ . (f) Cross-section of $f(x, v)$ at time $t = 2000$ for chirp interval $\Delta t = 400$ . . . . .	25
1.16	Plots of (a) $\phi_{max}$ , and (b) the percentage of excess density $\delta n_{max}/n_0$ of the saturated PSV states at $t = 2000$ after turning off the drive with different chirp intervals $\Delta t_d$ . . . . .	26
2.1	Logarithmic plot of the initial spatially averaged velocity distributions, for three different values ( $q < 1, q = 1, q > 1$ ) of the nonextensive index $q$ . . . . .	38
2.2	A cartoon figure of $(\omega, t)$ showing frequency turn on-off of external drive. Downward chirp is applied for $(0 \leq t \leq t_1)$ . Here, $\alpha, \beta$ are constant coefficients. . . . .	39
2.3	Plot of evolution of spatially averaged velocity distribution $\hat{f}(v)$ when external downward chirp is given from the start for $\Delta t = 250$ . . . . .	40
2.4	Plot of $f(x, v, t)$ at $t=2000$ when external downward chirp is applied from the start for a period $\Delta t = 250$ in the range $[0 \leq v \leq 4.3]$ . (a) Zoomed plot of $f(x, v, t)$ at time $t = 2000$ . (b) Cross-section of $f(x, v)$ at time $t = 2000$ . . . . .	41
2.5	Plots of relative entropy $S_{rel}$ and energy with time. The vertical lines represent times at which drive is turned on and turned off. . . . .	41
2.6	Plot of evolution of spatially averaged velocity distribution $\hat{f}(v)$ , when external downward chirp is given from the start for $\Delta t = 250$ , at $t = 2000$ comparing cases with $0.85 \leq q \leq 1$ . . . . .	43
2.7	Plot of $f(x, v, t)$ at $t=2000$ when external downward chirp is applied from the start for a period $\Delta t = 250$ in the range $[0 \leq v \leq 5.1]$ for $q = 0.95$ . (a) Zoomed plot of $f(x, v, t)$ at time $t = 2000$ . (b) Cross-section of $f(x, v)$ at time $t = 2000$ . . . . .	43
2.8	Plot of relative entropy $S_{rel}$ with time when external downward chirp is given from the start for $\Delta t = 250$ comparing cases with $0.85 \leq q \leq 0.95$ . The vertical line represents time $t$ at which chirp is turned off. . . . .	44
2.9	Plot of evolution of spatially averaged velocity distribution $\hat{f}(v)$ , when external downward chirp is given from the start for $\Delta t = 250$ , at $t = 2000$ comparing cases with $1 \leq q \leq 1.10$ . . . . .	45
2.10	Plot of relative entropy $S_{rel}$ with time when external downward chirp is given from the start for $\Delta t = 250$ comparing cases with $1 \leq q \leq 1.10$ . The vertical line represents time $t$ at which chirp is turned off. . . . .	46

2.11	Plot of $f(x, v, t)$ at $t=2000$ when external downward chirp is applied from the start for a period $\Delta t = 250$ in the range $[0 \leq v \leq 4.1]$ for $q = 1.05$ . (a) Zoomed plot of $f(x, v, t)$ at time $t = 2000$ . (b) Cross-section of $f(x, v)$ at time $t = 2000$ . . . . .	47
2.12	Phase-space portrait of the electron distribution $f(x, v)$ for $q = 1.10$ , starting from $t = 250$ (when the drive is turned off) to $t = 2000$ . These portraits show dynamic activity in subharmonic region at different instances after the drive is switched off. These kind of interesting features are seen for all the values of $q$ studied. . . . .	48
2.13	Plot of $f(x, v)$ for chirp interval $\Delta t = 250$ when external downward chirp is given from $\omega_{high} = 0.8$ to $\omega_{low} = 0.4$ for $q = 0.90, 1, 1.10$ respectively. [(a), (b)] Plots of $f(x, v, t)$ for $q = 0.90$ at time $t = 250$ and $t = 2000$ respectively. [(c), (d)] Plots of $f(x, v, t)$ for $q = 1$ at time $t = 250$ and $t = 2000$ respectively. [(e), (f)] Plots of $f(x, v, t)$ for $q = 1.10$ at time $t = 250$ and $t = 2000$ respectively. . . . .	50
2.14	(a)Plot of $\delta K$ and $\delta P$ at $t=2000$ when external downward chirp is applied from the start for a period $\Delta t = 250$ in the range $[0.85 \leq q \leq 1.10]$ . (b) Plot of $\delta n_{max}/n_0$ and $\phi_{max}$ of the saturated states after turning off the drive at $t = 250$ for $q$ values in range $[0.85 \leq q \leq 1.10]$ . . . . .	51
A.1	The distribution function as a function of the velocity. The trapped range is denoted by III, and the range II (I) refers to untrapped resonant (nonresonant) particles. . . . .	54
A.2	The gradient of the real part of the complex plasma dispersion function $-\frac{1}{2}Z'(v)$ is plotted for real arguments for immobile ions. . . . .	57
A.3	Dispersion curves or “ <i>Thumb</i> ” curves for the electrostatic waves (LAN, EAW) in $k - \omega$ plane, obtained by both Pseudo potential method as well as by assuming zero damping. . . . .	57
B.1	The effective potential $V_{eff}$ and the corresponding trajectories in $(d\Phi/dt, \Phi)$ space indicating potential wells and trapped trajectories in phase space exist in this case. . . . .	64

---

---

## List of Tables

1.1	Chirp Parameters for $k$ .	20
2.1	Chirp ranges for $q \leq 1$ .	43
2.2	Chirp ranges for $q \geq 1$ .	45



---

## Introduction

*This Thesis addresses the study of electrostatic modes and phase space vortices in an unbounded, unmagnetized, homogeneous, one dimensional Vlasov-Poisson plasma in the presence of static and mobile kinetic ions background. Studies include both collisionless and collisional regimes. In this Chapter, I provide introduction, review earlier work and motivation for my study.*

### I. INTRODUCTION

Plasma is a quasi-neutral ionized medium consisting of, in general, charged and neutral particles, that exhibits collective behavior due to Coulomb forces. Each particle in plasma feels all the other particles, but mainly the collective fields. Collisionless plasmas, by definition, are characterized by charged particles undergoing several small angle Coulomb collisions leading to a rare large angle collision. Rarity of such large angle collisions renders these plasmas “collisionless” and such plasmas are well described by kinetic models in the limit of weak particle-particle correlations. Collisionless plasmas are often found in natural conditions such as space plasmas as well as in laboratory conditions such as Tokamaks, for example.

In a warm quasi neutral plasma, when a bunch of electrons are displaced from their mean

(equilibrium) position, the resulting electrostatic interaction, causes electrons to oscillate about their equilibrium position, thus, sustaining steady plasma oscillations due to the restoring electric field with a characteristic electron plasma frequency. In 1946, Landau [1] discovered that in the limit of small amplitude perturbations in a warm collisionless plasma, these plasma oscillations can be exponentially damped, due to interaction with particles streaming with velocities close to the wave phase speed  $v_\phi$ . For warm unmagnetized uniform plasmas, the damping/growth rate of wave is generally proportional to the slope of the equilibrium particle velocity distribution at wave phase velocity of the distribution. Therefore, for monotonically falling equilibrium velocity distribution functions (such as the usual Maxwellian, for example), plasma waves are damped exponentially in time. However, when the amplitude of the perturbation is increased, the process of particle trapping in the wave potential well can inhibit Landau damping, by flattening the velocity distribution near the wave phase speed due to contributions from the non-linear or finite amplitude effects on the propagation of plasma waves, as was analyzed first by O'Neil [2].

In collisionless plasmas, the trapped particles oscillate in the trough of the wave approximately with the time period,  $\tau_r = 2\pi/\sqrt{\alpha}$ , where  $\alpha$  is the amplitude of density perturbation. The plasma wave thus formed is dissipated by Landau damping (LD) before particles are trapped i.e., unless  $\gamma_L\tau_r < 1$ , where  $\gamma_L$  is the linear Landau damping rate. Hence, when the amplitude of electric field is large enough to overcome LD, particles may get trapped in electric field pockets, which in turn flattens the distribution locally near the phase velocity of the wave, thus rendering the Landau damping ineffective as LD is proportional to  $|\partial f/\partial v|_{v_\phi}$ . This wave-particle interaction leads to formation of coherent structures in phase-space. A well known class of such coherent phase space structures are Bernstein-Greene-Kruskal (BGK) structures. These are exact stationary solutions for electrostatic, collisionless plasmas described by the Vlasov-Poisson model [3]. These BGK modes are in general, spatially inhomogeneous and therefore exhibit a finite amplitude self-consistent electric potential and field structures. These structures have continued to attract attention as they may represent the final saturated state of instabilities which are stabilized by particle trapping in the potential well formed by the finite amplitude waves. Plasmas support a great variety of nonlinear coherent structures which include phase

space vortices, double layers, solitary waves, solitons, shocks etc [64]. Such nonlinear coherent structures, which are observed in both laboratory and space plasmas, involve both nonlinearities and dispersion with collisionless and collisional dissipation [65]. In order to investigate the formation and dynamics of these nonlinear structures, both fluid and kinetic models are frequently used. While fluid models provide macroscopic plasma behavior, a kinetic model provides the microscopic aspects of plasma behavior including the wave-particle interactions. In kinetic treatment, these nonlinear coherent structures are generally referred to as BGK modes. These BGK modes have also been referred to by a variety of related terms: coherent waves, time domain structures, phase space structures, phase space vortices, solitary structures, Debye scale structures, electron holes, ion holes, localized potential structures etc. For simplicity, I will refer to all these structures by the name “phase space vortices” or PSVs in my Thesis.

The existence of these phase space vortices have been demonstrated in both laboratory experiments, space plasmas, numerical simulation and by satellites in the Earth’s ionosphere and magnetosphere. In laboratory plasmas, the formation and dynamics of solitary phase space vortices as well as accelerated periodic phase space vortices have been observed [66, 67, 68, 69, 70, 71, 72]. In non-neutral plasma experiments, using Penning-Malmberg traps, the trapped-particle modes have also been shown which are associated with anomalous transport across the external magnetic field [73]. Numerous satellites and spacecraft missions have reported and documented the characteristic signature of solitary PSVs in the form of pulses of the parallel component of electric field to the geomagnetic field direction. Such characteristic electric field signal signatures, observed in spacecraft and satellites data, which is parallel to the magnetic field, clearly results from the rapid propagation past the spacecraft of a localized structure having positive or negative potential along the magnetic field line [74, 75, 76, 77, 78]. In fusion experiments, energetic particle driven Alfvénic instabilities are often observed which exhibit a variety of nonlinear scenarios from a steady-state saturated mode amplitude evolution to a bursting one. The latter type is often associated with significant fast particle losses and the frequency shift or chirping patterns which can be attributed to the formation of long-living PSVs (also known as holes and clumps). These nonlinear studies are essential for understanding the global energetic

particles transport, particle redistribution and losses [79, 40, 80]. Therefore, the study of such wave-particle interactions leading to PSVs is an important class of laboratory plasmas, fusion plasmas as well as space plasmas.

The seminal work of BGK[3] opened a new window which described ways to construct a large class of above said nonlinear states. Since then, there has been an enormous body of work that speculates about which of these states might occur in nature,[4, 5, 6] in experiments,[7, 8, 9] and in numerical simulations,[10] in a variety of situations. In the past, in a series of papers, [11]-[12] nonlinear solutions and nonlinear dispersion relation (NDR) have been obtained to describe a large class of coherent phase space structures such as electron-ion holes, cnoidal holes, double layers and more. The stability of these structures has also been of great interest[10, 13].

Several investigations aim to understand the features of the dynamics at ion scales and electron scales in space plasmas by analyzing both spacecraft data [14, 15, 16] as well as numerical results from kinetic or phase space simulations [17, 18, 19, 20, 21, 22, 23]. For example, quasiregular packets of Langmuir waves (LAN) are frequently observed in the solar wind and magnetospheric plasmas [24, 25, 26]. The high frequency regions of the energy spectra, obtained by analyzing solar-wind measurements from the Helios spacecraft are dominated by longitudinal electrostatic modes, identified as ion-acoustic (IA) waves [27, 28, 29]. Recent observations and studies [30, 31, 32, 33, 34] point out that besides these LAN and IA branches, in agreement with spacecraft and solar-wind observations, two other novel branches of electrostatic waves exists. These waves have been dubbed as electron acoustic waves (EAW) and ion-bulk (IBk) waves, as their phase velocities are nearly constant and are comparable to the electron thermal velocity ( $v_{the}$ ) and ion thermal ( $v_{thi}$ ) velocity, respectively. Generally, these electrostatic modes at finite amplitude lead to nonlinear BGK mode with charged particles trapped in the wave troughs. As described earlier, because of the trapped particles, the charged particle distribution becomes effectively flat at the wave phase velocity which in turn minimize Landau damping (LD) as it is proportional to  $|\partial f/\partial v|_{v_\phi}$ .

## 1.1 Motivation

Energetic particles produced in fusion experiments, solar wind and magneto spheric plasmas etc can excite various modes and leads to various frequency bursts over the spatial and temporal scales. Associated nonlinear wave-particle interactions can generate significantly enhanced levels of energetic particle transport which can happen both along and across the magnetic field lines. For example, increased energetic particle transport by Alfvén eigenmodes has been correlated with a fast frequency oscillation (chirping) with a sub-millisecond period that has been observed in many experiments [43]. The high frequency regions of the energy spectra, obtained by analyzing solar-wind measurements from the Helios spacecraft, are dominated by quasiregular packets of Langmuir waves (LAN) and a longitudinal electrostatic modes, identified as ion-acoustic (IA) waves [24]. In such cases, the presence of energetic heavy ions are known to play an important role in the transfer of energy from the external drive to the bulk plasma. In Tokamaks, source of energetic particles typically are fusion-born alpha particles, neutral beam injected for heating and current drive kinetic component created from Radio-Frequency heating and current drive which are governed by collision-less dynamics. Similarly, for Astroplasmas (for eg Sun's atmosphere), a pre-existing collision-less plasma is often driven by external sources which tend to relax and create non-Maxwellian structures.

Several investigations aim to understand the features of dynamics of wave-particles interaction such as excitation of electrostatic modes and phase space structures, at ion scales and electron scales in space plasmas by analyzing both spacecraft data, solar wind observations and numerical results from kinetic or phase space simulations [39, 40, 17, 36]. Ideal way to model these kinetic processes is develop a 3D-3V Vlasov Maxwell solver with particle (and energy) sources and sinks. A next simplest model would be to use 1D-1V Vlasov-Poisson model along the magnetic field and fluid model across the magnetic field with sources and sinks-a hybrid model coupled through Maxwell equations. A simplest approach is to model the unbounded or periodic direction (eg. along the B-field in Tokamaks and in Astroplasmas) using a 1D-1V Vlasov-Poisson model where an external electric field is used

to produce kinetic species. In this work, it is shown that even this simple approach, but with both electrons and ions treated as kinetic species, in the presence of an external drive in an unbounded plasma yields crucial insights.

A natural way to study wave-particle interaction which leads to a PSV or BGK state (both are used interchangeably throughout) is to increase the amplitude of initial density perturbation without directly perturbing the distribution in velocity space. The amplitude should be large enough to trap particle and to overcome Landau damping[2, 10]. More recently, external drives with time dependent frequency  $\omega(t)$  or chirp, have been used to obtain BGK modes in bounded systems [36, 37, 38, 39, 40, 41]. For example, in a pure electron plasma confined in a Penning-Malmberg trap, it was shown that phase space holes can be created by choosing the frequency chirp window to be around axial electron bounce frequency [36, 37, 38]. Similarly, a downward frequency sweeping has been performed in a pure ion plasma experiment where extreme modification of initial distribution has been observed (for eg. splitting of an initial Maxwellian distribution into two counterpropagating distributions)[42].

The above said studies were performed for the bounded systems. However, in many cases, such as fusion experiments, solar wind and magnetospheric plasmas etc, various plasma modes and various frequency bursts has been seen over the spatial and temporal scales. Associated nonlinear wave-particle interactions can generate significantly enhanced the levels of energetic particle transport which can happen both along and across the magnetic field lines[43]. In such cases, along the magnetic field lines in a Tokamak or for periodically bounded systems, the presence of energetic heavy ions and the associated wave-particle interaction (like formation and dynamics of coherent structures) are known to play an important role in the transfer of energy from the external drive the bulk plasma. For unbounded or periodic systems, a detailed study of formation and saturation of PSVs in a 1D Vlasov plasma has not been addressed in the past. In general the following questions have been attempted:-

- How an external drive of constant frequency,  $\omega_0$ , wavenumber  $k$ , and an infinitesimal amplitude, excites electrostatic plasma modes over a range of frequencies along with

harmonics in a Maxwellian, homogeneous plasma with Periodic Boundary Conditions (basically unbounded)?

- What would happen if a plasma subjected to a Periodic Boundary Conditions (basically unbounded), and an external drive with time dependent frequency  $\omega(t)$  (or chirp) is applied for a short time interval  $\Delta t$ ?
- What would be the plasma response to the external chirp with different chirp rates and in different frequencies regimes?
- What would be the effect of chirp dynamics on the non- Maxwellian systems or plasmas with non-extensive velocity distributions?
- What would happen to excitation of electrostatic modes and phase space dynamics, when the ion motion is considered? For long drawn chirps or when chirp rate is reduced, would the ion dynamics become relevant?
- What would happen to phase space vortices when weak dissipative effects/collisions are included?

In this Thesis, by performing numerical experiment with a 1D1V Vlasov-Poisson solver, I present details and results from investigations of a variety of electrostatic modes and driven phase space vortices starting in an unmagnetized homogeneous plasma Periodic Boundary Conditions (basically unbounded). A more systematic Chapter-wise presentation of driven phase space vortices is presented below.

## 1.2 Thesis organization

The Chapters of this thesis are organized in the following fashion:-

## Chapter 2 : One Dimensional Vlasov-Poisson System - The Numerical Scheme

In this Chapter, the details of the development and upgradation of numerical techniques used to simulate driven homogeneous plasma . For purpose of suitable code, an Eulerian approach is applied with a 1D Vlasov-Poisson (VP) numerical solver that simulates 1D collisionless dynamics of plasmas and can self-consistently solve both the Vlasov and Poisson equations and advances the solution in time [58]. The well known “time-splitting” method [59] which rests on splitting the Vlasov solver into separate spatial advection at constant speed and velocity advection at constant space updates. In order to solve these advection equations, the third-order-accurate, positivity and monotonicity preserving “piecewise parabolic method” (PPM) [60] has been applied to simulate the evolution of phase space distributions of both electrons and ions governed by the 1D Vlasov equations. All the basic components of the numerical solver have been explained. In addition to these, a number of important modifications have been made in the solver. All phenomena considered in this Thesis have been studied by upgrading an in-house developed 1D electrostatic Vlasov-Poisson Solver VPPM-1.0 code to VPPM-version 2.0 with various additions and important modifications such as (1) Inclusion of external drive, (2) Inclusion of Vlasov-Yukawa (VY) system - Kinetic Ions and Boltzmann Electrons, (3) Inclusion of Ion dynamics- facilitates the study of both Kinetic Ions and Kinetic Electrons, (4) Inclusion of Collisions which are modeled through one dimensional operators of the type Bhatnagar-Gross-Krook (Krook)/Zakharov-Karpman (ZK) operator etc, which will be described in detail in this Chapter[21, 22, 23, 61, 62].

## Chapter 3: Driven Phase Space Vortices (PSV) In the background of Immobile Ions

In this Chapter, excitation of electrostatic modes and formation of steady state phase space coherent structures or phase space vortices (PSV), sometimes also called Bernstein-Greene-Kruskal (BGK) modes, is investigated in a collisionless, unbounded, one-dimensional plasma, modelled using Periodic Boundary Conditions (PBC). Using a high resolution one-dimensional Vlasov-Poisson solver (VPPM 2.0), the excitation of Electron Acoustic wave (EAW) along with Langmuir wave (LAN) and formation of giant PSVs are addressed numerically. An EAW wave is heavily Landau damped within the linear theory as its wave phase velocity is comparable to the electron thermal velocity  $v_{the}$ . However, it has been shown that this nonlinear EAW wave can be successfully excited when a relatively low amplitude external electric field driver is applied for a sufficiently long time (i.e. several trapping periods). This drive excites both EAWs as well as LAN along with some harmonics and create particle trapping (BGK/PSV) in both regions, which survives at a nearly constant amplitude long after the drive is turned off. In order to drive the systems as well as to identify the resulting modes, for a chosen  $k$ , the value of  $\omega_0$  is obtained with the help of dispersion relation. This dispersion relation is obtained by assuming weak flattening of the distribution followed by neglecting the imaginary part of the dielectric function in the background of immobile ions resulting in a “Thumb curve” dispersion [for Langmuir (LAN) and Electron Acoustic (EAW) waves] with kinetic electrons.

Also, for an infinitesimal external drive amplitude and wavenumber  $k$ , the existence of a window of chirped external drive frequency is demonstrated which leads to formation of giant PSV. A linear, small amplitude, external drive, when chirped, is shown to couple effectively to the plasma and increase both streaming of “untrapped” and “trapped” particle fraction. The steady state attained after the external drive is turned off is shown to lead to a giant PSV with multiple extrema and phase velocities, with excess density fraction, defined as the normalized deviation from the Maxwellian background. It is shown that the process depends on the chirp time duration  $\Delta t$  and chirp frequency range in  $\omega$ . Novel

features such as “shark”-like structures and transient “honeycomb”-like structures in phase space are discussed. Both undamped electrostatic modes (EAW and LAN) and steady state giant PSV, with multiple extrema due to embedded holes and clumps, are shown to survive long after the external drive is turned off [P. Trivedi and R. Ganesh, *Physics of Plasmas* 23, 062112 (2016)].

## **Chapter 4: Driven phase space vortices in plasmas with nonextensive velocity distribution**

The evolution of chirp-driven electrostatic waves in unmagnetized plasmas is numerically investigated by using a one-dimensional (1D) Vlasov-poisson solver with periodic boundary conditions. Initial velocity distribution of the 1D plasma is assumed to be governed by nonextensive  $q$  distribution. For an infinitesimal amplitude of external drive, the effects of chirp driven dynamics are investigated that leads to the formation of giant phase space vortices (PSV) for non-Maxwellian ( $q \neq 1$ ) plasmas and these results are compared with the results obtained in Chapter 3 earlier (for Maxwellian ( $q = 1$ ) plasmas). For non-Maxwellian plasmas, the formation of giant PSV with multiple extrema and phase velocities is shown to be dependent on the strength of “ $q$ ”. Novel features such as “shark”-like and transient “honeycomb”-like structures in phase space are discussed for non-Maxwellian plasmas [P. Trivedi and R. Ganesh, *Physics of Plasmas* 24, 032107 (2017)].

## **Chapter 5: Formation and Dynamics of Electrostatic Phase space Vortices: The Role of Kinetic Ions**

In this Chapter, the role of ions on the phase space dynamics has been studied using two different models:- (1) Boltzmann electrons and kinetic ions using *Vlasov-Yukawa (VY)*

model, and (2) Kinetic Ions and Kinetic Electrons (*KIKE*) model. In the previous Chapters, electrostatic waves have been studied in the background of immobile ions resulting in a “Thumb curve” dispersion [for Langmuir (LAN) and Electron Acoustic (EAW) waves] with kinetic electrons. In this Chapter, the role and effect of ions on the phase space dynamics, has been studied in two parts:-

(1) In the first part, the study electrostatic waves has been attempted at ion scale, with Boltzmann electrons treating ions as kinetic species, with a newly developed Vlasov-Yukawa (VY) solver. This model results in a “Teardrop” dispersion curve [for Ion Acoustic (IA) and Ion Bulk (IBk) waves]. Using 1D1V VY solver Landau damping and electrostatic waves at ion scales (IA and IBk waves) have been studied. Also, formation and dynamics of chirp driven phase space vortices at ion scales have been studied for different temperature ratios.

(2) In the second part, the electron scale physics and ion scale physics have been studied by including both ion and electron scale dynamics self consistently and simultaneously in a model using symmetric framework. With this model both high frequency and low frequency solutions can be obtained simultaneously which consists of a high frequency branch (LAN/IA) and a low frequency branch(EAW/IBk). Therefore, an attempt has been made by means of numerical simulations, considering kinetic electrons and kinetic ions both on the same physics footing, wherein the Vlasov equations are integrated for both electron and ion species without any approximations in length scale or time scales. The numerical results obtained show that both electron and ion waves can be excited simultaneously in phase space. In appropriate limits, it is shown that the “Thumb” and “Teardrop” curves are different parts of a general symmetric dispersion relation and are recovered in appropriate limits of that dispersion relation. Also, formation and dynamics of chirp driven electron phase space vortices have been studied for different mass ratios and for long drawn chirps, relevance of ion dynamics using both VY and KIKE models is addressed.

## Chapter 6 : Eulerian Simulations of Collisional Effects on Electrostatic Phase Space Vortices

In this Chapter, the effect of collisions on electrostatic phase space vortices formed in a collisionless process is analyzed by means of Eulerian simulation for two different collision models. In the absence of collisions, PSVs exhibits as the formation of a plateau, due to trapping of resonant particles in the resonant region of the particle velocity distribution function, thus preventing Landau damping. In the presence of collisions, this plateau is smoothed out since collisions drive the velocity distribution towards Maxwellian irrespective of how weak the collisions are as long as they are non-zero. In these conditions, kinetic processes and collisionality would be in competition and the evolution of the plasma would, therefore, be a result of nontrivial combination of these two effects. Therefore, an attempt has been made by means of numerical simulations, to study effect of weak collisionality on the electrostatic driven phase space vortices with two types of collision operators: (1) Boltzmann collision operator, where the colliding particles can be treated as isolated pairs and, (2) Fokker-Planck (FP) collision type operator in one dimension, where many weak collisions lead to particle diffusion in velocity space. It is shown that depending on the collision models used, the nature of smoothing in velocity space of giant PSVs results in different structures. However, irrespective of the collision model used, substantial excess density fractions are retained.

## Chapter 7: Conclusion and future work

In this Chapter, I discuss all the major findings, unresolved issues and elaborate future possibilities for extending the present work in various limits.

---

# One Dimensional Vlasov-Poisson System - The Numerical Scheme

## 2.1 Introduction

Due to the nature of the plasma which is an ensemble of charged particles, electromagnetic effects in many instances dominate the plasma dynamics. Therefore, it is vital to include an appropriate description, not only of external fields, but also of the fields that are self-consistently generated by the plasma particles under consideration. The most fundamental and classical model for a plasma to a good approximation is therefore the Vlasov equation which describes a collisionless, correlationless plasmas. Vlasov equation is exploited for numerous problems in plasma kinetic theory; it describes the evolution of a single particle phase space density function  $f(x, v, t)$  under the influence of electric and magnetic fields in the absence of any collision and correlations. If coupled to an appropriate field model of interest such as the the Poisson equation, the so called Vlasov-Poisson equations result. In some physical situations, further simplified models can be derived from the Vlasov-Poisson system. Even so, only a few very problems can actually be solved analytically in VP system. For this reason, numerical simulations of Vlasov

## CHAPTER 2. ONE DIMENSIONAL VLASOV-POISSON SYSTEM - THE NUMERICAL SCHEME

---

Poisson equation have become an important tool for the understanding of plasma dynamics.

Popular numerical approaches in solving the Vlasov-Poisson (VP) system can be classified as three types: Eulerian, Lagrangian and Semi Lagrangian (SL)[81]. The Lagrangian type particle methods, evolve the solution by following the nonlinear trajectories of large number of macroparticles in phase space, while the Eulerian approach evolves the state variable according to the Partial Differential Equation (PDE) on a fixed numerical grid in phase space. The SL approach is a mixed approach of Lagrangian and Eulerian in the sense that it has a fixed numerical grid; however, over each time step, the state variable is evolved by propagating information along nonlinear characteristics. Both Eulerian and the SL approaches can be designed to be of very high order accuracy, an advantage when compared with the Lagrangian approach. In the present studies, we have used the Eulerian approach for solving the VP system.

In this work, an Eulerian approach based to 1D Vlasov-Poisson (VP) numerical solver that simulates 1D collisionless dynamics of plasmas and can self-consistently solve both the Vlasov and Poisson equations and advance the solution in time is used. The well known “time-splitting” method [59] which is second order in time ( $\Delta t$ ) and the third order accurate “piecewise parabolic method” (PPM) [60] are applied to simulate the evolution of phase space distributions of both electrons and ions governed by the 1D Vlasov equations using the numerical method as presented in Sec.?? of this Chapter. All the basic components of the numerical solver have been explained. In addition to these, a number of additions/modifications made in the solver, have been briefly described in Sec.?? of this Chapter.

## 2.2 1D Electrostatic Vlasov-Poisson Solver- VPPM Solver

Phenomena considered in this Thesis have been studied by upgrading an already existing 1D electrostatic Vlasov-Poisson Solver code with Piecewise Parabolic Method (VPPM-1.0) developed at IPR [58]. I have upgraded the existing code with various additions/modifications [VPPM-2.0] such as (1) Inclusion of an external drive, (2) Inclusion of Vlasov-Yukawa (VY) system - Kinetic Ions and Boltzmann Electrons, (3) Inclusion of Ion dynamics, which facilitates the study of both Kinetic Ions and Kinetic Electrons, (4) Inclusion of Collisions which are modeled through one-dimensional operators of the Bhatnagar-Gross-Krook (Krook)/Zakharov-Karpman (ZK) operator type etc, which will be described in detail in the subsequent Sections.

### 2.2.1 Vlasov-Poisson System

The most fundamental description of a correlationless, collisionless plasma is derived from the kinetic properties of the constituent particles. The result is the so called Vlasov equation as given by,

$$\frac{\partial f_j}{\partial t} + \vec{v}_j \cdot \frac{\partial f_j}{\partial \vec{x}} + \frac{q_j}{m_j} (\vec{E} + \vec{v} \times \vec{B}) \cdot \frac{\partial f_j}{\partial \vec{v}_j} = 0 \quad (2.1)$$

where  $f_j(x, v, t)$  is the phase space density distribution function of  $j$ -th species,  $q_j$ ,  $m_j$  and  $v_j$  are the charge, mass and velocity of the  $j$ -th species, respectively. Here,  $\vec{E}$  and  $\vec{B}$  are the total electric and total magnetic field, respectively obtained from Maxwell equation. Along the  $\vec{B}$ -field ( $\vec{v} \times \vec{B} = 0$ ) or in absence of  $\vec{B}$ -field ( $B = 0$ ), Eqn.?? results into an one dimensional (1D) Vlasov equation. In simple Cartesian coordinates, it further simplifies to:-

$$\frac{\partial f_j}{\partial t} + v_j \frac{\partial f_j}{\partial x} + \frac{q_j}{m_j} E \frac{\partial f_j}{\partial v_j} = 0 \quad (2.2)$$

## CHAPTER 2. ONE DIMENSIONAL VLASOV-POISSON SYSTEM - THE NUMERICAL SCHEME

---

where electric field is obtained from charge densities, which in turn is to be determined from  $f_j(x, v, t)$ , by solving Poisson's equation:-

$$\frac{\partial E}{\partial x} = \frac{e}{\epsilon_0} \left( \int f_i dv_i - \int f_e dv_e \right) \quad (2.3)$$

where  $f_e(x, v, t)$  and  $f_i(x, v, t)$  are the electron and ion distribution function respectively. Here,  $E$  is the self consistent electric field. Both Eqns.?? and ?? make up 1D Vlasov-Poisson (VP) system.

Considering the motion of the electrons only and by treating the ions as a stationary, uniform background, these equations can be written as follows:-

$$\frac{\partial f}{\partial t} + v \frac{\partial f}{\partial x} - E \frac{\partial f}{\partial v} = 0 \quad (2.4)$$

$$\frac{\partial E}{\partial x} = 1 - \int f dv \quad (2.5)$$

where time has been normalized to the electron plasma frequency  $\omega_{pe} = \sqrt{n_0 e^2 / \epsilon_0 m_e}$ , space has been normalized to the electron Debye length  $\lambda_{De} = \sqrt{\epsilon_0 K T_e / n_0 e^2}$ , velocity has been normalized by the initial equilibrium thermal velocity  $v_{the} = \lambda_{De} \omega_{pe} = \sqrt{K T_e / m_e}$ . With these choices,  $f$  gets normalized by  $n_0 / v_{the}$  and  $E$  by  $m_e v_{the} / e \lambda_{De}$  where  $e$  is the electron charge. In this model, the ions form a stationary neutralizing background of number density  $n_0$  with numerical value 1 in the Poisson equation. (Please note that, in my published work [21, 22], the electric field  $E$  is normalized by  $-m_e v_{the} / e \lambda_{De}$ , which makes Eqn.?? and Eqn.?? as  $\partial f / \partial t + v \partial f / \partial x + E \partial f / \partial v = 0$  and  $\partial E / \partial x = \int f dv - 1$ .)

I set the simulation domain in phase space  $D(x, v) = [0, L_{max}] \times [-v_{max}^j, v_{max}^j]$  [see Fig.??],  $L_{max}$  is the system size and  $v_{max}^j$  is chosen sufficiently large so that velocity distribution functions approaches zero as  $|v^j|$  approaches  $v_{max}^j$ . The phase space is discretized with  $N_x$  grid points in the spatial domain and  $N_v$  in velocity domain such that there is sufficient resolution in both  $x$  and  $v^j$  grids. Phase Space and Time Discretization for this model is represented in Fig.?? for the following parameters:-

- $x_i = (i - 1)\Delta x$ ,  $i = 1, N_x$  and  $v_k = k\Delta v$ ,  $k = -N_v, N_v$
- $\Delta x = L_{max}/N_x$  and  $\Delta v = 2v_{max}/N_v$
- $t_n = n\Delta t$ ,  $n = 0, n_{step}$  and  $\Delta t \rightarrow$  CFL Condition (See Subsec.??)

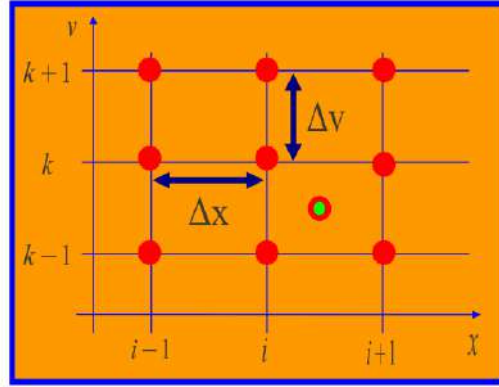


Figure 2.1: Phase space discretization

In order to solve 1D Vlasov-Poisson (Eqns.?? and ??), we have used the Time Stepping/Splitting Method suggested by Cheng and Knorr [59] coupled with the third order accurate Piecewise Parabolic Method (PPM) advection scheme [60] proposed by Colella and Woodward, the details of which will be given in the following subsections.

### 2.2.2 Time-Stepping/Splitting Method

It is well known that the Vlasov equation adequately describes the nonlinear evolution of collisionless plasmas. In kinetic simulations of plasma, the Strang splitting, first proposed by Cheng and Knorr [59], in which the Vlasov equation is integrated in the original phase space by splitting the convective and acceleration terms in such a way that the overall scheme is second-order accurate in  $\Delta t$ , has been successfully applied by several authors [82, 63, 10]. The advantage of performing such a splitting is that it decouples the Vlasov equation into lower dimensional equations of spatial advection and velocity ac/deceleration advection, which are linear and are much easier to evolve numerically. In the present work, we have adopted this time splitting method to reduce the VP Eqs.[??-??] into first order

## CHAPTER 2. ONE DIMENSIONAL VLASOV-POISSON SYSTEM - THE NUMERICAL SCHEME

advection equations.

In order to solve VP Eqs.[??-??], the time-stepping method for one time step  $\Delta t$  is given as following:

1. Spatial Advection:- solve  $\partial f/\partial t + v\partial f/\partial x = 0$  for  $\Delta t/2$ , for a given  $v$  in the  $x$ -domain for a given  $f(x, v, t = 0)$ . This result is  $f(x, v, \Delta t/2)$ . [Fig.??(a)]
2. Using this  $f(x, v, \Delta t/2)$ , solve the Poisson equation to obtain self consistent electric field  $E(x, \Delta t)$  at  $\Delta t$ .
3. Velocity Advection:- solve  $\partial f/\partial t - E\partial f/\partial v = 0$  for  $\Delta t$  [Fig.??(b)], where  $E(x, \Delta t)$  is obtained in the previous step.
4. Spatial Advection:- solve  $\partial f/\partial t + v\partial f/\partial x = 0$  for  $\Delta t/2$  , for a given  $v$  in the  $x$ -domain.[Fig.??(a)]

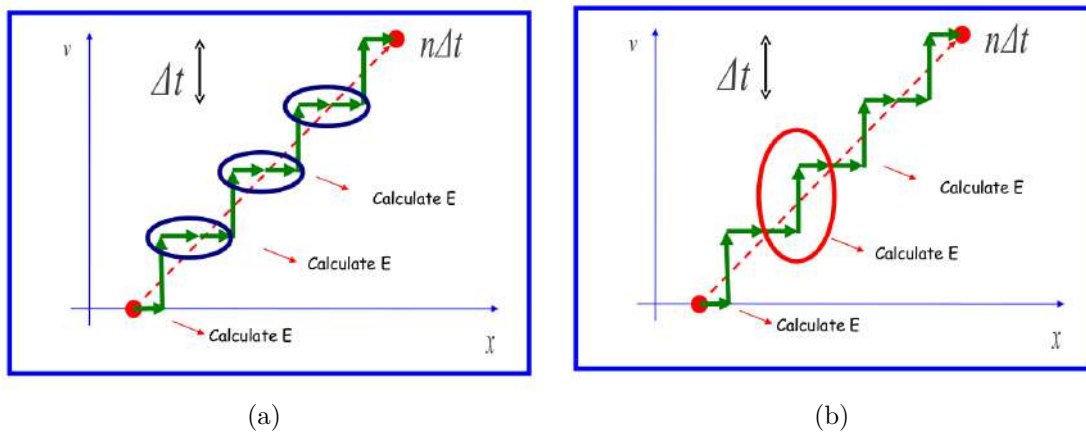


Figure 2.2: Cartoon diagram of Time-Stepping method:-(a) Spatial Advection at fixed velocity (b) Velocity Advection at fixed spatial value

Thus, the solution of the system is reduced to two 1D advection equations and a Poisson equation. This method formally incurs an error of the order  $\hat{O}[(\Delta t)^3]$ . Further, this splitting method requires a reliable advection solver and a Poisson solver, which will be described in the next subsection.

### 2.2.3 Piecewise Parabolic Method- PPM Advection Solver

The above described split-Eulerian technique rests on splitting the Vlasov solver into separate spatial and velocity space updates and has the advantage that each of these updates can then be treated as simple advections at constant “speed”. Since the groundbreaking, original work [59], most attention on fixed-grid Vlasov solvers have concentrated on improving the accuracy of the advection solvers. Previously examples include use of MacCormack’s method and other conservative schemes [83, 82]. One of the common problems with all the Vlasov solvers is that the Vlasov solutions often involve a fine-scale filamentation which increases in time. Also, there is no guarantee, except for first-order schemes, that the numerical solution has not introduced regions of negative distribution function i.e.  $f < 0$ . Moreover, some additional averaging is required with higher order schemes as they have a tendency to produce Gibbs overshoot [81].

Previously, Arber and Vann [81] have performed a comparison of various advection solvers to determine the best fixed grid Eulerian advection scheme for Vlasov problems. Attention was mainly focused on studying the importance of positivity, order, and monotonicity in the advection steps by comparing a variety of advection solvers with different properties, for example, Flux Balance Method (FB), Van Leer-Limited Scheme (VL), Piecewise Parabolic Method (PPM), Flux-Corrected Transport (FCT), High-Order Compact Finite Difference (Compact). It was found that for fixed Eulerian grid based solvers, PPM advection scheme [60], is successful in treating fine scales, automatically maintains positivity and monotonicity, and requires no additional smoothing. Therefore, I choose PPM advection method as my advection solver. The PPM advection method is formally third-order accurate away from the extrema and first-order accurate at the extrema [81]. Also, the monotonicity limiters of the PPM method ensure that the positivity of the distribution function is maintained.

The Piecewise Parabolic Method (PPM) scheme, developed by Colella and Woodward,

## CHAPTER 2. ONE DIMENSIONAL VLASOV-POISSON SYSTEM - THE NUMERICAL SCHEME

---

uses Parabolae as basic interpolation functions in a zone which allows for a more accurate representation of smooth spatial gradients, as well as a steeper representation of captured discontinuities, particularly contact discontinuities. For completion, the algorithm of the PPM scheme has been described below as given by Colella and Woodward[60]. I will describe the PPM scheme given in their paper [60] as follows:- Let us consider a general linear advection equation,

$$\frac{\partial a}{\partial t} + u \frac{\partial a}{\partial \xi} = 0 \quad (2.6)$$

where  $a = a(\xi, t)$  is the function being advected and  $u = u(\xi, t)$  is the constant velocity by which the function  $a$  is advected, and  $\xi, u$  are the generalized coordinates. The initial value for the problem is set as  $a(\xi, 0) = a_0(\xi)$ . In simplest steps, PPM scheme algorithm is as follows:-

Initial zone average  $a(\xi, t^n) \rightarrow$  Interpolation Step  $\rightarrow$  Monotonicity + Discontinuity check  $\rightarrow$  Integration Step  $\rightarrow$  next zone average  $a(\xi, t^{n+1})$ .

1. Initial Zone Average:- The average value of the discretized function  $a_j^n$  (where  $n$  is the timestep and  $j$  is the position step) is defined as the zone average of the underlying function  $a(\xi, t^n)$ , over the cell:

$$a_j^n = \frac{1}{\Delta \xi_j} \int_{\xi_{j-1/2}}^{\xi_{j+1/2}} a(\xi, t^n) d\xi \quad (2.7)$$

where  $\Delta \xi_j = \xi_{j+1/2} - \xi_{j-1/2}$  represents cell size and  $\xi_{j+1/2}, \xi_{j-1/2}$  are cell edges.

2. Interpolation Step :- The PPM scheme uses an interpolation which is piecewise continuous, with a given by a parabolic profile in each zone:

$$a(\xi) = a_j^n + x(\Delta a_{L,j} + (1-x)a_{6,j}) \quad (2.8)$$

- where  $x = (\xi - \xi_{j-1/2})/\Delta \xi_j$
- $\xi_{j+1/2} \leq \xi \leq \xi_{j-1/2}$
- $a_{6,j} = 6(a_j^n - 0.5(a_{R,j} + a_{L,j}))$
- $\Delta a_j = a_{R,j} - a_{L,j}$

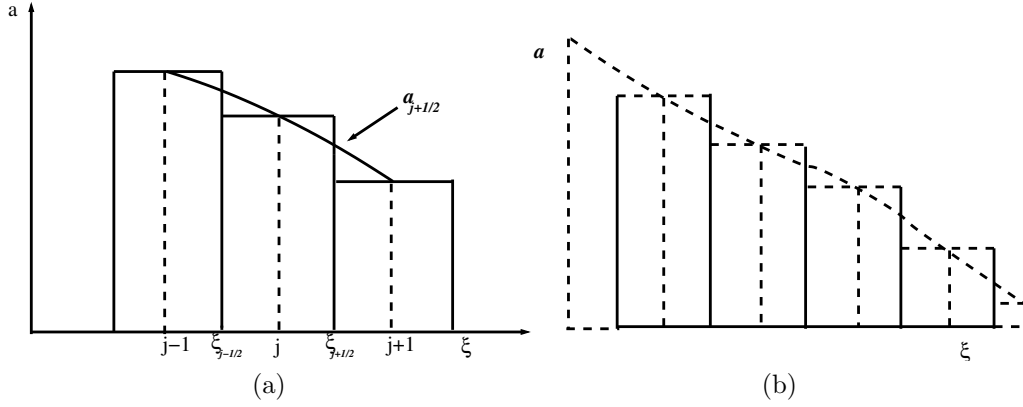


Figure 2.3: (a) Interpolation step:- The initial data (taken from [60]) are given as values of the variable “ $a$ ” averaged over the four zones shown. These averaged values are represented by dashed lines. From this data values of the variable  $a$  are interpolated at zone edges, using cubic curves which have the prescribed average values in the four zones nearest the edge. The interpolation parabolae within the zones, which are shown as solid lines, connect these edge values and give back the initial data when averaged over the zones. (b) Integration step :- New averages of the variable “ $a$ ” within the zones are obtained by integrating over the interpolated initial distribution shifted to the right by  $u\Delta t$ . This shifted distribution is shown by the dashed lines, and the new zone averages are shown by the solid lines. The scheme is third-order accurate in general; in the limit of very small time steps, for equally spaced zones, it is fourth-order accurate [60].

- $a_{R,j} = a(\xi_{j+1/2}, t^n)$  and  $a_{L,j} = a(\xi_{j-1/2}, t^n)$
- $a_R, a_L \rightarrow$  values of  $a$  at the cell edges).

3. Monotonicity check:- Once the interpolated cell-edge values are defined, one applies a monotonicity condition. Now, if  $a_j^n$  were the extremum, then the values of  $a_{R,j}$  and  $a_{L,j}$  are reset to the value of  $a_j^n$ . If  $a(\xi)$  achieved an extremum somewhere in the cell, then depending on where the extremum is close to, then one of the cell-edges is reset in such a way, so that the derivative at that cell edge is zero. This procedure maintains monotonicity of “ $a$ ”.
4. Discontinuity check:- Additionally, the values of  $a_{R,j}$  and  $a_{L,j}$  are reset depending on whether a discontinuity is detected. The discontinuity is detected as per assigned or expected tolerance, and this modifies the cell-edge function values to preserve the discontinuity during advection.
5. Integration Step:- the solution is just advection along the characteristics of the

problem, given by:

$$a_j^{n+1} = \frac{1}{\Delta \xi_j} \int_{\xi_{j-1/2}}^{\xi_{j+1/2}} a(\xi - u \times \Delta t) d\xi \quad (2.9)$$

6. Now that we have all the required parameters, we advect the function.

As described earlier, the PPM advection solver is third-order accurate away from the extrema and first order accurate at the extrema. However, for a given discontinuity, PPM method is relatively poor method in energy and enstrophy conservation in comparison to other methods (like spectral methods) but it is much stable, smoother and attains accurate solution even when the grid spacing is coarse [84]. Note that PPM advection solver is explicit in nature and hence has to obey the Courant-Frederichs-Lewy(CFL) condition [81, 85]:

$$k = \left| \frac{u \Delta t}{\Delta \xi} \right| \leq 1 \quad (2.10)$$

The PPM advection solver has been thoroughly benchmarked in a previous work [58].

## 2.2.4 Poisson Equation Solver-Fourier Transform (FFT) Method

As described in Sec.??, the Poisson equation is given by,

$$\frac{\partial E(x, t)}{\partial x} = \rho(x, t) \quad (2.11)$$

On taking Fourier Transform of above equation,

$$ik \tilde{E}(k, t) = \tilde{\rho}(k, t) \quad (2.12)$$

where  $k$  is the wave vector which represents conjugate variable of  $x$ . The transform of the original variable into  $k$ -space is represented by  $\sim$ . Therefore:

$$\tilde{E}(k, t) = -\frac{i \tilde{\rho}(k, t)}{k} \quad (2.13)$$

$E(x)$  is simply obtained by performing an inverse Fourier transform:

$$E(x, t) = FT^{-1}\left(-\frac{i\tilde{\rho}(k, t)}{k}\right) \quad (2.14)$$

where  $FT^{-1}$  represents the inverse Fourier transform. In VPPM solver, FFTW [86] is applied for performing the Fourier transforms which reduces the number of operations and makes this method more viable as compared to conventional integrators for Ordinary Differential Equations (ODEs). Depending on the model,  $\rho(x, t) = \int f_i dv_i - \int f_e dv_e$  or  $\rho(x, t) = 1 - \int f_e dv_e$  etc.

### 2.2.5 Integrator And Choice of Time Step (CFL Condition)

In order to perform the integration  $\int f dv$ , conventional trapezoidal rule [87] has been used,

$$Area = \frac{L}{N} \left( \frac{f_0 + f_n}{2} + \sum_{i=1}^{n-1} f_i \right) \quad (2.15)$$

Here, function  $f$  is assumed to be discretized over equally spaced  $n$  points with periodic boundary conditions (PBC) such that  $f_{n+1} = f_1$ . Also,  $L/N$  represents the stepsize. The theoretical error is  $(\frac{L^3}{12N^2})\max(f'')$ [58].

For the numerical solutions of the explicit time dependent partial differential equations, one has to focus on two important factors:- stability and convergence. The PPM advection solver is also explicit in nature that calculate the state of a system at a later time from the state of the system at the current time. Hence, to maintain stability and convergence, it has to obey the Courant-Frederichs-Lewy (CFL) condition[81, 85] i.e. the physical domain of dependence must be contained in the numerical domain of dependence:

$$\left| \frac{v\Delta t}{\Delta x} \right| \leq 1 \quad (2.16)$$

where  $\Delta t$  and  $\Delta x$  are the stepsizes in  $t$  and  $x$ . In simple words, the choice of the time step or mesh size cannot be independent. Thus, one has to choose the timestep such that the

maximum CFL number during the advancement of one timestep, does not violate Eqn.???. Therefore, we choose  $\Delta t$  such that:

$$\Delta t = \min\left(\frac{\Delta x}{v_{max}}, \frac{\Delta v}{\max |E|}\right) \quad (2.17)$$

where  $\max |E|$  is the maximum absolute value of the electric field,  $v_{max}$  is the value of maximum velocity on the velocity grid and  $\Delta x$ ,  $\Delta v$  are the step sizes on the  $x$  and  $v$  grid, respectively.

Now, we explain the assembly of the VPPM solver and introduce the additions/modifications made in the solver briefly.

## 2.2.6 Assembly of VPPM -Version 1.0 Solver

After setting up all the initial conditions, such as initial phase space distribution function  $f_0 = f(x, v, t = 0)$ , the grid-sizes  $N_x$  and  $N_v$ , time-step  $\Delta t$  etc, the Cheng-Knorr time-stepping method [59] is applied on Eqns.??-?? and perform the following process for one time step  $\Delta t$ :

- **$x$ -advection for  $\Delta t/2$** :- Solve  $\partial f/\partial t + v\partial f/\partial x = 0$  using PPM routine for half time-step  $\Delta t/2$  in  $x$ -domain, for various constant values of  $v$ .
- **FFT routine**:-Apply Poisson routine to get the self consistent electric field  $E$ .
- **$v$ -advection for  $\Delta t$** :- Solve  $\partial f/\partial t - E\partial f/\partial v = 0$  using PPM routine for a full time-step  $\Delta t$  in  $v$ -domain, for various constant values of  $E$  obtained from the previous FFT routine step.
- **$x$ -advection for  $\Delta t/2$** :- Solve  $\partial f/\partial t + v\partial f/\partial x = 0$  using PPM routine for another half time-step  $\Delta t/2$  in  $x$ -domain, for various constant values of  $v$ .

The above said solver was developed, tested, benchmarked and published in [58]. I have dubbed this solver as VPPM-1.0. In the following, I describe further generalization of VPPM-1.0 leading to VPPM-2.0 which is a part of the Thesis.

## 2.3 Development of the VPPM-2.0 solver

In the current upgraded version of VPPM solver i.e. VPPM-2.0, several physics terms have been added to simulate driven phenomena, for example, chirp driven phase space vortices in Maxwellian (Chapter 3) and Non-Maxwellian (Chapter 4) plasmas as well as to simulate the ion dynamics (Chapter 5) and to study collisional physics (Chapter 6). The details of these modifications and additional diagnostics; are listed below:-

### 2.3.1 External Drive

In the previous version of VPPM solver [VPPM-1.0], only the self consistent electric field  $E_s$  was present which was obtained from Poisson solver. In the upgraded version [VPPM-2.0], an external electric field has been added such that the VP equations defined as

$$\frac{\partial f}{\partial t} + v \frac{\partial f}{\partial x} - E_T \frac{\partial f}{\partial v} = 0 \quad (2.18)$$

$$\frac{\partial E_s}{\partial x} = \rho(x, t) = 1 - \int f dv \quad (2.19)$$

where  $E_T = E_s + E_{ext}$  is the total electric field, where  $E_s(x, t)$  is the self consistent electric field and  $E_{ext}$  is the external driver electric field, defined as:

$$E_{ext} = E_0 \sin(kx \pm \omega t) \quad (2.20)$$

where  $E_0$  is the amplitude of external drive. Here,  $k$  represents the perturbation wave number in the simulation box and  $\omega$  represents the driver frequency. As before here also, time has been normalized to the electron plasma frequency  $\omega_{pe}$ , space has been normalized to the Debye length  $\lambda_{De}$ , velocity has been normalized by the initial equilibrium thermal velocity  $v_{the} = \lambda_{De} \omega_{pe}$ . With these choices,  $f$  gets normalized by  $n_0/v_{the}$  and  $E$  by  $m_e v_{the}/e \lambda_{De}$  where  $e$  is the electron charge.

On addition of this driven term, the time stepping/splitting method modifies as follows:-

- ***x*-advection**:- Solve  $\partial f/\partial t + v\partial f/\partial x = 0$  for  $\Delta t/2$ , for a given  $v$  in the  $x$ -domain.
- **FFT routine**:-Using the  $f$  (obtained from previous step) solve the Poisson equation to obtain self consistent electric field  $E_s(x)$ .
- ***v*-advection**:- Solve  $\partial f/\partial t - E_T\partial f/\partial v = 0$  for  $\Delta t$ , for the  $E_T = E_s + E_{ext}$  where  $E_s$  is obtained in the previous step and  $E_{ext}$  is applied externally.
- ***x*-advection**:- Solve  $\partial f/\partial t + v\partial f/\partial x = 0$  for  $\Delta t/2$ , for a given  $v$  in the  $x$ -domain.

The driver frequency of the external electric field  $E_{ext}$  can be constant or time dependent, the details of which is presented later in the Thesis.

### 2.3.2 Vlasov-Yukawa Solver (VY):- Kinetic Ions and Boltzmann Electrons

The role of ions on the phase space dynamics of electrons is clearly related and important question. The above described Solver have been applied to study the dynamics of kinetic electrons in the background of immobile ions. In order to study of the kinetic dynamics of collisionless plasmas at short wavelengths (ion scales) which is a subject of active interest in the field of space plasma physics and other astrophysical plasmas, ion scale dynamics needs to be included. Among the several versions for the Vlasov-Poisson system, in this work, one of our interest lies in the self-consistent Vlasov-Yukawa system(VY) which consists of the Vlasov equation coupled with the Yukawa equation for the evolution of interaction potential. The Yukawa system is a short-range correction of the Poisson equation, which is sometimes called the screened Poisson equation in plasma physics. Necessary modifications are made in the VPPM solver to treat kinetic warm ions and Boltzmann electrons, analyzed by means of kinetic Eulerian simulations including a numerical Vlasov-Yukawa (VY) solver which treats kinetic ions in the presence of Boltzmann electrons [ $n_e = n_0 \exp(e\phi/KT_e) = n_0(1 + e\phi/KT_e)$ ] is given by,

$$\frac{\partial f}{\partial t} + v\frac{\partial f}{\partial x} + E_T\frac{\partial f}{\partial v} = 0, \quad (2.21)$$

$$\frac{\partial E_s}{\partial x} = -\frac{\partial^2 \phi}{\partial x^2} = n_i - n_e \quad (2.22)$$

Here,  $f$  is the ion distribution,  $n_e = (1 + T_R \phi)$  is the normalized Boltzmann electron distribution and  $T_R = T_i/T_e$  is the ion to electron temperature ratio. and  $E_T = E_s + E_{ext}$  is the total electric field, where  $E_s(x, t)$  is the self consistent electric field and  $E_{ext}$  is the external driver electric field defined as:

$$E_{ext} = E_0 \sin(kx \pm \omega t) \quad (2.23)$$

where  $E_0$  is the amplitude of external drive. Here,  $k$  represents the perturbation wave number in the simulation box and  $\omega$  represents the driver frequency. Therefore,

$$-\frac{\partial^2 \phi}{\partial x^2} + \frac{T_i}{T_e} \phi = \int f dv - 1. \quad (2.24)$$

Here, all the quantities are normalized in terms of ion parameters i.e. where time has been normalized to the ion plasma frequency  $\omega_{pi} = \sqrt{n_0 e^2 / \epsilon_0 m_i}$ , space has been normalized to the ion Debye length  $\lambda_{Di} = \sqrt{\epsilon_0 K T_i / n_0 e^2}$ , velocity has been normalized by the initial equilibrium ion thermal velocity  $v_{thi} = \lambda_{Di} \omega_{pi}$ . With these choices,  $f$  gets normalized by  $n_0 / v_{thi}$  and  $E$  is given by  $-\partial \phi / \partial x$ . In this model, only ion equations are solved using time-splitting method and effect of Boltzmann electrons considered in the screened Poisson equation. The details will be presented in the later part of the Thesis.

### 2.3.3 Inclusion of Ion Dynamics:- Kinetic Ions and Kinetic Electrons (KIKE)

In order to study the effect the ion dynamics, modifications have been made in the VPPM solver [VPPM-2.0] such that it can treat both kinetic electrons and kinetic ions on the same physics footing or symmetrically in terms of kinetics. This version of VPPM-2.0 is dubbed here as KIKE (Kinetic Ions and Kinetic Electrons) model.

To incorporate ion dynamics, the VP system can be described as followings:-

$$\frac{\partial f_e}{\partial t} + v_e \frac{\partial f_e}{\partial x} - E_T \frac{\partial f_e}{\partial v_e} = 0 \quad (2.25)$$

$$\frac{\partial f_i}{\partial t} + v_i \frac{\partial f_i}{\partial x} + \frac{1}{\mu} E_T \frac{\partial f_i}{\partial v_i} = 0 \quad (2.26)$$

$$\frac{\partial E_s}{\partial x} = \int f_i dv_i - \int f_e dv_e \quad (2.27)$$

where  $f_e(x, v, t)$  and  $f_i(x, v, t)$  are the distribution functions of electrons and ions, respectively,  $\mu$  is the mass ratio of ions to electrons i.e.  $\mu = M_i/m_e$  and  $E_T = E_s + E_{ext}$  is the total electric field. All the quantities are normalized in terms of electron parameters.

To solve both electron and ion Vlasov equations, the time-splitting method will be applied as follows:-

- Solve  $\partial f_e/\partial t + v_e \partial f_e/\partial x = 0$  and  $\partial f_i/\partial t + v_i \partial f_i/\partial x = 0$  for  $\Delta t/2$ , for a given  $v$  in the  $x$ -domain.
- Using this  $f_e$  and  $f_i$  solve the Poisson equation to obtain self consistent electric field  $E_s(x)$ .
- Solve  $\partial f_e/\partial t - E_T \partial f_e/\partial v_e = 0$  and  $\partial f_i/\partial t + (1/\mu) E_T \partial f_i/\partial v_i = 0$  for  $\Delta t$ , where  $E_T = E_s + E_{ext}$ ,  $E_s$  is obtained in the previous step and  $E_{ext}$  is applied externally.
- Again, solve  $\partial f_e/\partial t + v_e \partial f_e/\partial x = 0$  and  $\partial f_i/\partial t + v_i \partial f_i/\partial x = 0$  for  $\Delta t/2$ , for a given  $v$  in the  $x$ -domain.

### 2.3.4 Inclusion of Collisions

In most part of this Thesis, the plasma is considered to be collisionless. Many aspects of relatively dense but hot plasmas, such as those present in magnetic confinement fusion devices, can be analyzed using the Vlasov equation. However, there are certain plasma phenomena that can only be explained if a collision term is added to the VP model (such as

nearly collisionless regimes like, runaway electrons in magnetically confined fusion plasmas, magnetic reconnection in weakly collisional regime, low density edge in a tokamak plasma, solar plasma near sunspots, and non-neutral plasmas etc.) as will be described here. Therefore, a collision term has to be added to the Vlasov equation. The result is usually called the Boltzmann equation. The basic equations considered here can be written in the following dimensionless form:

$$\frac{\partial f}{\partial t} + v \frac{\partial f}{\partial x} - E_T \frac{\partial f}{\partial v} = \left. \frac{\partial f}{\partial t} \right|_{collision} = C(f) \quad (2.28)$$

where  $C(f)$  is a generic collision operator. For this model, time evolution of the distribution function is approximated by using a splitting scheme for collisional Eulerian codes [63] that decomposes the evolution of  $f$  in three different steps. To summarize this splitting scheme, for a single time step  $\Delta t$ :

- $\Delta t/2$  transport step  $\rightarrow \partial_t f + v \partial_x f - E \partial_v f = 0$  [Note that this step includes further time-splitting].
- $\Delta t$  collisional step  $\rightarrow \partial_t f = C(f)$ .
- $\Delta t/2$  transport step  $\rightarrow \partial_t f + v \partial_x f - E \partial_v f = 0$ .

Each transport step is in turn composed by three substeps, a first half-step advection in physical space followed by a full-step advection in velocity space and then by an additional half-step advection in physical space, according to the time splitting scheme first proposed by Cheng and Knorr in 1976. The Poisson equation for the electrostatic potential is solved after the first spatial advection step. Being  $\Delta t' = \Delta t/2$ , the time step for the transport advance, a single transport step for  $\Delta t'$  can be summarized as follows:

- $\Delta t'/2$   $x$ -advection  $\rightarrow \partial_t f + v \partial_x f = 0$
- Poisson routine  $E_s \rightarrow E_T = E_s + E_{ext}$ (if any)
- $\Delta t'$   $v$ -advection  $\rightarrow \partial_t f - E_T \partial_v f = 0$ .

- $\Delta t'/2$   $x$ -advection  $\rightarrow \partial_t f + v \partial_x f = 0$ .

Both  $x$ -advection and  $v$ -advection have been performed numerically using PPM advection scheme. In Thesis, we have considered two different 1D collisional operators:-

- *Bhatnagar-Gross-Krook (Krook) operator* [61]:-  $C = -\nu(f - f_{eq})$
- *Zakharov-Karpman (ZK) operator* [62]:-  $C = \nu \partial/\partial v (\partial f/\partial v + v f)$

where  $\nu$  is the collision frequency,  $f_{eq}$  is the local equilibrium value for the distribution of particles. Here, a systematic study has been presented with these two different collision models:- (1) Boltzmann collision operator or Bhatnagar-Gross-Krook (Krook) operator, where the colliding particles can be treated as isolated pairs and (2) Zakharov-Karpman (ZK) operator (a Fokker-Planck collision term in 1D[88]), where many weak collisions lead to particle diffusion in velocity space. The details of these operators will be presented in the later part of the Thesis.

## 2.4 Benchmarking of VPPM-2.0 Solver

In this Section, we benchmark the Vlasov-Poisson solver VPPM-2.0 with the Landau damping results previously obtained from VPPM-1.0 [58].

### 2.4.1 Benchmark of KIKE code

Benchmarking of KIKE code is done with VPPM-1.0 by assuming plasma to be consists of kinetic electrons and immobile ions ( $\mu/T_R = 10^{10}$ ) and an extensive comparison is carried out between simulation and theoretical results. For a collisionless plasma, where damping by collisions is negligible, when plasma is perturbed with an initial density perturbation ( $E_{ext} = 0$ ), by initializing the following distribution function:-

$$f(x, v, t = 0) = (1 + \alpha_0 \cos(x)) f_0(v) \quad (2.29)$$

where  $f_0(v) = 1/\sqrt{(2\pi)}exp(-v^2/2)$  is the initial Maxwellian velocity distribution function and  $\alpha_0$  is the strength of perturbation such that the oscillating period of the trapped particles in the trough of the plasma wave is approximately for the time period,  $\tau_r = 2\pi/\sqrt{\alpha_0}$ , after which time the linear solution breaks down and nonlinear phenomena become prominent. The plasma wave is dissipated by Landau damping before particles are trapped, unless  $\gamma_L\tau_r < 1$ , where  $\gamma_L$  is the linear Landau damping rate.[81]

With an initial amplitude, which is as small as near the linear region i.e. for  $\gamma_L\tau_r > 1$ , it leads to an exponential damping or linear Landau damping. For example, in Fig.[??], with simulation parameters:-  $\alpha_0 = 0.01$ ,  $k = 0.4$ , the numerically observed plasma frequency is  $\omega_r^{obs} = 1.282$  and the linear landau damping rate is  $\gamma = -0.0661$  which are in close agreement with analytical values  $\omega_r = 1.285$  and  $\gamma = -0.0661$ , respectively[89]. In Fig. ??, the total energy of the system is plotted, which is defined as:  $TE(t) = KE(t) + PE(t)$ , where kinetic energy is computed as  $KE(t) = (1/2) \int \int v^2 f(x, v, t) dx dv$  and potential energy computed as  $PE(t) = (1/2) \int E^2(x, t) dx$ . In Fig. ??(d), the relative total energy  $\delta W = TE(t) - TE(0)$ , the relative kinetic energy  $\delta K = KE(t) - KE(0)$  and the relative potential energy  $\delta P = PE(t) - PE(0)$  are plotted. One can see that the total energy remains conserved in time. As the amplitude of perturbation becomes larger, contribution

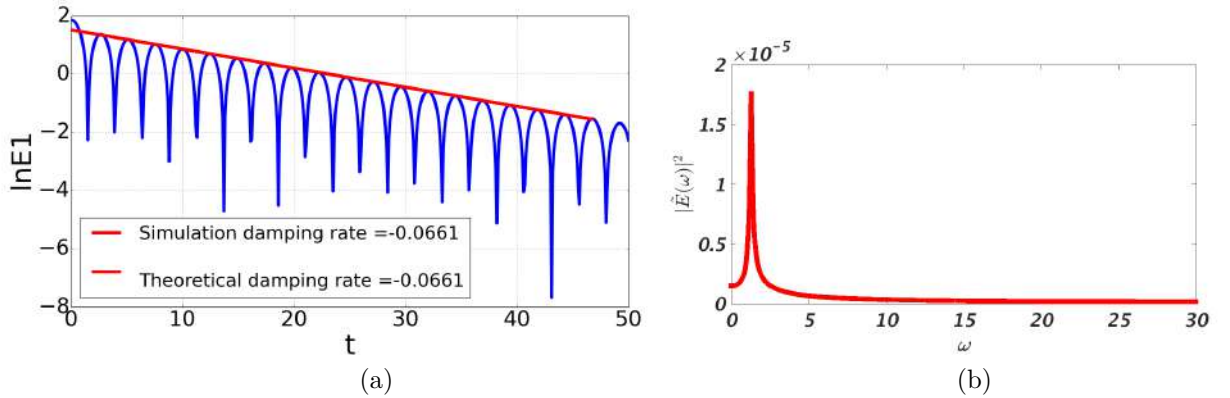


Figure 2.4: Linear Landau Damping (LLD) for  $k = 0.4$ ,  $\alpha_0 = 0.01$  (a) Logarithmic plot of time evolution of amplitude of the first fundamental harmonic of the electric field  $\log|E_1|$  - LLD rate. (b) The numerically observed plasma frequency  $\omega_r^{obs}$  for LLD.

from the nonlinear terms become more significant and the behavior deviates from uniform exponential damping. This causes interaction of particles with the electric field to form

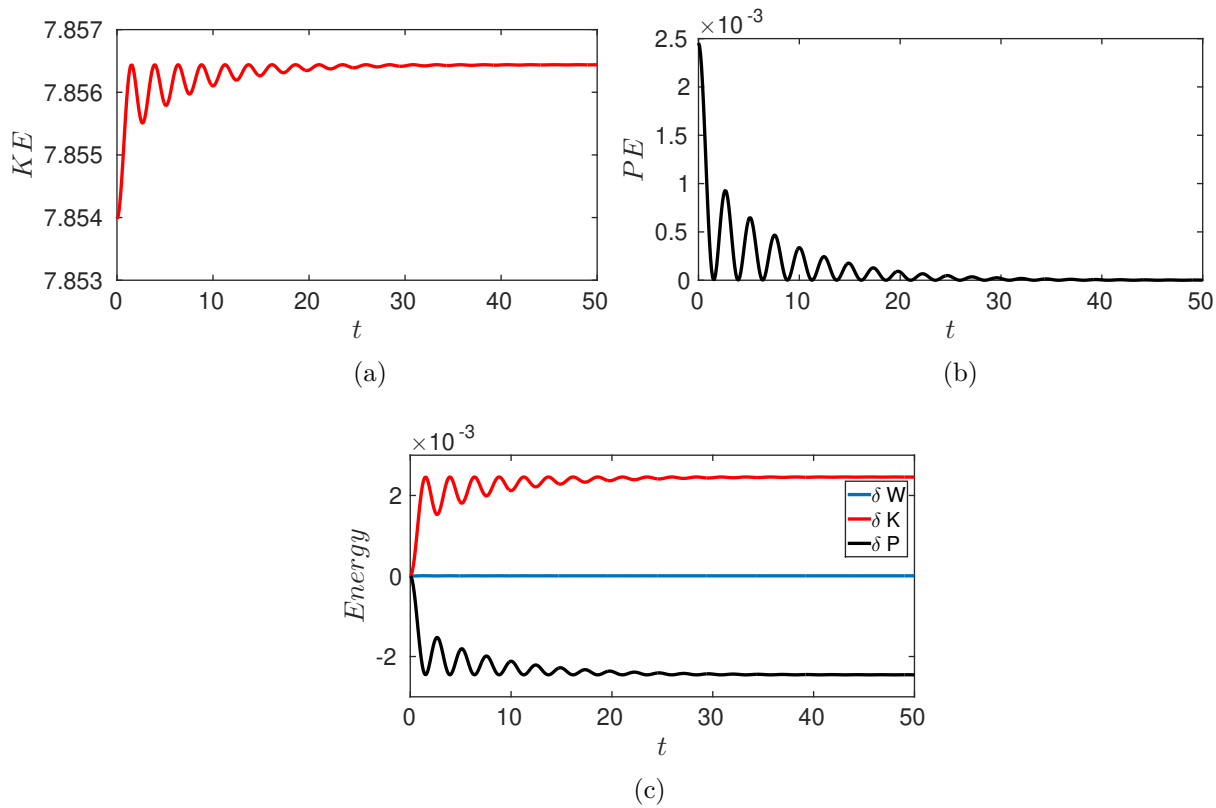


Figure 2.5: Linear Landau Damping (LLD) for  $k = 0.4$ ,  $\alpha_0 = 0.01$ . Plots for (a) Kinetic Energy (KE), (b) Potential Energy (PE) and (c) Plots for relative total energy, relative kinetic energy and relative potential energy.

pockets of trapped particles in the phase-space, due to trapping nonlinearity, leading to coherent structures in phase-space known as Bernstein-Greene-Kruskal (BGK) structures[3]. In Landau damping, the electrons with velocity  $v_\phi \simeq \omega_r/k$ , resonates with the plasma wave field and energy exchange takes place between resonant particles and wave. This results in the flattening of the distribution function. For example, for  $k = 0.4$ , the analytic value of  $\omega_r$  is 1.285; hence  $v_\phi = \omega_r/k = 3.21$ . As we can see in Fig.??, when plasma is perturbed with a nonlinear amplitude of perturbation  $\alpha_0 = 0.05$ , the velocity distribution function gets flattened near 3.21 and a corresponding phase space vortex is found at  $v_\phi = 3.21$ . This implies that there is a prominent potential well formed, and particles get trapped and detrapped to sustain the steady-state potential well, which can also be seen in Fig.??(c), where the time evolution of amplitude of the first fundamental harmonic of the electric field  $E_{k=1}$ , denoted by  $E1$ , is plotted. Since only one Fourier mode has been perturbed here, the fundamental harmonic  $E1$  would represent how this mode evolves with time [10, 58]. However, these initial density excitation with homogeneous Maxwellian plasma leads

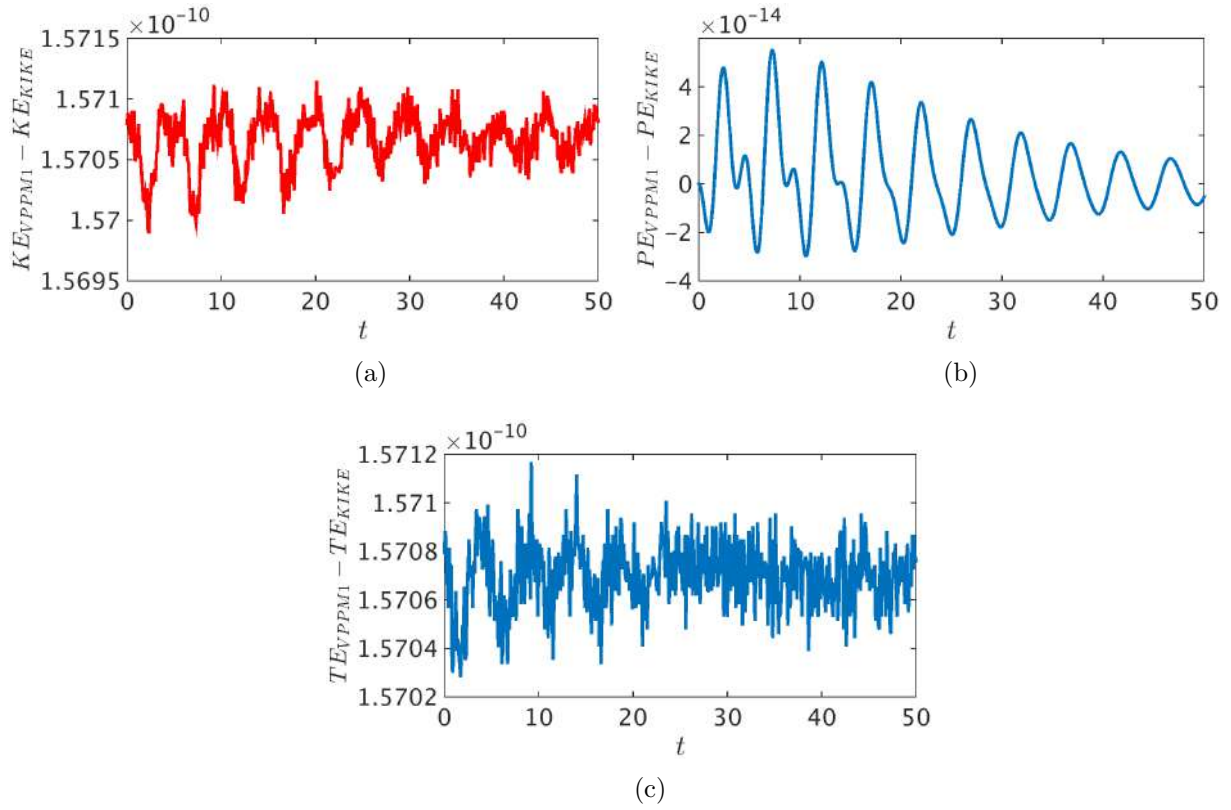


Figure 2.6: Linear Landau Damping (LLD) for  $k = 0.4$ ,  $\alpha_0 = 0.01$ . Plots of difference between data obtained from VPPM-1.0 and VPPM-2.0 solver for (a) Total Energy (TE), (b) Kinetic Energy (KE), (c) Potential Energy (PE)

to Langmuir waves only. In Figs. ??(a), ??(b) and ??(c), the total energy (TE), the kinetic energy (KE) and the potential energy (PE) of the system are plotted, respectively. In Fig. ??(d), the total relative energy  $\delta W = W(t) - W(0)$ , the total relative kinetic energy  $\delta K = K(t) - K(0)$  and the total relative potential energy  $\delta P = P(t) - P(0)$  are plotted. One can see that the total energy remains conserved upto third decimal. These results can be interpreted as benchmarking of VPPM-2.0-KIKE solver.

## 2.4.2 Benchmarking of VPPM-2.0 Solver - External Drive Version

Benchmarking of External drive version is done for both cases: (1) where ion species is not included in the code such that Vlasov equation is solved only for electrons [same as VPPM-1.0] and (2) KIKE model with  $\mu/T_R = 10^{10}$ , such that the plasma is assumed to be

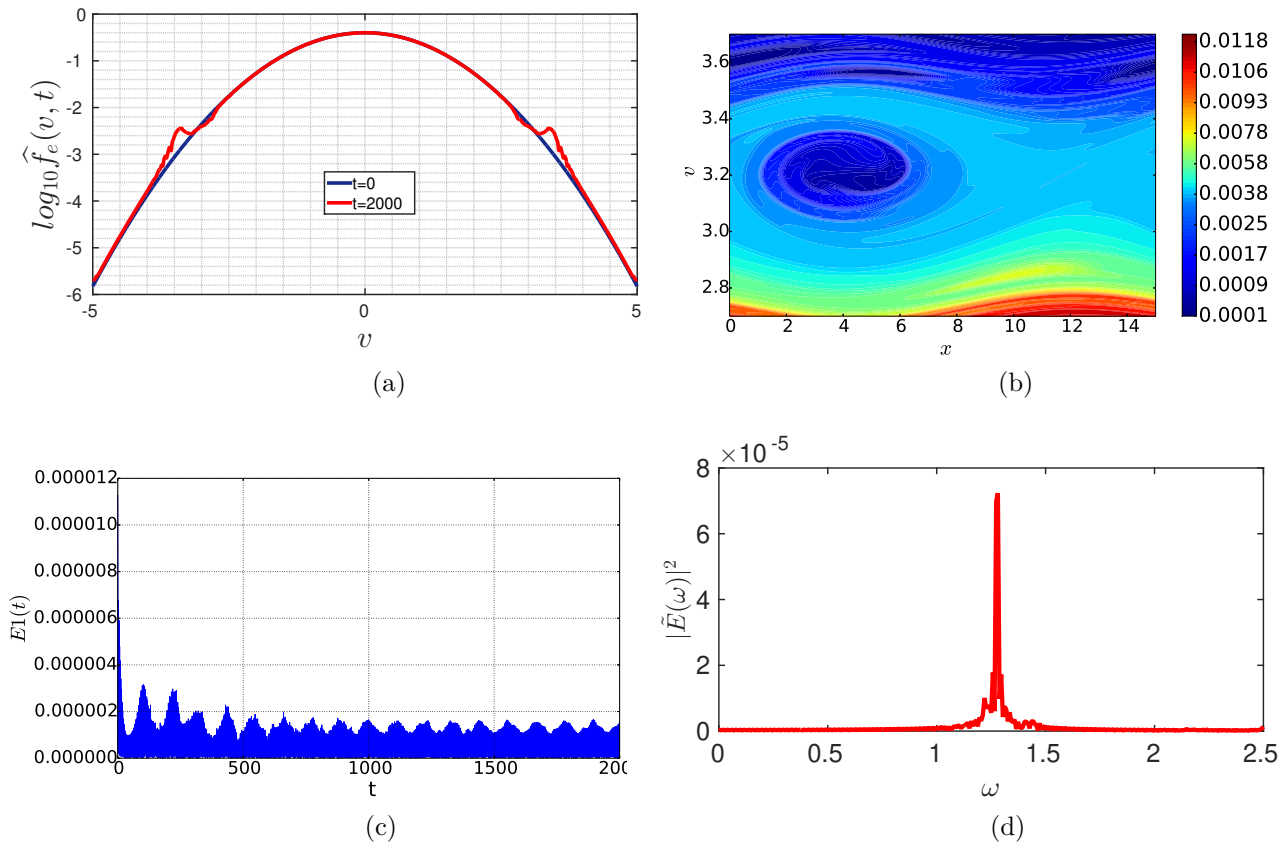


Figure 2.7: Non-linear Landau Damping - BGK modes for  $k = 0.4$ ,  $\alpha_0 = 0.05$  (a) Plot of velocity distribution function  $\hat{f}(v)$  in log scale. A small flattening can be seen at  $v = 3.21$ . (b) Phase space plot of  $f(x, v)$  at  $t = 2000$  with phase space vortex at  $v = 3.21$ . (c) Plot for the amplitude of the first harmonic of the electric field  $E1$  with time. (d) The numerically observed frequency  $\omega_r^{obs} \sim 1.28$  obtained at the end of simulation.

consists of kinetic electrons in the background of immobile ions. By assuming  $E_{ext} = 0$ , which makes  $E_T = E_s$ . The results exactly matches (1) with VPPM-1.0 for the first case and (2) with KIKE model results as shown above in Subsection.?? for the second case.

### 2.4.3 Benchmark of Vlasov-Yukawa (VY) code

Benchmarking of Vlasov-Yukawa (VY) code, where plasma is assumed to be consists of kinetic ions in the background of Boltzmann electrons, is presented from Chapter 5 where an extensive comparison is carried out between simulation and theoretical results.

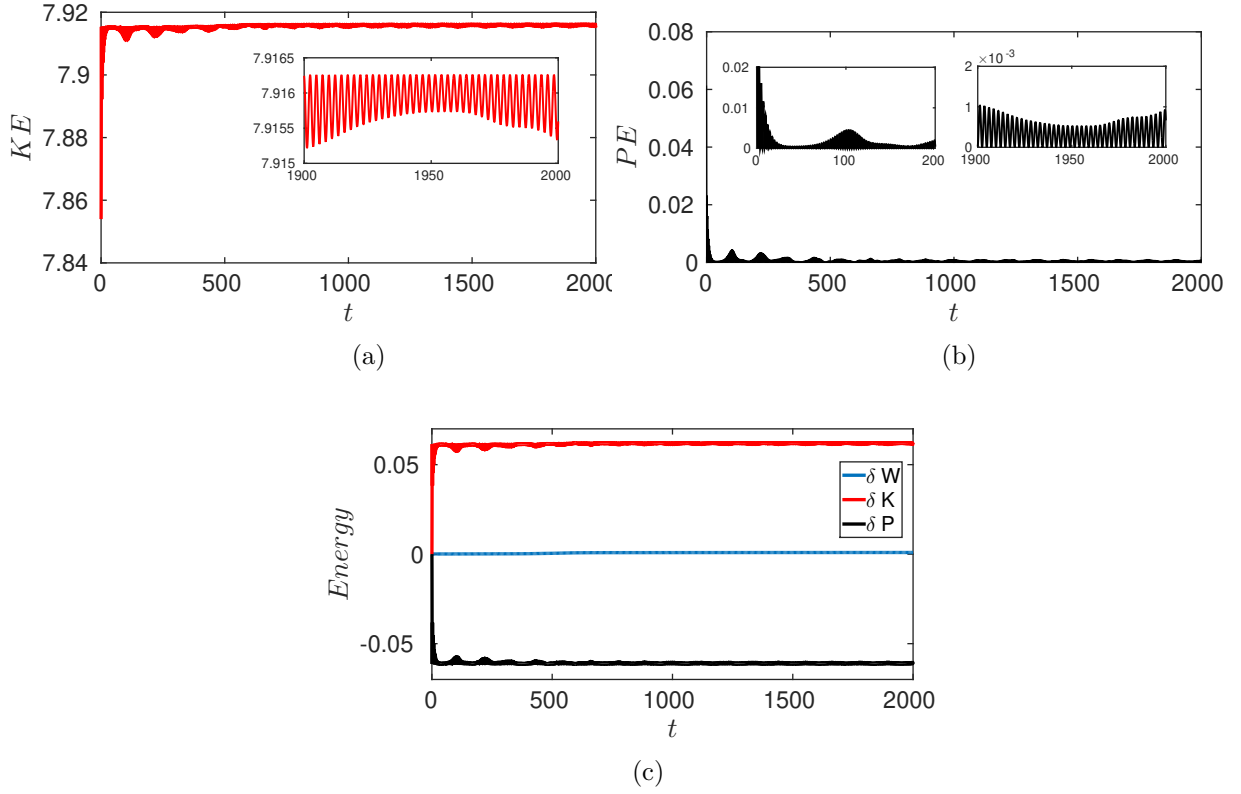


Figure 2.8: Non-linear Landau Damping (LLD) for  $k = 0.4$ ,  $\alpha_0 = 0.05$ . Plots for (a) Total Energy (TE), (b) Kinetic Energy (KE), (c) Potential Energy (PE) and (d) Plots for relative total energy, relative kinetic energy and relative potential energy.

#### 2.4.4 Benchmark of Collisional Solver

In this Section, we have benchmarked the collision time-step model with the usual time-step algorithm. Here, we have referred the VPPM 2.0 solver with single time-stepping as “old scheme” and VPPM-2.0-Collisional version of code, where time-stepping is done twice, with collision frequency  $\nu = 0$  as “new scheme”. For the purpose of the benchmark, we use previously obtained linear Landau damping and nonlinear Landau damping results. In the Fig.??,  $\log|E_1|$  for linear Landau damping case has been plotted for parameters:  $k = 0.4$ ,  $\alpha_0 = 0.01$ . The results obtained with “old scheme” as well as “new scheme” matches with each other. In Fig. ??(a), the time evolution of space averaged velocity distribution is plotted, which is given by

$$\hat{f}(v, t) = \frac{\int_0^L f(x, v, t) dx}{\int_{-v_{max}}^{v_{max}} \int_0^L f(x, v, t) dx dv} \quad (2.30)$$

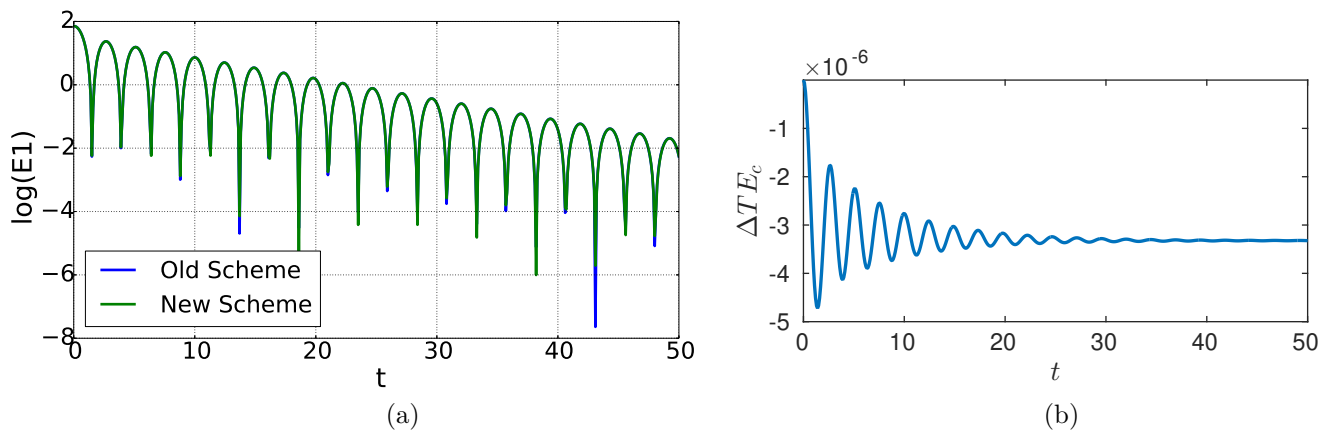


Figure 2.9: Linear Landau Damping (LLD) for  $k = 0.4$ ,  $\alpha_0 = 0.01$  and collision frequency  $\nu = 0$ . Fit of a straight line through the maxima of  $\log|E_1|$ , obtained with both “old scheme” and “new scheme”. (b) Plots of comparison of relative total energy obtained with both “old scheme” and “new scheme” i.e.  $\Delta TE_c = TE_{newscheme} - TE_{oldscheme}$ .

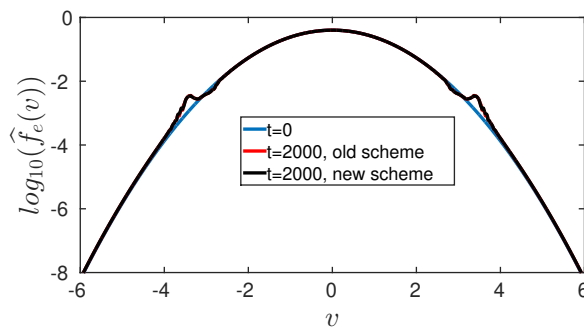


Figure 2.10: Non-Linear Landau Damping - BGK modes for  $k = 0.4$ ,  $\alpha_0 = 0.05$  and collision frequency  $\nu = 0$ . (a) Plot of space averaged velocity distribution function  $\hat{f}(v)$  in log scale, obtained with both “old scheme” and “new scheme”. A small flattening can be seen at  $v = 3.21$ .

As one can observe the space averaged velocity distribution at later time exactly matches for both “old scheme” as well as “new scheme”. In Fig.??(b), the difference of total energy TE obtained by “new scheme” and “old scheme” is shown as  $\Delta TE_c = \delta TE_{newscheme} - \delta TE_{oldscheme}$ . The difference between the two schemes is in the  $10^{-5}$  order, which indicates the order of accuracy in the results obtained by “new scheme”. Furthermore, phase space plots of  $f(x, v, t = 2000)$  have been shown on Fig.??, where one can observe the corresponding phase space vortex found at  $v_\phi = 3.21$  for both schemes. The position of the vortex in  $x$ -space is different due to difference in the time-splitting techniques used in both schemes as in “new scheme” or collision solver each time-step includes further

time-splitting. However, it does not affect the important results and the basic features of the results. These results can be interpreted as benchmarking of collisional version of VPPM 2.0 solver.

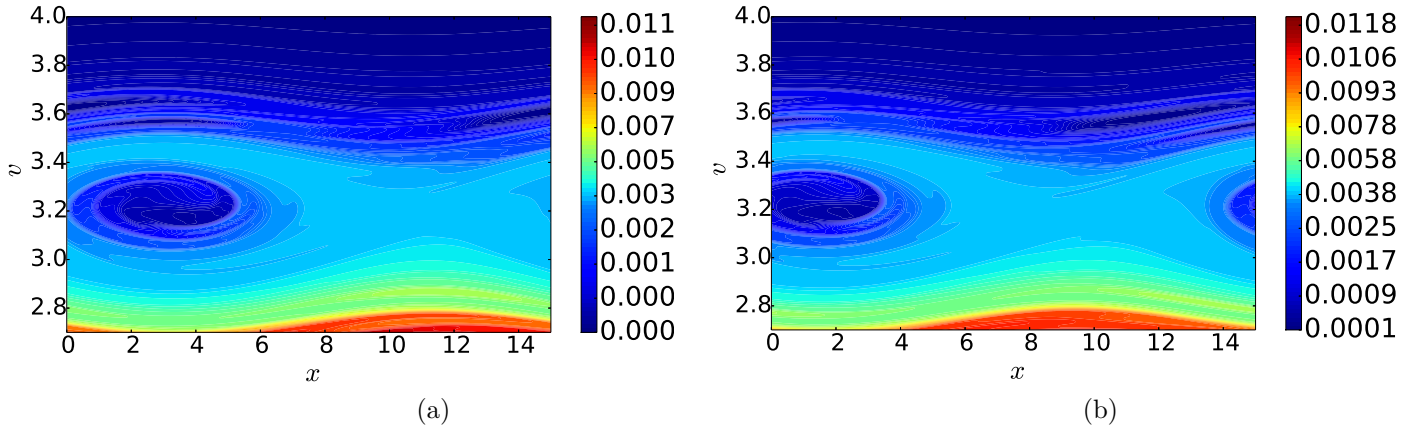


Figure 2.11: Non-Linear Landau Damping [10, 58] - BGK modes for  $k = 0.4$ ,  $\alpha_0 = 0.05$  and collision frequency  $\nu = 0$ . Phase space plot of  $f(x, v)$  at  $t = 2000$  with phase space vortex at  $v = 3.21$  obtained with both (a) “old scheme” and (b) “new scheme”.

In the following Chapters, formation and dynamics of coherent structures or phase space vortices by applying different models and by means of Eulerian simulation will be described.



---

## Electrostatic Modes and Driven Phase Space Vortices (PSV) In the background of Immobile Ions

*In this Chapter, excitation of electrostatic modes and formation of steady state phase space coherent structures or phase space vortices (PSV), sometimes also called Bernstein-Greene-Kruskal (BGK) modes, is investigated in a collisionless, unbounded, one-dimensional plasma, modelled using Periodic Boundary Conditions (PBC). Using a high resolution one-dimensional Vlasov-Poisson solver (VPPM 2.0), the excitation of Electron Acoustic wave (EAW) along with Langmuir wave (LAN) and formation of giant PSV is addressed numerically. An EAW wave is heavily Landau damped within the linear theory because its wave phase velocity is comparable to the electron thermal velocity. However, it has been shown that the nonlinear EAW wave can be successfully excited when a relatively low amplitude external electric field driver is applied for a sufficiently long time (i.e. several trapping periods). This process excites both EAWs as well as LAN along with some harmonics and create particle*

*trapping (BGK/PSV) in both phase regions, which survives at a nearly constant amplitude long after the drive is turned off. Also, for an infinitesimal external drive amplitude and given wavenumber  $k$ , the existence of a window of chirped external drive frequency is demonstrated which leads to formation of giant PSV. The linear, small amplitude, external drive, when chirped, is shown to couple effectively to the plasma and increase both streaming of “untrapped” and “trapped” particle fraction. The steady state attained long after the external drive is turned off is shown to lead to a giant PSV with multiple extrema and phase velocities, with excess density fraction, defined as the normalized deviation from the Maxwellian background. It is shown that the process depends on the chirp time duration  $\Delta t$  and chirp frequency range in  $\omega$ . The excess density fraction  $\Delta n/n_0$ , which contains both trapped and untrapped particle contribution, is also seen to scale with  $\Delta t$ , only inhibited by the gradient of the distribution in velocity space. Novel features such as “shark”-like structures and transient “honeycomb”-like structures in phase space are discussed. Both undamped electrostatic modes (EAW and LAN) and steady state giant PSV, with multiple extrema due to embedded holes and clumps, are shown to survive long after the external drive is turned off [P. Trivedi and R. Ganesh, *Physics of Plasmas* 23, 062112 (2016)].*

### 3.1 Introduction

In 1946, Landau[1] discovered that electrostatic plasma waves of vanishing amplitude excited as small amplitude perturbations in a collisionless uniform, Maxwellian, electrostatic plasma can be exponentially damped, due to their interaction with plasma particles that stream with velocities close to the wave phase speed  $v_\phi$  of the wave. For example, Langmuir waves (LAN). Landau’s treatment was rigorous, but strictly linear, meaning, the amplitude of the initial perturbation is assumed to be infinitesimal. As the amplitude of perturbation becomes finite, contributions from the non-linear effects become signif-

### CHAPTER 3. ELECTROSTATIC MODES AND DRIVEN PHASE SPACE VORTICES (PSV) IN THE BACKGROUND OF IMMOBILE IONS

---

icant which inhibit the uniform exponential damping, as was analyzed by O’Neil. [2], by flattening the velocity distribution near the wave phase velocity  $v_\phi$ . Consequently, certain nonlinear electrostatic oscillations, which tends to flatten the distribution locally due to particle trapping [30], can survive Landau damping and exist at even low amplitude, even when their phase velocities are comparable to the electron thermal velocity ( $v_{the}$ ). One such nonlinear electrostatic wave structure is known as Electron Acoustic Waves (EAW) as the dispersion relation is of the form  $\omega/k = 1.31v_{the}$  [35], where  $\omega$  is the angular frequency of the wave,  $k$  the wavenumber, and  $v_{the}$  the electron thermal velocity of the plasma. The EAWs are the nonlinear waves that involve only the electrons; in the background of immobile ions. However, within linear theory, these waves are heavily Landau damped because the wave phase velocity of EAWs is comparable to the  $v_{the}$ .

As described earlier, in collisionless plasmas, when the amplitude of electric field is increased, particles may get trapped in electric field pockets, which in turn flattens the distribution, thus rendering the Landau damping ineffective. This leads to formation of coherent structures in phase-space. A well known class of such coherent phase space structures are Bernstein-Greene-Kruskal (BGK) structures. These are exact stationary solutions for electrostatic, collisionless plasmas described by the Vlasov-Poisson model [3]. An undamped EAW is also a weakly nonlinear BGK mode with small populations of electrons trapped in the wave troughs. The distribution of electron velocities is effectively flat at the wave phase velocity because of the trapped electrons and this turns off Landau damping. In general, BGK modes are spatially inhomogeneous and therefore exhibit a finite self-consistent electric potential and field structures. These structures have continued to attract attention as they may represent the final saturated state of instabilities which are stabilized by particle trapping in the potential well formed by the finite amplitude waves.

The BGK paper[3] opened a new window which described ways to construct a large class of nonlinear states. Since then, there has been an enormous body of work that speculates about which of these states might occur in nature [4, 5, 6], in experiments [7, 8, 9], and in

### CHAPTER 3. ELECTROSTATIC MODES AND DRIVEN PHASE SPACE VORTICES (PSV) IN THE BACKGROUND OF IMMOBILE IONS

---

numerical simulations [10], in a variety of situations. In a series of papers, starting from 1972, H. Schamel and collaborators [11, 90, 91, 13, 92, 93, 94, 65, 95, 96, 12] have obtained nonlinear solutions and nonlinear dispersion relation to steady state Vlasov-Poisson equation. In their work, Sagdeev pseudo potential method is used to describe accurately a large class of coherent phase space structures such as electron-ion holes, double layers and more. Their procedure describes parameters estimating trapped particle fraction for a steady state coherent phase space structure with a single extrema. The stability of these structures is also of great interest [13, 10, 44]. The applicability of Sagdeev pseudo potential method to multiextrema phase space structures, such as the studies in the Thesis is questionable [21].

As described earlier, a natural way to achieve a BGK state is to increase the amplitude of initial density perturbation without directly perturbing the distribution in velocity space. The amplitude should be large enough to overcome Landau damping [2, 10]. These waves can be excited even at low amplitude by tailoring the particle velocity distribution or driving the plasma externally. These external drives can excite both LAN waves as well as EAW waves [35]. More recently, external drives with time dependent frequency  $\omega(t)$  or chirp, have been used to obtain BGK modes in bounded systems [36, 37, 38, 39, 40, 41]. For example, in a pure electron plasma confined in a Penning-Malmberg trap, it was shown that phase space holes can be created by choosing the frequency chirp window to be around axial electron bounce frequency [36, 37, 38]. Similarly a downward frequency sweeping has been performed in a pure ion plasma experiment where extreme modification of initial distribution has been observed (for eg. splitting of an initial Maxwellian distribution into two counter-propagating distributions) [42]. Possibility of obtaining BGK modes or PSVs, if the plasma is unbounded as in astrophysical plasmas or in the axial direction in a Tokamak, is an interesting open question. Interestingly such a paradigm may help understand alpha particle dynamics in Tokamaks as well as formation of the non-Maxwellian structures along the magnetic field lines in the astrophysical plasmas.

In the present work, a 1D unbounded Vlasov-Poisson system has been modeled using

## CHAPTER 3. ELECTROSTATIC MODES AND DRIVEN PHASE SPACE VORTICES (PSV) IN THE BACKGROUND OF IMMOBILE IONS

---

Periodic Boundary Conditions (PBC). The plasma is subjected to an infinitesimal external drive. As is well known, [Schamel2000, 30, 33, 42] both abrupt as well as adiabatic external drive of constant frequency, say  $\omega = \omega_0$ , wavenumber  $k$  and linear amplitude (i.e. infinitesimal) are expected to generate plasma modes over a range of frequencies along with its harmonics [as shown later]. In this work, the following questions have been addressed: what would happen in an unbounded plasma modeled using PBC, if the external drive frequency  $\omega(t)$  is chirped down in time interval  $\Delta t$ , say from  $\omega_{high}$  to  $\omega_{low}$ . It has been found out that this frequency chirping allow “continuous” flattening in the velocity space leading to large coherent structures in phase space with embedded holes and clumps resulting in Phase Space Vortices (PSV) with multiple extrema and phase velocities. The drive increases both kinetic energy and potential energy of the system. Meaning both untrapped and trapped particle fraction is seen to increase, leading to flattening of the distribution function. As the external drive is switched off, the above said large coherent phase space structure is found to attain a steady state leading to large amplitude steady PSV. This process of PSV formation also depends on the frequency regime in which chirp is given, which leads to one giant PSV structures to multiple PSVs. In general, the formation of PSV is found to strongly dependent on chirp frequency range and chirp time interval  $\Delta t$ . As described earlier, unlike single extrema PSVs, I believe that the multiple extrema PSVs are not describable well by Pseudo Potential method of Schamel and co-workers.

The rest of the Chapter is organized as follows: I proceed to describe the numerical scheme in Sec. 2.2. Simulations with different cases have been discussed in Sec. 2.3. In the Subsec.1.3.1, the formation of small “seed” flattenings have been shown on applying a constant frequency external drive to a PBC 1D VP plasma, which excites both LAN mode as well as EAW mode. In Subsec.1.3.2, it has been shown that a small amplitude downward chirp amplifies the trapping from LAN to EAW region and at the same time creates streaming of untrapped particles which in turn creates a large flattening in velocity distribution resulting in giant PSV with multiple extrema due to embedded holes and clumps (Subsec.1.3.2.1). These structures I call as multiple phase space vortices (Subsec.1.3.2.2). In Subsec.1.3.2.3, I study the evolution of “untrapped” and “trapped” particle dynamics

with different chirp intervals. In Subsec.1.4 discussion has been presented and phase space holes in Vlasov-Poisson system followed by our conclusions in Sec.2.5.

## 3.2 Governing Equations & Simulation Setup

A 1D unmagnetized, collisionless electrostatic plasma, in the framework of kinetic theory, is described by one dimensional Vlasov-Poisson (VP) model equations, viz:

$$\frac{\partial f}{\partial t} + v \frac{\partial f}{\partial x} - E_T \frac{\partial f}{\partial v} = 0 \quad (3.1)$$

$$\frac{\partial E_s}{\partial x} = 1 - \int f dv \quad (3.2)$$

where  $f(x, v, t)$  is the electron distribution function and  $E_T = E_s + E_{ext}$  is the total electric field, where  $E_s(x, t)$  is the self consistent electric field obtained by Eqn.1.2 and  $E_{ext}$  is the external drive electric field defined as:

$$E_{ext} = E_0 \sin(kx \pm \omega t) \quad (3.3)$$

where  $E_0$  is the amplitude of external drive. Here,  $k$  represents the wave number in the simulation box and  $\omega$  represents the drive frequency. In these above equations, time is scaled to electron plasma frequency ( $\omega_{pe}^{-1}$ ), where  $\omega_{pe} = \sqrt{n_0 e^2 / m_e \epsilon_0}$ , length is scaled to electron Debye length  $\lambda_{De} = \sqrt{KT_e \epsilon_0 / n_0 e^2}$  and velocities to  $v_{the} = \lambda_{De} \omega_{pe} = \sqrt{KT_e / m_e}$ , electron thermal velocity. With these choices,  $f$  gets normalized to  $n_0 / v_{the}$  and  $E$  to  $m_e v_{the} / e \lambda_{De}$ . In this model, the ions form a stationary neutralizing background of number density  $n_0$  with numerical value 1 in the Poisson equation [Eq.(1.2)]. (Please note that, in my published work [21], the electric field  $E$  is normalized by  $-m_e v_{the} / e \lambda_{De}$ , which makes Eqn.1.1 and Eqn.1.2 as  $\partial f / \partial t + v \partial f / \partial x + E_T \partial f / \partial v = 0$  and  $\partial E_s / \partial x = \int f dv - 1$ .)

The simulation domain has been set in phase space  $D = [0, L_{max}] \times [-v_{max}^e, v_{max}^e]$ , where

$L_{max} = 2\pi/k$  is the system size for wavenumber  $k$  such that the longest wavelength fits into the simulation box. and  $v_{max}$  is chosen sufficiently large so that electron velocity distribution function approaches zero as  $|v|$  approaches  $v_{max}$ . I apply periodic boundary conditions (PBC) along boundaries for both spatial and velocity domains.

### 3.2.1 Plasma Dispersion Relation

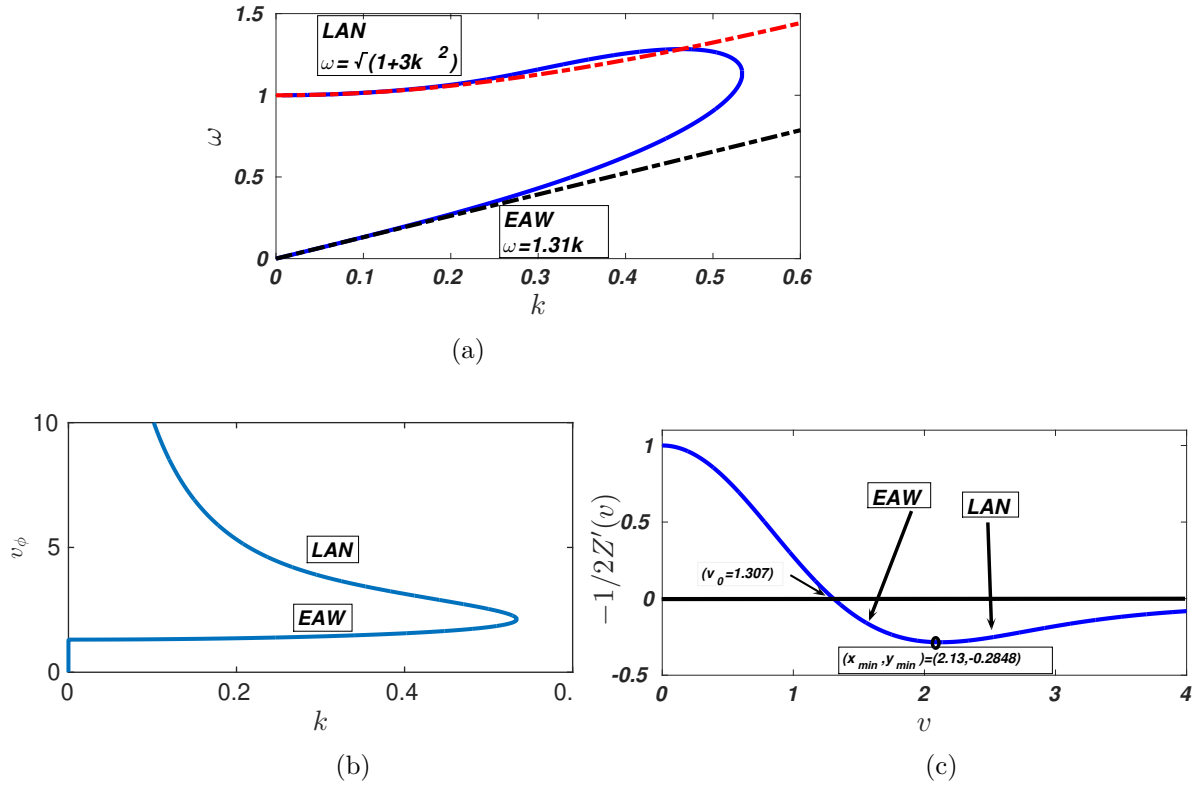


Figure 3.1: Dispersion curves or “Thumb” curves for the electrostatic waves (LAN, EAW) in  $k - \omega$  plane, obtained by assuming zero damping:- (a) The “Thumb” curve represents the solutions or the roots of Eq.(1.4). (b) The same “thumb” curve plotted in the  $k - v_\phi$  plane. (c) The gradient of the real part of the complex plasma dispersion function  $-\frac{1}{2}Z'(v)$  is plotted for real arguments for immobile ions.

Using the above normalizations, the Fourier transformation of linearized form of Eqs. (1.1)-(1.2) leads to the usual linear dispersion relation[16]:-

$$1 + \sum_j K_j(\mathbf{k}, \omega) = 0 \quad (3.4)$$

where  $K_j(\mathbf{k}, \omega) = -k_j^2/2k^2 Z'(\xi_j)$  is the susceptibility of the  $j^{th}(= e)$  species,  $\xi_j =$

### CHAPTER 3. ELECTROSTATIC MODES AND DRIVEN PHASE SPACE VORTICES (PSV) IN THE BACKGROUND OF IMMOBILE IONS

---

$\omega/\sqrt{2}kv_j$  and  $Z_j(\xi_j)$  represents the real part of the complex plasma dispersion function for real arguments[44]. Here, I consider the initial distribution to be Maxwellian,  $f_0(v) = \exp(-v^2/2)/\sqrt{(2\pi)}$ . By assuming a weak flattening (or trapped region) of vanishing velocity width i.e.  $(\partial f/\partial v)|_{v_\phi} \simeq 0$ , which allows us to neglect the contribution from the imaginary part of the dielectric function (For an alternative description as described by Schamel and coworkers [44], See Appendix A), the solution to the real part of the wave frequency  $\omega$  as a function of the wave number  $k$ , obtained numerically from Eq.(1.4) is shown in Fig.(1.1). Typically in the  $k - \omega$  diagram, at high frequencies (fixed/immobile ions), one obtains the “thumb” curve that represents Langmuir waves (upper branch of thumb) and EAWs (lower branch of thumb)[17]. At values of the wave number for which the effects of charge separation are no longer negligible, both electron branches (LAN and EAW) coalesce [Fig.1.1(a)]. In the bottom plot Fig.1.1(b), the same thumb curve is displayed in the  $k - v_\phi$  plane.

In Eqn.(1.4), the term  $-\frac{1}{2}Z'(v)$  can be interpreted as a gradient of the real part of the complex plasma dispersion function for real arguments. A plot of the function  $-\frac{1}{2}Z'(v)$  for kinetic electrons and immobile ions is displayed in Figs.(1.1(c)), where it divides the phase velocity regions and reveals different branches of the dispersion relation. In the limit of immobile ions, the function  $-\frac{1}{2}Z'(v)$  represents electron contribution, where all the negative values of this function represents the real solutions for electrostatic waves. It has one zero transition (at  $v = 1.307$ ) and one minimum (at  $v = 2.13$ ) which results in two separated regions for the phase velocity[96]:-(i)  $v \leq 2.13$  (EAW), (ii)  $v \geq 2.13$  (LAN)). The function is positive for  $v < 1.307$  and negative for other values of  $v$  and vanishes at infinity. From these plots in Fig.1.4, it is evident that there are mainly two undamped roots and no undamped roots exist beyond a critical value of the wavenumber  $k$ . Moreover, this thumb curve also represents that each point in the  $k - \omega$  plane along the thumb curve corresponds to a different particle velocity distribution function. This so-called “thumb” dispersion curve is obtained by assuming the small wavenumber  $k$  and retaining only the principle part in the velocity integral of the Landau dispersion relation.[1]

### 3.3 Simulation

In this Section, I systematically present the numerical results of driven Vlasov-Poisson system using VPPM-2.0 solver. I have considered in detail two different physical phenomena: (a) when plasma is driven with a constant frequency drive, (b) the second concerns the response of the plasma when a time dependent external drive is used.

#### 3.3.1 Driven Electrostatic Modes :- Constant Frequency Drive

Within linear theory, the electron acoustic waves (EAWs) are heavily damped as their wave phase velocities are close to electron thermal velocity ( $v_{the}$ ). In the past, the EAW has been studied in the context of two temperature plasmas, such as those in fusion devices and in the auroral ionosphere [97, 98], where it has often been found that the electrons consist of two distinct groups, one hot and one cold. In the usual acoustic mode dynamics for EAW waves, when plasma constitutes of two different electron components, bulk hot component and less dense (or thinner) cold component with the neutralizing immobile ion background. In such case, the restoring force of the cold electrons comes from the pressure of the hot component, whereas the effective inertia is provided by the cold component. However, for a single temperature electron species plasma, an undamped EAW is a nonlinear BGK mode where electrons trapped in the wave troughs which makes the electron velocity distribution effectively flat at the wave phase velocity, consequently turns off Landau damping. With a Maxwellian plasma, there are no trapped particles. But if the plasma is driven externally, it can form trapping distribution dynamically as the wave evolves. For an external electric field  $E = E_0 \sin(kx - \omega t)$ , the trapping time to form the trapped particle fraction is approximately  $\tau_r = 2\pi / \sqrt{kE_0}$  (in my normalization). However, the EAWs can be excited by a small amplitude driver if the driver is applied resonantly over few trapping periods  $\tau_r$ . The driver continuously replenishes the energy removed by Landau damping. Therefore, the trapped particle distribution survives and the undamped EAWs are eventually produced. the excitation of trapped particle structures

can also be understood by single resonance dynamics, as described in Appendix B.

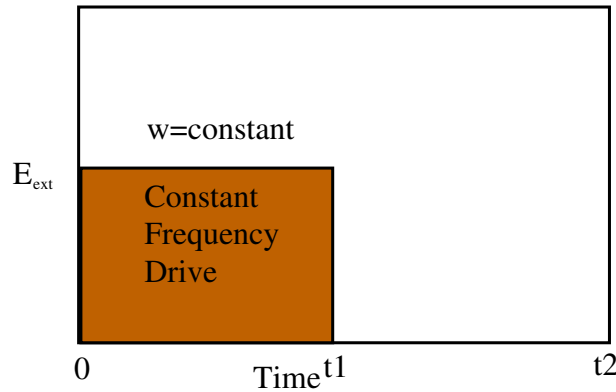


Figure 3.2: A cartoon figure of  $(E_{ext}, t)$  showing frequency turn on-off of external drive. Constant frequency drive is applied for  $(0 \leq t \leq t_1)$ .

In order to excite undamped EAWs, I initialize simulation with a collisionless plasma having a homogeneous density distribution in space and an initial Maxwellian velocity distribution:

$$f_M = \exp(-v^2/2) / \sqrt{2\pi} \quad (3.5)$$

which is driven with an external drive of amplitude  $E_0$ , [Eq.(2.4)], wave number  $k$  and frequency  $\omega$  chosen to be consistent with the  $\omega$  values obtained from “thumb curve”. [17, 35, 99, 33, 42] The drive is applied for time  $0 \leq t \leq t_1$  [See Fig.(1.8)], where  $t_1 \simeq \text{few } \tau_r$ , where  $\tau_r = 2\pi / \sqrt{kE_0}$ .

It is important to note that the amplitude of external drive,  $E_0$ , is chosen to be small enough such that when an initial value problem is performed, the trapping time  $\tau_r = 2\pi / \sqrt{kE_0}$  is much larger than the Landau damping time  $\gamma_L^{-1}$  ensuring Landau damping. [58] For example, consider plasma is driven with parameters:-  $k = 0.4$ ,  $E_0 = \alpha_0/k = 0.01/0.4 = 0.025$ ,  $\omega_d^{EAW} = 0.6241$  (obtained from “thumb” curve), for time period  $\Delta t_d = 1000$ . Here  $\alpha_0$ , is the amplitude perturbation applied in the initial value problems. Then the system is allowed to relax for another several  $\omega_{pe}^{-1}$  i.e. until  $t = 2000$ . In Fig.1.3, the space averaged normalized velocity distribution function is plotted, which is given by

$$\hat{f}_e(v, t) = \frac{\int_0^L f_e(x, v, t) dx}{\int_{-v_{max}}^{v_{max}} \int_0^L f_e(x, v, t) dx dv} \quad (3.6)$$

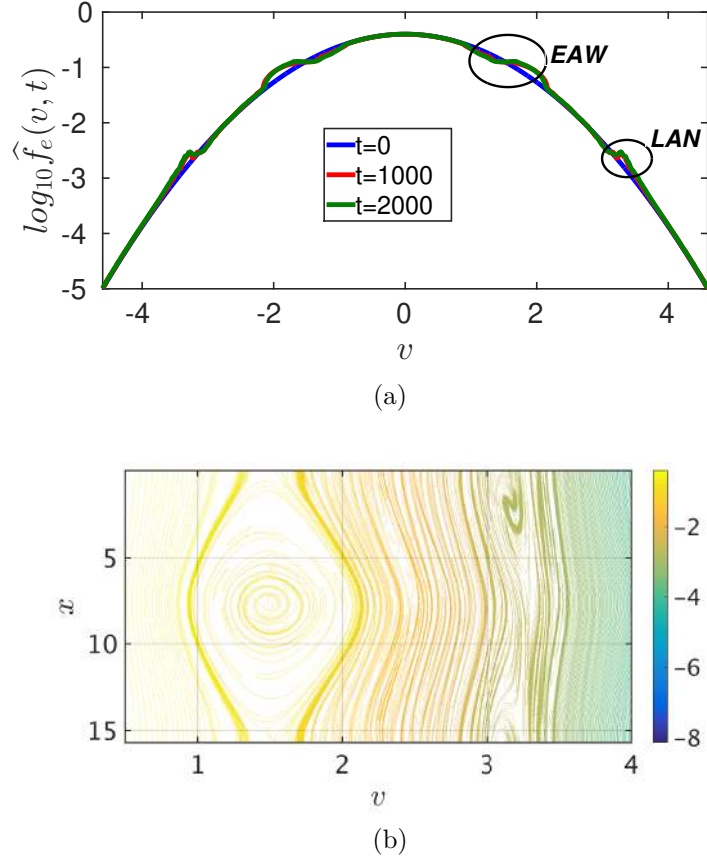


Figure 3.3: (a) Plot of electron velocity distribution function  $\widehat{f}_e(v)$  at different times. Two small “seed” flattening can be seen at  $v_\phi^{EAW} \simeq 1.572$  and  $v_\phi^{LAN} \simeq 3.162$ . (b) Contour plot of  $\log_{10} f(x, v)$  at  $t=2000$  indicating both EAW and LAN regions.

As can be seen in Fig.1.3, this “weakly nonlinear drive” creates a velocity space distribution with two small “seed” flattening, one in nonlinear EAW region and another in LAN region. The corresponding trapping structures can be seen in the phase space plot of  $f(x, v)$  at  $t = 2000$  [see Fig.1.3(b)]. Both small “seed” flattening are seen both at  $v_\phi^{EAW} \simeq 1.572$  and  $v_\phi^{LAN} \simeq 3.162$ . These values are slightly different from the values obtained via “thumb” curve ( $v_\phi^{EAW} \simeq 1.56$  and  $v_\phi^{LAN} \simeq 3.14$ ) due to trapping region of small but finite velocity width. In Fig.1.4(a) and Fig.1.4(c), evolution of excess density fraction  $\delta n(x, t)/n_0 = \int f(x, v, t)dv - \int f_0(v)dv$  is plotted with time and with space. The total energy of the system is defined as:  $W(t) = K(t) + P(t)$ , where kinetic energy is computed as  $K(t) = (1/2) \int \int v^2 f(x, v, t) dx dv$  and potential energy computed as  $P(t) = (1/2) \int E^2(x, t) dx$ . The In Fig.1.4(b), the total relative energy  $\delta W = W(t) - W(0)$ , the total relative kinetic energy  $\delta K = K(t) - K(0)$  and the total relative potential energy  $\delta P = P(t) - P(0)$  are plotted. It is clear that as the drive is kept on, the relative kinetic

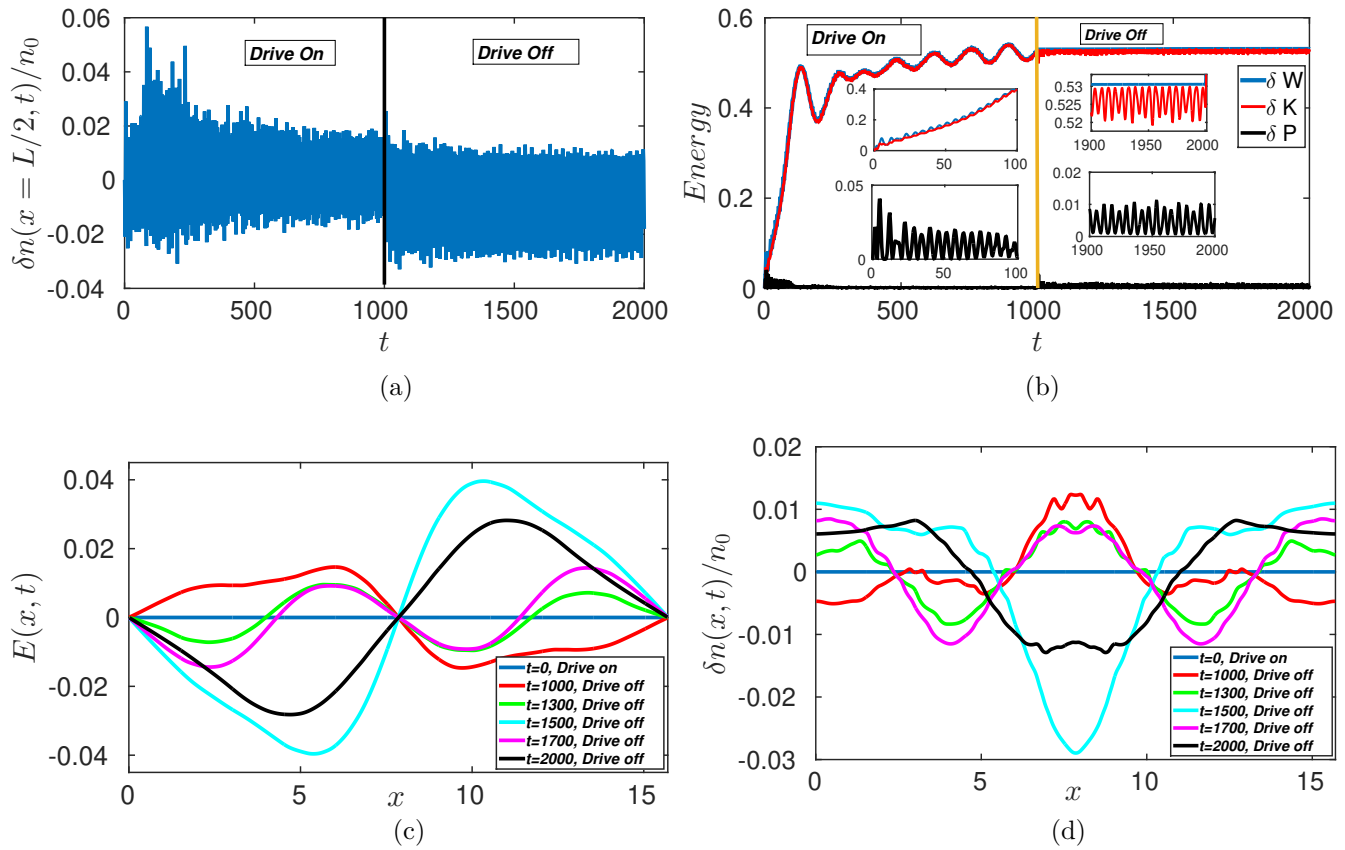


Figure 3.4: (a) Plot of time evolution of excess density fraction  $\delta n(x, t)/n_0 = \int f(x, v, t)dv - \int f_0(v)dv$  at  $x = L/2$ . (b) Plot of relative energy with time, when plasma is driven with a constant frequency for  $\Delta t = 1000$  for the following parameters:-  $k = 0.4$ ,  $\omega_d = 0.6241$ .(c) Plot of evolution of electric field  $E(x, t)$  with  $x$  at different times. (d) Plot of evolution of excess density fraction  $\delta n(x, t)/n_0 = \int f(x, v, t)dv - \int f_0(v)dv$  with  $x$  at different times. The vertical line in Fig. (a) and (b) represents the time at which drive is turned off.

energy of the system increases which reflects the increase in untrapped particle populations. The relative potential energy of the system first increases the attains a certain value during the drive. As the drive is turned off, relative kinetic energy decreases a little and relative potential energy increases which reflects the increase in trapped particle populations.

However, one trapping period ( $\tau_r = 2\pi/\sqrt{kE_0}$ ) as the duration of external constant frequency drive is enough to excite the EAW waves, which depends upon the parameters  $k$  and  $E_0$ . In Fig.1.5, for  $k = 0.4$ , two cases have been shown:- (1) for  $E_0 = 0.01$ ,  $\tau_r \simeq 99.34$  and (2) for  $E_0 = 0.025$ ,  $\tau_r \simeq 62.831$ . For both cases, plasma is driven for one trapping period i.e.  $\Delta t_d = 1\tau_r$ . This weakly nonlinear drive excites EAWs for both cases where the

trapping width increases with increasing amplitude of  $E_0$ .

As is well known, the external electric field  $E_{ext}$  (defined in Eq.(2.4)), may be turned on

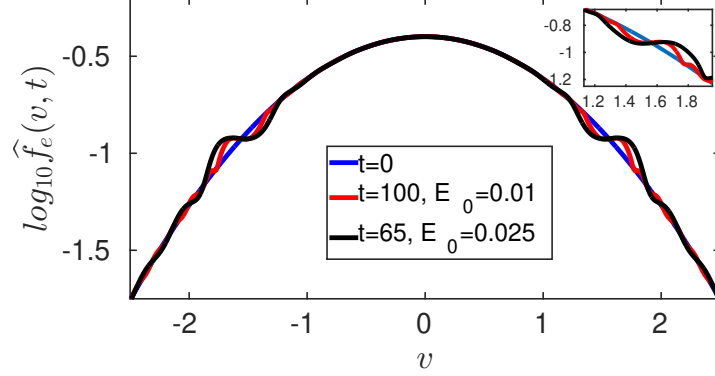


Figure 3.5: Plot of electron velocity distribution function  $\widehat{f}_e(v)$  indicating flattening in EAW region for two different values of  $E_0 = 0.01$  and  $E_0 = 0.025$  after one  $\tau_r$  for each case, respectively.

and turned off either adiabatically (i.e.  $E_{adiabatic} = E_{ext}[1 + (t - \tau)^n / \Delta\tau^n]^{-1}$ ) (See Fig.1.7) [17] or abruptly (i.e.  $E_{abrupt} = E_{ext}$ ) in time. In Fig.1.7, the same experiment has been done to excite EAWs for different adiabatic profiles. For  $E_{adiabatic} = E_{ext}[1 + (t - \tau)^n / \Delta\tau^n]^{-1}$ , a comparison has been shown [Fig.1.7(a)] for the adiabatic profile  $g(t)$  with  $n = 10, 20, 50, 1000$ . As the value of  $n$  increases, the profile becomes more steeper. Both methods would excite Langmuir waves (LAN) as well as weakly nonlinear electron acoustic waves (EAW) along with other harmonics[99]. In Fig.(1.6), I present a benchmark result demonstrating the correctness of our numerical methods used here, when  $E(t)$  is swept from zero to  $E_0$  in a very short time. The abrupt drive is same as given in Eq.(2.4) for  $\delta t_d = 1000$  and the adiabatic drive is given by  $E_{adiabatic} = E_{ext}[1 + (t - \tau)^n / \Delta\tau^n]^{-1}$  where I choose  $\tau = 1000, \Delta\tau = 700$  and  $n = 20$ [33]. For  $k = 0.4$ , the circle indicates the LAN plasma frequency for our parameters where the other peaks indicate weakly nonlinear EAW. As can be expected, for an adiabatic drive, the amplitudes of excited modes are lower than that of the abrupt drive but the frequencies coincide.

Here, the plasma is driven in EAW region for one trapping period  $\tau_r$  for different values of  $n$ . As can be seen in Fig.1.7(b), for all the values of  $n$ , the flattening of electron velocity distribution indicates the trapping and excitation EAWs which persists at a nearly constant amplitude long after the drive is turned off. Profiles with the higher values of  $n$  also

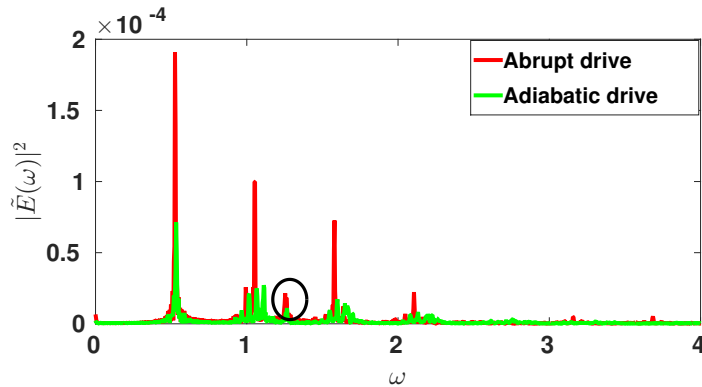


Figure 3.6: Frequency spectrum of perturbed electric field after switching off the constant frequency drive given in EAW region (both adiabatic and abrupt drive) obtained by Fourier transform of electric field during off time i.e. time  $t_1 < t < t_2$ . The abrupt drive is same as given in Eq.(2.4) and the adiabatic drive is given by  $E_{adiabatic} = E_{ext}[1 + (t - \tau)^n / \Delta\tau^n]^{-1}$  [17] where I choose  $\tau = 1000, \Delta\tau = 700$  and  $n = 20$ . [33] For  $k = 0.4$ , the circle indicates the LAN plasma frequency for our parameters where the other peaks indicate weakly nonlinear EAW and its harmonics.

produce the similar results and are equivalents to abrupt drive cases. In the present work, the external drive is always turned on abruptly.

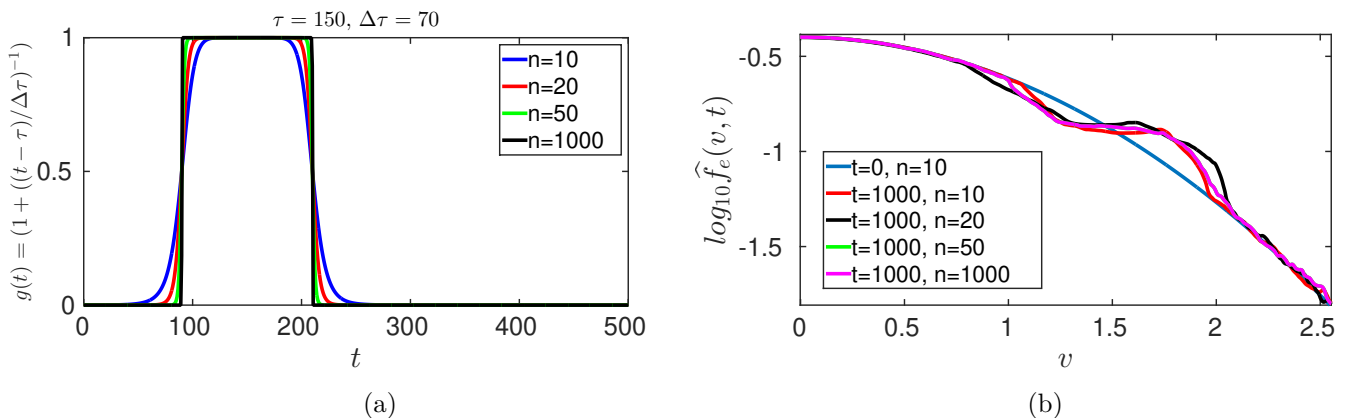


Figure 3.7: Excitation of EAW by driving the homogeneous Maxwellian plasma for nearly one trapping period  $\tau_r$ . (a) Different Adiabatic profile for which plasma is driven with  $E_{adiabatic} = E_{ext}g(t)$  where  $g(t) = [1 + (t - \tau)^n / \Delta\tau^n]^{-1}$  [17]. Here, I choose  $\tau = 150, \Delta\tau = 70$  for different  $n$  values indicating different profiles from adiabatic to nearly abrupt. (b) Plot of electron velocity distribution function  $\hat{f}_e(v)$  indicating flattening in EAW region for corresponding adiabatic profiles. Profiles with the higher values of  $n$  also produce the similar results and are equivalents to abrupt drive cases. In the present work, the external drive is always turned on abruptly.

### 3.3.2 Chrip Driven Phase Space Vortices

In the previous Section 1.3.1, the excitation of electrostatic plasma waves (both LAN and EAWs along with harmonics) in the background of immobile ions is shown for a 1D periodic (unbounded) system. These excited waves creates particle trapping in the resonant regions, also known as undamped Bernstein-Greene-Kruskal (BGK) modes or Phase Space Vortices (PSVs). One can create large amplitude, transient kinetic structures in plasmas, but more often than not, these structures are frequently unstable and short lived and do not necessarily form a long lasting BGK/PSVs. Here, I report that the long lasting, large amplitude PSVs can be excited by an external, oscillating, chirped frequency drive. I start with a stable, Maxwellian Plasma with homogeneous density in space. The idea is to apply a very low amplitude external drive with a downward shifting frequency (or “*chirp*”) for a qualitative short period of time. This process creates localized, growing coherent phase space structures in phase space which are shown to attain a steady state leading to large amplitude PSVs.

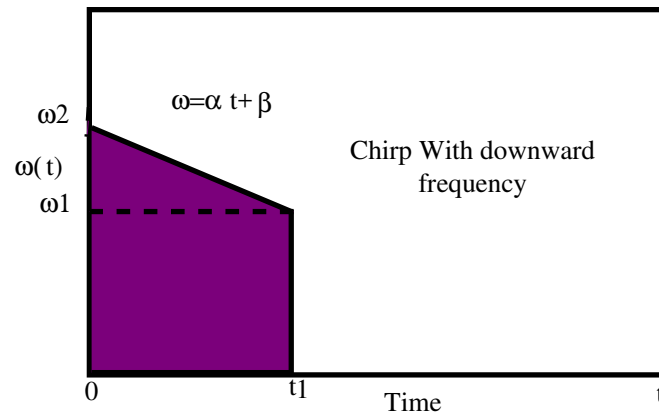


Figure 3.8: A cartoon figure of  $(\omega, t)$  showing frequency turn on-off of external drive. A downward chirp  $\omega = \alpha t + \beta$  is applied for  $(0 \leq t \leq t_1)$ .

### 3.3.2.1 Chirp Driven Giant PSVs

Consider a Maxwellian homogeneous plasma driven by an external downward frequency chirp ( $\omega = \alpha t + \beta$ ) which is applied to the plasma right at  $t = 0$  for time duration  $\Delta t_d$  till  $t = t_1$  from  $\omega_{high}$  (or  $\omega_2$ ) to  $\omega_{low}$  (or  $\omega_1$ ). The parameters for simulations are:-  $k = 0.4$ ,  $E_0 = 0.025$ ,  $\Delta t_d = 200$ ,  $\omega_{high} = 2$ ,  $\omega_{low} = 1$ . The chirp parameter are  $\alpha = -5 \times 10^{-3}$  and  $\beta = 2$ . In order for the transients to relax the system is evolved till  $t_2 = 2000$ .

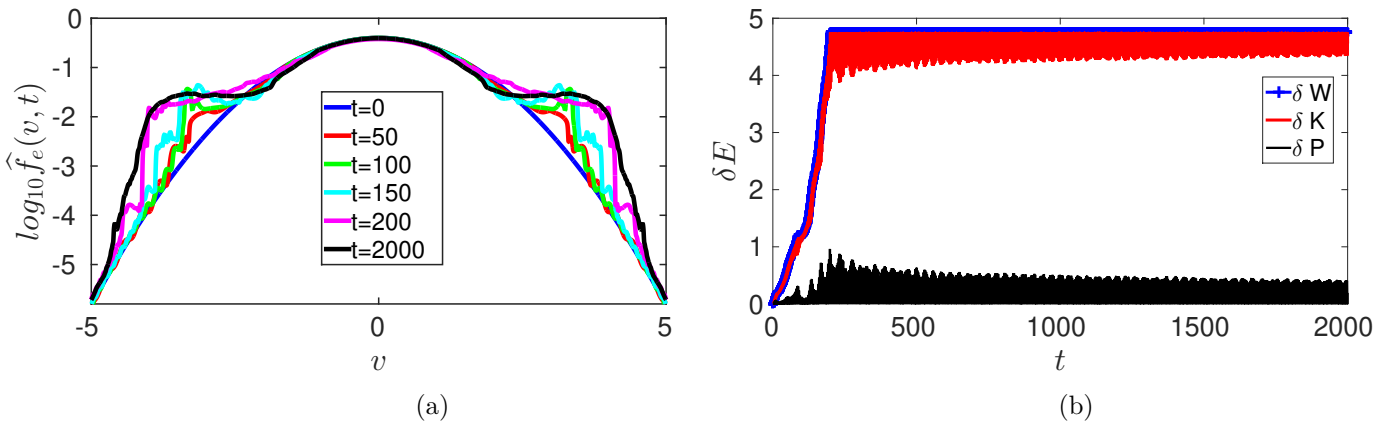


Figure 3.9: Plots of (a) Electron velocity distribution function  $\widehat{f}_e(v)$  at different times in log scale, and (b) Relative energy  $\delta E$  with time, when plasma is driven with a downward frequency chirp from  $\omega_{high} = 2$  to  $\omega_{low} = 1$  for  $\Delta t_d = 200$  after which the drive is turned off.

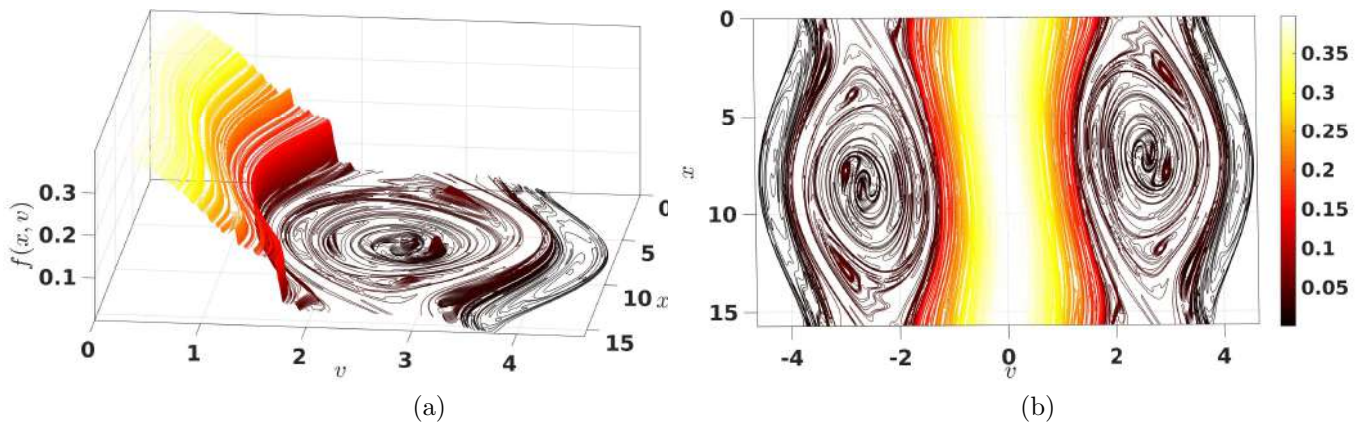


Figure 3.10: Phase space plot of  $f(x, v)$  at  $t=2000$ , when plasma is driven with a downward frequency chirp for  $\delta t_d = 200$ . The large PSV structure contains peaked spikes and holes embedded in it along with a “shark”-like structure, i.e., a bunch of particles moving together within the giant phase space vortices.

### CHAPTER 3. ELECTROSTATIC MODES AND DRIVEN PHASE SPACE VORTICES (PSV) IN THE BACKGROUND OF IMMOBILE IONS

---

Figure 1.9(a) shows the resultant spatially averaged velocity distribution at different time intervals with an increasing plateau region. In the constant frequency drive case [ See Fig.1.3], in spite of the extended time of drive, the flattening is limited to the small regions in velocity space. However, when the drive frequency is chirped from high frequency to low frequency, the initial flattening is seen to grow into a giant stationary region in velocity space and grows till the drive is on. As the chirp is turned off at  $\Delta t = 200$ , the distribution shows a weak relaxation leading to a steady configuration with a giant flat region.

The total energy of the system is defined as:  $W(t) = K(t) + P(t)$ , where kinetic energy is computed as  $K(t) = (1/2) \int \int v^2 f(x, v, t) dx dv$  and potential energy computed as  $P(t) = (1/2) \int E^2(x, t) dx$ . The In Fig. 1.9(b), the total relative energy  $\delta W = W(t) - W(0)$ , the total relative kinetic energy  $\delta K = K(t) - K(0)$  and the total relative potential energy  $\delta P = P(t) - P(0)$  are plotted. It is clear that as the chirp frequency is swept downwards, both relative kinetic energy and relative potential energy of the system increases which reflects the increase in untrapped and trapped particle populations, respectively.

The iso-contour of the electron phase-space distribution  $f(x, v, t)$  at final time ( $t = 2000$ ) is shown in Fig.(1.10), where a steady state vortex structure is created by a combination of both untrapped and trapped particle dynamics during chirp. This phase space structure exhibits several interesting features, like the large hole/ PSV structure contains peaked spikes and holes embedded in it along with a “shark”-like structure, i.e., a bunch of particles moving together within the giant phase space vortices. Also, apart from a large electron hole at one phase velocity ( $v_\phi = 2.569$ ), a second hole structure at higher phase velocity ( $v_\phi = 3.691$ ) is seen. A large region of “separatrices” are seen to be squashed between these two giant hole structures. Furthermore, these hole structures in turn contain peaked spikes or clumps and holes embedded in the larger electron hole surrounded by large region of separatrix as described earlier. This is an example of steady state multiple extrema PSV. Thus, the numerical results predicts that even though the amplitude of drive is much below the “linear limit”, it causes increased particle trapping and simultaneous increase in kinetic energy which in turn facilitates the formation of giant PSV in an unbounded (periodic) system with enormous structural complexity in phase space which is

preserved till the end of the simulation [Fig.1.10].

The time evolution of excess density fraction  $\delta n/n_0$ , as defined in Eq.(2.12), at  $x = L/2$ , is shown in Fig.(1.11(a)). The excess density fraction  $\delta n(x, t)/n_0$  may be defined as:

$$\delta n(x, t)/n_0 = \int f(x, v, t)dv - \int f_0(v)dv \quad (3.7)$$

In response to the small amplitude chirp, excess particle density increases linearly in time till the drive is on. The growth of excess density fraction is arrested when the drive is turned off. Then the system relaxes and saturates to attain a certain value of excess density fraction i.e.  $\delta n/n_0 \simeq 16 - 17\%$  and remains the same till the end of simulation.

The entropy of the system is given by:

$$S(t) = - \int_0^L \int_{-v_{max}}^{+v_{max}} f(x, v, t) \log f(x, v, t) dv dx \quad (3.8)$$

It is plotted as relative entropy [See Fig.(1.11(b))], defined as  $S_{rel} = (S(t) - S(0))/S(0)$  with time. Strictly speaking, for a collisionless plasma  $dS/dt = 0$ . However, because of the numerical scheme, entropy does increase with time (which is a measure of finite grid size effects in simulation) and then saturates [100]. The numerical entropy is a measure of the information “lost” from the simulation. As is well known, the evolving distribution function exhibits filamentation which generates a small-scale structure in phase-space. The numerical entropy saturates when the small-scale structures generated are dissipated when this filamentation reaches the grid size, rendering a numerical steady-state. Here, the relative entropy is seen to grow initially but saturates as soon as the drive is turned off. The numerical experiments have been tested for different phase space grid resolutions also. The growth in the entropy is found to be slower for the higher resolution case, although eventually all different resolution cases saturate at nearly the same level. Results are found to be invariable to grid sizes beyond certain resolutions. All the grid sizes for numerical results in the Thesis have been carefully chosen. After the grid size study, the resolution has been chosen without compromising the quality or quantity of the results. Here, the

CHAPTER 3. ELECTROSTATIC MODES AND DRIVEN PHASE SPACE  
VORTICES (PSV) IN THE BACKGROUND OF IMMOBILE IONS

---

relative entropy is seen to grow when the drive is on but saturates as soon as the drive is turned off. Also, the simulation is extended till  $t = 2000$  in order to confirm the formation of a steady-state solution.

It is important to note that this novel nonlinear phase space structure with rich internal

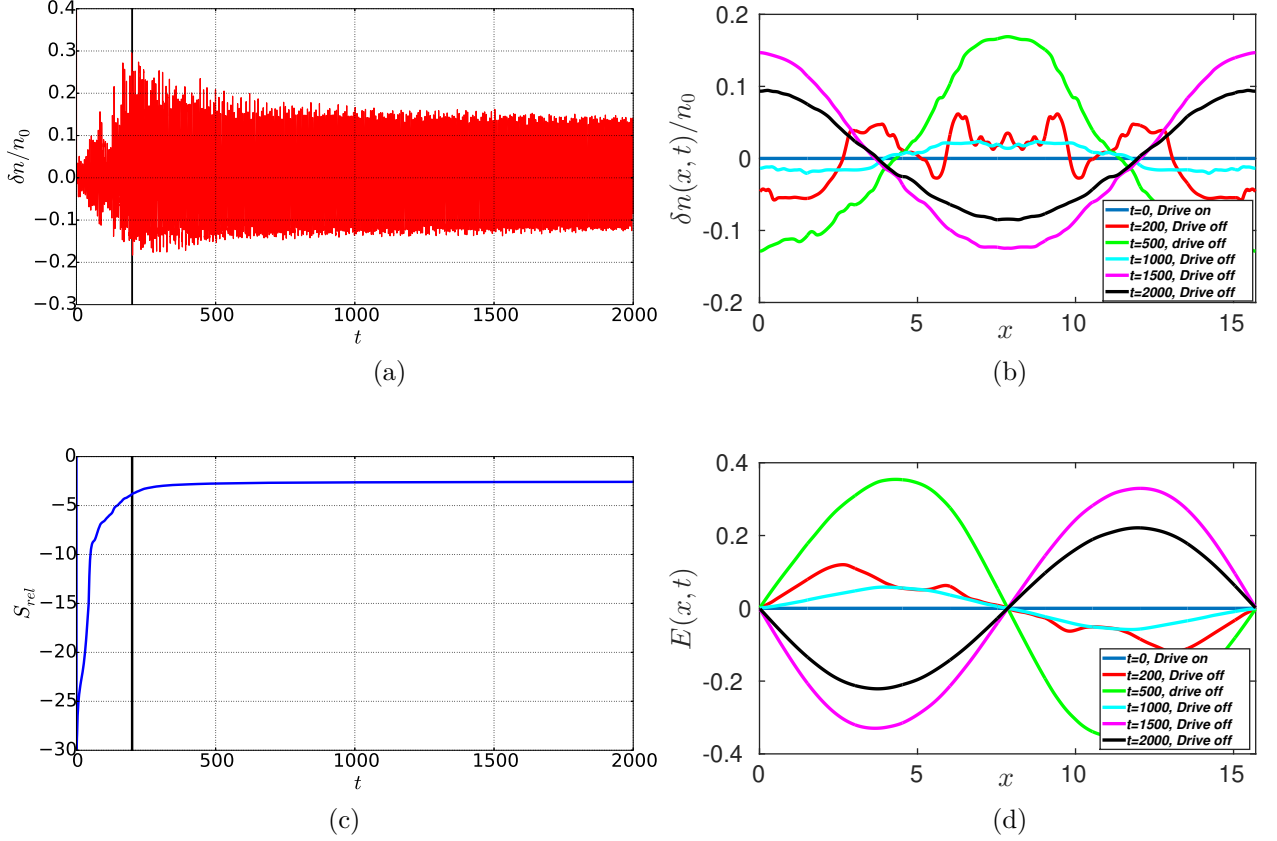


Figure 3.11: Plots for the case where plasma is driven with a downward frequency chirp for  $\delta t_d = 200$  for  $k = 0.4$ :- (a) Plot of excess density fraction (defined in Eq.2.12) evolution at  $x = L/2$  with time. (b) Plot of excess density fraction (defined in Eq.2.12) evolution with  $x$  at different time. (c) Plot of relative entropy  $S_{rel}$  with time. The vertical line represents time at which drive is turned off. (d) Plot of electric field  $E(x,t)$  with  $x$  at different times. The vertical line represents time at which drive is turned off.

structures is a steady state solution [See Fig.(1.10)]. In Fig.1.12, the response of the plasma is shown for different values of wavenumber  $k = 0.3, 0.4, 0.5$ . Considering the “thumb” curve analysis [Fig.1.12(a)], the plasma is driven from LAN region to EAW region for all three values of  $k$  [as shown in Table 1.1]. As can be seen, for lower values of  $k$ , the frequency range from LAN to EAW regime is broader which makes it possible for the chirp drive to excite both electrostatic modes along with their harmonics. As a result, all the

adjacent excitations/resonances overlap which leads to giant phase space structures.

Table 3.1: Chirp Parameters for  $k$ .

$k$	$\omega_{high}$	$\omega_{low}$
0.3	1.2	0.4
0.4	1.5	0.5
0.5	1.4	0.8

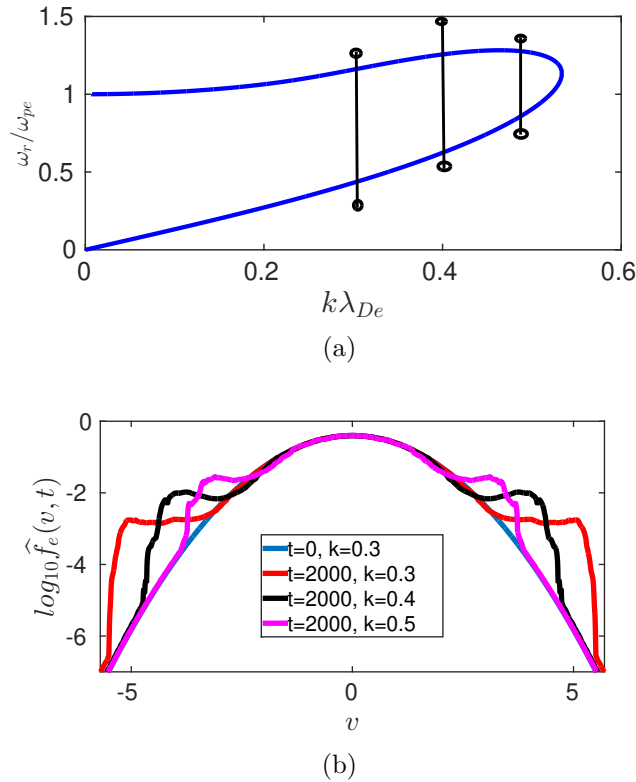


Figure 3.12: Plots of (a) “Thumb” curve indicating chirp frequency ranges used for different  $k$  values, and (b) Electron velocity distribution function  $\widehat{f}_e(v)$  for different  $k$  values in log scale, when plasma is driven with a downward frequency chirp for chirp interval  $\Delta t_d = 200$  from LAN to EAW region [see Table 1.1].

### 3.3.2.2 Transient Honeycomb Structures

The above numerical experiment has also been used to analyze the response of the plasma to the downward chirp in the smaller frequency regime and to study the process of formation and growth of the PSVs in the distribution function. It has been found that downward chirp in smaller frequency regime leads to formation of multiple phase space vortices, all

### CHAPTER 3. ELECTROSTATIC MODES AND DRIVEN PHASE SPACE VORTICES (PSV) IN THE BACKGROUND OF IMMOBILE IONS

---

appearing at different regions of phase space, which gives a “honeycomb”-like transient structure of the distribution function. Here, I report the results of the excitation of the plasma with a drive amplitude of  $E_0 = 0.025$ , with frequency swept from  $\omega_{high} = 0.8$  to  $\omega_{low} = 0.4$  with a sweep rate of  $\alpha = -2 \times 10^{-3}$  for  $\Delta t_d = 250$ .

As the  $\omega(t)$  of the drive chirps down from  $\omega_{high}$  to  $\omega_{low}$  with a single mode number, the entire sub-harmonic region of phase space is seen to be driven strongly which results in an interacting, finite amplitude phase-space structures during the drive phase. The phase space portrait of the plasma as shown in Fig. 1.13 provides a convincing visualization of the effect of the downward chirp on the process of formation and development of the multiple PSV in the subharmonic region. In the first part of the driving process, only the large density fluctuations are visible but at later times, the smaller PSV become more prominent. The growth of the density fluctuations is arrested when the drive is switched off but the phase space structures created by the drive persists till the end of the simulation. These excitations at various phase velocities gives the distribution a “honeycomb” like appearance.

In the past,[37, 38] with chirped frequency drive, a study of axial 1D dynamics of a bounded system (Malmberg-Penning trap) confining pure electrons has been reported. In this work, the external drive with high spatial harmonic content ( $k$ - spectrum) is used to search and lock the axially bouncing electrons. These phase-locked electrons at higher phase velocity are chirp-dragged (“bucket”) to lower velocity region of the distribution function resulting in multiple non-overlapping phase space holes or “honey-comb-like” structures in phase space. In their work, these structures are reported to overlap or interact only at large amplitude of chirp drive. However, our work, I have shown that these transient multi-extrema phase structures in sub-harmonic region or “honeycomb”-like structures thus created are seen to continuously interact, long after the linear drive is switched off, with smaller structures slowly “merging”, as it can be expected in a 2D inverse cascade process leading to a quasi-steady phase space structures.

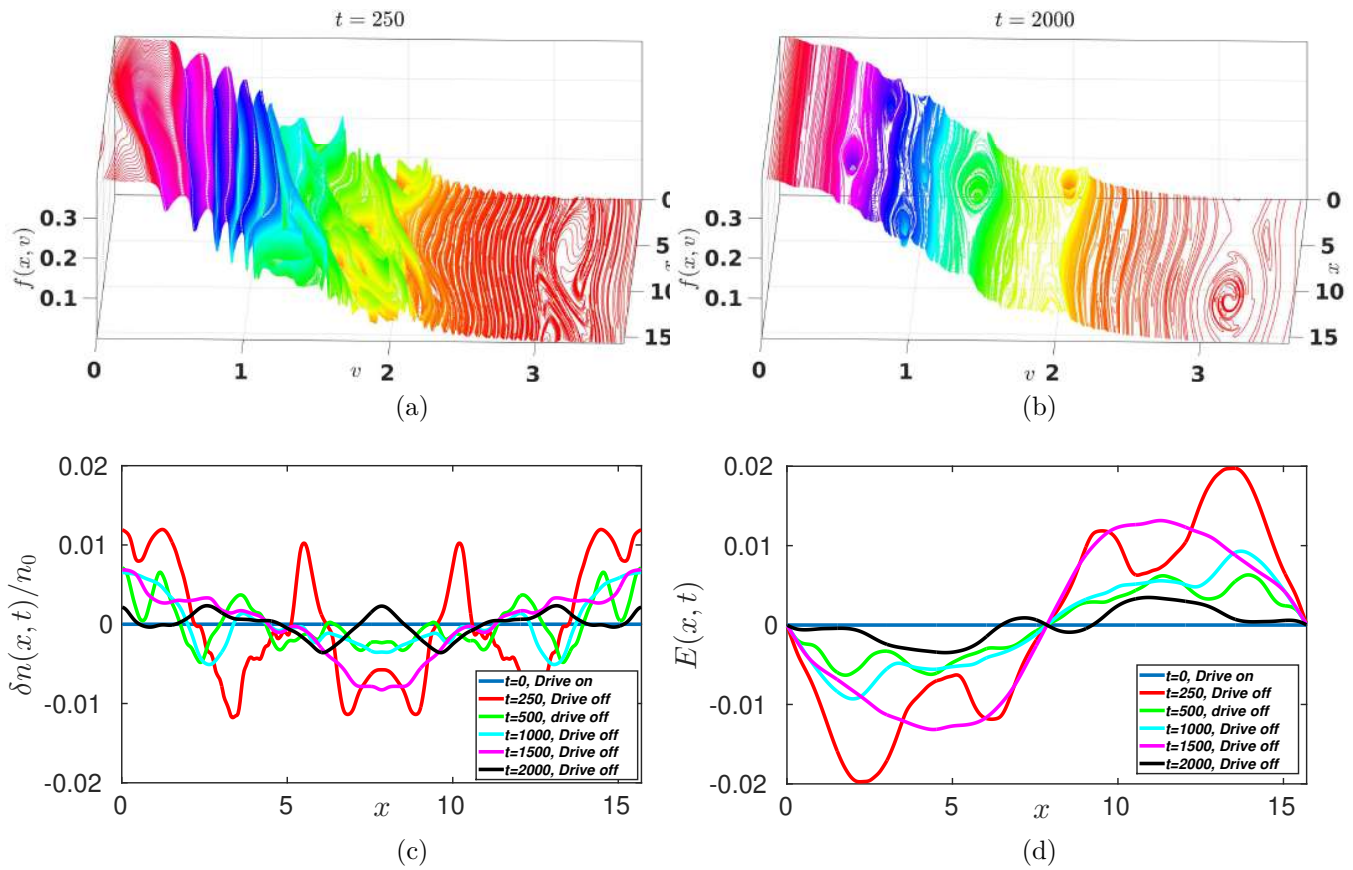


Figure 3.13: Phase-space portrait of the electron distribution  $f(x, v)$ , when plasma is driven in subharmonic region from  $\omega_{high}=0.8$  to  $\omega_{low} = 0.4$  for  $\Delta t_d = 250$ . Contour plots (a)  $t = 250$ , when drive is turned off, and (b) at  $t = 2000$ , at the end of simulation. These portraits show dynamic activity in subharmonic region leading to transient multi-extrema phase structures in sub-harmonic region or “honeycomb”-like structures. (c) Plot of excess density fraction evolution with  $x$  at different time. (d) Plot of electric field  $E(x, t)$  with  $x$  at different times.

### 3.3.2.3 Response of the system to the different chirp intervals

In this Section, the plasma is driven with the same drive amplitude  $E_0 = 0.025$  and the drive frequency is swept within the same range (from  $\omega = 2$  to  $\omega = 1$ ) as in the earlier Section, but for different chirp time intervals ( $\Delta t = 50, 100, 150, 200, 250, 300, 350, 400$ ). The results are shown in Fig.1.14(a), where the width of the flattened regime is shown to increase with chirp time interval. The longer is the chirp time (i.e.  $\Delta t$ ), larger the flattening in velocity distribution. Fig.1.14(b) shows that the system attains a steady state and the relative entropy does not change throughout the simulation long after the drive is turned off. With increase in chirp interval, the structure grows in amplitude but beyond a

certain chirp interval, the amplitude saturates as  $\frac{\partial \langle f \rangle}{\partial v}$  attains very large negative value.

The phase space portrait of the system at the end of the simulation is shown in Fig.(1.15),

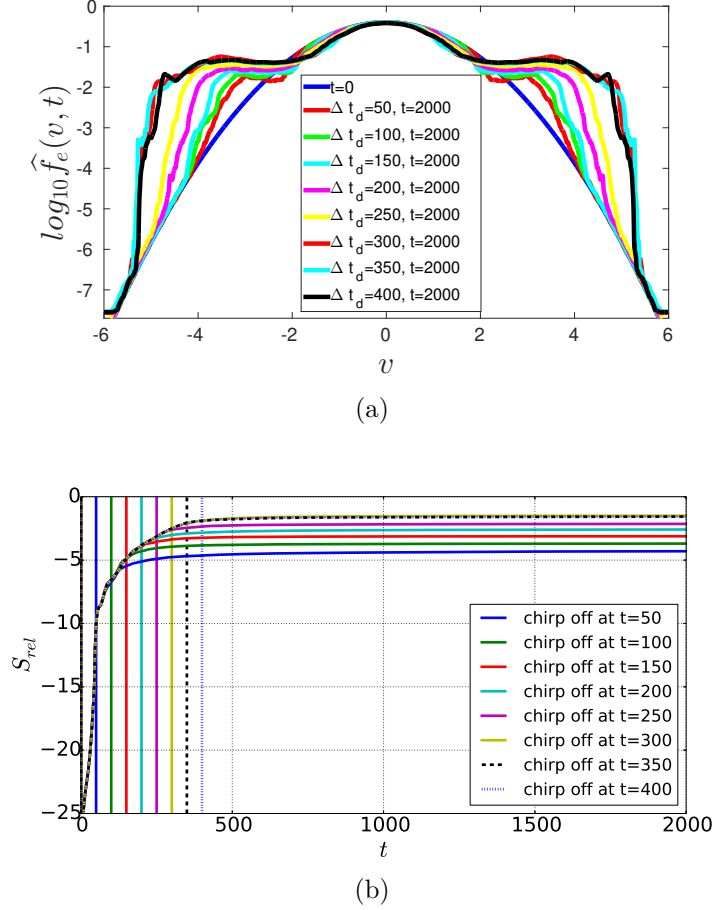


Figure 3.14: (a) Plot of velocity distribution function  $\widehat{f}_e(v)$ , when external downward chirp is given from the start ( $t = 0$ ) for different time intervals. (b) Plot of relative entropy  $S_{rel}$  with time when external downward chirp is given from the start ( $t = 0$ ) for different time intervals. The vertical lines represent time  $t$  at which chirp is turned off.

for different chirp intervals. In Fig.[1.15(a),1.15(c),1.15(e)], a giant PSV structure embedded with holes and clumps can be seen clearly. The size of these steady state PSV structures increases with chirp interval. In the figure, besides the large PSV structure, the presence of a second structure create a significant excess density trapping which is seen last till the end of simulation even in the absence of drive. The increase in the size of the second phase space structure can be seen clearly with increase in chirp interval, where it attains maximum growth after  $\Delta t = 200$ . These structures are seen to persist till the end of simulation. It is important to note that the multiple extrema PSV are formed soon after

the chirp is turned off (typically  $t \sim 800$ ) and remain so, without any further coalescence, for the entire length of the simulation ( $t \sim 2000$ ).

The response of the system in terms of maximum potential well depth and maximum relative density fraction, obtained after switching of the drive, as a function of chirp interval has been shown in Figs. 1.16(a) and 1.16(b) respectively.

### 3.4 Discussion

I have studied numerically a simple, novel and efficient way to obtain giant Phase Space Vortices (PSV) in a 1D unbounded Vlasov plasma modelled using periodic boundary conditions. A very low amplitude external drive with frequency chirping is found to drive giant structures in phase space at steady state. In the first part, 1D simulations have been performed to excite LAN mode which represents the damping and trapping phenomenon of plasma for initial density perturbation problems as well as work as benchmark of our solver. Then, by assuming an initially homogeneous Maxwellian distributional, plasma is driven with constant frequency  $\omega_0$ . This drive creates two “seeds” flattening, one at weakly nonlinear EAW frequency and other is at LAN frequency. Both EAW and LAN are excited with this constant frequency drive which are seen to persist long after the weakly nonlinear drive is turned off.

In the second part, it has been demonstrated that large steady state PSV structures can be excited when the drive frequency is swept from the start ( $t = 0$ ) for a short time period  $\Delta t_d$  from  $\omega_{high}$  to  $\omega_{low}$ .

It was found that when a low amplitude external drive with  $(\omega, k)$  is turned on for longer than several trapping periods, this drive resonantly couples to particles around  $\omega/k$  in phase space leading to linear and weakly nonlinear form of natural modes of the system, for eg. EAW. The modes do not grow any further and the linear and weakly nonlinear dispersions can be obtained. This exercise leads to “thumb” dispersion curve.

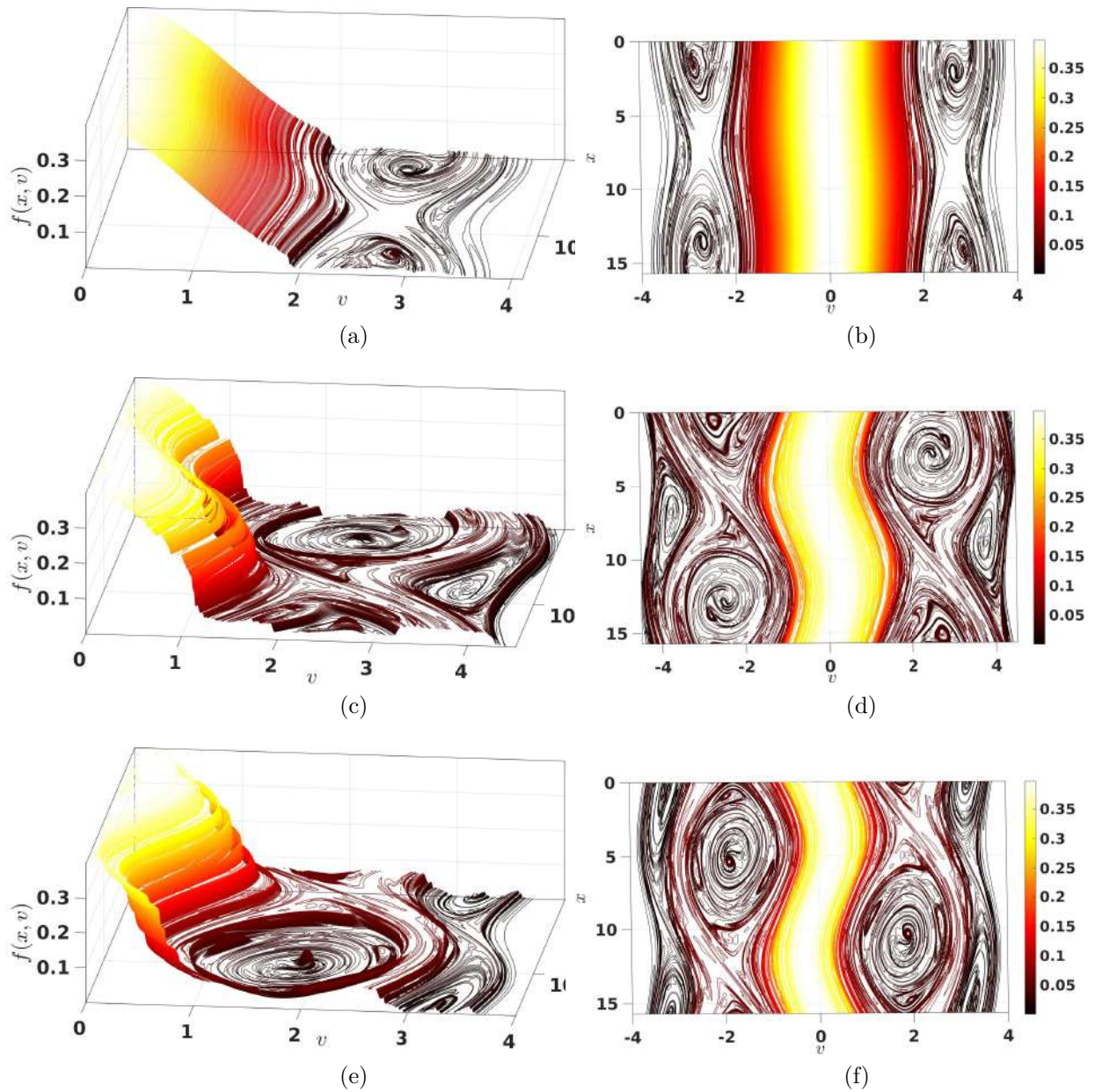


Figure 3.15: Phase space plots of  $f(x, v)$  at  $t = 2000$  when external downward chirp is given from the start for different time intervals. (a) Plot of  $f(x, v)$  at time  $t = 2000$  for chirp interval  $\Delta t = 50$ . (b) Cross-section of  $f(x, v)$  at time  $t = 2000$  for chirp interval  $\Delta t = 50$ . (c) Plot of  $f(x, v)$  at time  $t = 2000$  for chirp interval  $\Delta t = 250$ . (d) Cross-section of  $f(x, v)$  at time  $t = 2000$  for chirp interval  $\Delta t = 250$ . (e) Plot of  $f(x, v)$  at time  $t = 2000$  for chirp interval  $\Delta t = 400$ . (f) Cross-section of  $f(x, v)$  at time  $t = 2000$  for chirp interval  $\Delta t = 400$ .

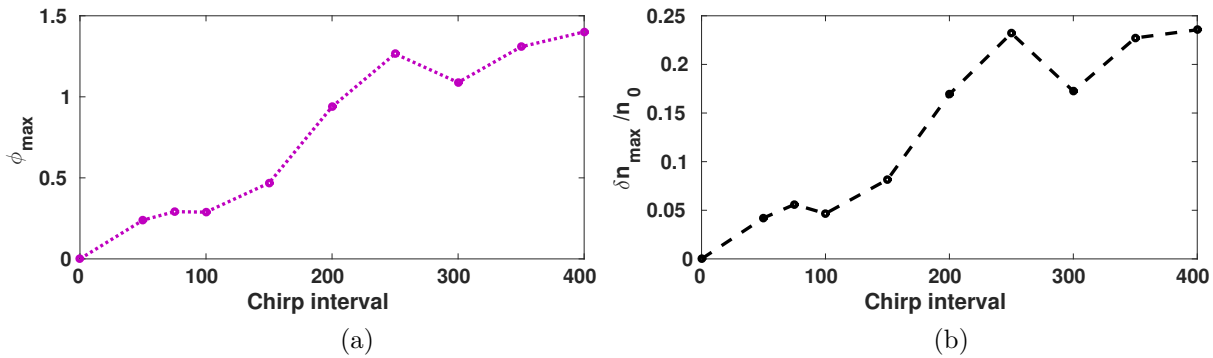


Figure 3.16: Plots of (a)  $\phi_{max}$ , and (b) the percentage of excess density  $\delta n_{max}/n_0$  of the saturated PSV states at  $t = 2000$  after turning off the drive with different chirp intervals  $\Delta t_d$ .

Instead of keeping  $\omega$  a constant, if  $\omega = \omega(t)$  is swept in time or chirped, then groups of particles in the distribution  $f(v)$  resonantly couple to  $\omega(t)/k_0$  leading to several “near-resonant” coupling through the whole range of velocity distribution. As the chirp rate is slowed, the sum of the half widths of the adjacent resonances becomes greater than the distance between the centers of the resonances i. e. the adjacent resonances starts to overlap. Resonance overlap leads to mixing between the two adjacent resonant regions and can lead to overlapped resonant regions with multiple features in it (“shark” like PSVs).

Keeping other parameters fixed, the response of the plasma on applying different chirp rates reveals that the longer the frequency is swept (i.e. slower the chirp rate), the greater is the region of flattening in velocity space. The growth of these coherent phase space structures are arrested beyond a certain chirp interval as  $\frac{\partial \langle f \rangle}{\partial v}$  attains large negative value. In general, the chirp driven phase space structures repeated here are seen to possess multiple extremas of  $f(x, v)$  embedded within the giant hole structure. Moreover, more than one giant hole structures are squashed together amongst separatrix like structures, each of these structures moving at a different phase velocities. The complexity of these structures are seen to increase with  $\Delta t$ .

As described in the Introduction, Schamel and coworkers, [11, 90, 91, 13, 92, 93, 94, 65, 95, 96, 12] construct the phase space holes or vortices, by applying Sagdeev Pseudopotential method to Vlasov-Poisson system of equation. Given a phase velocity  $v_\phi$  of a

### CHAPTER 3. ELECTROSTATIC MODES AND DRIVEN PHASE SPACE VORTICES (PSV) IN THE BACKGROUND OF IMMOBILE IONS

---

single nonlinear phase space structure, mode number  $k_0$  and the amplitude of the nonlinear potential well  $\Psi$ , Schamel and co-workers provide a clear prescription via a nonlinear dispersion relation (NDR), to calculate trapped fraction for a single phase space structure with phase velocity  $v_\phi$ . For a nonlinear phase structure which exists as a steady state solution with more than one extrema embedded with holes and clumps, each of these extrema travel at its own  $v_\phi$ . Moreover these extrema of  $\phi(x)$ , namely  $\Psi$ , would be same for all the structures. Thus in our understanding, while it is possible to apply Pseudo potential theory of phase space holes to steady state nonlinear coherent phase space solution with one  $v_\phi$  and one  $\Psi$  for a given  $k_0$  corresponding to a single extrema, it is unclear as to how this methodology[11, 90, 91, 13, 92, 93, 94, 65, 95, 96, 12] is to be applied to the multiple extrema steady state coherent structures found here.

In the past, with chirped frequency drive, BGK like structures have been studied for bounded system,[36, 37, 38] for example, a pure electron plasma is confined in Penning-Malmberg trap. The extended frequency of drive is applied in such a way that it resonates with a group of axially bouncing electrons. Then the drive frequency is swept downwards such that the bounce-resonant particles remain phase locked to the drive which creates a hole in the electron phase space distribution. Electron population with certain axial bounce frequency is “phase-locked” using an external frequency chirp drive with certain amplitude. The drive contains high spatial harmonics ( $k$ - spectrum) and the frequency chirp is used to “search and lock” the axially bouncing electrons. The chirp range is so chosen that  $\omega_{high} > \frac{\omega_{bounce}}{k_1} > \omega_{low}$  where  $k_1$  is the lowest and prominent mode number. The phase-locked electrons at higher phase velocity and low density (or population) are chirp-dragged to lower velocity (but higher density) region of the distribution function forming a “phase space hole”. This trap-drag-drop idea is akin to a “bucket”. Higher  $k$ -harmonics are shown to create non-overlapping phase space holes of different depths at velocities lower than  $\frac{\omega_{bounce}}{k_1}$ . Thus simultaneous presence of multiple  $k$  values ( $k$ -harmonics) and dynamics of bounce-electron results in “honey-comb-like” structures in phase space. However, these structures do not overlap or interact until the amplitude of the chirp drive is increased to nonlinear levels akin to the well known Chirikov-like condition.

In my work, I study essentially an unbounded 1D plasma modeled using periodic boundary conditions with ions forming a stationary neutralizing background. Thus in the undisturbed plasma there are no trapped electrons. Trapped particles arises only due to the chirp-driven nonlinear phase space vortices. For the entire study, I consider a single  $k$ -mode, the lowest possible  $k$ -mode ( $k = \frac{2\pi}{L}$ ,  $L$ -is the system size) and have investigated the effect of chirped frequency drive with infinitesimal or “linear-like” amplitude  $E_0$  (meaning, at this amplitude, when I perform a standard initial value problem, the mode simply Landau damps linearly). When plasma is driven in high frequency range (from LAN to EAW), the phase of the drive resonates with particle velocity and consequently increases both the kinetic energy and potential energy of the system in that high frequency region. This process creates deep potential well leading trapping as well as streaming of untrapped particles. As the drive is turned off, the system is seen to relax to a phase space vortices but with multiple extrema “shark” like structures squashed between ergodic regions of separatrices. However, for the frequency regime smaller than electron plasma frequency, as  $\omega(t)$  of the drive chirps down from  $\omega_{high}$  to  $\omega_{low}$  with a single mode number  $k$ , the entire sub-harmonic region of phase space is shown to be driven strongly even for “linear-like” drive amplitudes. This results in strongly interacting, finite amplitude phase-space structures during the drive phase. These transient multi-extrema phase structures in sub-harmonic region or “honey-comb-like structures” thus created are seen to continuously interact, long after the linear drive is switched off, with smaller structures slowly “merging”, as it can be expected in a 2D inverse cascade process leading to a quasi-steady phase space structures.

### 3.5 Summary and Conclusions

- The aim of my work presented in this Chapter, is to find, by numerically solving the driven VP system self-consistently, long after the small amplitude drive is switched off, whether or not the VP system supports steady Coherent Phase Space Structures, in a 1D periodically bounded problem. The strength of our numerical method is that

it strictly conserves physical quantities such as the total energy and total number, positivity of the distribution, while at the same time, has very little numerical dissipation. Thus the solutions are very accurate.

- I have studied the excitation of undamped electrostatic modes (LAN and EAW) and formation of giant multiple extrema PSV structures in a homogeneous unbounded plasma modelled using periodic boundary conditions. Application of an external linear drive with a constant frequency and slowly down-chirped frequency (i.e. from  $\omega_{high}$  to  $\omega_{low}$  such that  $\omega_{high} < \omega < \omega_{low}$ ) is shown to create both electrostatic modes with their harmonics and a giant flat region in velocity distribution function indicating formation of multiple extrema PSV structure, respectively. These structures are seen to sustain for very long times after the extended drive is switched off.
- Choice of the amplitude for our external drive  $E_0$  is such that, if an initial value problem is performed with the very same amplitude value  $E_0$  of external drive, the Landau damping time would be much smaller than the conventional trapping time and hence the perturbation would be fully damped.
- The driven dynamics of this Chapter can be divided into the following parts : First part simply present the temporal response of the VP system to an small amplitude external drive which has a sharp temporal rise - It is expected that the plasma would be subjected to a range of frequencies : from the weakly nonlinear slow electron acoustic frequency to the warm plasma frequency and harmonics. This should be observable irrespective of whether the external drive is switched on adiabatically or abruptly. Fig.(1.6) shows this response of plasma  $E(\omega)$  Vs  $\omega$  for adiabatic and abrupt switch on of external drive. This response of the plasma as yet another stringent test for the numerical correctness of our numerical method.

The second part contains the results of constant frequency external drive turned on abruptly with drive frequency  $\omega$  chosen to be consistent with the  $\omega$  values obtained from “thumb curve”. Our results show for the constant frequency drive in EAW region (or near EAW region), the plasma responds by generating a slow weakly nonlinear

Electron Acoustic Wave (EAW) and a weakly nonlinear Langmuir structure (LAN) at higher phase velocity along with some harmonics as shown in Fig.(1.3). Now when chirp is introduced from LAN to EAW region, novel multiple extrema (“shark”-like structures) steady state phase space structure or in short a multiple extrema BGK mode or PSVs which more clearly exhibits enormous details and complexity of clumps and holes embedded inside a large electron hole with large secondary coherent structures separated from the primary structure by a large region of separatrices (Fig.1.10).

In the third part, I perform the chirp experiment for various chirp intervals. Our results clearly shows existence of giant PSVs of increasing size and complexity with increasing chirp interval. As the chirp becomes slower, the amount of trapped and untrapped particle increases nearly linearly, only bounded by the slope of the distribution. This creates a large flattening in velocity distribution resulting in giant PSV with multiple extrema due to embedded holes and clumps. These large PSV structures, once formed, are seen to persist, without any further coalescence, for the entire length of the simulation ( $t \sim 2000$ ). We also find that the multiple extrema phase space vortex structure is formed soon after the chirp is turned off (typically  $t \sim 800$ ) and remain so, without any further coalescence, for the entire length of the simulation. The same is also reflected in our relative entropy data. Thus, I believe that the multiple extrema structures to be a true steady state numerical solution of 1D Vlasov-Poisson system.

The above said studies were for the initial velocity distributions which were Maxwellian. For systems with short range interactions, the energy of the system is extensive. However, for a variety of interesting physical problems such as thermodynamics of self gravitating systems with long range interactions, energy is non-extensive.[45, 46] For such systems, in the nonextensive statistical mechanics framework, non-extensive distributions are needed, for example,  $q$ -nonextensive distributions where  $q$  is the strength of nonextensivity. This formalism has found many applications in systems with the non-Maxwellian particle distribution functions observed in space and laboratory. These include the solar wind

### CHAPTER 3. ELECTROSTATIC MODES AND DRIVEN PHASE SPACE VORTICES (PSV) IN THE BACKGROUND OF IMMOBILE IONS

---

and the long-range interacting systems containing plentiful superthermal particles[48, 49], the peculiar velocity distributions of galaxy clusters[50], and the solar neutrino problem[51]. This formalism has also been extended to study non-linear Landau damping and formation of Bernstein-Greene-Kruskal structures for plasmas with  $q$ -nonextensive velocity distributions[57, 58]. In the next Chapter, a numerical study has been performed to study the formation and dynamics of phase space vortices as the effect of the frequency chirp on the  $q$ -nonextensive distribution as initial distribution function [*P. Trivedi and R. Ganesh, Physics of Plasmas 24, 032107 (2017)*].



---

## Driven phase space vortices in plasmas with nonextensive velocity distribution

*The evolution of chirp-driven electrostatic waves in unmagnetized plasmas is numerically investigated by using a one-dimensional (1D) Vlasov-Poisson solver with periodic boundary conditions. Initial velocity distribution of the 1D plasma is assumed to be governed by Tsalli's [47] nonextensive  $q$  distribution. For an infinitesimal amplitude of external drive, investigate the effects of chirp driven dynamics that leads to the formation of giant phase space vortices (PSV) for non-Maxwellian ( $q \neq 1$ ) plasmas and compare the results with the results obtained in Chapter 3 earlier for Maxwellian plasmas i.e for  $q = 1$ . For  $q$  non-Maxwellian plasmas, the formation of giant PSV with multiple extrema and phase velocities is shown to be dependent on the strength of non-extensivity parameter " $q$ ". Novel features such as "shark"-like and transient "honeycomb"-like structures in phase space are also discussed.*

## 4.1 Introduction

For over a century, the equilibrium of statistical systems has been studied based on the Boltzmann-Gibbs-Shannon entropy (BGS)[101],

$$S_{BGS} = k_B \sum_i p_i \ln p_i \quad (4.1)$$

where  $k_B$  is the Boltzmann constant and  $p_i$  denotes the probability of the  $i$ -th microscopic configuration. For a given composite system  $A + B$ , constituted by two independent subsystems  $A$  and  $B$ , the probability of system  $A + B$  in  $i + j$  state is,  $p_{i+j}^{A+B} = p_i^A \cdot p_j^B$ , where  $i$  is the microstate of system  $A$  and  $j$  is the microstate of system  $B$ . For such case, The BGS entropy satisfies the additivity of entropy of the system, i.e.  $S_{BGS}^{A+B} = S_{BGS}^A + S_{BGS}^B$ , which shows that the entropy is an extensive quantity.

As is well known, for systems with short range interactions, the energy of the system is extensive. Thus the “canonical” distribution is a “Maxwellian” and may be obtained by extremizing Boltzmann-Gibbs-Shannon (BGS) entropy subject to energy constraint. However, for a variety of interesting physical problems such as thermodynamics of self gravitating systems with long range interactions, energy is non-extensive [45, 46]. Recently, there have been several attempts to define a BGS like entropy for nonextensive systems. For example, Tsalli’s definition [47] of  $q$ -nonextensive entropy where  $q$  is the strength of nonextensivity and the corresponding “canonical” distribution function has been derived using nonextensive statistical mechanics framework. This formalism has found many applications in systems with the non-Maxwellian particle distribution functions observed in space and laboratory. These include the solar wind and the long-range interacting systems containing plentiful superthermal particles [48, 49], the peculiar velocity distributions of galaxy clusters [50], and the solar neutrino problem [51]. The  $q$  distribution lend themselves to applications in vast number of problems in areas of ion acoustic waves, electron acoustic solitons and other areas of plasmas [52, 53, 54, 49, 55]. On the theoretical front, a

comprehensive discussion of plasma oscillations, Landau damping and dispersion relation for electrostatic waves, which can be found and solved for an equilibrium distribution function, in a collisionless thermal plasma has been provided based on  $q$ -statistics [56]. The dispersion relation is found to fit experimental data better than a Maxwellian. This formalism has also been extended to study non-linear Landau damping and formation of Bernstein-Greene-Kruskal structures for plasmas with  $q$ -nonextensive velocity distributions [57, 58].

In the previous Chapter, an external drive with time dependent frequency  $\omega(t)$  or chirp was successfully applied to obtain multiple extrema phase space vortices (PSV) in an infinite plasma modeled using periodic boundary conditions (PBC) along with “shark”-like structures in phase space [21]. Starting from a uniform plasma with a Maxwellian velocity distribution, the plasma is subjected to a linear, small amplitude, external drive of constant frequency  $\omega_0$  which was properly chosen so that a small population of particles are resonant. Then, the external drive frequency  $\omega(t)$  was chirped down slowly in time interval  $\Delta t$  from  $\omega_{high}$  to  $\omega_{low}$  such that  $\omega_{high} < \omega_0 < \omega_{low}$  which was shown to couple effectively to the plasma and increase both streaming of “untrapped” and “trapped” particle fraction. The steady state attained after the external drive was turned off, was shown to lead to a giant PSV with multiple extremas with embedded holes and clumps or “shark”-like modes. It was also shown that the excess density fraction, which define as a deviation from initial Maxwellian contains both trapped and untrapped particles, which was found to increase with chirp duration  $\Delta t$ . This downward sweeping is shown to create multiple extrema phase space vortices with a giant flat region in velocity distribution function [21].

The above said studies were for the initial velocity distributions which were Maxwellian. The purpose of the present Chapter is to study numerically the effect of the downward frequency chirp on the  $q$ -nonextensive distribution as initial distribution function. For this purpose, a one dimensional (1D) Vlasov-Poisson solver has been used. Starting with a  $q$  nonextensive equilibrium distribution, I study the plasma behavior as a function of

different values of the non-extensivity parameter  $q$ , and compare the numerical results with Maxwellian case. I find that the chirp dynamics and trapping phenomenon is strongly affected by the deviations from the Maxwellian distribution. The process of PSV formation and the amount of both trapped and untrapped particle fraction is shown to be dependent on the strength “ $q$ ” of nonextensivity along with some novel features of PSV such as “shark”-like and transient “honeycomb”-like structures.

## 4.2 Mathematical Model And Numerical Scheme

In an unmagnetized, collisionless plasma, in the framework of kinetic theory, the propagation of electrostatic waves can be described by a normalized one dimensional Vlasov-Poisson system, which is given by

$$\frac{\partial f}{\partial t} + v \frac{\partial f}{\partial x} - E_T \frac{\partial f}{\partial v} = 0 \quad (4.2)$$

$$\frac{\partial E_s}{\partial x} = 1 - \int f dv \quad (4.3)$$

where  $f(x, v, t)$  is the electron distribution function and  $E_T = E_s + E_{ext}$  is the total electric field, where  $E_s(x, t)$  is the self consistent electric field and  $E_{ext}$  is the external driver electric field defined as:

$$E_{ext} = E_0 \sin(kx \pm \omega t) \quad (4.4)$$

where  $E_0$  is the amplitude of external drive. Here,  $k$  represents the perturbation wave number in the simulation box and  $\omega$  represents the driver frequency.

As described earlier in the Chapter 2, in solving the equations (2.2) and (A.6), time has been normalized to the electron plasma frequency  $\omega_{pe}$ , space has been normalized to the Debye length  $\lambda_{De}$ , velocity has been normalized by the initial equilibrium thermal velocity  $v_{the} = \lambda_{De} \omega_{pe}$ . With these choices,  $f$  gets normalized by  $n_0/v_{the}$  and  $E$  by  $m_e v_{the}/e \lambda_{De}$  where  $e$  is the electron charge. In this model, the ions form a stationary neutralizing background of number density  $n_0$  with numerical value 1 in the Poisson equation [Eq.(A.6)]. Please note that, in my published work [22], the electric field  $E$  is normalized by  $-m_e v_{the}/e \lambda_{De}$ , which makes Eqn.?? and Eqn.?? as  $\partial f/\partial t + v \partial f/\partial x + E \partial f/\partial v = 0$

and  $\partial E/\partial x = \int f dv - 1$ .

In the previous Chapter [21], the above described model has predicted important features of the chirp-driven process in case of Maxwellian plasmas. In order to study the effects of chirp-driven process and frequency sweep on the non-Maxwellian plasmas, I consider an initial distribution function to be a Tsalli's distribution with non-extensivity parameter  $q$ , which is given as follows[56],

$$f_{q0}(v) = C_q [1 - (q - 1) \frac{v^2}{2}]^{1/(q-1)} \quad (4.5)$$

where  $f_{q0}$  is the initial  $q$ -nonextensive velocity distribution function. Here,  $q$  is the strength of nonextensivity and  $C_q$  is the normalization constant given by

$$C_q = \begin{cases} \frac{\Gamma(\frac{1}{1-q})}{\Gamma(\frac{1}{1-q} - \frac{1}{2})} \sqrt{\frac{1-q}{2\pi}}, & \text{For } -1 < q < 1. \\ \frac{1+q}{2} \frac{\Gamma(\frac{1}{q-1} + \frac{1}{2})}{\Gamma(\frac{1}{q-1})} \sqrt{\frac{q-1}{2\pi}}, & \text{For } q > 1. \end{cases} \quad (4.6)$$

where  $\Gamma(m)$  represents the standard Gamma function. For  $q = 1$ , this distribution reduces to the Maxwellian with  $C_1 = 1/\sqrt{2\pi}$ . I present results mainly for three specific values of non-extensivity parameter  $q$ , namely  $q = 0.95, 1, 1.05$ . The corresponding profiles of velocity distributions are displayed in Fig. (2.1), where the logarithmic plot of initial spatially averaged distribution function in velocity space is shown. For  $q < 1$ , the tail(s) of the distribution is(are) extended as compared to a Maxwellian function which implies that there are more particles with the velocities faster than the thermal speed  $v_{th}$  and high energy (i.e.  $E = mv^2/2$  for non relativistic particles) states are more probable than in the extensive case. While, for  $q > 1$ , the function becomes narrower than a Maxwellian one which shows there is large fraction of particles with velocities that are slower than the thermal speed  $v_{th}$ . Therefore, for  $q > 1$ , high energy states are less probable than in the extensive case and the function exhibits a velocity cutoff on the maximum value allowed for the velocity of the particles, namely  $|v_{cutoff}| = \sqrt{2/(q-1)}$ , beyond which no energy states exist.[56]

We set the simulation domain in phase space  $D = [0, L_{max}] \times [-v_{max}^e, v_{max}^e]$ , where

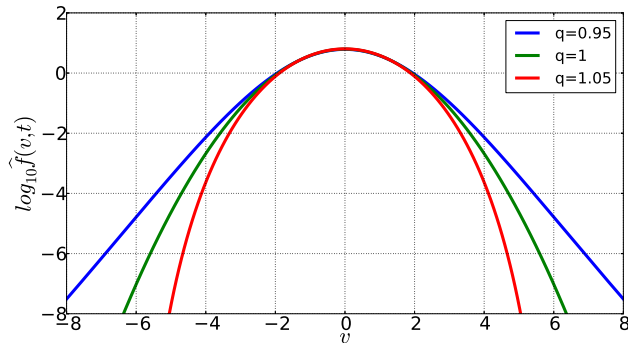


Figure 4.1: Logarithmic plot of the initial spatially averaged velocity distributions, for three different values ( $q < 1, q = 1, q > 1$ ) of the nonextensive index  $q$ .

$L_{max} = 2\pi/k$  is the system size and  $v_{max}$  is chosen sufficiently large so that electron velocity distribution function approaches zero as  $|v|$  approaches  $v_{max}$ . The grid spacing is given by  $\Delta x = L/N_x$  and  $\Delta v = 2v_{max}/N_v$ , where  $N_x$  and  $N_v$  are grid points in spatial space and velocity space respectively. Here, for the value of  $k = 0.4$ , I set gridsize  $N_x = 512$  and  $N_v = 8000$  in such a manner that there is sufficient resolution in both  $x$  and  $v$  for all values of nonextensive parameter “ $q$ ” considered.

### 4.3 Simulation Results

To begin with, initialize simulations with a collisionless plasma with homogeneous density distribution in space having the following velocity distribution function:

$$f_{q0}(v) = \begin{cases} \exp(-v^2/2)/\sqrt{2\pi}, & \text{For } q=1. \\ C_q[1 - (q-1)v^2/2]^{1/(q-1)}, & \text{For } q \neq 1. \end{cases} \quad (4.7)$$

which is driven by an external drive  $E_{ext}$  of amplitude  $E_0$  with a downward frequency chirp  $\omega = \alpha t + \beta$  from  $t = 0$  to  $t = t_1$  with appropriately chosen chirp coefficients  $(\alpha, \beta)$  [see Fig. (2.2)]. By doing so, the total electric field  $E_T$  ( $E_T = E_{ext} + E_s$ ) acting on the particles produces a plateau in the resonant region. In this way, the energy of both trapped and untrapped particles increases till the chirp is on followed by complete energy conservation

once the chirp is turned off, until the end of simulation. In order to check the correctness of numerical method, a constant frequency drive has also been applied for multiple values of  $q$ , namely  $q = 0.95, 1, 1.05$ . This linear drive excites weakly slow electron acoustic waves (EAW) and Langmuir waves (LAN) along with other harmonics for all above values of  $q$  including  $q = 1$  as previously shown results.[21]

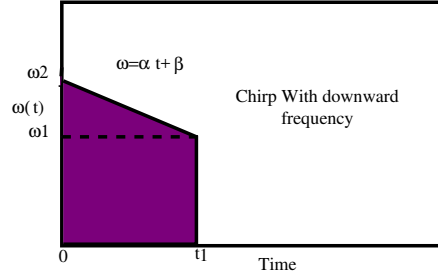


Figure 4.2: A cartoon figure of  $(\omega, t)$  showing frequency turn on-off of external drive. Downward chirp is applied for  $(0 \leq t \leq t_1)$ . Here,  $\alpha, \beta$  are constant coefficients.

### 4.3.1 Case $q=1$

In the following, I have considered a simulation for  $q = 1$  case, which is the normalized Maxwellian. This case has been reported in the previous Chapter in great detail [21]. Here I will summarize the relevant results along with some detail regarding the initial conditions for later comparison. The homogeneous plasma is subjected to an external drive of amplitude  $E_0 = 0.025$  right at  $t = 0$  for time duration  $\Delta t = 250$  from  $\omega = 1$  to  $\omega = 0.5$  for a full time step. The chirp parameters are  $\alpha = -2 \times 10^{-3}$  and  $\beta = 1$ . It was found that this downward frequency chirping allows “continuous” flattening in the velocity space leading to large coherent structures in phase space with multiple extrema with “shark” like features in phase space.

Fig.(2.3) shows the resultant spatially averaged velocity distribution showing growth of plateau region with time. The velocity distribution function is given by

$$\hat{f}(v, t) = \frac{\int_0^L f(x, v, t) dx}{\int_{-v_{max}}^{v_{max}} \int_0^L f(x, v, t) dx dv} \quad (4.8)$$

## CHAPTER 4. DRIVEN PHASE SPACE VORTICES IN PLASMAS WITH NONEXTENSIVE VELOCITY DISTRIBUTION

It can be clearly seen, as the drive frequency is chirped downwards, the size of the “flat region” is seen to grow into a giant stationary region till the drive is on. After turning off the chirp, the transient structures relax and eventually a nonlinear steady state structure is established which is seen to last till the end of simulation.

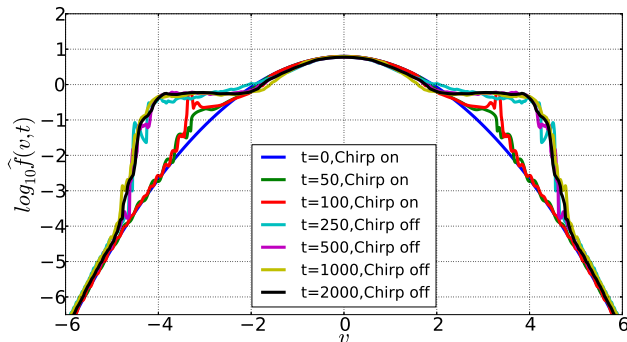


Figure 4.3: Plot of evolution of spatially averaged velocity distribution  $\hat{f}(v)$  when external downward chirp is given from the start for  $\Delta t = 250$ .

The iso-contour of the electron phase-space distribution  $f(x, v)$  at final time ( $t = 2000$ ) is shown in Fig. (2.4). As one can observe, there is a significant density of trapped particles and those of surrounding untrapped particles forming a large electron hole at  $v = 2.53$  and at higher phase velocity  $v = 4.39$ . At  $t = 0$ , when chirp is applied, a phase space “dip” forms at  $v = 2.5$  with a small amount of particle trapped in it and as the frequency decreases, the “dip” grows in size with addition of more and more new particles in it till the drive is on and. Furthermore, the larger hole structure contains peaked spikes and holes embedded in it along with a “shark”-like structure i.e. a bunch of particles moving together within the giant phase space vortices.

The numerical entropy  $S(t)$  of the system, for  $q = 1$ , is computed by

$$S(t) = - \int_0^L \int_{-v_{max}}^{+v_{max}} f(x, v, t) \log f(x, v, t) dv dx \quad (4.9)$$

It is plotted as relative entropy [See Fig. 2.5(a)], defined as  $S_{rel} = (S(t) - S(0))/S(0)$  with time. At first, entropy increases with time due to finite gridsize effects and then saturates soon after turning off the chirp and remains stable throughout the simulation

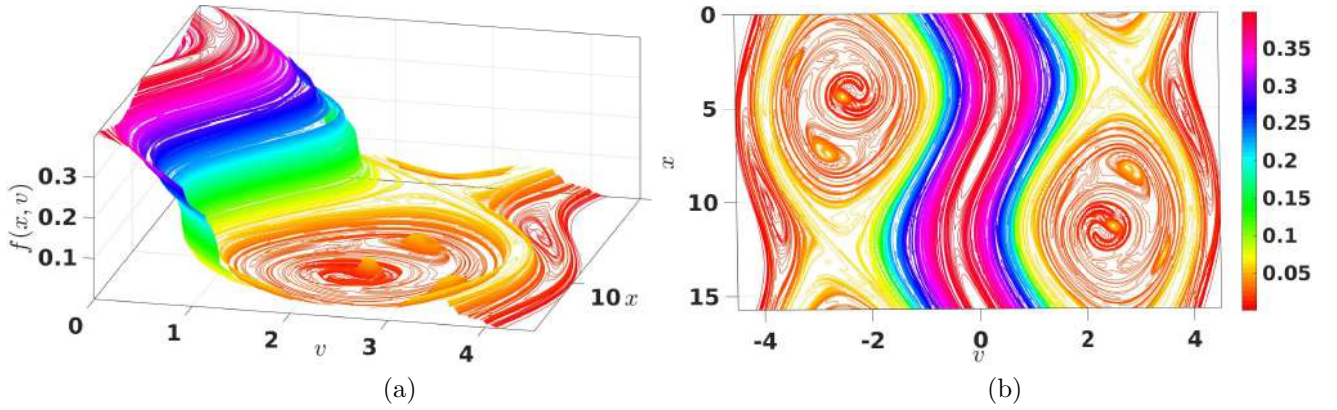


Figure 4.4: Plot of  $f(x, v, t)$  at  $t=2000$  when external downward chirp is applied from the start for a period  $\Delta t = 250$  in the range  $[0 \leq v \leq 4.3]$ . (a) Zoomed plot of  $f(x, v, t)$  at time  $t = 2000$ . (b) Cross-section of  $f(x, v)$  at time  $t = 2000$ .

which confirms the formation of stationary structures (here PSVs).

The total energy of the system is defined as :  $W(t) = K(t) + P(t)$ , where  $K(t) = (1/2) \int \int v^2 f(x, v, t) dx dv$  is the kinetic energy and  $P(t) = (1/2) \int E^2(x, t) dx$  is the potential energy. The actual total energy, at any given, is the half of  $W(t)$ . It is clear from the Fig. 2.5(b) that, when drive is swept downwards, both kinetic energy [In Fig. as  $\delta K = K(t) - K(0)$ ] and potential energy [In Fig. as  $\delta P = P(t) - P(0)$ ] increases which reflects the increase in untrapped and trapped particle populations respectively.

To summarize  $q = 1$  results, it has been observed that an external linear drive with a

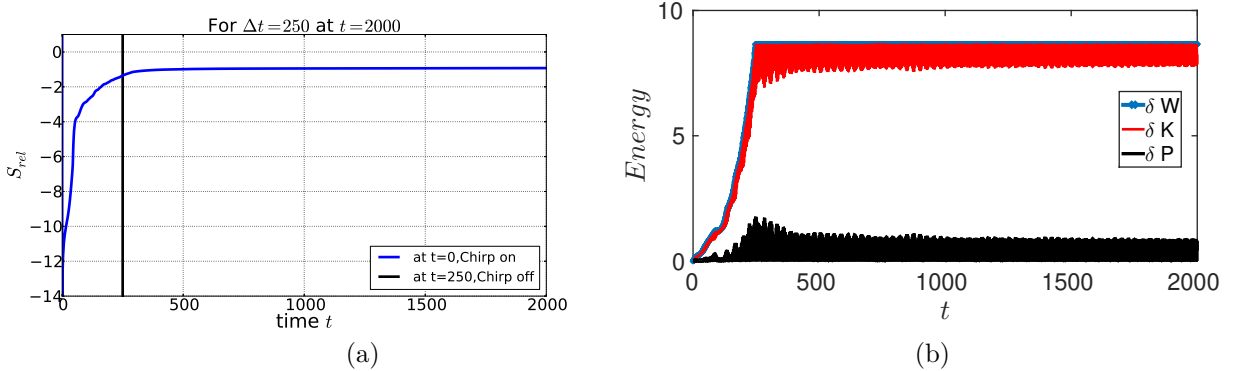


Figure 4.5: Plots of relative entropy  $S_{rel}$  and energy with time. The vertical lines represent times at which drive is turned on and turned off.

slowly down-chirped frequency creates a giant flat region in velocity distribution function indicating the increased amount of both trapped and surrounding untrapped particle population. In phase space, it can be seen as a giant phase space vortices with multiple

extrema squashed between ergodic regions of separatrices.

Now that I have recollected the results for  $q = 1$  distribution leading to multiple extrema PSVs, I wish to study the long-time fate of similar downward chirp on  $q \neq 1$  distributions. For this purpose, two sets of different  $q$  values have been taken to perform the comprehensive study.

### 4.3.2 Case $q < 1$

As shown in Fig. (2.1), for  $q < 1$  case, the initial distribution function exhibits a lower peak and a longer tail as compared to Maxwellian. For non-Maxwellian  $q$ -distributed plasmas, Lima *et al*[56], derived analytic formulas for the undamped a generalized Langmuir dispersion relation,

$$\omega^2 = 1 + 3k^2 \left( \frac{2}{3q - 1} \right) \quad (4.10)$$

which depends on the non-extensivity index  $q$ . Here, it is worth noting that in the limit  $q \rightarrow 1$ , the dispersion relation based on the Maxwellian distribution is recovered [102].

The following parameters are used. Runs are presented for  $0.85 \leq q < 1$  varied in steps of 0.05 and I choose  $v_{max} = 12.5$ ,  $N_v = 8000$  and  $N_x = 512$  by keeping rest of the initial conditions same as case [2.3.1]. Simulations have been performed to see the evolution of PSV's for different  $q$  values. As one can observe from the Eq. (2.10), for any  $q$ -distribution taken in this set, the phase velocity  $v_\phi = \omega/k$  lies well within the range, far "inside" from  $v_{max}$ . In Fig. (2.6), the change in giant flat region in spatially averaged distribution can be seen easily. At  $q = 0.95$ , the chirp seems to be more effective in creating two large phase space vortices well separated by separatrix [See Fig. 2.7(a) and 2.7(b)]. But as I go down in  $q$  values, this second structure at higher phase velocity vanishes and remains only a single large structure with peaked spikes and holes within it. With the same initial conditions as for  $q = 1$ , the following chirp ranges have been used for different  $q$  values:-

Table 4.1: Chirp ranges for  $q \leq 1$ .

$q$	$C_q$	$\omega_{high}$	$\omega_{low}$
0.85	0.3760	1	0.5
0.90	0.3838	1	0.5
0.95	0.3914	1	0.5
1.00	0.3989	1	0.5

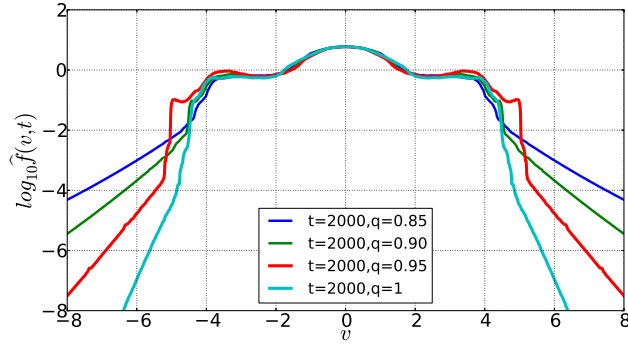


Figure 4.6: Plot of evolution of spatially averaged velocity distribution  $\hat{f}(v)$ , when external downward chirp is given from the start for  $\Delta t = 250$ , at  $t = 2000$  comparing cases with  $0.85 \leq q \leq 1$ .

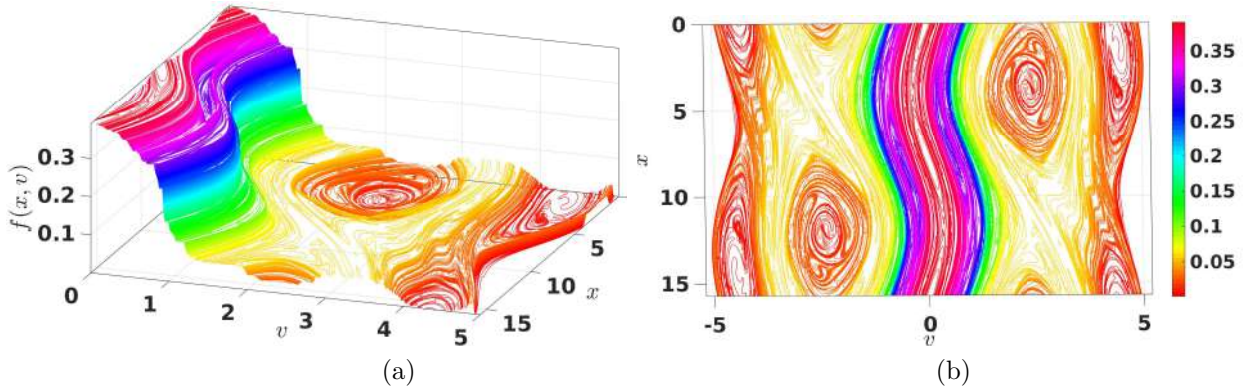


Figure 4.7: Plot of  $f(x, v, t)$  at  $t=2000$  when external downward chirp is applied from the start for a period  $\Delta t = 250$  in the range  $[0 \leq v \leq 5.1]$  for  $q = 0.95$ . (a) Zoomed plot of  $f(x, v, t)$  at time  $t = 2000$ . (b) Cross-section of  $f(x, v)$  at time  $t = 2000$ .

Now, for this case, entropy  $S(t)$  is defined as[47]

$$S_q(t) = - \int_0^L \int_{-v_{max}}^{+v_{max}} f(x, v, t) \left( \frac{1 - f(x, v, t)^{q-1}}{q-1} \right) dv dx \quad (4.11)$$

which reduces to Eq.(2.9) for the limit  $q = 1$ . As can be seen from Fig. (2.8), because of the numerical scheme, entropy does increase with time and then saturates. Also, one can notice that with increasing  $q$  values, relative entropy seems to grow and then stabilize after turning off the chirp. I extend the simulation till  $t = 2000$  in order to confirm the formation

of steady state solution.

Furthermore, in terms of different chirp rates, the simulation with  $q = 0.95$ , has been

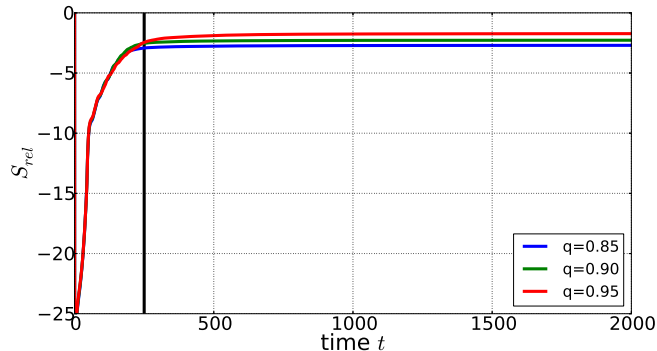


Figure 4.8: Plot of relative entropy  $S_{rel}$  with time when external downward chirp is given from the start for  $\Delta t = 250$  comparing cases with  $0.85 \leq q \leq 0.95$ . The vertical line represents time  $t$  at which chirp is turned off.

studied for  $\Delta t = 50, 150, 250$ . Similar to the previous study of Maxwellian plasma[21], as the chirp becomes slower, the amount of trapped and surrounding untrapped particles increases nearly linearly. This creates a a giant PSV at first and as the chirp rate decreases, a second coherent structure forms at higher phase velocity [as it is shown in Fig. 2.7(a)].

### 4.3.3 Case $q > 1$

It is clear from the velocity distribution function Eq.(2.7) that for  $q > 1$ , the distribution exhibits higher peak and a shorter tail as compared to Maxwellian and a velocity cutoff at  $v_{cutoff} = \sqrt{2/(q-1)}$ , beyond which the function becomes unphysical. Also, for  $q > 1.2$ , the phase velocity  $v_\phi > v_{cutoff}$ , therefore I do not consider cases for  $q \geq 1.2$ .

Again, similar to case  $q < 1$ , simulations are performed for  $1 < q \leq 1.10$  varied in steps of 0.025 and I choose  $v_{max} = v_{cutoff}$  by keeping the grid size and rest of the initial conditions except chirp range. Now, in this case, the periodic boundary conditions (PBC) on the velocity domain may affect the simulation if the resonant region is close to the boundaries. Therefore, only those cases have been considered for which the resonant region and chirp range are sufficiently far away from the boundaries. Hence, to accommodate both chirp range and  $v_{max}$ , cases with  $q = 1.05, 1.075, 1.10$  have been considered. With the same

CHAPTER 4. DRIVEN PHASE SPACE VORTICES IN PLASMAS WITH  
NONEXTENSIVE VELOCITY DISTRIBUTION

---

initial conditions as for  $q = 1$ , the following chirp ranges have been used for different  $q$  values:-

In Fig.(2.9), a semi-log plot for the velocity distribution  $\hat{f}(v)$  shows the difference in

Table 4.2: Chirp ranges for  $q \geq 1$ .

$q$	$C_q$	$\omega_{high}$	$\omega_{low}$
1.000	0.3989	1	0.5
1.050	0.4064	1	0.5
1.075	0.4100	0.9	0.4
1.100	0.4137	0.8	0.4

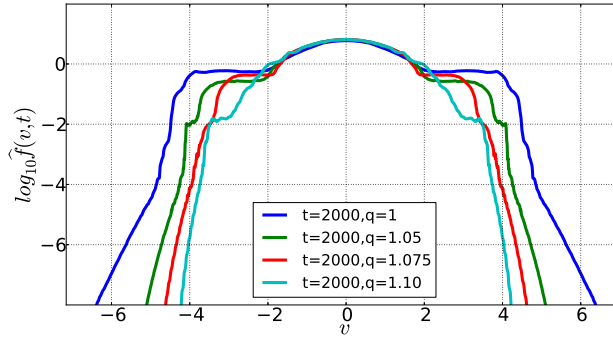


Figure 4.9: Plot of evolution of spatially averaged velocity distribution  $\hat{f}(v)$ , when external downward chirp is given from the start for  $\Delta t = 250$ , at  $t = 2000$  comparing cases with  $1 \leq q \leq 1.10$ .

behavior of resonant flattening for different  $q$  cases. Because of the change in chirp range and with increasing  $q$  values, the particle trapping decreases. As the  $q$  values increases, this chirp affects the modes present at lower velocities more.

For the cases  $1.05 \leq q \leq 1.10$ , the relative entropy curves are plotted in Fig. (2.10). Similar to the previous cases, entropy increases due to the measure of finite gridsize effects in simulation and then it saturates after turning off the chirp. In terms of nonextensivity parameter, the saturation value of relative entropy decreases with increasing value of  $q$ .

The phase space portrait of the system for  $q = 1.05$  at the end of the simulation is shown in Fig.2.11(a) and 2.11(b). Similar to the previous results, one can see the particle trapped in a large PSV which contains peaked spikes and holes embedded in it along with a small “shark”-like structure.

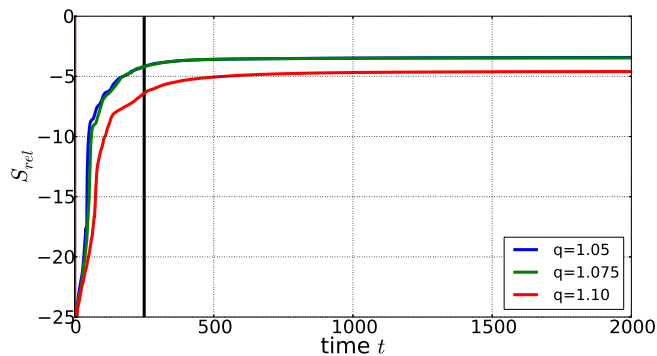


Figure 4.10: Plot of relative entropy  $S_{rel}$  with time when external downward chirp is given from the start for  $\Delta t = 250$  comparing cases with  $1 \leq q \leq 1.10$ . The vertical line represents time  $t$  at which chirp is turned off.

However, for higher  $q$ -values, one can increase the value of  $k$  so as to make the value of  $v_\phi = \omega/k$  lie within the bulk of the distribution function. For this purpose, I perturb with a higher value of  $k = 0.7$ , initialized with  $q = 1.15$ , by keeping rest of the conditions same as in  $q = 1$  case. For  $k = 0.7$ , phase velocity  $v_\phi \sim 1.6854$  and  $v_{cutoff} \sim 3.6515$ . On sweeping downwards, I have found the phase space vortices and a flattened region in velocity distribution which is smaller in comparison to previous cases with same initial conditions and  $k = 0.4$ . Thus trapping decreases with increase in  $k$  values and chirp dynamics becomes less effective in terms of  $q$ -values for higher values of  $k$  in this case.

### 4.3.4 Transient Honeycomb Structures

The above numerical experiment has also been used to analyze the response of the plasma to the downward chirp in the smaller frequency regime and to study the process of formation and growth of the holes in the distribution function. It has been found that this downward chirp in smaller frequency regime leads to formation of multiple phase space vortices, all appearing at different regions of phase space, which gives a “honeycomb”-like transient structure of the distribution function. Here, I report the results of the excitation of the plasma with a drive amplitude of  $E_0 = 0.025$ , with frequency swept from  $\omega_{high} = 0.8$  to  $\omega_{low} = 0.4$  with a sweep rate of  $\alpha = -16 \times 10^{-3}$  for different  $q$  values, namely  $q = 0.90, 1, 1.10$ .

As the  $\omega(t)$  of the drive chirps down from  $\omega_{high}$  to  $\omega_{low}$  with a single mode number, the

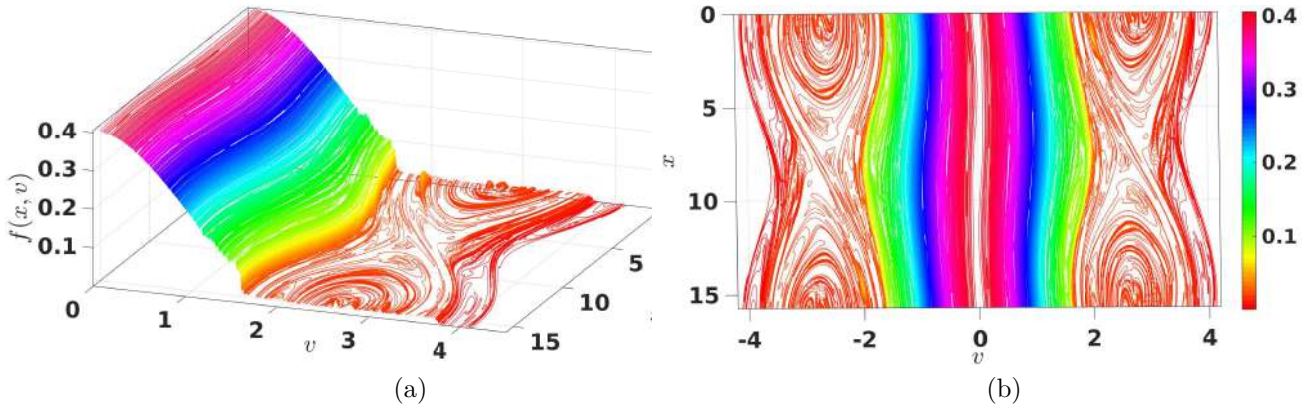


Figure 4.11: Plot of  $f(x, v, t)$  at  $t=2000$  when external downward chirp is applied from the start for a period  $\Delta t = 250$  in the range  $[0 \leq v \leq 4.1]$  for  $q = 1.05$ . (a) Zoomed plot of  $f(x, v, t)$  at time  $t = 2000$ . (b) Cross-section of  $f(x, v)$  at time  $t = 2000$ .

entire sub-harmonic region of phase space is seen to be driven strongly which results in an interacting, finite amplitude phase-space structures during the drive phase. The phase space portrait of the plasma as shown in Fig. 2.12 provides a convincing visualization of the effect of the downward chirp on the process of formation and development of the multiple PSV in the subharmonic region. In the first part of the driving process, only the large density fluctuations are visible but at later times, the smaller PSV become more prominent. The growth of the density fluctuations is arrested when the drive is switched off but the phase space structures created by the drive persists till the end of the simulation. These excitations at various phase velocities gives the distribution a “honeycomb” like appearance. These transient multi-extrema phase structures in sub-harmonic region or “honeycomb-like structures” thus created are seen to continuously interact, long after the linear drive is switched off, with smaller structures slowly “merging”, as it can be expected in a 2D inverse cascade process leading to a quasi-steady phase space structures.

In the past,[37, 38] with chirped frequency drive, a study of axial 1D dynamics of a bounded system (Malmberg-Penning trap) confining pure electrons has been reported. In this work, the external drive with high spatial harmonic content ( $k$ - spectrum) is used to search and lock the axially bouncing electrons. These phase-locked electrons at higher phase velocity are chirp-dragged (“bucket”) to lower velocity region of the distribution function

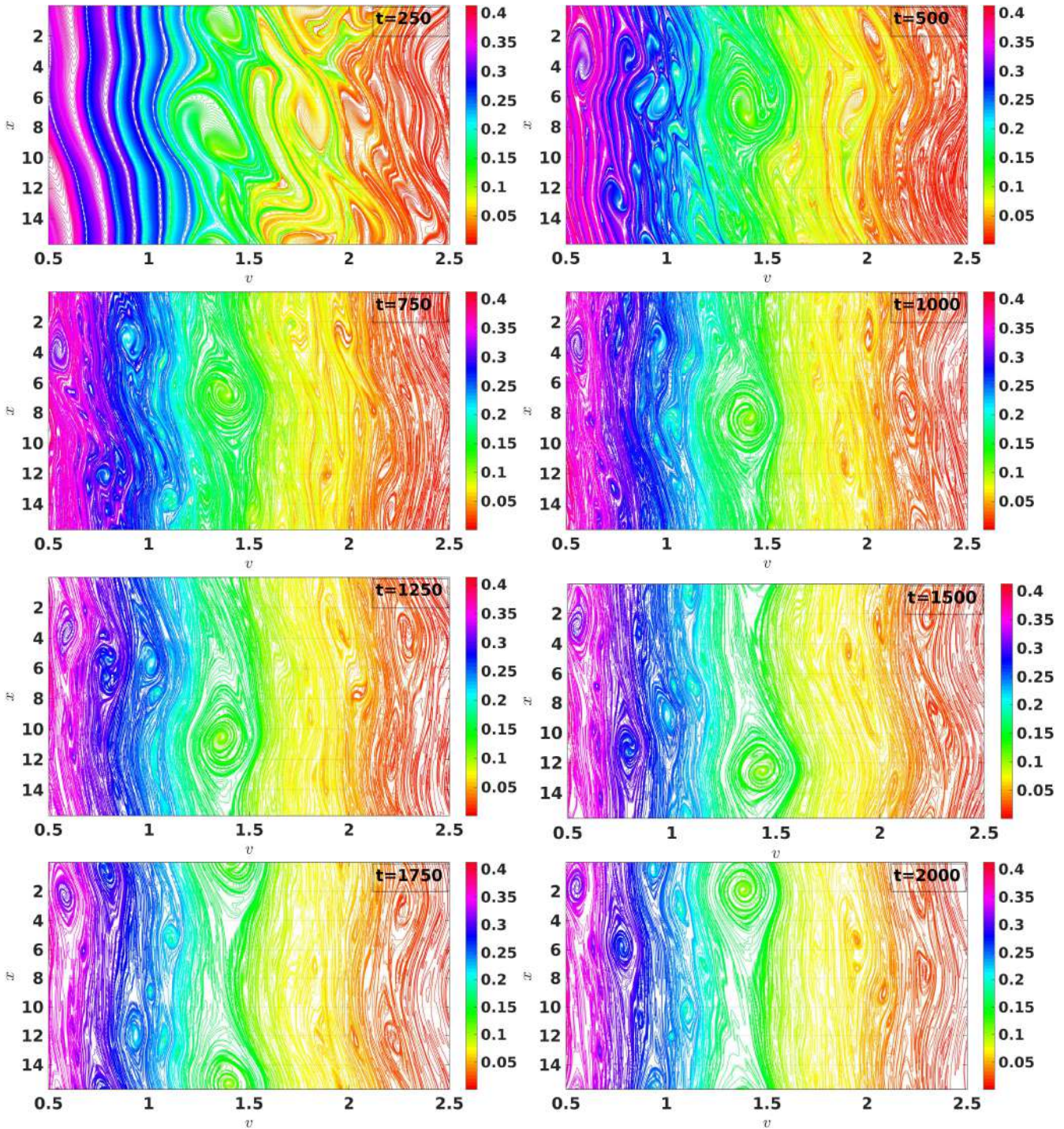


Figure 4.12: Phase-space portrait of the electron distribution  $f(x, v)$  for  $q = 1.10$ , starting from  $t = 250$  (when the drive is turned off) to  $t = 2000$ . These portraits show dynamic activity in subharmonic region at different instances after the drive is switched off. These kind of interesting features are seen for all the values of  $q$  studied.

resulting in multiple non-overlapping phase space holes or “honey-comb-like” structures in phase space. However, in this work, these structures are reported to overlap or interact only at large amplitude of chirp drive.

In the present chapter, I have investigated the effect of chirped frequency drive with infinitesimal amplitude on an unbounded plasma with single  $k$ -mode for both Maxwellian and non-Maxwellian plasmas. In Fig. 2.13, I have shown the effect of the downward chirp on the process of the excitation of multiple PSV and the formation of “honeycomb” like structures for different  $q$  values. As one can observe, the number of these multiple PSV is more for  $q > 1$  than the cases with  $q = 1$  and  $q < 1$ .

## 4.4 Discussion

Let us compare the results obtained from the runs corresponding to  $0.85 \leq q \leq 1.10$ , for which phase space vortices are formed on applying a low amplitude external downward chirp. In order to do so, the response of the system in terms of relative kinetic energy ( $\delta K$ ) and relative potential energy ( $\delta P$ ) for different entropy index  $q$  has been plotted in Fig. 2.14(a). As one can observe, the overall energy (i.e.  $\delta K + \delta P$ ) of particles increases with  $q$  values for  $q \leq 1$  and then it decreases for  $q > 1$ . The maximum trapping is reflected from the potential well depth which is highest for Maxwellian plasma i.e.  $q = 1$ . As the giant flattening in velocity distribution indicates the increment in both trapped and surrounding untrapped particle population. Here Fig. 2.14(a) shows the effect of chirp on the kinetic energy of untrapped regions which is maximum for  $q = 0.95$  case explaining the large separatrix between the two giant PSVs in Fig. (2.7).

Similarly, the response of the system in terms of maximum potential well depth and maximum excess density fraction, defined as:

$$\delta n(x, t)/n_0 = \left( \frac{\int f(x, v, t) dv - \int f_0(v) dv}{\int f_0(v) dv} \right) \quad (4.12)$$

which was obtained after switching off the drive, as a function of entropy-index  $q$  has been shown in Fig. 2.14(b). Again, it can be clearly seen that  $\phi_{max}$  is maximum for  $q = 1$  case

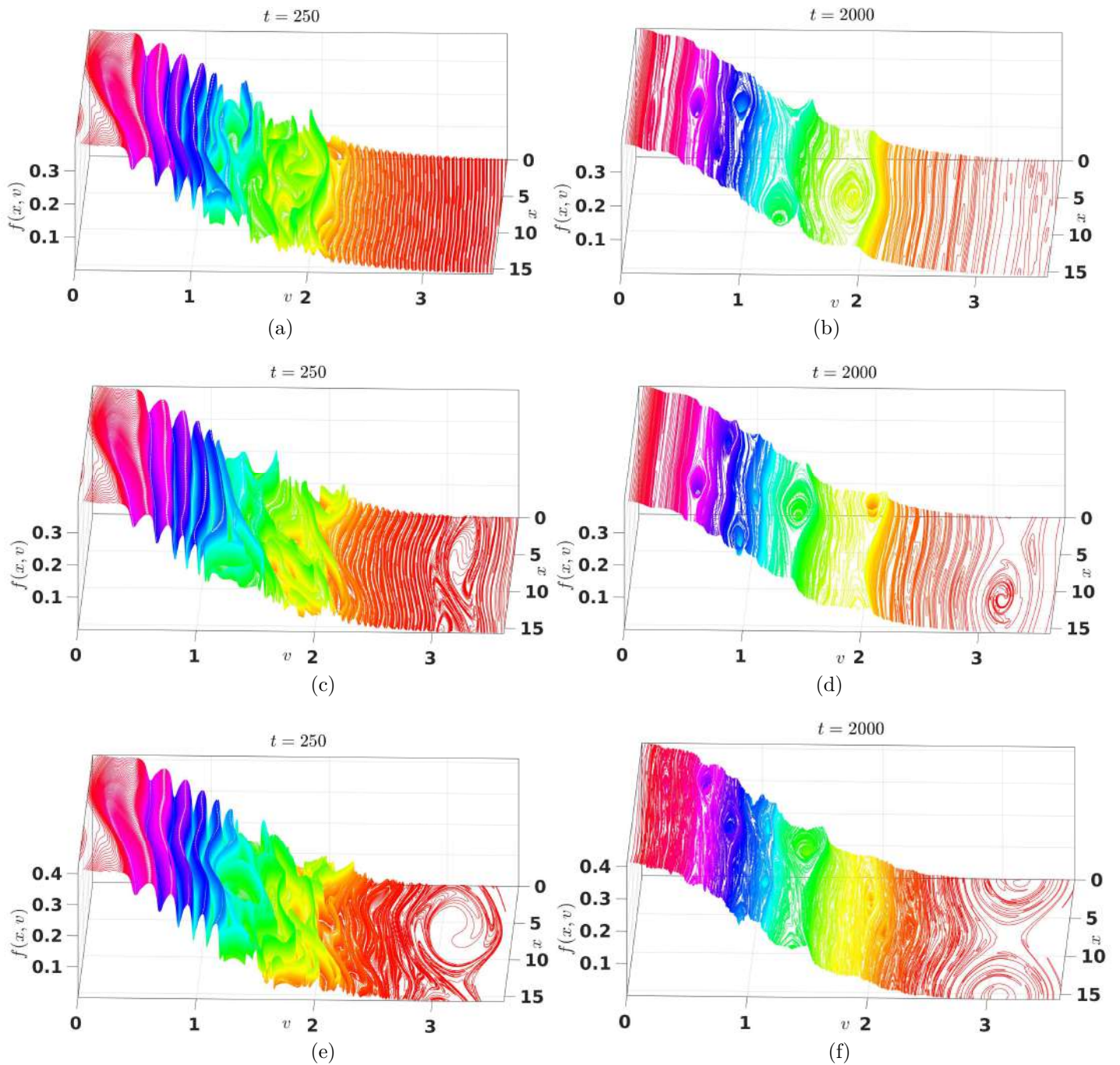


Figure 4.13: Plot of  $f(x, v)$  for chirp interval  $\Delta t = 250$  when external downward chirp is given from  $\omega_{high} = 0.8$  to  $\omega_{low} = 0.4$  for  $q = 0.90, 1, 1.10$  respectively. [(a), (b)] Plots of  $f(x, v, t)$  for  $q = 0.90$  at time  $t = 250$  and  $t = 2000$  respectively. [(c), (d)] Plots of  $f(x, v, t)$  for  $q = 1$  at time  $t = 250$  and  $t = 2000$  respectively. [(e), (f)] Plots of  $f(x, v, t)$  for  $q = 1.10$  at time  $t = 250$  and  $t = 2000$  respectively.

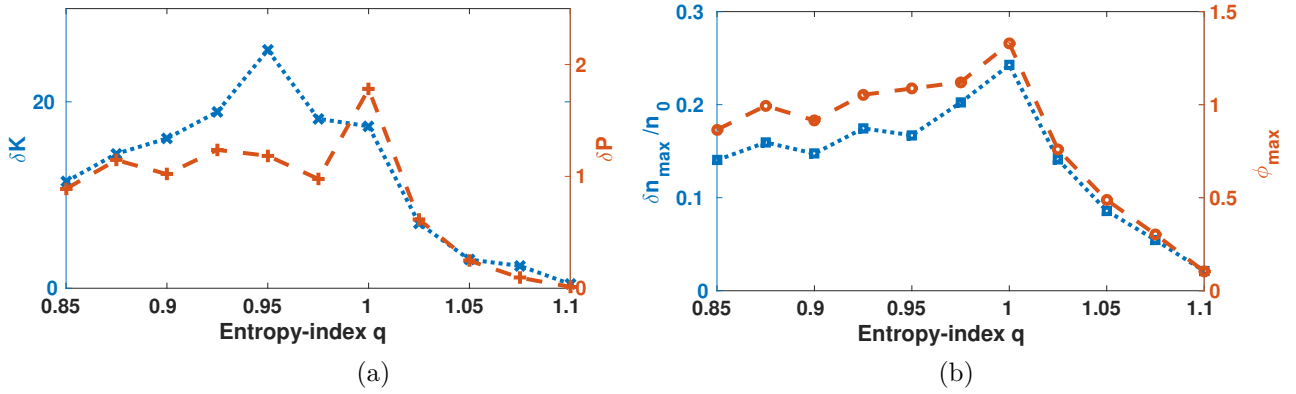


Figure 4.14: (a) Plot of  $\delta K$  and  $\delta P$  at  $t=2000$  when external downward chirp is applied from the start for a period  $\Delta t = 250$  in the range  $[0.85 \leq q \leq 1.10]$ . (b) Plot of  $\delta n_{max}/n_0$  and  $\phi_{max}$  of the saturated states after turning off the drive at  $t = 250$  for  $q$  values in range  $[0.85 \leq q \leq 1.10]$ .

which shows the maximum trapping for Maxwellian plasma and the excess density fraction is also maximum for  $q = 1$ .

## 4.5 Summary and Conclusions

For a non Maxwellian plasma described by  $q$ -distribution, I have studied numerically a simple and efficient way to obtain phase space vortices in a 1D unbounded Vlasov plasma, modeled using periodic boundary conditions. I have numerically addressed the nonlinear evolution of Maxwellian and  $q$ -nonextensive Maxwellian plasma when perturbed with an external drive, of very low amplitude, which is slowly chirped downwards. From our numerical results, I conclude that the chirp dynamics and trapping phenomenon is strongly affected by the deviations from the Maxwellian distribution. In other words, the trapping efficiency is related to the region around wave phase velocity or the velocity derivative of the initial distribution function near the resonance region.

It is found that, for values of the entropy-index less than unity, trapping decreases with decrease in  $q$  values. On the contrary, for large value of  $q$ , trapping decreases with increase in  $q$  values. This implies the trapping efficiency for a given set of parameters is maximum for Maxwellian plasma. As  $q$  increases beyond unity, the phase velocity

## CHAPTER 4. DRIVEN PHASE SPACE VORTICES IN PLASMAS WITH NONEXTENSIVE VELOCITY DISTRIBUTION

---

comes closer to the velocity cutoff for the distribution which makes an upper limit for  $q$  below which I find PSVs. For increasing values of  $k$ , I observe that trapping fraction reduces.

We have shown, using high-resolution Vlasov-Poisson solver for long-times up to  $t = 2000\omega_p^{-1}$  that the formation of phase space vortices seem to depend on the nonextensive parameter  $q$  and chirp rate. Study of excitation of giant phase space vortices which contains peaked spikes and holes embedded in it along with a “shark”-like structure and excitation of multiple PSV forming a “honeycomb”-like transient feature is novel.

Moreover, In these Chapter and the earlier Chapter 3, ions have been assumed to be immobile. However, ion motion may significantly change the evolution of high and low frequency motions which in turn may affect the trapping and formation of PSVs. In the next Chapter, I will present several interesting features of ion modes and driven electron and ion phase space structures, in Maxwellian plasma, analyzed by means of kinetic Eulerian simulations, composed of (a) kinetic warm ions and Boltzmann electrons and (b) kinetic warm ions and Kinetic electrons . The details of which will be presented.

---

## Formation and Dynamics of Electrostatic Phase space Vortices: Kinetic Ions

*In this Chapter, the role of ions on the phase space dynamics has been studied using two different models:- (1) Boltzmann electrons and kinetic ions using Vlasov-Yukawa (VY) model, and (2) Kinetic Ions and Kinetic Electrons (KIKE) model. In the previous Chapters, electrostatic waves have been studied in the background of kinetic electrons and immobile ions resulting in a “Thumb curve” dispersion [for Langmuir (LAN) and Electron Acoustic (EAW) waves]. In this Chapter, the role and effect of ions on the phase space dynamics, has been studied in two parts:-*

*(1) In the first part, the study electrostatic waves in ion scale with Boltzmann electrons treating ions as kinetic species has been attempted with a newly developed Vlasov-Yukawa (VY) solver. This model results in a “Teardrop” dispersion curve [for Ion Acoustic (IA) and Ion Bulk (IBk) waves]. Using 1D1V VY solver, Landau damping and electrostatic waves at ion scales (IA and IBk waves) have been studied. Also, formation and dynamics of chirp driven phase space vortices at ion scales have been studied for different temperature*

*ratios.*

*(2) In the second part, the electron scale physics and ion scale physics have been studied by including both ion and electron scale dynamics self consistently and simultaneously in a model using symmetric framework. With this model, it is shown that both high frequency and low frequency solutions can be obtained simultaneously which consists of a high frequency branch (LAN/IA) and a low frequency branch(EAW/IBk). The numerical results obtained show that both electron and ion waves can indeed be excited simultaneously in phase space without any approximation in length scale or time scale. In appropriate limits, it is shown that the “Thumb” and “Teardrop” curves are recovered from a general symmetric dispersion relation [P. Trivedi and R. Ganesh, Physics of Plasmas 25, 112102 (2018)].*

## 5.1 Introduction

As discussed in the earlier Chapters, the study of phase space dynamics of a collisionless plasma is currently a subject of extensive efforts both for the case of interplanetary environments and for laboratory plasma systems. Several investigations aim to understand the features of the dynamics at ion scales and electron scales in space plasmas by analyzing both spacecraft data [14, 15, 16] as well as numerical results from kinetic (or phase space simulations) [17, 18, 19, 20, 21, 22]. For example, in space craft data, one usually deals with modes, covering practically the entire frequency range from electron to ion response times. For example, quasiregular packets of Langmuir waves (LAN) are frequently observed in the solar wind and magnetospheric plasmas [24, 25, 26]. The high frequency regions of the energy spectra, obtained by analyzing solar-wind measurements from the Helios spacecraft are dominated by longitudinal electrostatic modes, identified as ion-acoustic (IA) waves [27, 28, 29]. Recent observations and studies [30, 44, 31, 32, 33, 34] point out that besides these LAN and IA branches, in agreement with spacecraft and solar-wind observations, two other novel branches of electrostatic waves exists. These waves have

been dubbed as electron acoustic waves (EAW) and ion-bulk (IBk) waves, as their phase velocities are nearly constant and are comparable to the electron thermal velocity ( $v_{the}$ ) and ion thermal ( $v_{thi}$ ) velocity, respectively. These waves have been studied either in the background of immobile ions resulting in a “*thumb curve*” dispersion (for LAN and EAW waves) with kinetic electrons or in the frame of Boltzmann electrons resulting in a “*teardrop*” curve (for IA and IBk waves)[17, 19, 34] with kinetic ions. Thus, the electron scale physics and ion scale physics have been separately studied and applied whereas more consistent physical picture would emerge only when both ion and electron scale dynamics are included self consistently and simultaneously in a model or symmetric framework where both high frequency (“*thumb curve*”) and low frequency (“*teardrop*”) branches can be obtained simultaneously. From this symmetrical framework, both electron scale dispersion (“*thumb curve*”-LAN and EAW) and ion scale dispersion (“*teardrop*”-IA and IBk) can be obtained in appropriate limits of where each of them again consists of a high frequency branch (LAN/IA) and a low frequency branch(EAW/IBk).

In the present work, an attempt has been made by means of numerical simulations, to study the role and effect of ions on the phase space dynamics in two parts:-

In the first part, considering kinetic ions and Boltzmann electrons, wherein the Vlasov equations are integrated for ion species with no approximations in length scale or time scales in terms of ion parameters. This is performed by solving Vlasov-Yukawa (VY) equations which consists of the Vlasov equation coupled with the a short-range correction of the Poisson equation (Yukawa equation or screened Poisson equation). The weakly driven Vlasov-Yukawa (VY) equations has been solved which facilitates weak flattening of distribution function or weak trapping. The numerical results leads to a “Teardrop” curve for Ion Acoustic (IA) and Ion Bulk (IBk) waves. Using 1D1V Vlasov-Yukawa solver which treats kinetic ions and Boltzmann electrons, Landau damping of electrostatic waves at ion scales (IA and IBk waves) has been studied. Also, formation and dynamics of chirp driven phase space vortices at ion scales has been studied for different temperature ratios in this Thesis.

## CHAPTER 5. FORMATION AND DYNAMICS OF ELECTROSTATIC PHASE SPACE VORTICES: KINETIC IONS

---

In the second part, considering both kinetic electrons and kinetic ions on the same physics footing, the Vlasov equations are integrated for both electron and ion species without any approximations in length scale or time scales. First, the weakly driven fully nonlinear Vlasov-Poisson (VP) equations has been solved which facilitates weak flattening of distribution function or weak trapping. To identify the electrostatic modes (LAN, EAW, IA, IBk), the  $\omega_r$  is need to be calculated. The eigenvalue values thus obtained for various wavenumbers are compared with frequencies obtained from solving the linearized eigenvalue equations considering weak trapping which allows us to neglect the contribution from the imaginary part of the dielectric function. The numerical results obtained show that both electron and ion waves can be excited simultaneously in phase space. In appropriate limits, it is shown that the “thumb” and “teardrop” curves are different parts of a general symmetric dispersion relation and are recovered in appropriate limits of that dispersion relation.

Using a one dimensional (1D), two component Vlasov-Poisson system which treats both electrons and ions symmetrically in terms of kinetics, I report, perhaps for the first time, the the following major findings:- (i) continuous connectivity of electron (or “Thumb curve”)[17] and ion (or the “Teardrop curve”)[34] branches using a general symmetric dispersion relation. The hitherto separately studied “Thumb curve” and the “Teardrop curve” show a “symmetry” in the dispersion curve as each of them consists of a high frequency branch and a low frequency branch. The entire physical picture on the same scale is presented using a general symmetric dispersion curve which again consists of a high frequency part (“Thumb curve”-LAN, EAW) and a low frequency part(“Teardrop curve”-IA, IBk), (ii) all four branches (LAN, EAW, IA, IBk)[17, 19, 34] have been recovered both via obtaining a general symmetric dispersion relation from solving weakly driven fully nonlinear VP equations which facilitates weak trapping as well as by performing a numerical simulation where plasma is driven with an infinitesimal external electric field. (iii) for realistic mass ratios, simultaneous excitation of all the normal modes:-LAN, EAW, IA, IBk.

The rest of the Chapter is divided into two main sections: (1) In the first Section [Sec.??],

the formation and dynamics of electrostatic waves at ion scale has been studied in the background of Boltzmann electrons and kinetic ions using *Vlasov-Yukawa* (VY) model, and (2) In the second Section [Sec.??], considering both kinetic electrons and kinetic ions on the same physics footing, the Vlasov equations are integrated for both electron and ion species without any approximations in length scale or time scales:- *Kinetic Ions & Kinetic electrons* (KIKE) model. Each of these sections is organized as follows: the numerical scheme of VY model is described in Subsec. ?? and the numerical scheme of KIKE model is described in Subsec.?.?. Simulations using VY model with different cases have been discussed Subsec.?? and simulations using KIKE model with different cases have been discussed Subsec.?.?. In Sec.2.5 summary and conclusions have been presented.

## 5.2 Vlasov-Yukawa Plasmas (VY):- Kinetic Ions and Boltzmann Electrons

In this Section, the numerical simulations are performed considering kinetic ions and Boltzmann electrons, wherein the Vlasov equations are integrated for ions and electron contribution comes only through the temperature ratio of ions to electrons.

### 5.2.1 Governing Equations & Wave Dispersion Relation for VY Plasmas

The self-consistent Vlasov-Yukawa system(VY) which consists of the Vlasov equation coupled with the Yukawa equation. The Yukawa equation is obtained from the Poisson equation by making the assumption that the electrons are Boltzmann and sometimes called the screened Poisson equation. As described in Chapter 2, necessary modifications are made in the VPPM solver to treat kinetic warm ions and Boltzmann electrons, analyzed by means of kinetic Eulerian simulations. A numerical Vlasov-Yukawa (VY) solver which treats kinetic ions in the presence of Boltzmann electrons [ $n_e = n_0 \exp(e\phi/KT_e) = n_0(1 + e\phi/KT_e)$ ]

is given by,

$$\frac{\partial f}{\partial t} + v \frac{\partial f}{\partial x} + E_T \frac{\partial f}{\partial v} = 0, \quad (5.1)$$

$$\frac{\partial E_s}{\partial x} = -\frac{\partial^2 \phi}{\partial x^2} = n_i - n_e \quad (5.2)$$

Here,  $f$  is the ion distribution,  $n_i = \int f dv$ ,  $n_e = (1 + T_R \phi)$  is the normalized Boltzmann electron distribution,  $T_R = T_i/T_e$  is the ion to electron temperature ratio and  $E_T = E_s + E_{ext}$  is the total electric field, where  $E_s(x, t)$  is the self consistent electric field and  $E_{ext}$  is the external driver electric field defined as:

$$E_{ext} = E_0 \sin(kx \pm \omega t) \quad (5.3)$$

where  $E_0$  is the amplitude of external drive. Here,  $k$  represents the perturbation wave number in the simulation box and  $\omega$  represents the driver frequency. In this Vlasov-Yukawa model, the electron response is taken to be the standard Boltzmann response as  $n_e = n_0 \exp(e\phi/KT)$  which in terms of ion normalization becomes  $n_e = \exp(\phi T_R)$ . In this Chapter, all the parameters have been chosen such a way that  $\phi T_R \ll 1$  throughout the simulation period. Therefore, the relationship between the electron density and the electrostatic potential becomes linear  $n_e = (1 + \phi T_R)$ . For the parameters chosen, numerically solving the Poisson equation with  $\exp(\phi T_R)$  was thus not necessary and hence, was not used. Therefore, Poisson eqn.?? becomes

$$-\frac{\partial^2 \phi}{\partial x^2} + \frac{T_i}{T_e} \phi = \int f dv - 1. \quad (5.4)$$

Here, all the quantities are normalized in terms of ion parameters. In this model, only ion equations are solved using time-splitting method and effect of Boltzmann electrons considered in the screened Poisson equation. The simulation domain in phase space  $D(x, v) = [0, L_{max}] \times [-v_{max}^i, v_{max}^i]$ ,  $L_{max} = 2\pi/k$  is the system size and  $v_{max}^i$  is chosen

sufficiently large so that velocity distribution functions approaches zero as  $|v^i|$  approaches  $v_{max}^i$ . In all these simulations, the mode with the largest wavelength that fits in the numerical domain is excited at  $t = 0$ , in order to prevent the sideband frequency generation in the system. The phase space is discretized with  $N_x = 1024$  grid points in the spatial domain and  $N_v = 4000$  in velocity domain. Using the above normalizations, the Fourier

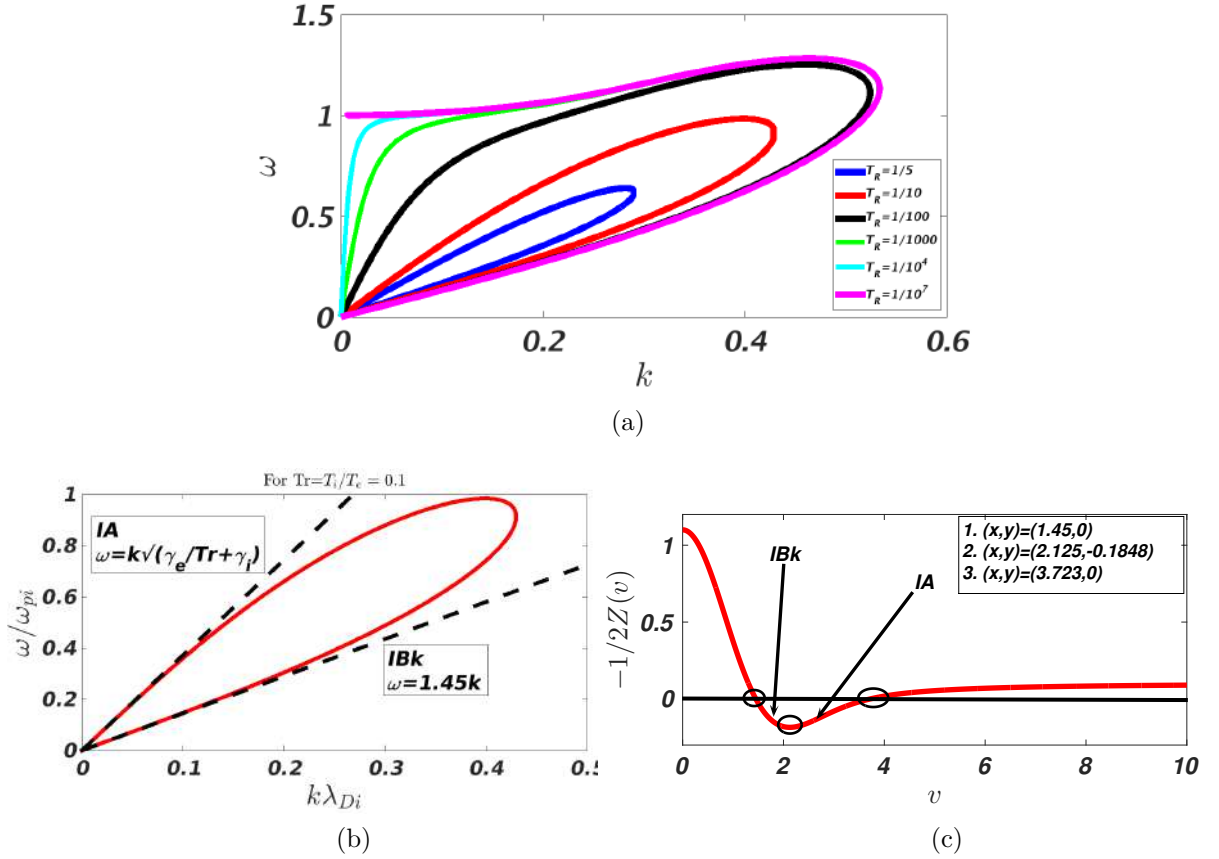


Figure 5.1: Dispersion curves or “Teardrop” curves for the electrostatic waves (IA, IBk) in  $k - \omega$  plane, obtained by assuming zero damping as a function of  $T_R$  [Fig. (a)], (ii) Teardrop curve for  $T_R = 0.1$  [Fig. (b)]. Also, the gradient of the real part of the complex plasma dispersion function  $-\frac{1}{2}Z'(v)$  is plotted for real arguments in Fig.(c)  $T_R = 0.1$ .

transformation of linearized form of Eqs. (??)-(??) leads to the dispersion relation[16]:-

$$1 + \sum_j K_j(\mathbf{k}, \omega) = 0 \quad (5.5)$$

where  $K_j(\mathbf{k}, \omega) = -k_j^2/2k^2 Z'(\xi_j)$  is the susceptibility of the  $j^{th}(= i, e)$  species,  $\xi_j = \omega/\sqrt{2}kv_j$  and  $Z_j(\xi_j)$  represents the real part of the complex plasma dispersion func-

tion for real arguments[44]. Here, we consider the initial distribution to be Maxwellian,  $f_0(v) = \exp(-v^2/2)/\sqrt{2\pi}$ . By assuming a weak flattening (or trapped region) of vanishing velocity width i.e.  $(\partial f/\partial v)|_{v_\phi} \simeq 0$  (which allows us to neglect the contribution from the imaginary part of the dielectric function), the solution to the real part of the wave frequency  $\omega$  as a function of the wave number  $k$ , obtained numerically from Eq.(??) is shown in Fig.(??). Typically in the  $k - \omega$  diagram, at low frequencies (Boltzmann electrons and kinetic ions), one obtains the “teardrop” curve that represents Ion Acoustic (IA) (upper branch of teardrop) and IBk (lower branch of teardrop)[17]. At values of the wave number for which the effects of charge separation are no longer negligible, both ion branches (IA and IBk) coalesce [see fig.??(a)]. As the ion to electron temperature ratio  $T_R$  decreases, the “teardrop” becomes a “thumbcurve” for ions. Finally, when  $T_R > 0.3$  the VY solution disappear.

In the bottom plot Fig.??(b), the same “teardrop” dispersion is plotted for  $T_R = 0.1$ .

In Eqn.(??), the term  $-\frac{1}{2}Z'(v)$  can be interpreted as a gradient of the real part of the complex plasma dispersion function for real arguments. A plot of the function  $-\frac{1}{2}Z'(v)$  for Kinetic ions and Boltzmann electrons for  $T_R = 0.1$  is displayed in Figs.??(c)), where it divides the phase velocity regions and reveals different branches of the dispersion relation. In the limit of Boltzmann electrons, the function  $-\frac{1}{2}Z'(v)$  represents ion contribution, where it has two zero transitions (at  $v = 1.45$  and at  $v = 3.723$ ) and one minimum (at  $v = 2.125$ ) which results in two separated regions for the physical phase velocity:-(i)  $1.45 \leq v \leq 2.125$  (IBk), (ii)  $2.125 \leq v \leq 3.723$  (IA)). The function is positive for  $v < 1.45$  and  $v > 3.723$ .

## 5.2.2 Simulation I

In this Section, we systematically present the numerical results of the VY plasmas where kinetic ions in the background of Boltzmann electrons are considered. In order to study the low frequency (ion dominated) electrostatic waves, the numerical results are presented for

the following three cases:- where plasma is subjected to (i) an initial density perturbation i.e. Landau damping at ion scales, (ii) a constant frequency external drive which concerns the excitation of electrostatic modes at ion scales (IA and IBk) by applying a constant frequency external drive and (iii) a time dependent external drive or chirp at ion scales in the background of Boltzmann electrons.

### 5.2.2.1 Ion Landau Damping

In the following, to study the Landau damping at ion scales, the oscillations are excited by initializing a single Fourier mode  $k$  with the following initial ion distribution:

$$f_i(x, v_i, t = 0) = \frac{1}{\sqrt{2\pi}} [1 + \alpha \cos(kx)] \exp\left(-\frac{v_i^2}{2}\right) \quad (5.6)$$

where  $\alpha$  is the amplitude of initial ion density perturbation. Here, electron follows the normalized Boltzmann [ $n_e = (1 + T_R \phi)$ ] distribution and  $T_R = T_i/T_e$  is the ion to electron temperature ratio. In the following simulation case, numerical experiments have been performed for  $v_{max}^i = 8$  and different  $k$ ,  $\alpha$  and  $T_R$  values.

When the plasma is perturbed with an initial amplitude, it leads to formation of ion acoustic wave which is exponentially damped or Landau damped. The ion acoustic frequency is given by  $\omega_r = k \sqrt{\gamma_e/T_R + \gamma_i}$ , in ion normalization.

In Fig.??(a), comparison of time evolution of the electric field for various values of wavenumber  $k$  is shown which indicated that the Landau damping increases with increase in  $k$  and  $\omega_r$  also increases with increase in  $k$ , as expected [Fig.??(b)]. In Fig.(??), comparison of time evolution of the electric field for various values of initial amplitude of perturbation  $\alpha$  and  $T_R$  has been shown. The time evolution of electric field for various values of  $T_R$  indicates that the Landau damping increases with increase in  $T_R$ .

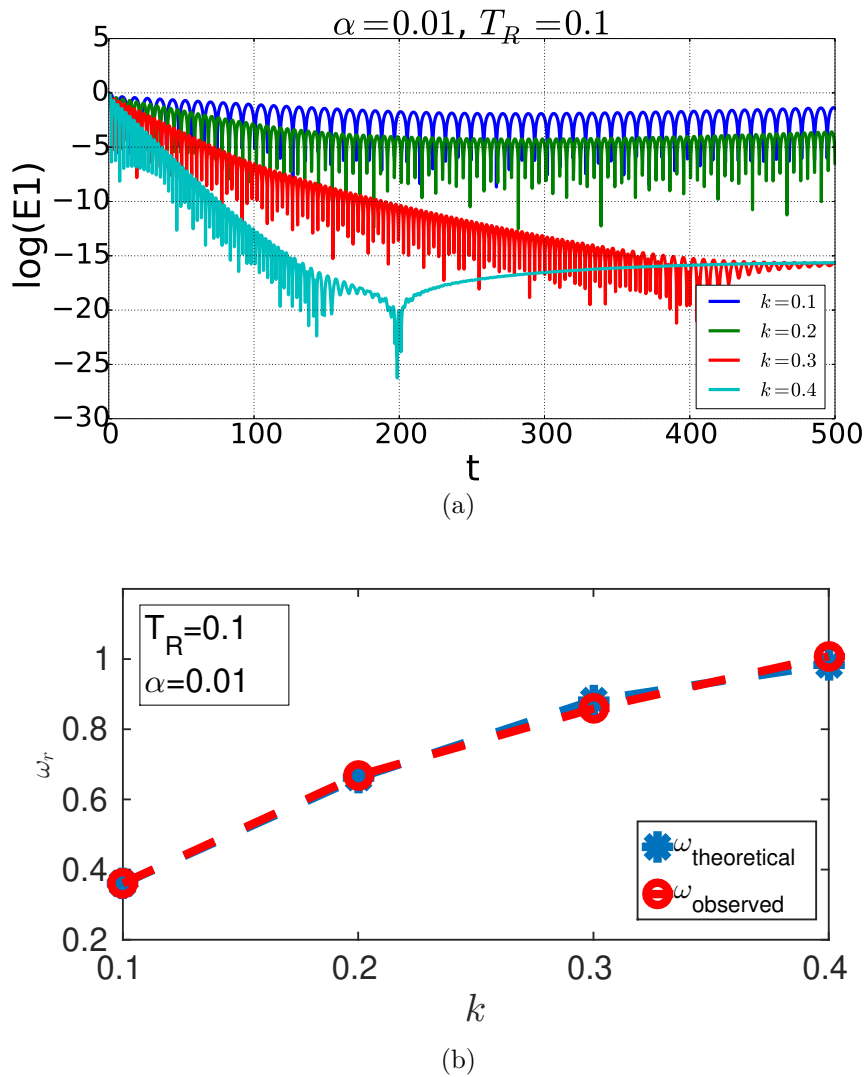


Figure 5.2: (a) Comparison of time evolution of the electric field for various values of wavenumber  $k$ , and (b) the corresponding  $\omega_r - k$  plot of theoretical and observed values for various values of wavenumber  $k$ .

### 5.2.2.2 Driven Ion Electrostatic Modes :- Constant Frequency Drive

Within linear theory, the Ion Bulk (IBK) waves are heavily damped as their wave phase velocities is close to ion thermal velocity ( $v_{thi}$ ), respectively. However, this wave is also a nonlinear BGK mode where ions trapped in the wave troughs which makes the ion velocity distribution effectively flat at the wave phase velocity, and turns off Landau damping. Initially there is no trapped particle distribution exist. But if the plasma is driven externally, it can form trapping distribution dynamically as the wave evolves. For an external electric field  $E = E_0 \sin(kx - \omega t)$ , the trapping period to form the trapped

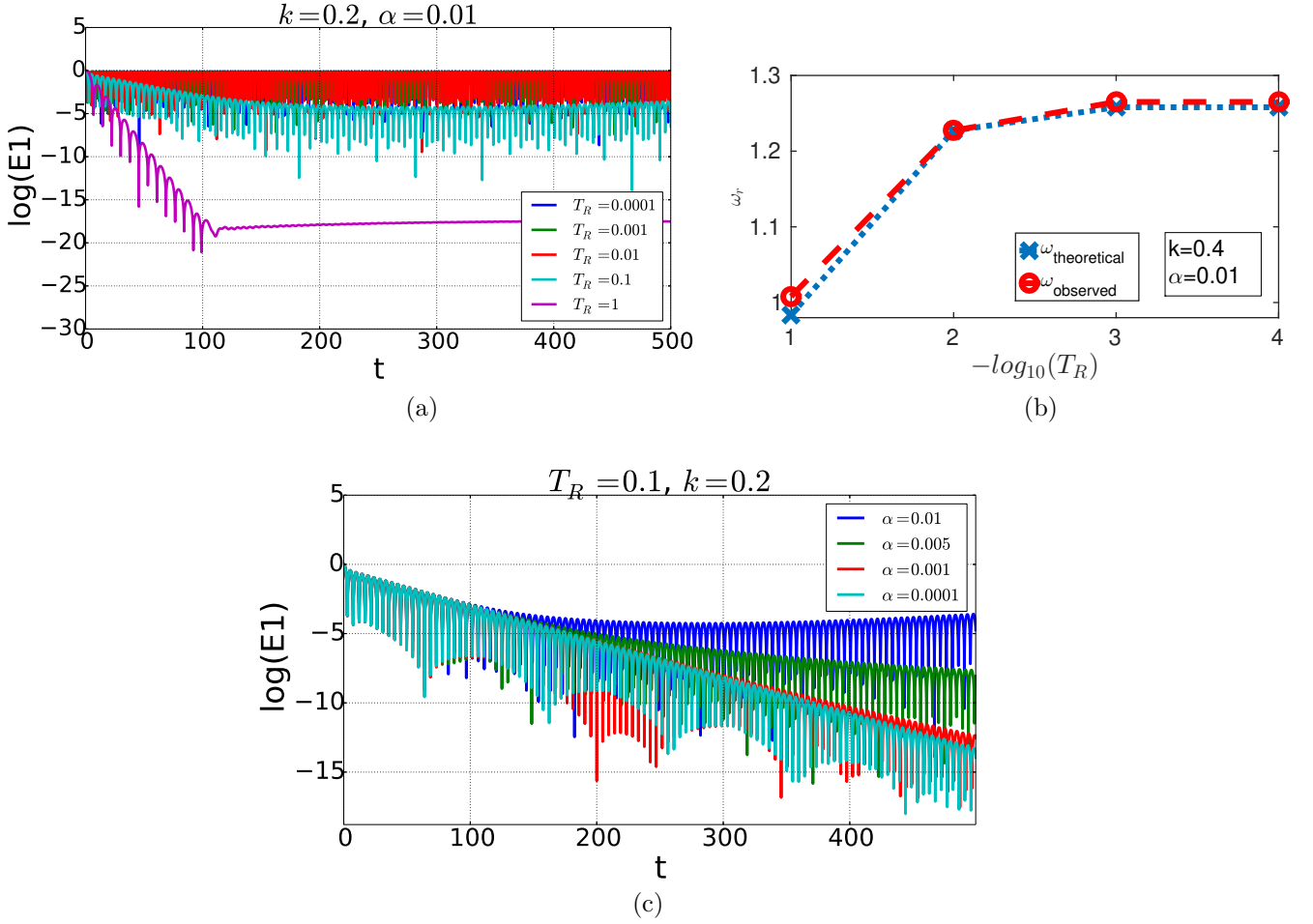


Figure 5.3: Comparison of time evolution of the electric field (a) for various values of  $T_R$ , (b) The corresponding  $\omega_r - k$  plot of theoretical and observed values for various values of  $T_R$  on log scale and (c) for various values of initial amplitude of perturbation  $\alpha$ .

particle distribution is approximately  $\tau = 2\pi / \sqrt{kE_0}$  (in this normalization). Thus, the IBks can be excited by a small amplitude driver if the driver is applied resonantly over few trapping periods. The driver continuously replenishes the energy removed by Landau damping. Therefore, the trapped particle distribution survives and the IBks are eventually produced.

In order to excite both electrostatic modes at ion scales (IA, IBk), the following numerical simulation is performed: at  $t = 0$ , ions are considered to be Maxwellian velocity distributions [ $f_i = (1/\sqrt{2\pi})\exp(-v_i^2/2)$ ] homogeneous density and electrons have a Boltzmann distribution. The external electric field applied to induce weak trapping has the form

## CHAPTER 5. FORMATION AND DYNAMICS OF ELECTROSTATIC PHASE SPACE VORTICES: KINETIC IONS

$E_{ext} = E_0 \sin(kx \pm \omega t)$ . The external driver electric field is applied directly to the ions in the Vlasov equation. The longest wavelength is driven that fits into the simulation box. The trapping time  $\tau_r$  for ions is  $\tau_r = 2\pi / \sqrt{kE_0}$ . Moreover, the external drive of amplitude  $E_0 = 0.025$  is switched on at  $t = 0$  for a period  $\Delta t$  [see Fig.??(a)], where  $\tau_r \leq \Delta t \leq 5\tau_r$  and then let the system to relax for atleast another few  $\omega_{pi}^{-1}$  by switching off the external drive. After the drive has been turned off, the plasma response is analyzed. the simulation has been performed for the following parameters:-  $k = 0.2$  ( $\tau_r = 88.85$ ), temperature ratio  $T_R = 0.1, 0.01, 10^{-7}$ ,  $v_{max} = 8$ ,  $\Delta t = 100$  [see Fig.??(b)]. I

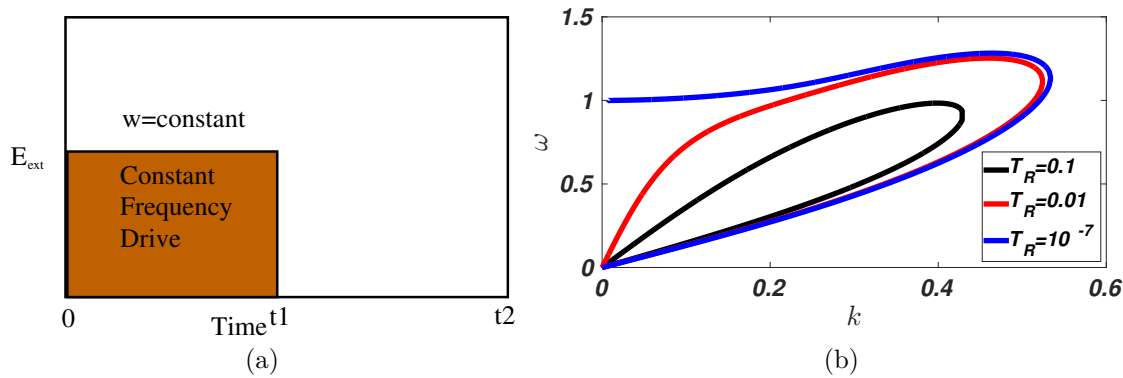


Figure 5.4: (a) A cartoon figure of  $(E_{ext}, t)$  showing frequency turn on-off of external drive. Constant frequency drive is applied for  $(0 \leq t \leq t_1)$ . (b) Dispersion curves or “Teardrop” curves for the electrostatic waves (IA, IBk) in  $k - \omega$  plane, obtained by assuming zero damping as a function of  $T_R$ .

simulate the excitation of the modes with  $k - \omega$  values obtained from the studies shown in Fig.??(b)). In order to characterize the plasma response, three cases have been considered with  $T_R = 0.1, 0.01, 10^{-7}$ . First, let us consider the plasma with  $T_R = 0.1$  case. When plasma is driven externally with  $\omega = \omega_d = 0.3043$  (in IBk region) during  $0 \leq t \leq 100$ , where  $\omega_d$  is considered from  $k - \omega$  curve for wavenumber  $k = 0.2$ , it produces both “Ion Acoustic” and “Ion Bulk” structures in ion distribution at  $v \simeq 1.545$  and  $v \simeq 3.295$  respectively [Figs.??(a) and ??(b)]. These values are slightly different from the values obtained via the dispersion relation shown in Fig.??(b) for IA and IBk waves ( $v_\phi^{IA} \simeq 3.3$  and  $v_\phi^{LAN} \simeq 1.5215$ ) due to the fact that the trapping region created in the simulations by the external driver is of small but finite velocity width. Fourier analysis, for this case, in Fig ??(b) reveals that after the drive has been turned off, the electric signal is shown to

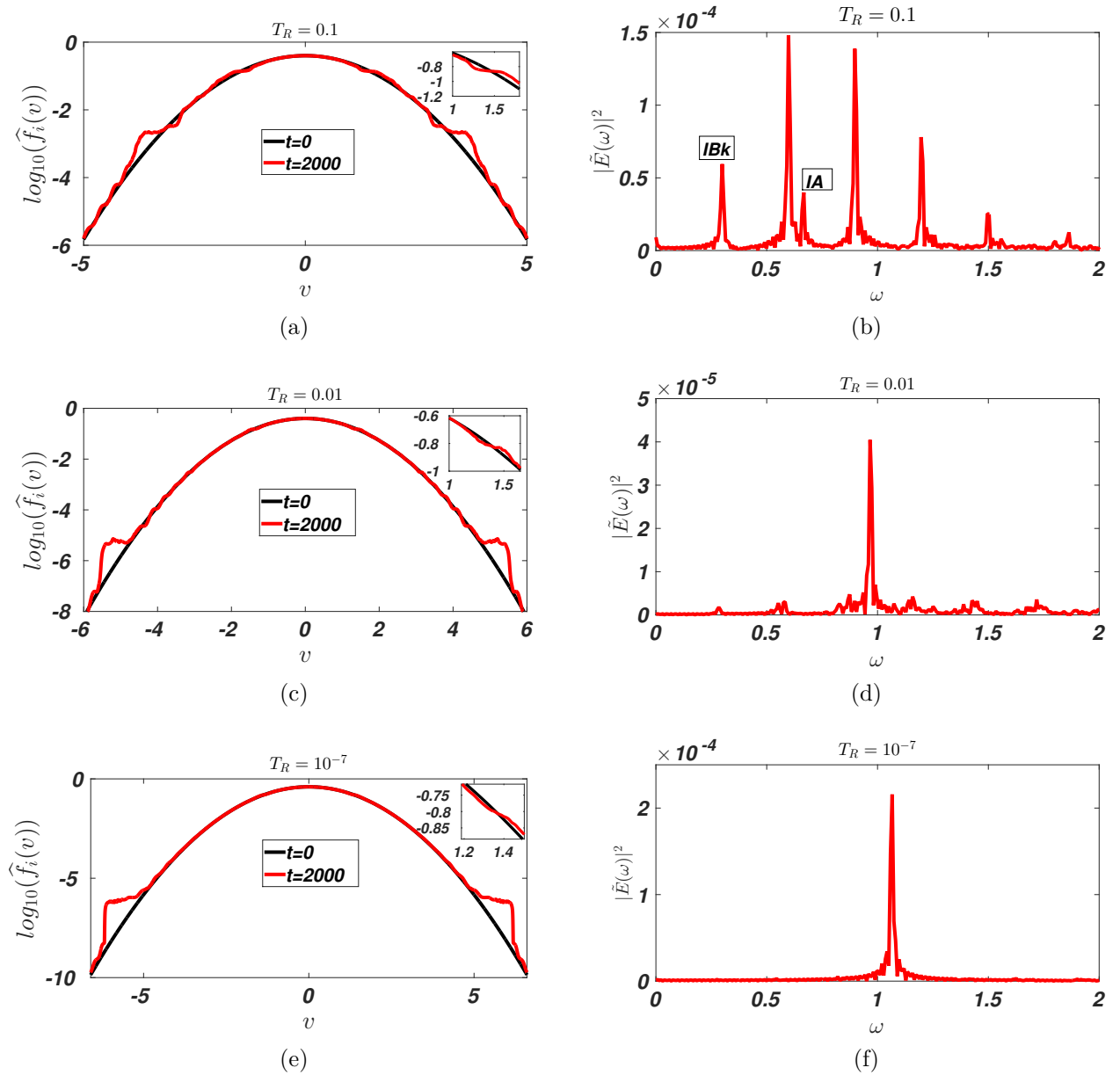


Figure 5.5: Plots of space averaged ion velocity distributions for:- Fig.(a)  $T_R = 0.1$ , Fig.(c)  $T_R = 0.01$ , Fig.(e)  $T_R = 0.1$  and (b) FFT plots of electric field, when plasma is driven for  $k = 0.2$  with  $\omega_d = \omega^{IBk}$ :- Fig.(b)  $T_R = 0.1$ , Fig.(d)  $T_R = 0.01$ , Fig.(f)  $T_R = 0.1$ .

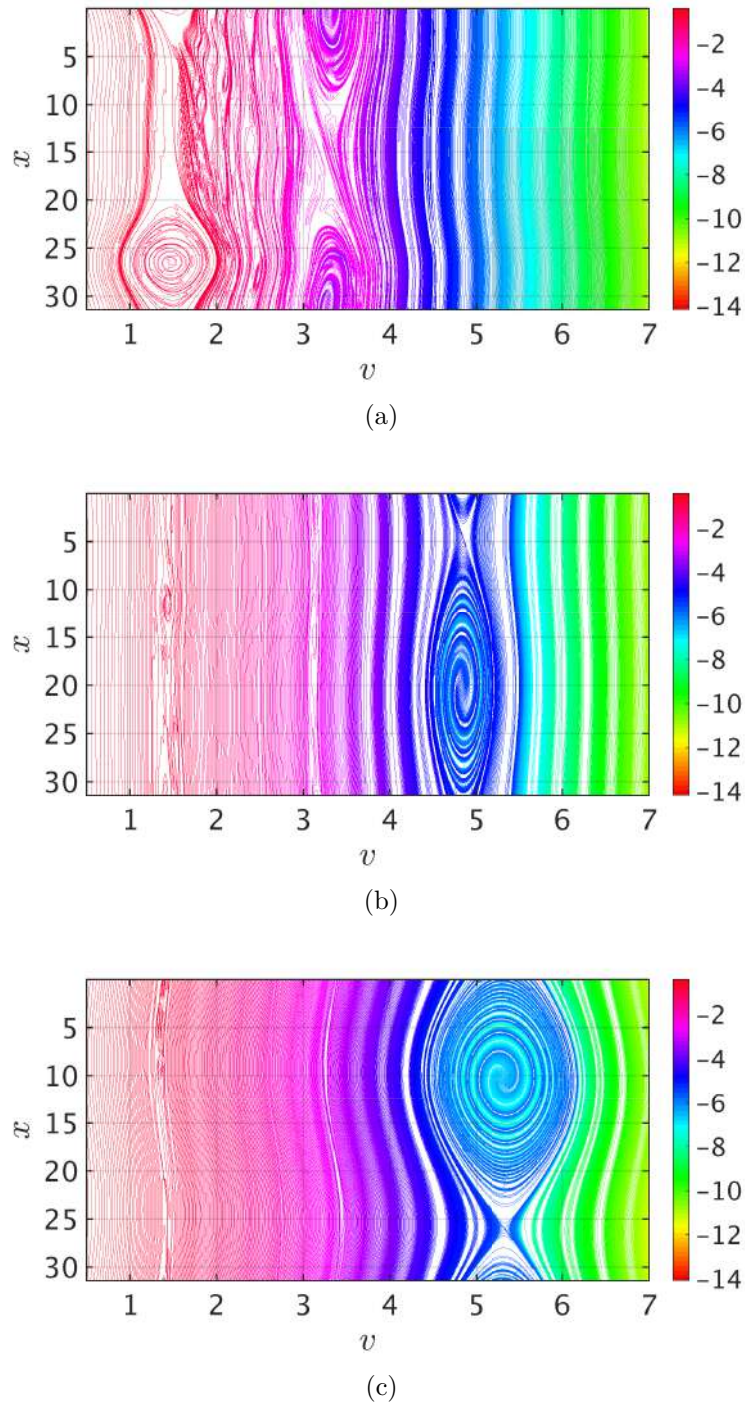


Figure 5.6: Ion phase space plots  $f_i(x, v, t = 2000)$  on log scale, when plasma is driven for  $k = 0.2$  with  $\omega_d = \omega^{IBk}$ :- Fig.(a)  $T_R = 0.1$ , Fig.(b)  $T_R = 0.01$ , Fig.(c)  $T_R = 10^{-7}$ .

be composed of both IA and IBk modes and their harmonics. However, when plasma is drive for  $T_R = 0.01$  with  $\omega_d = 0.2751$  (in IBk region) and  $T_R = 10^{-7}$  with  $\omega_d = 0.2722$  (in IBk region), it creates a large amount of trapping in IA region but no significant trapping in the IBk region. These is also indicated in fft plots of electric signal in Figs.??(c) to

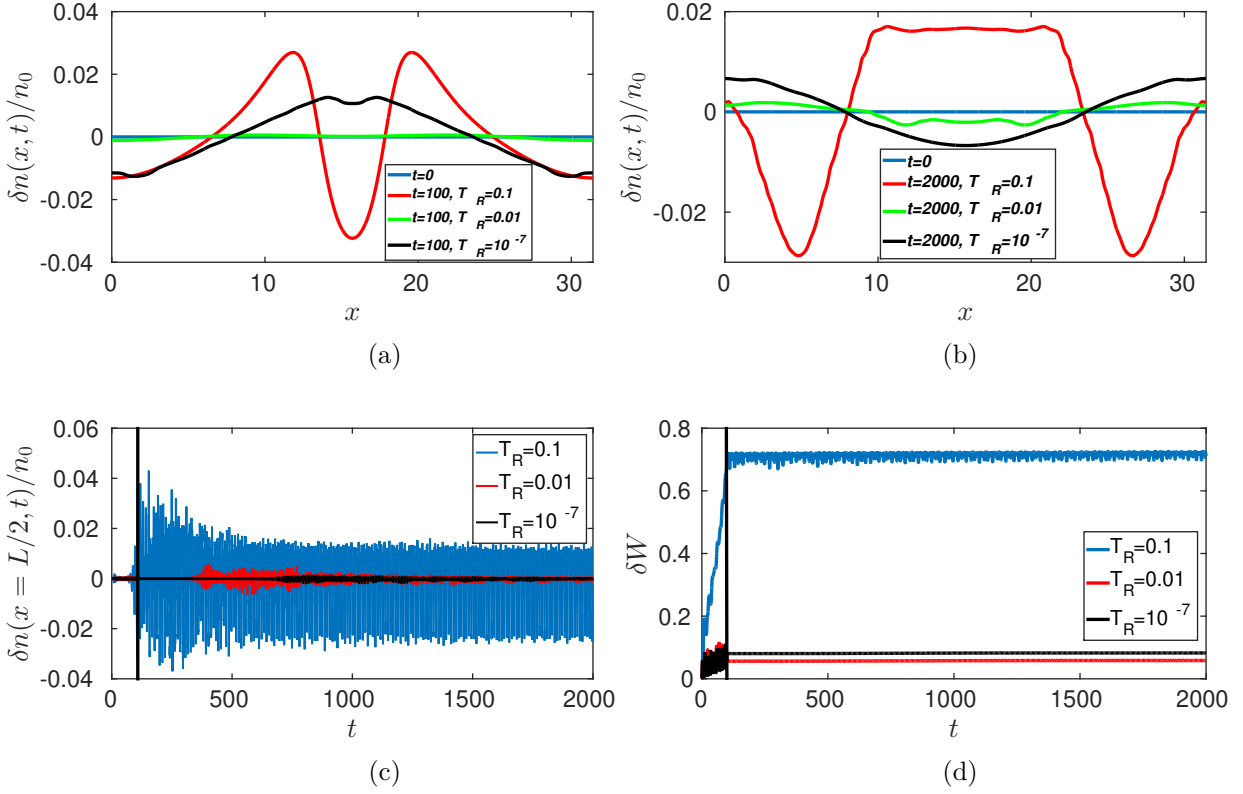


Figure 5.7: (a) Plot of excess density fraction  $\delta n/n_0(x, t)$  with  $x$  at time  $t = 100$  when the drive is turned off. (b) Plot of excess density fraction  $\delta n/n_0(x, t)$  with  $x$  at time  $t = 2000$  i.e. at the end of simulation, (c) Plot of time evolution of excess density fraction  $\delta n/n_0(x, t)$  at  $x = L/2$  and (d) relative total energy, when plasma is driven for  $k = 0.2$  with  $\omega_d = \omega^{IBk}$  for  $T_R = 0.1$ ,  $T_R = 0.01$ ,  $T_R = 10^{-7}$ .

??(f). In Fig.??(a), ??(b), ??(c), the snapshots of phase space distribution of ions have been shown corresponding to the above cases. These evidences suggest that the weak external driver has successfully created the trapped particle regions or weak flattening of distribution function simultaneously in IA and IBk regions for  $T_R = 0.1$ . However, for  $T_R = 0.01$  and  $T_R = 10^{-7}$ , the weak external drive creates significant trapping in IA region only.

In Fig.??(a), the time evolution of excess density fraction  $\delta n/n_0$ , as defined by  $\delta n(x, t)/n_0 = \int f_i(x, v, t)dv - \int f_{0i}(v)dv$ , at  $x = L/2$ , has been shown, where maximum  $\delta n/n_0$  gained by  $T_R = 0.1$  case and minimum is gained by  $T_R = 10^{-7}$  case. The total energy of the system is defined as:  $W(t) = K(t) + P(t)$ , where kinetic energy is computed as  $K(t) = (1/2) \int \int v^2 f_i(x, v, t)dx dv$  and potential energy computed as  $P(t) = (1/2) \int E^2(x, t)dx$ . In

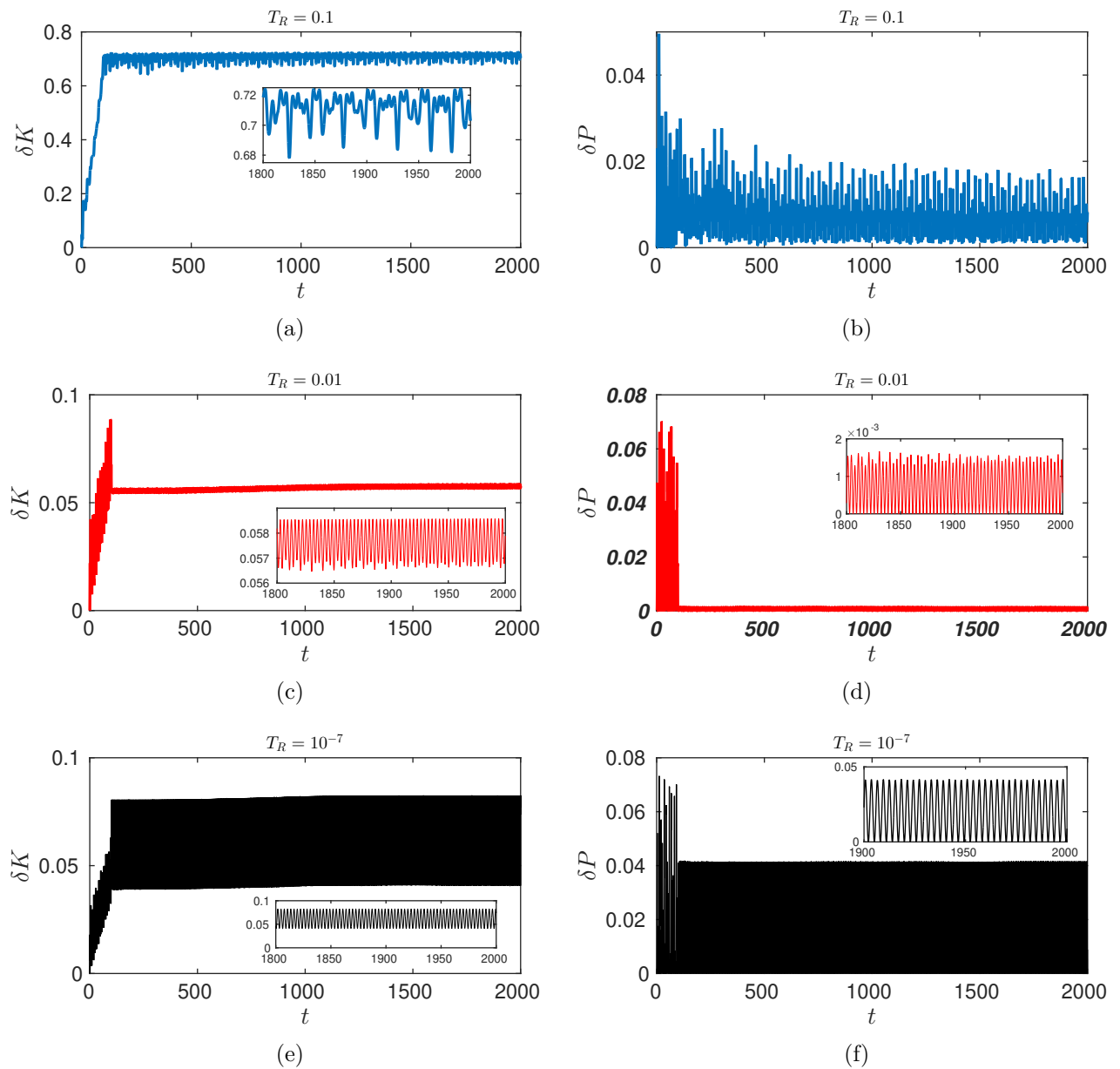


Figure 5.8: Plots of relative kinetic energy and relative potential energy , when plasma is driven for time period  $\Delta t = 100$ . Parameters used are:-  $k = 0.2$  with  $\omega_d = \omega^{IBk}$  for  $T_R = 0.1$ ,  $T_R = 0.01$ ,  $T_R = 10^{-7}$ .

Fig. ??(b), (a) the total relative energy  $\delta W = W(t) - W(0)$ , (b) the total relative kinetic energy  $\delta K = K(t) - K(0)$  and (c) the total relative potential energy  $\delta P = P(t) - P(0)$  are plotted. It is clear that during the external drive is on, both relative kinetic energy and relative potential energy of the system increases which reflects the increase in untrapped and trapped particle populations, respectively. The growth of these relative energies is arrested when the drive is turned off. Then the system relaxes and saturates to attain a certain value of  $\delta W$ ,  $\delta K$ ,  $\delta P$  and remains almost the same till the end of the simulation.

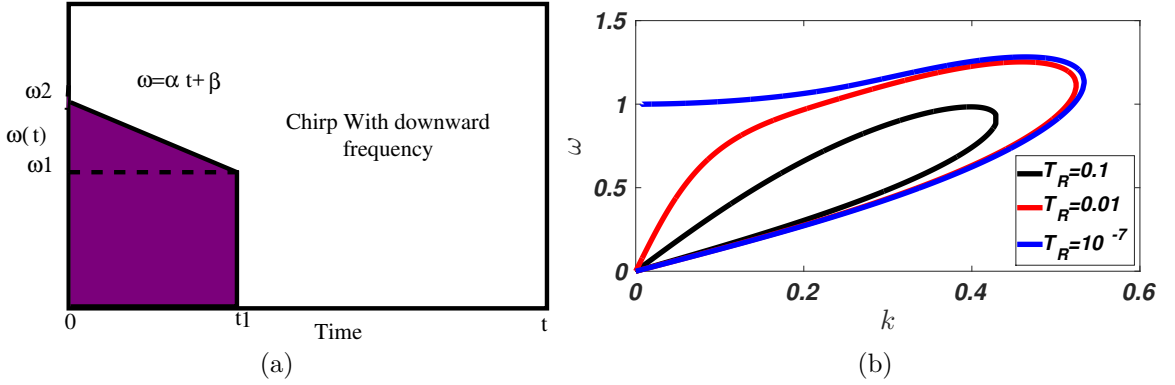


Figure 5.9: (a) A cartoon figure of  $(E_{ext}, t)$  showing frequency turn on-off of external drive. Downward frequency chirp is applied for  $(0 \leq t \leq t_1)$ . (b) Dispersion curves or “Teardrop” curves for the electrostatic waves (IA, IBk) in  $k - \omega$  plane, obtained by assuming zero damping as a function of  $T_R$ .

However, the maximum growth and the saturated values attained by these relative energies are shown to be dependent on  $T_R$ . The maximum saturated relative total energy  $\delta W$  is gained by  $T_R = 0.1$  case whereas minimum value is gained by  $T_R = 0.01$ .

### 5.2.2.3 Chirp Driven Ion Phase Space Vortices

In the following, we consider an initial Maxwellian homogeneous plasma which is driven by an external drive  $E_{ext}$  of amplitude  $E_0$  with a downward frequency chirp  $\omega = \alpha_0 t + \beta_0$  from  $t = 0$  to  $t = t_1$  with appropriately chosen chirp coefficients  $(\alpha_0, \beta_0)$  for different temperature ratios  $T_R = 0.1, 0.01, 10^{-7}$ . By doing so, the total electric field  $E_T$  ( $E_T = E_{ext} + E_s$ ) acting on the particles produces trapping in the resonant region. In this way, the energy of both trapped and untrapped particles increases, till the chirp is on, followed by complete energy conservation once the chirp is turned off, till the end of simulation.

In Fig.(??), the homogeneous plasma is subjected to an external drive of amplitude  $E_0 = 0.025$  right at  $t = 0$  for time duration  $\Delta t = 250$  from  $\omega_{high} = 0.5$  to  $\omega_{low} = 0.1$  for different values of  $T_R$ , namely,  $T_R = 0.1, 0.01, 10^{-7}$ . The chirp parameters are  $\alpha_0 = -1.6 \times 10^{-3}$  and  $\beta_0 = 0.5$ .

In order to characterize the plasma response, we have considered three cases with  $T_R = 0.1, 0.01, 10^{-7}$ . In all three cases, plasma is externally driven with a downward chirp

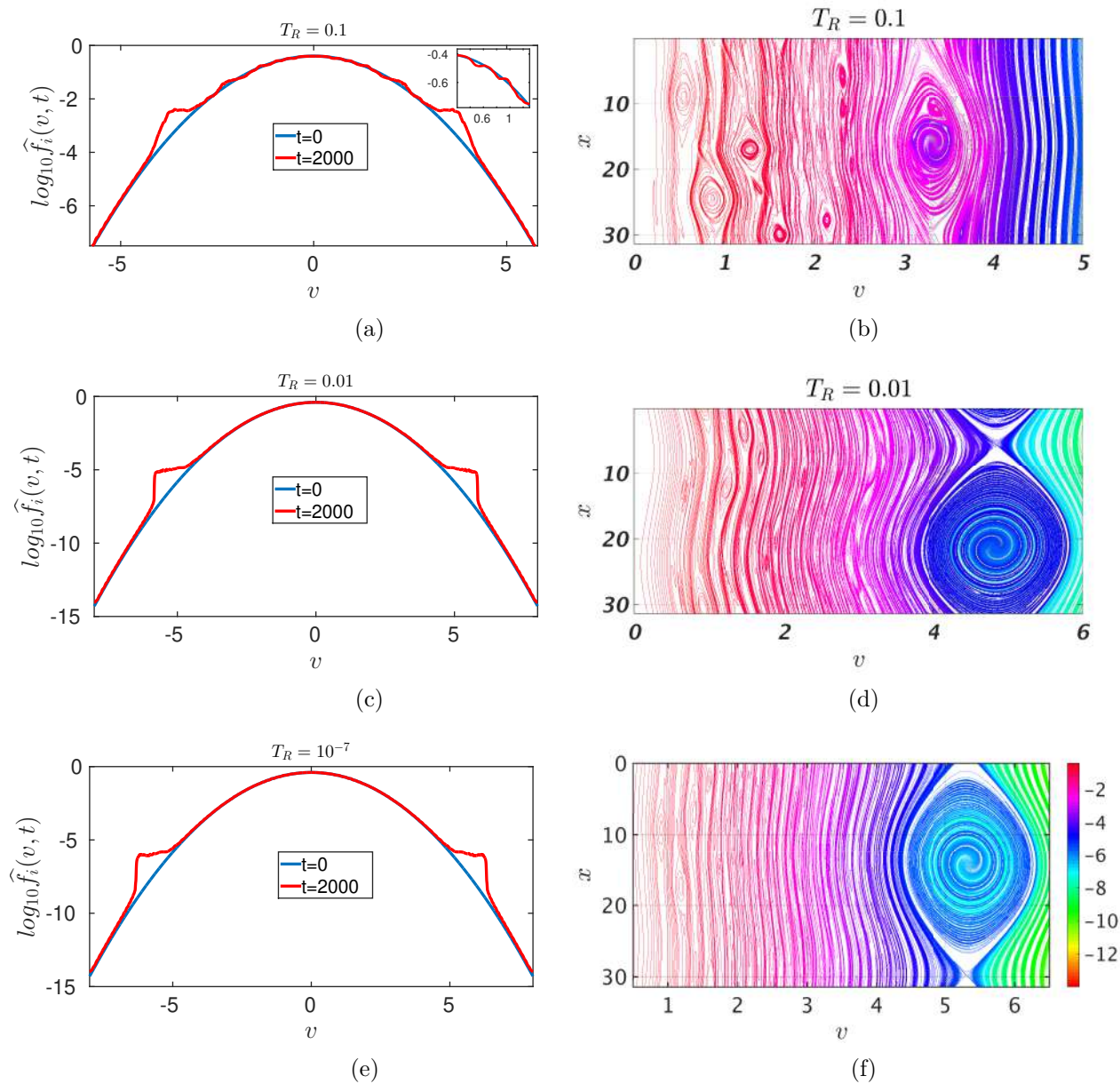


Figure 5.10: Plots of space averaged ion velocity distributions for:- Fig.(a)  $T_R = 0.1$ , Fig.(c)  $T_R = 0.01$ , Fig.(e)  $T_R = 0.1$  and Ion phase space ( $f_i(x, v, t = 2000)$ ) plots on log scale, when plasma is driven for time duration  $\Delta t = 250$  from  $\omega_{high} = 0.5$  to  $\omega_{low} = 0.1$  and for  $k = 0.2$ :- Fig.(b)  $T_R = 0.1$ , Fig.(d)  $T_R = 0.01$ , Fig.(f)  $T_R = 10^{-7}$ .

in the IBk region. First, let us consider the plasma with  $T_R = 0.1$  case. In Fig.??(a), the time evolution of space averaged ion velocity distribution is shown for  $T_R = 0.1$ , where plasma is subjected to an external drive of amplitude  $E_0 = 0.025$  for time duration  $\Delta t = 250$  from  $\omega_{high} = 0.5$  to  $\omega_{low} = 0.1$ . This chirp affects the plasma from IA to IBk region which in turn creates multiple PSVs in between IA to IBk region. This can also be seen in the corresponding phase space plot of  $f_i(x, v, t = 2000)$ , as shown in Fig.??(b).

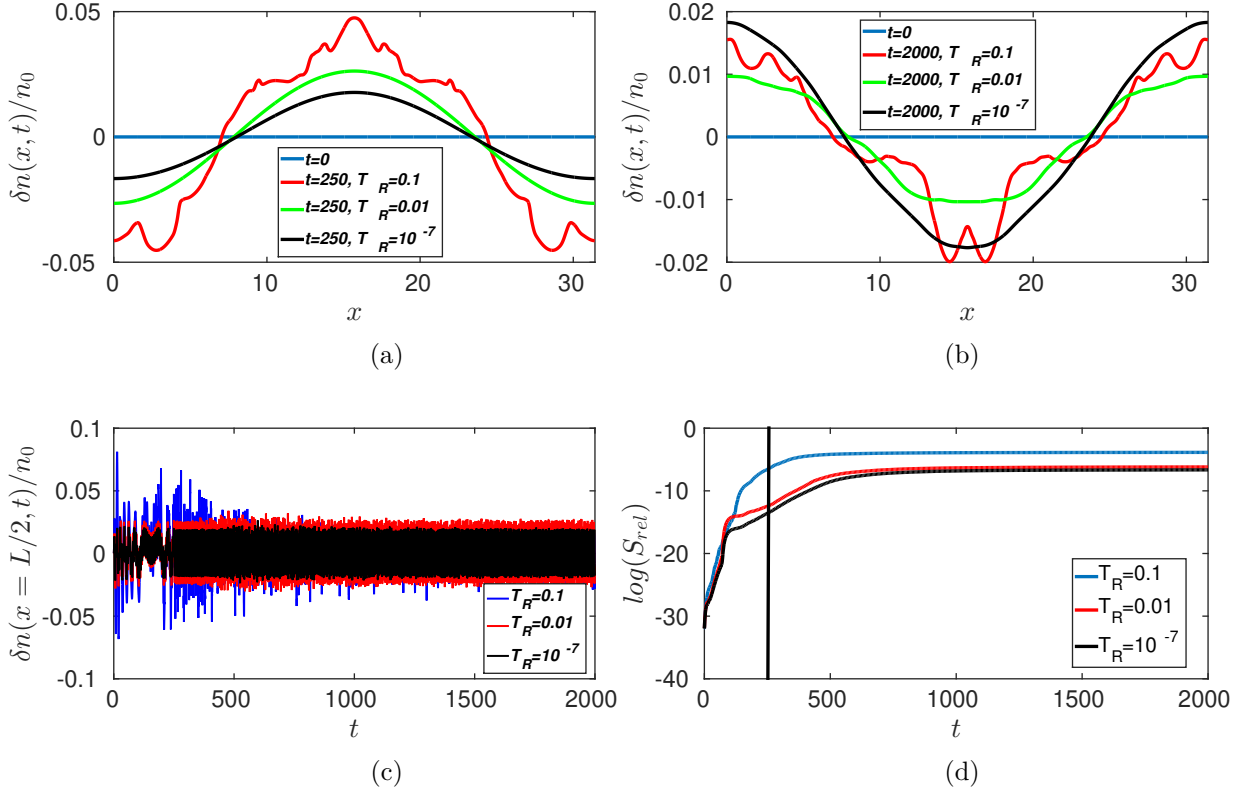
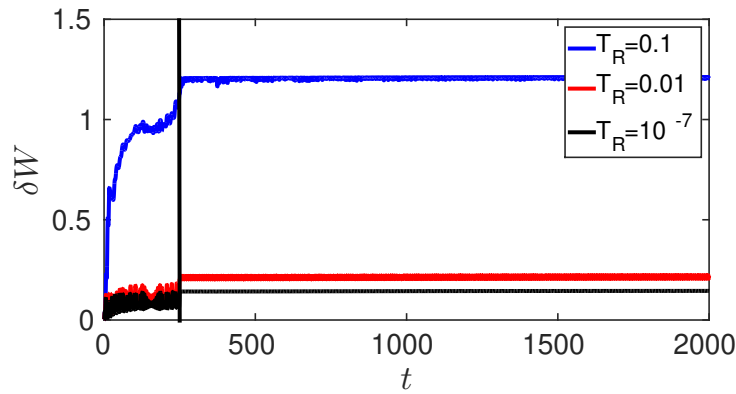


Figure 5.11: (a) Plot of space evolution of excess density fraction  $\delta n/n_0$  at  $t = 250$  (when the chirp is turned off) for  $T_R = 0.1$ ,  $T_R = 0.01$ ,  $T_R = 10^{-7}$ . (b) Plot of space evolution of excess density fraction  $\delta n/n_0$  at  $t = 2000$  for  $T_R = 0.1$ ,  $T_R = 0.01$ ,  $T_R = 10^{-7}$ . (c) Plot of time evolution of excess density fraction  $\delta n/n_0$  at  $x = L/2$ . (d) relative entropy, when plasma is driven time duration  $\Delta t = 250$  from  $\omega_{high} = 0.5$  to  $\omega_{low} = 0.1$  and for  $k = 0.2$  for  $T_R = 0.1$ ,  $T_R = 0.01$ ,  $T_R = 10^{-7}$ .

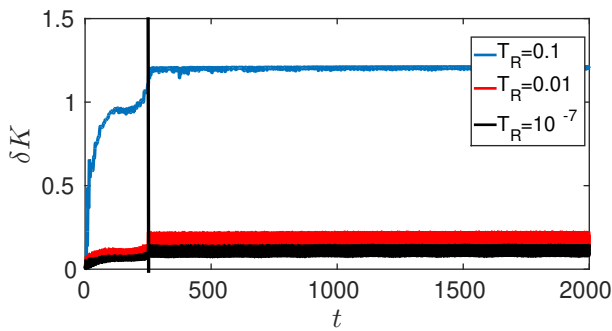
As the ion to electron temperature ratio  $T_R$  decreases, the “teardrop” curve becomes broader and the distance between IA branch and IBk branch increases. For such cases, this downward chirp excites the IA region more than the IBk region, which created giant PSV in the IA region [see Fig.??(c) and Fig.??(d)]. For very small value of  $T_R$ , for example  $T_R = 10^{-7}$ , contribution from electrons become negligible, in that case only IA region gets excited while applying the external chirp [see Fig.??(e) and Fig.??(f)].

### 5.3 Kinetic Ions and Kinetic Electrons (KIKE)

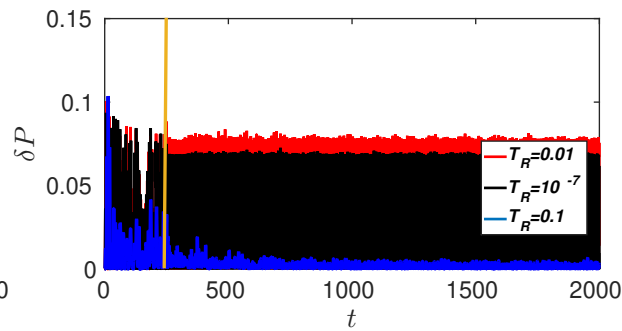
In this Section, an attempt has been made by means of numerical simulations, considering both kinetic electrons and kinetic ions on the same physics footing, wherein the Vlasov



(a)



(b)



(c)

Figure 5.12: Plot of (a) relative total energy, (b) relative kinetic energy and (c) relative potential energy, when plasma is driven time duration  $\Delta t = 250$  from  $\omega_{high} = 0.5$  to  $\omega_{low} = 0.1$  and for  $k = 0.2$  for  $T_R = 0.1$ ,  $T_R = 0.01$ ,  $T_R = 10^{-7}$ .

equations are integrated for both electron and ion species without any approximations in length scale or time scales. First, the weakly driven fully nonlinear Vlasov-Poisson (VP) equations has been solved which facilitates weak flattening of distribution function or weak trapping. To identify the modes, the  $\omega_r$  is need to be calculated. The eigenvalue values thus obtained for various wavenumbers are compared with frequencies obtained from solving the linearized eigenvalue equations considering weak trapping which allows us to neglect the contribution from the imaginary part of the dielectric function. My numerical results show that both electron and ion waves can be excited simultaneously in phase space. In appropriate limits, it is shown that the “thumb” and “teardrop” curves are different parts of a general symmetric dispersion relation and are recovered in appropriate limits of that dispersion relation.

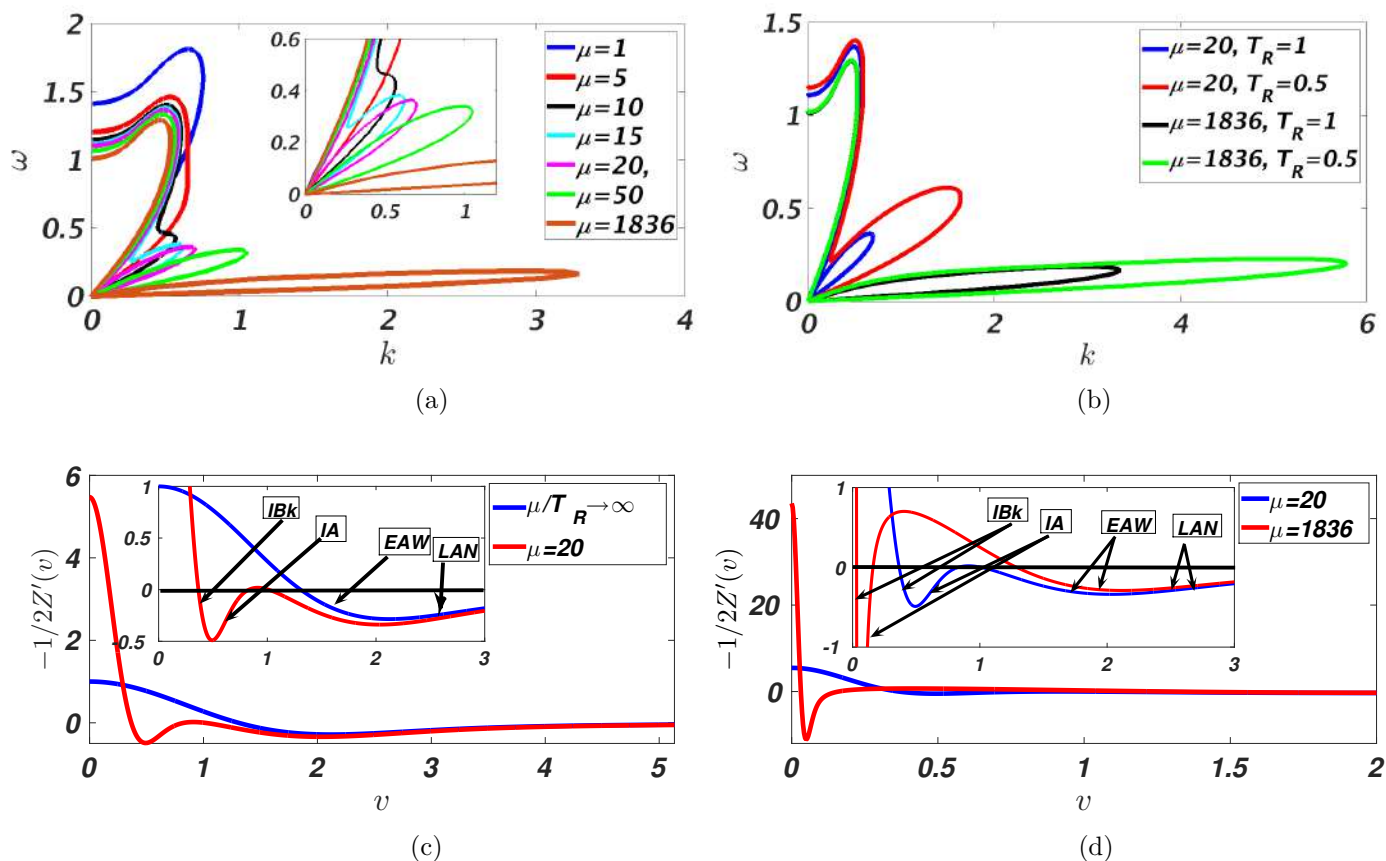


Figure 5.13: Dispersion curves or “*Thumb-Teardrop*” curves for the electrostatic waves (LAN, EAW, IA, IBk) in  $k - \omega$  plane, obtained by assuming zero damping: (i) as a function of  $\mu$  for  $T_R = 1$  [Fig. (a)], (ii) as a function of  $\mu$  and  $T_R$  [Fig. (b)]. These curves represent the solutions or the roots of Eq.(??). Also, the gradient of the real part of the complex plasma dispersion function  $-\frac{1}{2}Z'(v)$  is plotted for real arguments in Figs.(c) and (d) for immobile ions,  $\mu = 20$  and  $\mu = 1836$ .

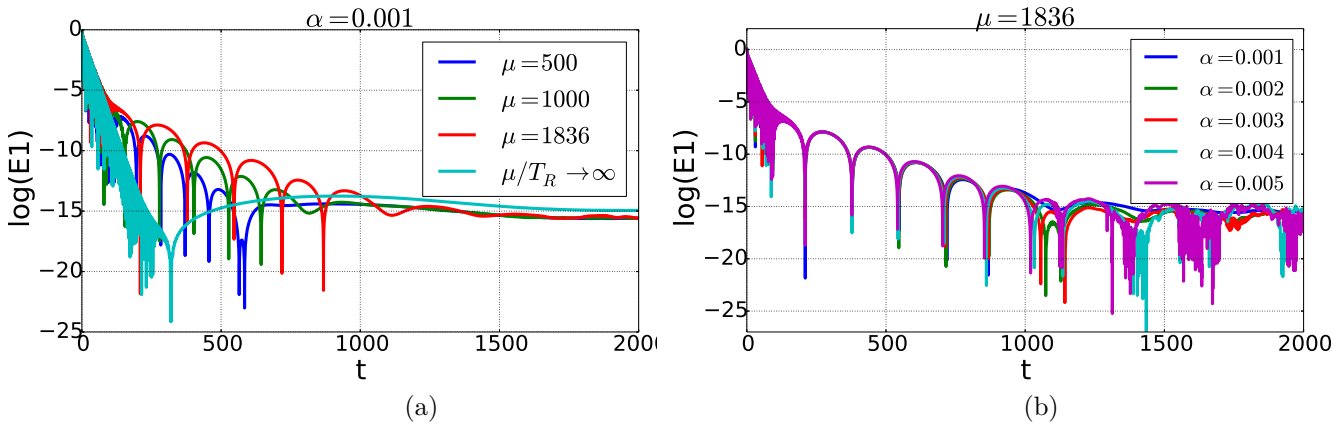


Figure 5.14: Comparison of time evolution of the electric field (a) for various values of initial amplitude of perturbation  $\mu$ , and (b) for various values of initial amplitude of perturbation  $\alpha$ .

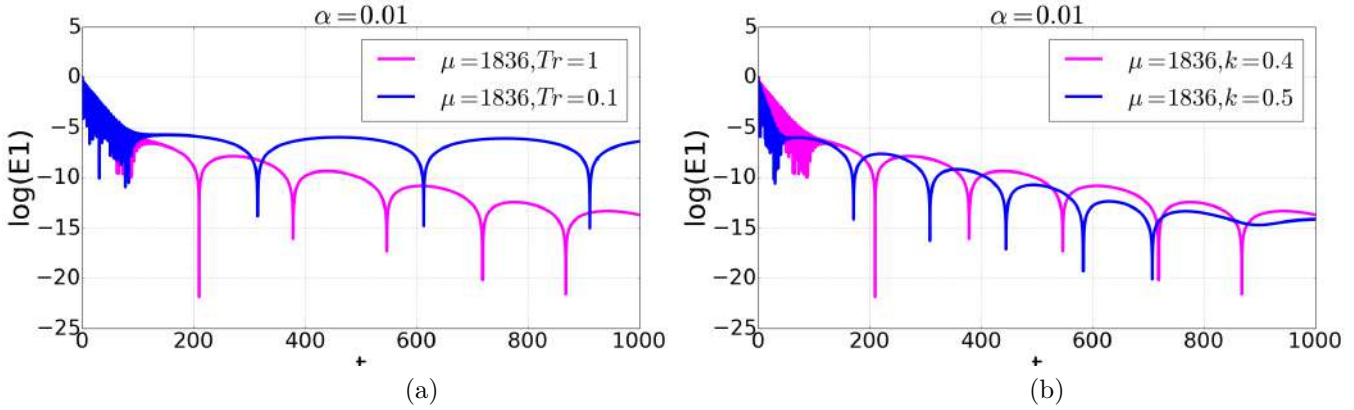


Figure 5.15: Comparison of time evolution of the electric field (a) for various values of ion to electron temperature ratio  $T_R$ , and (b) for various values of wavenumber  $k$ .

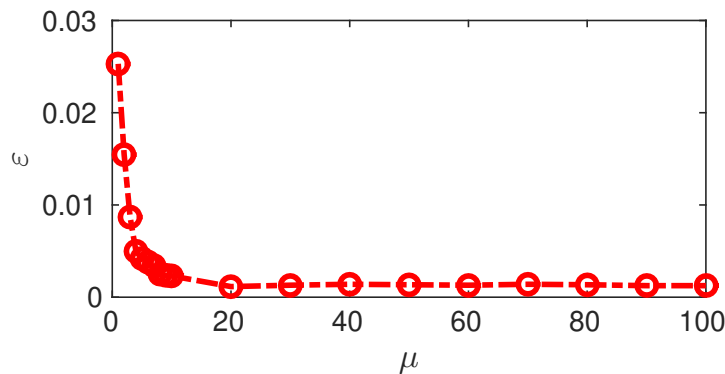


Figure 5.16: Plot the maximum value of the electric energy  $\epsilon = \int E^2 dx$  as a function of  $\mu$  for  $\alpha = 0.05$  in the time interval  $[1500, 2000]$ .

### 5.3.1 Governing Equations & Wave Dispersion Relation for KIKE Plasmas

A 1D unmagnetized, collisionless electrostatic plasma, in the framework of kinetic theory considering both kinetic electrons and kinetic ions, is described by one dimensional Vlasov-

Poisson (VP) model equations, viz:

$$\frac{\partial f_e}{\partial t} + v_e \frac{\partial f_e}{\partial x} - E_T \frac{\partial f_e}{\partial v_e} = 0 \quad (5.7)$$

$$\frac{\partial f_i}{\partial t} + v_i \frac{\partial f_i}{\partial x} + \frac{1}{\mu} E_T \frac{\partial f_i}{\partial v_i} = 0 \quad (5.8)$$

$$\frac{\partial E}{\partial x} = -\frac{\partial^2 \phi}{\partial x^2} = \int f_i dv_i - \int f_e dv_e \quad (5.9)$$

where  $f_e(x, v, t)$  and  $f_i(x, v, t)$  are the distribution functions of electrons and ions, respectively,  $\mu$  is the mass ratio of ions to electrons i.e.  $\mu = M_i/M_e$ ,  $\phi$  is the electrostatic potential,  $E_T = E_s + E_{ext}$  is the total electric field, where  $E_s = -\partial\phi/\partial x$  is the self consistent electric field and  $E_{ext}$  is the external driver electric field defined as:

$$E_{ext} = E_0 \sin(kx \pm \omega t) \quad (5.10)$$

where  $E_0$  is the amplitude of external drive. Here,  $k$  represents the perturbation wave number in the simulation box and  $\omega$  represents the driver frequency.

In the above equations [Eqs.(??)-(A.6)], time is scaled to  $\omega_{pe}^{-1}$ , length is scaled to electron Debye length  $\lambda_{De}$  and velocities to  $v_{the} = \lambda_{De}\omega_{pe}$ , electron thermal velocity. Using these normalizations, the Fourier transformation of linearized form of Eqs. (??)-(A.6) leads to the usual linear dispersion relation[16]:-

$$1 + \sum_j K_j(\mathbf{k}, \omega, \mu, T_R) = 0 \quad (5.11)$$

where  $K_j(\mathbf{k}, \omega, \mu, T_R) = -k_j^2/2k^2 Z'(\xi_j, \mu, T_R)$  is the susceptibility of the  $j^{th}$  ( $= i, e$ ) species,  $T_R (= T_i/T_e)$  is the temperature ratio,  $\xi_j = \omega/\sqrt{2}kv_j$  and  $Z_j(\xi_j, \mu, T_R)$  represents the real part of the complex plasma dispersion function for real arguments[44]. By assuming a weak flattening (or trapped region) of vanishing velocity width i.e.  $(\partial f/\partial v)|_{v_\phi} \simeq 0$  (which allows us to neglect the contribution from the imaginary part of the dielectric function), the solution to the real part of the wave frequency  $\omega$  as a function of the wave number  $k$ , obtained numerically from Eq. (??) is shown in Fig.(??) for various values of  $\mu$  and  $T_R$ .

Typically in the  $k - \omega$  diagram, at high frequencies (fixed ions), one obtains only the “thumb” curve that represents Langmuir waves (upper branch of thumb) and EAWs (lower branch of thumb)[17], where as in the low-frequency regime (Boltzmann electrons), one obtains only the “teardrop” curve that represents IA waves (upper branch of teardrop) and IBk waves (lower branch of teardrop)[19]. Perhaps for the first time, we have shown a unified “*thumb-teardrop*” diagram in Fig[(??)(a)], which includes kinetic response from both electron and ion branches simultaneously. For small values of  $\mu$ , the electron and ion parts of the solution are not separately visible from each other and the “*thumb*” curve represents contributions of both electrons and ions. As the value of  $\mu$  is increased, the curve begins to break into two different set of solutions where “*thumb*” shape represents the electron contribution (LAN and EAW waves) and the “*teardrop*” shape represents the ion contribution (IA and IBk waves). Depending on the value of  $T_R$  and  $k$ , at values of the wave number for which the effects of charge separation are no longer negligible, both electron branches (LAN and EAW) and both ion branches (IA and IBK) coalesce [Fig.??(b)]. Moreover, as  $\mu/T_R \rightarrow \infty$ , the “*teardrop*” curve becomes more and more narrow in  $\omega$  and flattens onto the  $k$ -axis, after which  $\omega/k \rightarrow 0$  in the teardrop and only “*thumb*” curve of electrons survives. Also, as the ion to electron temperature ratio  $T_R$  decreases, “*teardrop*” curve enlarges until eventually the IA branch is replaced by the ion Langmuir waves (ILWs) beyond which “*teardrop*” continuously changes into a “*thumb*” curve for ions.

In Eqn.(??), the term  $-\frac{1}{2}Z'(v)$  can be interpreted as a gradient of the real part of the complex plasma dispersion function for real arguments. A plot of the function  $-\frac{1}{2}Z'(v)$  for different values of  $\mu$  is displayed in Figs.(??(c)) and (??(d)), where it divides the phase velocity regions and reveals different branches of the dispersion relation. In the limit of immobile ions (see Fig.??(c)), the function  $-\frac{1}{2}Z'(v)$  represents electron contribution only. Therefore, it has one zero transition (at  $v = 1.307$ ) and one minimum (at  $v = 2.13$ ) which results in two separated regions for the phase velocity [96]. However, when both electron and ion contributions are considered such that both “*thumb*” and “*teardrop*” are well separated, for example for  $\mu = 20$  case [see Fig.(??(c))], the function  $-\frac{1}{2}Z'(v)$  represents four separated regions for the phase velocity:-(i)  $0.3662 \leq v \leq 0.4932$  (IBk), (ii)

$0.4932 \leq v \leq 0.8302$  (IA), (iii)  $0.10109 \leq v \leq 2.052$  (EAW) and (iv)  $v \geq 2.052$  (LAN). The function is positive for  $v < 0.3662$  and  $0.8302 < v < 1.0109$  else negative for other values of  $v$  and vanishes at infinity. Similarly, for  $\mu = 1836$ , the function  $-\frac{1}{2}Z'(v)$  again divides phase velocity into four different regions to present both ion and electrons contributions. This demonstrate the simultaneous existence of all four branches.

To further corroborate the results from the solution of the dispersion relation wherein weak local flattening of the distribution function or weak trapping was assumed (i.e. by neglecting the imaginary part of the dielectric function), the numerical simulations are performed with a well benchmarked VPPM 2.0 solver that uses Eulerian algorithm to solve the VP Eqs.(??)-(A.6) in one dimensional phase space  $(x, v)$  and advances the solution in time [21, 22, 58]. The simulation domain in phase space is  $D = [0, L_{max}] \times [-v_{max}^j, v_{max}^j]$ , where  $j = e$  (for electron) and  $j = i$  (for ions),  $L_{max} = 2\pi/k$  is the system size and  $v_{max}^j$  is chosen sufficiently large so that electron and ion velocity distribution functions approaches zero as  $|v^j|$  approaches  $v_{max}^j$ . The phase space is discretized with  $N_x = 512$  grid points in the spatial domain, where periodic boundary conditions are imposed, and  $N_{ve} \in [3000, 10000]$ ,  $N_{vi} = 4000$  in velocity domain such that there is sufficient resolution in both  $x$  and  $v_j$  grids for all values of  $\mu$  and  $T_R$  considered.

### 5.3.2 Simulation II

In this Section, I systematically present the numerical results of the two species case where both kinetic electrons and kinetic ions are considered on the same physics footing. In order to study the effect of ion motion on the evolution of high frequency (electron dominated) and the low frequency (ion dominated) electrostatic waves, the numerical results are presented for the following three cases:- where plasma is subjected to (i) an initial density perturbation i.e. the effect of ion motion on the Landau damping, (ii) a constant frequency external drive which concerns the excitation of all four normal electrostatic modes by applying a constant frequency external drive and (iii) a time dependent external drive or

chirp in the presence of kinetic ions in the collisionless plasma.

### 5.3.2.1 Effect of Ion Motion On Landau Damping of Electrons Langmuir waves (LAN)

In the following, to study the effects of ion dynamics on linear and non-linear Landau damping of LAN, the oscillations are excited by initializing a single Fourier mode  $k$  with the following initial electron distribution:

$$f_e(x, v_e, t = 0) = \frac{1}{\sqrt{2\pi}} [1 + \alpha \cos(kx)] \exp\left(-\frac{v_e^2}{2}\right) \quad (5.12)$$

where  $\alpha$  is the amplitude of initial electron density perturbation. Ions are initially uniform in the  $x$ -space and follow the Maxwellian distribution in the velocity space  $f_i(x, v_i, t = 0) = (\sqrt{2\pi})^{-1} (\sqrt{\mu/T_R}) \exp(-v_i^2 \mu / 2T_R)$ . In the following simulation case, we have kept a fixed wave number  $k = 0.4$ ,  $v_{max}^e = 6$  and  $T_R = 1$ , unless it is specified otherwise.

When the plasma is perturbed with an initial amplitude, which is as small as near the linear region, and ions are considered to be immobile i.e.  $\mu/T_R \rightarrow \infty$ , it leads to an exponential damping or linear Landau damping. However, in presence of ion motion, the linear Landau damping develops at the beginning but then the electric field evolution starts to deviate from the linear Landau damping and soon, the Landau damping almost disappears. Instead, the electric field evolution appears to decay slowly with comparatively large oscillating periodic structure which should be associated with ion motion [see Fig.(??)]

.When the ion mass is equal to the electron mass (i.e.  $\mu = 1$ ), the damping exist only for a few cycles with reduced damping rate because of quick excitation of ion density perturbation. Afterwards, the system evolution is mainly dominated by energy exchange between electrons and ions via electric fields. As the ion mass increases, their motion stop the linear Landau damping at some time and the large oscillating structures excited due to ion motion dominates the system evolution at the later stage. In Fig.(??), comparison of time evolution of the electric field for various values of initial amplitude of perturbation  $\alpha$  and  $\mu$  has been shown. The time evolution of electric field for various values of  $\alpha$

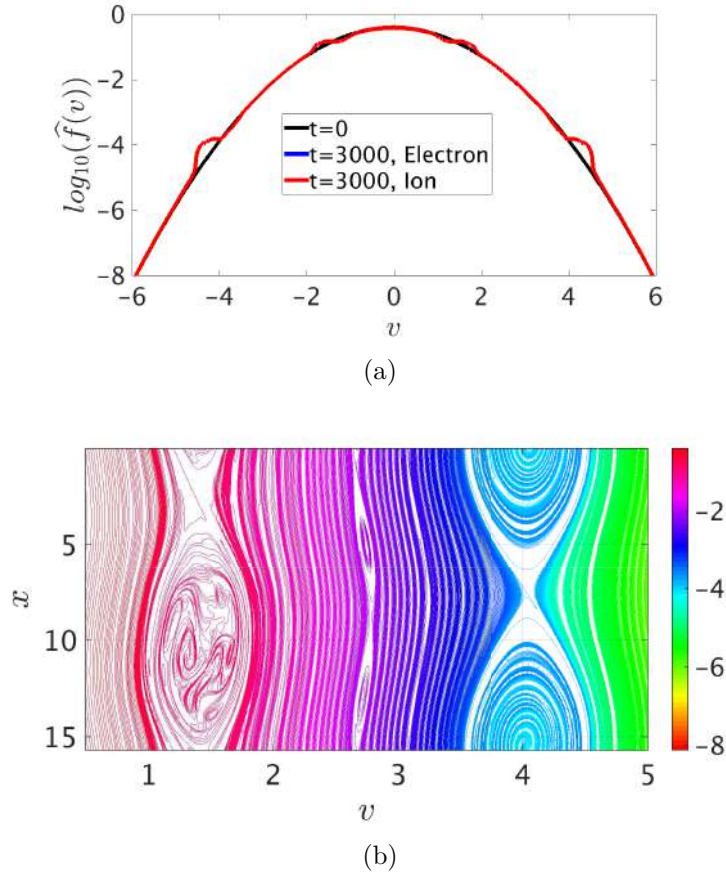


Figure 5.17: (a) Plots of space averaged electron and ion velocity distribution, (b) Contour plot of electron phase space distribution for  $\mu = 1$ , where plasma is driven for  $k = 0.4$  with  $\omega_d = 0.05712$ .

indicates the beginning of linear Landau damping at the start but then due to the effect of motion of comparatively massive ions the electric field evolution appears to decay slowly with comparatively large oscillating periodic structures at later stage. These large oscillating structures are again composed of smaller oscillations which indicates the decay of electric field due to both electron and ion motion simultaneously. The amplitude of these oscillations at later times is found to be increasing with increases in amplitude of perturbation.

Moreover, with the increase in the ion mass, the influence of ion motion on the linear Landau damping occurs later with larger oscillation periods accordingly [see Figs.??]. The frequency of the second large oscillation is found to be near the ion acoustic frequency. In the present normalization, the ion acoustic frequency is given by  $\omega_r^{IA} = k \sqrt{\gamma_e + \gamma_i T_R / \mu}$ , where both  $\gamma_e = \gamma_i = 3$ , corresponding to one-dimensional motion. Form this formula, for a given  $T_R$  and  $\mu$ ,  $\omega_r^{IA} \propto k$  and for a given  $k$  and  $\mu$ ,  $\omega_r^{IA} \propto \sqrt{T_R}$ . Therefore, in order to

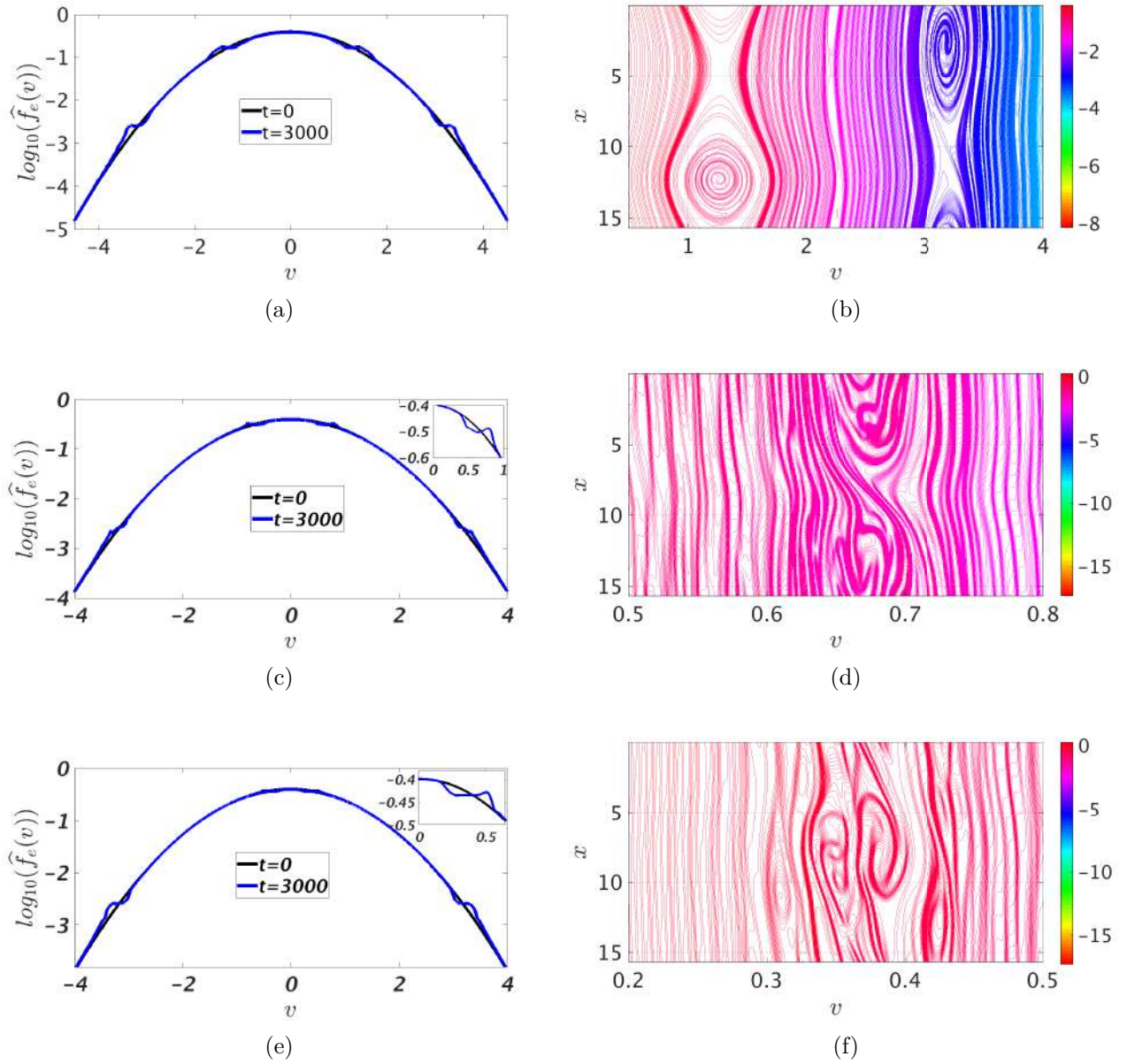


Figure 5.18: (i) Time Evolution of space averaged electron velocity distribution for  $\mu = 20$ . The plasma is driven during  $0 \leq t < t_1$  for  $k = 0.4$  in different regions:- (a) EAW ( $\omega_d = 0.5363$ ) for  $t_1 = 300$ , (c) IA ( $\omega_d = 0.275$ ) for  $t_1 = 1000$ , (e) IBk ( $\omega_d = 0.1545$ ) for  $t_1 = 1000$ . (ii) Phase space plots of electron distribution  $f_e(x, v, t = 3000)$  [(b) EAW and LAN] and ion distribution  $f_e(x, v, t = 3000)$  [(d) IA and (f) IBk].

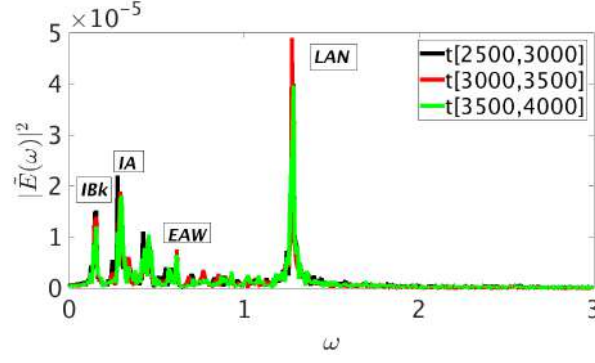


Figure 5.19: Fourier transform of electric field performed for different time windows, where plasma is driven during  $0 \leq t \leq 1000$  with  $\omega_d = 0.1545$  (IBk region) for  $\mu = 20$ .

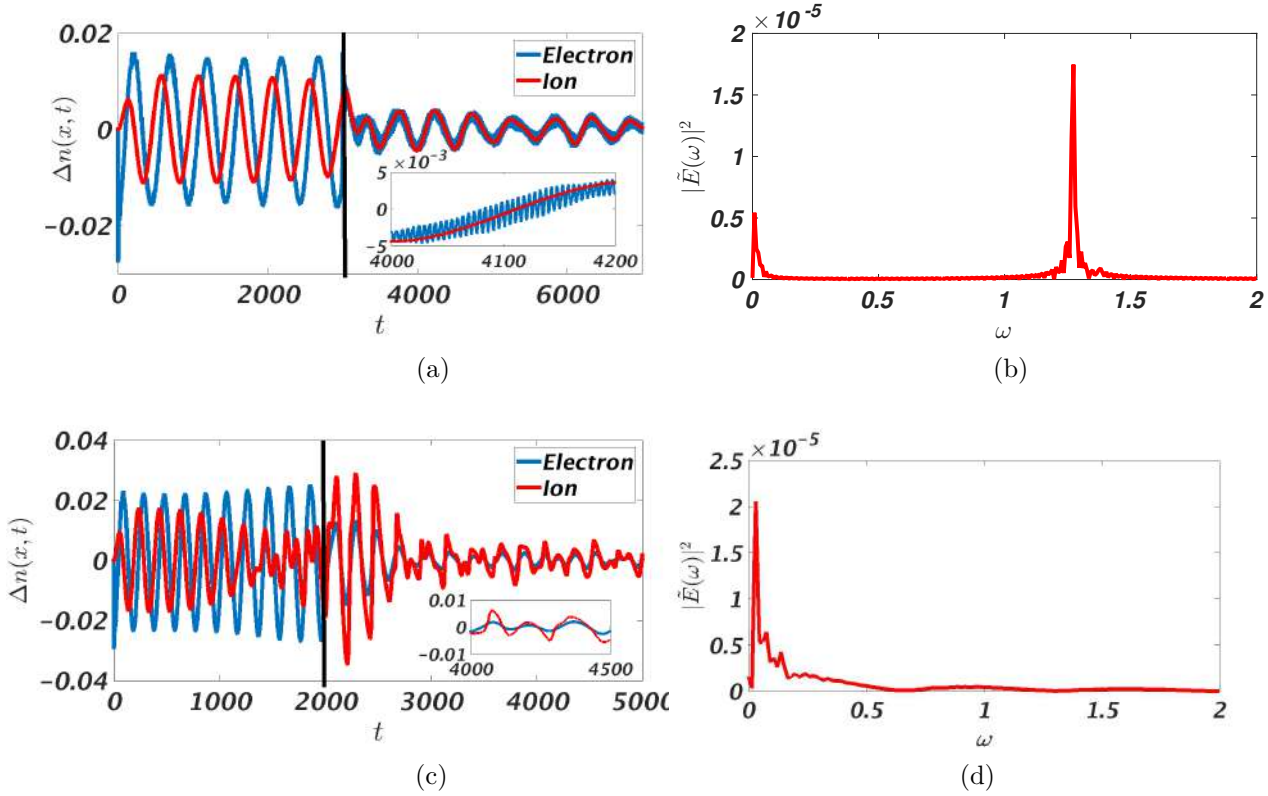


Figure 5.20: Time evolution of density fluctuation  $[\Delta n(x, t) = n(x, t) - n_0(x, t_0)]$  at  $x = L/2$  [Figs.(a), (c)] and Fourier analysis of electric field [Figs.(b), (d)], after the driver is turned off for  $\mu = 1836$ . The plasma is driven in IBk region during  $0 \leq t < 2\tau_r$  for the following sets of parameters:- (i)  $k = 0.4$ ,  $\omega_d = 0.0127$  [Figs. (a), (b)], (ii)  $k = 1$ ,  $\omega_d = 0.0321$  [Figs. (c), (d)]. The vertical line represents the time at which driver is turned off.

confirm that the second large oscillation is ion acoustic, the initial density perturbation numerical experiment is performed with two sets of parameters: (i)  $\alpha = 0.001$ ,  $\mu = 1836$ ,  $k = 0.4$ ,  $T_R = 1, 0.1$  and (ii)  $\alpha = 0.001$ ,  $\mu = 1836$ ,  $k = 0.4, 0.5$ ,  $T_R = 1$ . The corresponding

electric field plots are shown in Fig.??, where the large oscillation frequency increases with increase in  $k$  and decreases with  $\sqrt{T_R}$ . Thus, small amplitude perturbation excites both Langmuir oscillations and IA oscillations in a KIKE plasma.

When the initial density perturbation is large enough in the quasi-nonlinear regime, the behavior deviates from uniform exponential damping and trapping occurs. When the ion mass is comparable to the electron mass, both electron and ion contribute in the trapping dynamics but as the ion mass increases, the influence of ion motion becomes weak and the system is mainly determined by the electron dynamics. In Fig.(??), to characterize the plasma response for the nonlinear amplitude of perturbation  $\alpha = 0.05$ , the maximum value of the electric energy  $\varepsilon = (1/2) \int E^2 dx$  is plotted in the time interval [1500,2000] as a function of  $\mu$ . For smaller values of  $\mu$ , the  $\varepsilon$  value is high which shows contribution of both electrons and ions in trapping . However as the value of  $\mu$  increases, the ion influence becomes weak and trapping decreases till the trapping dynamics mainly dominated by electrons, thus value of  $\varepsilon$  attains a saturated value.

### 5.3.2.2 Driven Electron-Ion Electrostatic Modes :- Constant Frequency Drive

Within linear theory, the Electron acoustic waves (EAWs) and Ion bulk (IBK) waves are heavily damped as their wave phase velocities is close to electron thermal velocity ( $v_{the}$ ) and ion thermal velocity ( $v_{thi}$ ), respectively. However, these waves also a nonlinear BGK mode where electrons (or ions) trapped in the wave troughs which makes the electron (or ion) velocity distribution effectively flat at the wave phase velocity, and turns off Landau damping. Initially there is no trapped particle distribution exist. But if the plasma is driven externally, it can form trapping distribution dynamically as the wave evolves. For an external electric field  $E = E_0 \sin(kx - \omega t)$ , the trapping period to form the trapped particle distribution is approximately  $\tau = 2\pi / \sqrt{kE_0}$  for electrons and for ions  $\tau_r^i = 2\pi \sqrt{\mu} / \sqrt{kE_0}$  (in this normalization). Thus, the EAWs and IBks can be excited by a small amplitude driver if the driver is applied resonantly over few trapping periods. The driver continuously

replenishes the energy removed by Landau damping. Therefore, the trapped particle distribution survives and the EAW/IBks are eventually produced.

In order to excite all four electrostatic modes (LAN, EAW, IA, IBk), the follow-

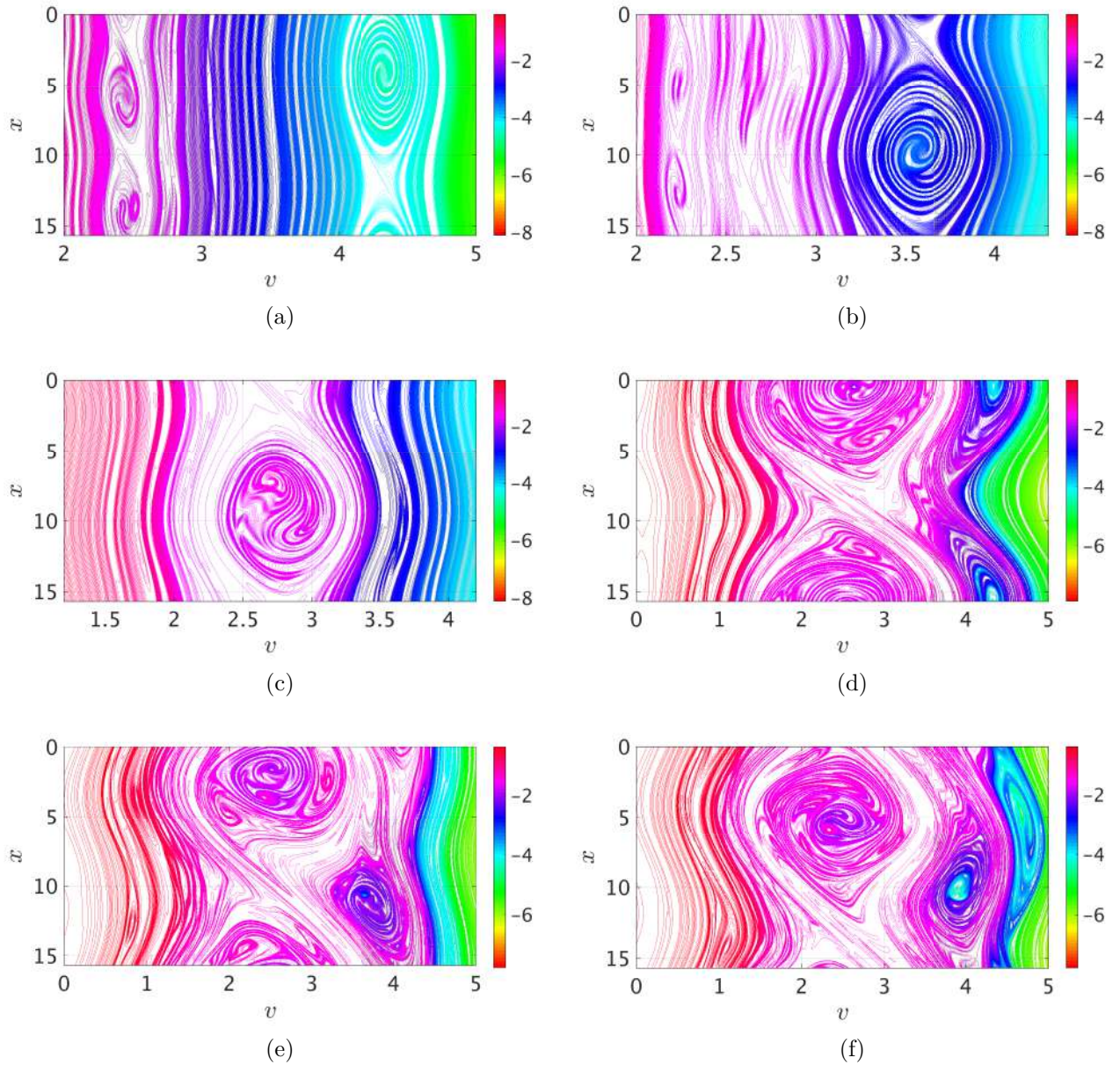


Figure 5.21: Phase space plots of  $f_e(x, v, t = 2000)$  for chirp interval  $\Delta t = 250$  when external downward chirp is given from  $\omega_{high} = 1$  to  $\omega_{low} = 0.5$  for (a)  $\mu = 1$ , (b)  $\mu = 3$  (c)  $\mu = 5$  (d)  $\mu = 50$  (e)  $\mu = 1836$  (f)  $\mu/T_R \rightarrow \infty$ .

ing numerical simulation has been performed: at  $t = 0$ , both electrons and ions are considered to be Maxwellian velocity distributions [ $f_e = (1/\sqrt{2\pi})\exp(-v_e^2/2)$  and  $f_i = (1/\sqrt{2\pi})(\sqrt{\mu/T_R})\exp(-v_i^2\mu/2T_R)$ ] and homogeneous density. The external electric field

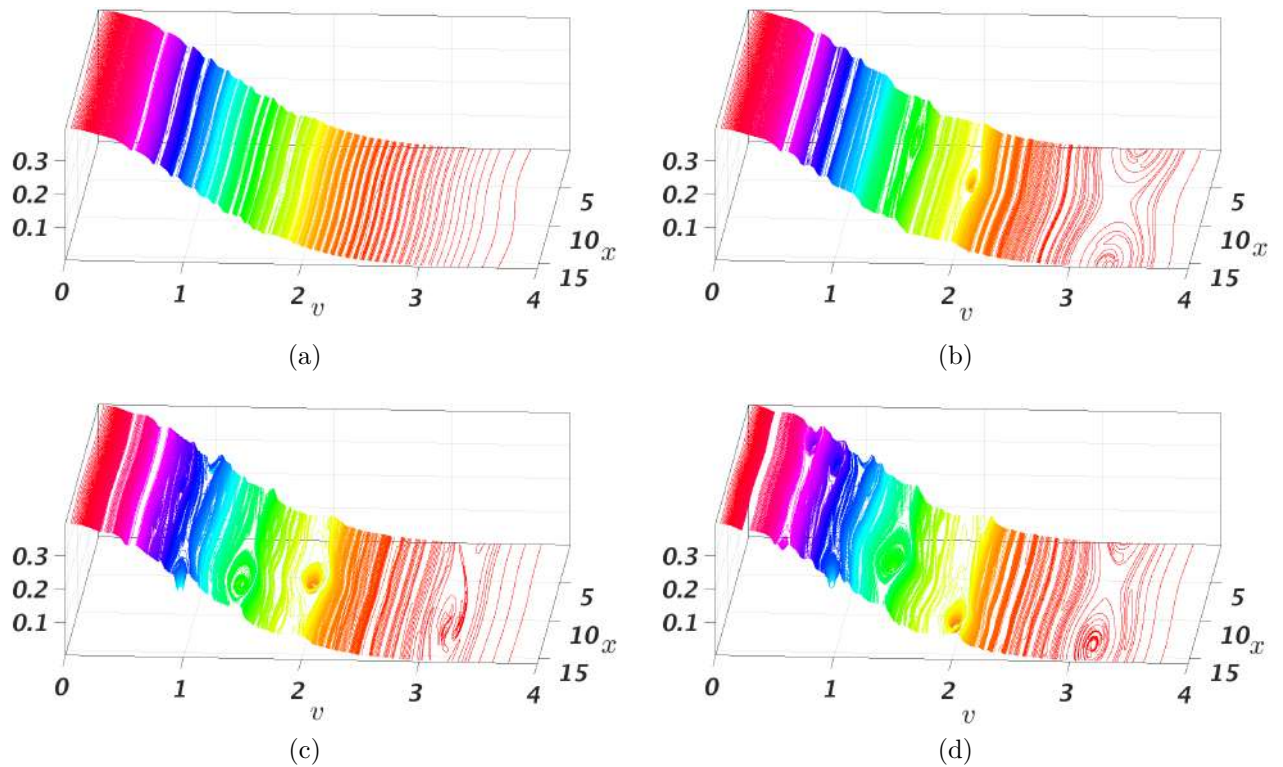


Figure 5.22: Phase space plots of  $f_e(x, v, t = 2000)$  for chirp interval  $\Delta t = 250$  when external downward chirp is given from  $\omega_{high} = 0.8$  to  $\omega_{low} = 0.4$  for (a)  $\mu = 1$  (b)  $mu = 5$  (c)  $mu = 20$  (d)  $\mu/T_R \rightarrow \infty$ .

applied to induce weak trapping has the form  $E_{ext} = E_0 \sin(kx \pm \omega t)$ . The external driver electric field is applied directly to the electrons and ions in the Vlasov equation. The longest wavelength is driven that fits into the simulation box. It is important to note that the amplitude of external drive,  $E_0$ , is chosen to be small enough that when an initial value problem is performed with this value of  $E_0$ , the trapping time  $\tau_r^j$  (for electrons  $\tau_r^e = 2\pi / \sqrt{kE_0}$  and for ions  $\tau_r^i = 2\pi \sqrt{\mu} / \sqrt{kE_0}$ ) is much larger than the Landau damping time  $\tau_{LD} = \gamma_L^{-1}$ . Moreover, the external drive of amplitude  $E_0 = 0.025$  is switched on at  $t = 0$  for a period  $\Delta t$ , where  $\tau_r^j \leq \Delta t \leq 5\tau_r^j$  and then we let the system to relax for atleast another  $t = 2000$  or  $t \sim 32\tau_r^e$  by switching off the external drive. After the drive has been turned off, the plasma response is analyzed. The temperature ratio is fixed  $T_R = 1$ , unless it is specified otherwise.

I simulate the excitation of the modes with  $k - \omega$  values obtained from the studies shown in Fig.??(a). In order to characterize the plasma response, I have considered three cases

with  $\mu = 1$ ,  $\mu = 20$  and  $\mu = 1836$ . First, let us consider the plasma with  $\mu = 1$  case, for which the space averaged velocity distribution of electrons and ions are always the same due to their identical masses and equal and opposite charges [Fig.(??)]. In case of immobile ion ( $\mu/T_R \rightarrow \infty$ ), an infinitesimal density perturbation leads to linear Landau damping and as the amplitude of perturbation becomes larger, LAN mode sets in and the weak trapping ensues of resonant particles in the wave troughs. Moreover, when the plasma is driven with an infinitesimal amplitude external drive in the background of immobile ions, it drives a well known “acoustic” mode, also known as “EAW”, besides the well known “LAN” mode in electron distribution. However, when ion motion is considered, for example  $\mu = 1$ , for an infinitesimal density perturbation, the ion motion significantly suppresses the linear Landau damping and the system evolution is mainly dominated by energy exchange between electrons and ions via electric fields [103]. For electron-positron plasma i.e.  $\mu = 1$ , when plasma is driven externally with  $\omega = \omega_d = 0.5172$  (in EAW region) during  $0 \leq t \leq 300$ , where  $\omega_d$  is considered from  $k - \omega$  curve for wavenumber  $k = 0.4$ , it produces both “acoustic” and “Langmuir” structures in electron as well as ion distribution at  $v \simeq 1.419$  and  $v \simeq 4.0275$  respectively [Figs.(?(a)) and (?(b))]. These values are slightly different from the values obtained via the dispersion relation shown in Fig.(?(a)) for “acoustic” and “Langmuir” waves ( $v_\phi^{EAW} \simeq 1.42$  and  $v_\phi^{LAN} \simeq 4.0287$ ) due to the fact that the trapping region created in the simulations by the external driver is of small but finite velocity width.

In Fig.(?), the  $k-\omega$  dispersion curve indicates that as we move towards larger values of  $\mu$ , the single  $k-\omega$  thumb curve begins to break into two parts. For  $\mu = 20$ , at which both thumb and teardrop are well separated [Fig.(?)], four simultaneous roots for  $k = 0.4$  (EAW, LAN, IA, IBk) are obtained using nonlinear VPPM solver. In Fig.(?), we show the time evolution of the space averaged velocity distribution for  $\mu = 20$  where plasma is driven in three different regions:- (i) EAW, (ii) IA and (iii) IBk, with  $(k - \omega)$  values obtained from dispersion predictions [Fig.?(a)]. When the plasma is driven in the EAW region with  $\omega_d = 0.5363$ , it creates two observable flattenings in the electron velocity distribution, one of which is EAW (at  $v \simeq 1.295$ ) and the other one is LAN (at  $v \simeq 3.164$ ) [Fig.(?(a))]. Similarly, when plasma is driven in IA region with  $\omega_d = 0.275$ , as shown in Fig.(?(c)), it

also creates two observable flattenings in the velocity distribution, one of which is IA (at  $v \simeq 0.675$ ) and the other one is LAN (at  $v \simeq 3.2975$ ). Also, when driven in IBk region with  $\omega_d = 0.1545$  results in two trapping regions, one of which is IBk (at  $v \simeq 0.375$ ) and the other one is LAN (at  $v \simeq 3.25$ ) [Fig.(??(e))]. These values are also slightly different from the values obtained via the dispersion relation shown in Fig.?? for EAW, LAN, IA and IBk waves ( $v_\phi^{EAW} \simeq 1.3407$ ,  $v_\phi^{LAN} \simeq 3.3075$ ,  $v_\phi^{IA} \simeq 0.6875$  and  $v_\phi^{IBk} \simeq 0.38675$ ) due to the trapping region of small but finite velocity width.

In Fig.(??(c), ??(d), ??(f)), we have shown the snapshots of phase space distribution of electrons and ions corresponding to the above cases. These evidences suggest that the weak external driver has successfully created the trapped particle regions or weak flattening of distribution function simultaneously for all four branches. Fourier analysis, for case (iii), in Fig (??) reveals that after the drive has been turned off, the electric signal is shown to be composed of all four modes and their harmonics.

For higher values of  $\mu$ , the system evolution is mainly determined by the electron dynamics at small wavenumbers. However, as shown in Fig.(??(b)), at slightly higher wavenumbers, the dispersion relation predicts solutions for ion branches only and no solutions for electron branches. For example, with more realistic values of  $\mu$ , say  $\mu = 1836$ , one gets four roots for  $k = 0.4$  (EAW, LAN, IA, IBk) and two roots for  $k = 1$  (IA and IBK) from analytical estimate. In Fig.(??(a)) and Fig.(??(c)), we show the time evolution of the density fluctuation, defined as  $\Delta n(x, t) = n(x, t) - n_0(x, t_0)$  where  $n(x, t) = \int f dv$ . In Fig.(??(a)) and Fig.(??(c)), the density fluctuation vs time is shown at  $x = L/2$  for  $k = 0.4$  (with  $\omega_d = 0.0127$ ) and  $k = 1$  (with  $\omega_d = 0.00321$ ), where the plasma is driven in IBk region. For this massratio, plasma is simulated for  $7000/\sqrt{1836} \simeq 163$  ion plasma periods for  $k = 0.4$  and  $5000/\sqrt{1836} \simeq 117$  ion plasma periods for  $k = 1$ . As it is clear from these plots, electron dynamics is present along with ion dynamics for  $k = 0.4$ , during and after the driving process, whereas for  $k = 1$ , ion dynamics dominates. After the driver has been turned off, the electric field oscillates at an almost constant amplitude. Fourier analysis [Figs. (??(b)), (??(d))] reveals that for  $k = 0.4$ , both electron (LAN) and ion (IBk) modes are generated whereas for  $k = 1$ , only ion mode is present.

In this work:- (i) a general symmetric dispersion relation which shows a continuous connectivity of electron (or “Thumb curve”) and ion (or the “Teardrop curve”) branches is shown, (ii) Demonstration of the simultaneous excitation of all four normal mode branches (LAN, EAW, IA and IBk waves) of a two species Vlasov plasma in a symmetric framework, both via dispersion solution as well as by applying a small amplitude external electric field that creates a weak population of trapped particles resulting in weak flattening of the distribution function.

### 5.3.2.3 Chirp Driven Phase Space Electron Vortices- Role of Ion motion

In the following, I have considered an initial Maxwellian homogeneous electron plasma and an initial Maxwellian homogeneous ion plasma which is driven by an external drive  $E_{ext}$  of amplitude  $E_0$  with a downward frequency chirp  $\omega = \alpha t + \beta$  from  $t = 0$  to  $t = t_1$  with appropriately chosen chirp coefficients  $(\alpha, \beta)$ . By doing so, the total electric field  $E_T$  ( $E_T = E_{ext} + E_s$ ) acting on the particles produces trapping in the resonant region. In this way, the energy of both trapped and untrapped particles increases, till the chirp is on, followed by complete energy conservation once the chirp is turned off, till the end of simulation.

In Fig.(??), the homogeneous plasma is subjected to an external drive of amplitude  $E_0 = 0.025$  right at  $t = 0$  for time duration  $\Delta t = 250$  from  $\omega_{high} = 2$  to  $\omega_{low} = 1$  in high frequency regime for different values of  $\mu$ , namely,  $\mu = 1, 3, 5, 50, 1836$  and  $\mu/T_R \rightarrow \infty$ . The chirp parameters are  $\alpha = -4 \times 10^{-3}$  and  $\beta = 2$ . In the limit of immobile ions ( $\mu/T_R \rightarrow \infty$ ), this downward frequency chirping leads to large coherent structures in phase space with multiple extrema with “shark” like features in phase space. As described earlier, the constant frequency linear drive excites electron acoustic waves and Langmuir waves along with other harmonics. Now, when the downward chirp is applied instead of the linear drive, it excites the whole resonant region from LAN to EAW along with its harmonics in a very short time period. Therefore, all these excited modes overlap to form giant phase space vortices (PSVs). However, when the ion motion is considered, the thumb shape of dispersion curve gets wider as the value of  $\mu$  decreases. Therefore, chirp efficiency decrease

and at smaller value of  $\mu$ , only two main modes i.e. LAN and EAW gets excited.

Also, in the smaller frequency regime near EAW branch, the downward chirp leads to the formation of multiple phase space vortices, all appearing at different regions of phase space, which gives a “honeycomb”-like transient structure of the distribution function. As shown in Fig. (??), the plasma is excited with the same drive amplitude  $E_0 = 0.025$  and frequency is swept  $\omega_{high} = 0.8$  to  $\omega_{low} = 0.4$  with a sweep rate of  $\alpha = -1.6 \times 10^{-3}$  for different  $\mu$  values, namely,  $\mu = 1, 5, 20$  and  $\mu/T_R \rightarrow \infty$ . In the limit of immobile ions ( $\mu/T_R \rightarrow \infty$ ), this downward frequency chirping excites the entire sub-harmonic region of phase space, which results in multiple non-overlapping phase space holes or “honeycomb”-like structures in phase space. However, when the ion motion is considered, trapping efficiency decreases at smaller value of  $\mu$ .

## 5.4 Summary and Conclusions

In the first part of this Chapter, the study of electrostatic waves in ion scale has been performed in the frame of Boltzmann electrons with kinetic ions using Vlasov-Yukawa (VY) solver. This model results in a “teardrop” curve (for IA and IBk waves). Using 1D1V VY solver Landau damping and electrostatic waves at ion scales (IA and IBk waves) have been studied. Also, formation and dynamics of chirp driven phase space vortices at ion scales have been studied for different temperature ratios.

Using a one dimensional (1D), two component Vlasov-Poisson system which treats both electrons and ions symmetrically in terms of kinetics, the the following major findings are reported:- (i) continuous connectivity of electron (or “Thumb curve”)[17] and ion (or the “Teardrop curve”)[34] branches with a general symmetric dispersion relation. The hitherto separately studied “Thumb curve” and the “Teardrop curve” show a “symmetry” in the dispersion curve as each of them consists of a high frequency branch and a low frequency branch. We present the whole physical picture on the same scale using a general symmetric dispersion curve which again consists of a high frequency part (“Thumb curve”-LAN,

EAW) and a low frequency part (“Teardrop curve”-IA, IBk), (ii) when plasma is subjected to small amplitude initial density perturbation, it excites both Langmuir oscillations as well as IA oscillations in a KIKE plasma, (iii) all four branches (LAN, EAW, IA, IBk)[17, 19, 34] have been recovered both via performing a numerical simulation where plasma is driven with an infinitesimal external electric field and from obtaining a general symmetric dispersion relation from solving weakly driven fully nonlinear VP equations which facilitates weak trapping. (vi) for realistic mass ratios, simultaneous excitation of all the normal modes:-LAN, EAW, IA, IBk. (v) the formation and dynamics of chirp driven PSVs are found to be dependent on  $\mu$  values.

Furthermore, the results presented in this and the earlier Chapters are for the collisionless plasmas. However, in systems governed by kinetic processes, nearly collisionless limits are not the same as the limit of zero collisionality. Since particle collisions work to restore thermal equilibrium, it is clear that their effect can eventually change the features of the kinetic dynamics of a plasma, even in situations where collisionality can be considered very weak. The evolution of the plasma is a result of nontrivial combination of kinetic processes and collisionality. Therefore, in the next Chapter, an attempt has been made by means of numerical simulations, to study effect of weak collisionality on the electrostatic driven phase space vortices. The details of which will be presented in the Chapter 6.



---

## Eulerian Simulations of Collisional Effects on Electrostatic Phase Space Vortices

*In this Chapter, the effect of collisions on electrostatic phase space vortices formed in a collisionless process is analyzed by means of Eulerian simulation for two different collision models. As seen in earlier Chapters, in the absence of collisions, phase space vortices manifests as the formation of a plateau in the resonant region of the particle velocity distribution function, due to trapping of resonant particles. In the presence of collisions, over long time this plateau is smoothed out since collisions drive the velocity distribution towards Maxwellian irrespective of how weak the collisions are as long as they are non-zero. In these conditions, kinetic processes and collisionality would be in competition and the evolution of the plasma would, therefore, be a result of nontrivial combination of these two effects. Therefore, an attempt has been made by means of numerical simulations, to study effect of weak collisionality on the electrostatic driven phase space vortices with two types of collision operators: (1) Boltzmann collision operator, where the colliding particles can be treated as isolated pairs and, (2) Fokker-Planck (FP) collision type operator in one*

*dimension, where many weak collisions lead to particle diffusion in velocity space. It is shown that depending on the collision models used, the nature of smoothing in velocity space of giant PSVs results in different structures. However, irrespective of the collision model used, substantial excess density fractions are retained.*

## 6.1 Introduction

The understanding of collision dynamics in plasmas is a very fascinating and important concept and it has been the subject of a relevance for both laboratory plasmas as well as astrophysical plasmas. Various authors have approached the study of collisional effects in plasmas, by modeling particle interactions through different collision operators, with different physical features and mathematical structures [1, 88, 61, 62, 104]. For example, highly collisional plasmas, collision operators involving a few low-order moments are found to be enough to derive transport equations [105, 106, 107, 108]. However, plasmas with low collisionality (or nearly collisionless) require calculation of high-order moments [109, 110, 111]. In order to calculate the effect of collisional dynamics on plasmas, several different model operators and numerical methods have been developed and applied [112, 113, 114, 115, 116].

While studying plasma dynamics, collisions are usually considered either dominant, so as to maintain the velocity distribution function near Maxwellian (fluid model), or negligible (Vlasov model). For physical systems, such as the solar wind, that exhibit a weak but non-negligible collisionality, both kinetic and collisional approaches are necessary to understand the phase space dynamics and phase space structures formed. In systems governed by kinetic processes, limit of low collisionality (or nearly collisionless regimes) is not the same as the limit of zero collisionality. This is mainly because, kinetic processes in a plasma are determined by the details of the particle distribution function in velocity space and on the nature of subtle trapping-detrapping processes. For example, a slight departure from a Maxwellian may not produce any significant change in the real frequency

but can produce significant modifications in the growth/damping of electrostatic waves. Since particle collisions work to restore thermal equilibrium, it is clear that their effect can eventually change the features of the kinetic dynamics of a plasma, even in situations where collisionality may be regarded very weak. Nearly collisionless regimes are important to a number of physical processes, including runaway electrons in magnetically confined fusion plasmas, magnetic reconnection in weakly collisional regime, low density edge in a tokamak plasma, solar plasma near sunspots, and non-neutral plasmas etc [117, 118, 119, 120]. For such kind of plasma phenomena, kinetic dynamics along the magnetic field lines can only be explained if a collision model is added to the model described here. In these conditions, kinetic processes and collisionality are in competition between each other: while the first process works to produce deformations of the particle distribution function away from a Maxwellian, the latter tends to restore the Maxwellian configuration. The evolution and phase space structure of the plasma is, therefore, a result of nontrivial combination of these two effects.

In the past, many attempts have been made to deal with the dynamics due to collision processes, for eg., a spectral method has been proposed for the numerical evaluation of the Landau collision integral, based on the use of Fast Fourier Transform (FFT) routines which significantly reduce the computational weight with respect to finite difference schemes [63]. The inclusion of collisional effects in the splitting scheme has been performed using Bhatnagar-Gross-Krook (Krook) operator to study the damping of electrostatic waves in the linear limit [61]. In order to reduce computational weight of the numerical approximation to the Landau integral, collisional operators have been simplified by decreasing their dimensionality in velocity space to study Coulomb collision effects [62, 121]. Recently, a detailed numerical study of the simplified operators has been performed through a 1D-1V Eulerian simulations to study the collisional effects on electrostatic plasma waves [122, 123].

In the present work, an attempt has been made by means of Eulerian phase spacenumerical

## CHAPTER 6. EULERIAN SIMULATIONS OF COLLISIONAL EFFECTS ON ELECTROSTATIC PHASE SPACE VORTICES

---

simulations, to study effect of weak collisionality on the linear Landau damping, non-linear Landau damping and driven electrostatic driven phase space vortices. In this Thesis, two types of collision operators have been used to study the same physical phenomenon and results have been compared. The collision operators are:- (1) Boltzmann collision operator, where the colliding particles can be treated as isolated pairs and (2) Fokker-Planck (FP) collision type operator in one dimension, where many weak small angle-like collisions lead to particle diffusion in velocity space.

In this Chapter, the inclusion of collisional effects in Eulerian time-splitting algorithm has been performed to the study the effect of weakly dissipative/collisional effects on driven electrostatic phase space vortices (PSV). Collisions are modeled through one dimensional operators of the Bhatnagar-Gross-Krook (Krook)/Fokker-Planck or Zakharov-Karpman (ZK) type [61, 62, 63]. The accuracy of the numerical code is discussed by comparing the numerical results to the analytical predictions obtained in some limiting cases to evaluate the effects of collisions on linearly stable (Landau damping) distributions and in the dissipation of Bernstein-Greene-Kruskal modes. Particular attention is devoted to the study of collisional effects on the formation and dynamics of driven PSVs which have been studied in previous Chapters, for an unbounded collisionless plasma with both Maxwellian and non-Maxwellian distributions [*P. Trivedi and R. Ganesh, Physics of Plasmas 23, 062112 (2016)*, *P. Trivedi and R. Ganesh, Physics of Plasmas 24, 032107 (2017)*]. Depending on the collision models used, it is shown that the giant PSVs smoothen out, yet retain overall large excess density fractions. In this Chapter, using VPPM-2.0 solver which includes collisional models, I bring out several interesting features of driven phase space structures in the presence of weakly collisional environment, starting from a Maxwellian plasma, the details of which will be presented below.

The rest of the Chapter is organized as follows: I proceed to describe the numerical scheme in Sec. 2.2. Simulations with different cases have been discussed in Sec. 2.3. In the Subsec.??, the effects of collisions on linear Landau damping has been elucidated using both

Krook and ZK operators. In Subsec.??, the collisional effects on Bernstein-Greene-Kruskal waves or phase space vortices (PSV) has been reported. In Subsec.??, the effect of collisions on the driven PSVs with multiple extrema due to embedded holes and clumps , or multiple phase space vortices has been presented using both Krook and ZK operator. In Sec.2.5 summary and conclusions have been presented.

## 6.2 Collision Model And Numerical Scheme

In the framework of kinetic theory, the propagation of 1D electrostatic plasma waves in the absence of collisions can be described by the 1D-1V Vlasov-Poisson equations. In the present case, I analyze in detail the properties of two different one-dimensional collisional operators and their effects on the propagation of plasma waves and electrostatic phase space vortices, by means of Eulerian kinetic simulations, which has been achieved by including in the right hand side of the Vlasov equation, different collision operators. In our analysis, only electron-electron collisions are taken into account.

The basic equations considered here can be written in the following dimensionless form:

$$\frac{\partial f}{\partial t} + v \frac{\partial f}{\partial x} - E_T \frac{\partial f}{\partial v} = \frac{\partial f}{\partial t} \Big|_{collision} = C(f) \quad (6.1)$$

$$\frac{\partial E_s}{\partial x} = 1 - \int f dv \quad (6.2)$$

where  $C(f)$  is a generic collisional operator and  $E_T = E_s + E_{ext}$  is the total electric field, where  $E_s(x, t)$  is the self consistent electric field and  $E_{ext}$  is the external driver electric field defined as:

$$E_{ext} = E_0 \sin(kx \pm \omega t) \quad (6.3)$$

where constant  $E_0$  is the amplitude of external drive. Here,  $k$  represents the perturbation wave number in the simulation box and  $\omega$  represents the driver frequency. Also, time has been normalized to the electron plasma frequency  $\omega_{pe}$ , space has been normalized to the electron Debye length  $\lambda_{De}$ , velocity has been normalized by the initial equilibrium electron thermal velocity  $v_{the} = \lambda_{De} \omega_{pe}$ . With these choices, electron distribution  $f$  gets normalized

## CHAPTER 6. EULERIAN SIMULATIONS OF COLLISIONAL EFFECTS ON ELECTROSTATIC PHASE SPACE VORTICES

---

by  $n_0/v_{the}$  and  $E$  by  $m_e v_{the}/e\lambda_{De}$  where  $e$  is the electron charge. In this model, the ions form a stationary neutralizing background of number density  $n_0$  with numerical value 1 in the Poisson equation.

In this Thesis, I have considered two different 1D collisional operators:-

1. *Bhatnagar-Gross-Krook (Krook) operator* [61]:-  $C = -\nu(f - f_{eq})$
2. *Zakharov-Karpman (ZK) operator* [62]:-  $C = \nu\partial/\partial v(\partial f/\partial v + vf)$

where  $\nu$  is the collision frequency,  $f_{eq}$  is the local equilibrium profile for the distribution of particles. The first operator is Bhatnagar-Gross-Krook (Krook) operator (also known as Krook model), is the simplest collisional operator. If a plasma is close to the isotropic thermal equilibrium, i.e. , close to the local equilibrium value  $f_{eq}$  (or Maxwellian  $f_0 = 1/\sqrt{(2\pi)}exp(-v^2/2)$ ), the effects of binary collisions can be modeled by means of Krook operator. The model is useful because of its simplicity and for weakly ionized plasmas ( where charge-neutral collisions are dominant), it is a good approximation, but it assumes identical relaxation times for all the moments (density, momentum, energy etc) which may not be necessarily true in all situations, hence is restrictive. In the past, Krook operator has been used to introduce the method to compute the transport coefficients (as plasma conductivities etc) [124].

The second operator under consideration is the linear Zakharov-Karpman (ZK) operator[62], whose form is equivalent to that discussed by Lenard and Bernstein [88] to study the linear evolution of plasma oscillations in presence of small-angle collisions. It has been obtained by linearizing the original Landau integral in the resonant region and assuming distribution functions are close to Maxwellian. This collision term is a simplified form of the Fokker-Planck (FP) collision operator and neglects the velocity dependence of the collision frequency, but respects important properties of the FP operator:- (a) the property of conserving the number of electrons, (b) the property of representing diffusion in velocity space, and (c) the property of yielding the steady state solution as Maxwellian in absence

of spatial anisotropies and forces. In the ZK model, collision frequency is considered low, in the sense that trapped particles bounce many times in the wave trough, before being detrapped due to a ZK collision. Both Krook and ZK operators used here do not conserve either momentum or energy. However, the Krook operator does conserve the number of particles. There are other operators with better conservation properties such as Gaussian BGK model, ESBGK model, the BGK model with velocity dependent collision frequency, Dougherty collisional operator etc [125, 126]. However, in order to perform a qualitative comparison study using simplistic collision operators, both Krook and ZK operators have been used here. Quantitatively, there will be indeed some differences between the results obtained using other operators than the results obtained from Krook and ZK operators. However, I believe that there will be no difference qualitatively.

For the collision models considered here, time evolution of the distribution function is approximated by using a splitting scheme for collisional Eulerian codes [63] that decomposes the evolution of  $f$  in three different steps. To summarize this splitting scheme, for a time step  $\Delta t$ :

- (1).  $\Delta t/2$  transport step  $\rightarrow \partial_t f + v\partial_x f + E\partial_v f = 0$ .
- (2).  $\Delta t$  collisional step  $\rightarrow \partial_t f = C(f)$ .
- (3).  $\Delta t/2$  transport step  $\rightarrow \partial_t f + v\partial_x f + E\partial_v f = 0$ .

Each transport step is in turn composed of advance, a single transport step  $\Delta t'$  can be summarized as follows:

- a).  $\Delta t'/2$   $x$ -advection  $\rightarrow \partial_t f + v\partial_x f = 0$
- b). Poisson routine  $E_s \rightarrow E_T = E_s + E_{ext}$ (if any)
- c).  $\Delta t'$   $v$ -advection  $\rightarrow \partial_t f + E_T\partial_v f = 0$ .
- d).  $\Delta t'/2$   $x$ -advection  $\rightarrow \partial_t f + v\partial_x f = 0$ .

Both  $x$ -advection and  $v$ -advection have been performed numerically using PPM advection scheme [58].

We set the simulation domain in phase space  $D(x, v) = [0, L_{max}] \times [-v_{max}^j, v_{max}^j]$ ,  $L_{max} = 2\pi/k$  is the system size and  $v_{max}^j$  is chosen sufficiently large so that velocity distribution functions approaches zero as  $|v^j|$  approaches  $v_{max}^j$ . In all these simulations, the mode with the largest wavelength that fits in the numerical domain is excited at  $t = 0$ , in order to

prevent the sideband frequency generation in the system. The phase space is discretized with  $N_x = 512$  grid points in the spatial domain and  $N_v = 5000$  in velocity domain such that there is sufficient resolution in both  $x$  and  $v^j$  grids.

## 6.3 Simulation Results

In this Section, I systematically present the numerical results of our collisional Eulerian code using two different collisional operators for various values of collision frequencies. I have considered in detail three different physical phenomena: (a) the first is collisional effects on linear Landau damping, (b) the second concerns the collisional damping of PSV excited by large amplitude initial density perturbation, and (c) the third concerns the study of chirp driven PSVs in the weakly collisional plasma.

### 6.3.1 Linear Landau Damping: Effect of Collisions

As predicted by Landau in 1946, in the absence of collisions electrostatic waves are damped exponentially in time for small amplitude of initial density perturbations. In order to study the effects of collisions on linear Landau damping, two different collisional operators:- (a) Krook operator and (b) ZK operator have been used.

In this set of simulations, the initial distribution function is considered a Maxwellian in velocity space, over which a perturbation in physical space with amplitude  $\alpha$  and wave number  $k$  is superposed,

$$f_0(x, v, t = 0) = (1 + \alpha \cos(x)) f_0(v) \quad (6.4)$$

where  $f_0(v) = 1/\sqrt{(2\pi)} \exp(-v^2/2)$  is the initial Maxwellian velocity distribution function. Here, the plasma is perturbed with a small amplitude initial density perturbation for two different collisional operators:-

(1) In the first set [Table ??], Krook operator is used with the following set of parameters:-

CHAPTER 6. EULERIAN SIMULATIONS OF COLLISIONAL EFFECTS ON  
ELECTROSTATIC PHASE SPACE VORTICES

---

(2) In the second set of simulations [Table ??], ZK operator is used for the following

Table 6.1: Krook operator for LLD simulations

$k$	$\alpha$	$\nu$
0.4	$1 \times 10^{-2}$	$0, 1 \times 10^{-5}, 1 \times 10^{-3}, 1 \times 10^{-2}, 1 \times 10^{-1}$
0.5	$5 \times 10^{-3}$	$0, 1 \times 10^{-2}, 5 \times 10^{-2}, 1 \times 10^{-1}$

parameters:-

In Fig.??, logarithmic of time evolution of amplitude of the first fundamental harmonic

Table 6.2: ZK operator for LLD simulations

$k$	$\alpha$	$\nu$
0.4	$1 \times 10^{-2}$	$0, 1 \times 10^{-4}, 1 \times 10^{-5}, 1 \times 10^{-6}$

of the electric field  $E_{k=1}$ , denoted by  $E1$ , is plotted (or linear Landau damping rate  $\gamma$ ) for  $k = 0.4$  and  $k = 0.5$  for various values of collision frequency  $\nu$  for Krook operator. As the collision frequency increases, the damping of the plasma wave also increases. The corresponding values have been shown in Table ?? and ?. In Fig.??,  $\gamma$  is plotted for  $k = 0.4$  and  $k = 0.5$  for various values of collision frequency  $\nu$  for ZK operator. In ZK operator does not affect the linear Landau damping rate  $\gamma$  (See Table??) in the linear regime (i.e. before  $\tau_{bounce} = 2\pi/\sqrt{\alpha} = 62.831$ , after which the linear solution breaks down and nonlinear phenomena become prominent). The effect of collisional frequency with ZK operator comes into play in the non-linear regime where plasma wave damps faster with increase in collision frequency. Moreover, for small collision frequency (for eg.  $\nu = 10^{-5}$ ), the ZK operator is much more effective than Krook operator at long time evolution.

Table 6.3: Krook operator for  $k = 0.4$

Table 6.4: Krook operator for  $k = 0.5$

$\nu$	$\omega_r$	$\gamma$	$\nu$	$\omega_r$	$\gamma$
0.00	1.285	-0.06612	0.00	1.415	-0.15339
0.00001	1.285	-0.06612	0.00001	1.415	-0.15339
0.001	1.285	-0.06724	0.01	1.415	-0.1634
0.01	1.285	-0.07639	0.05	1.415	-0.20331
0.1	1.285	-0.16603	0.1	1.415	-0.25215

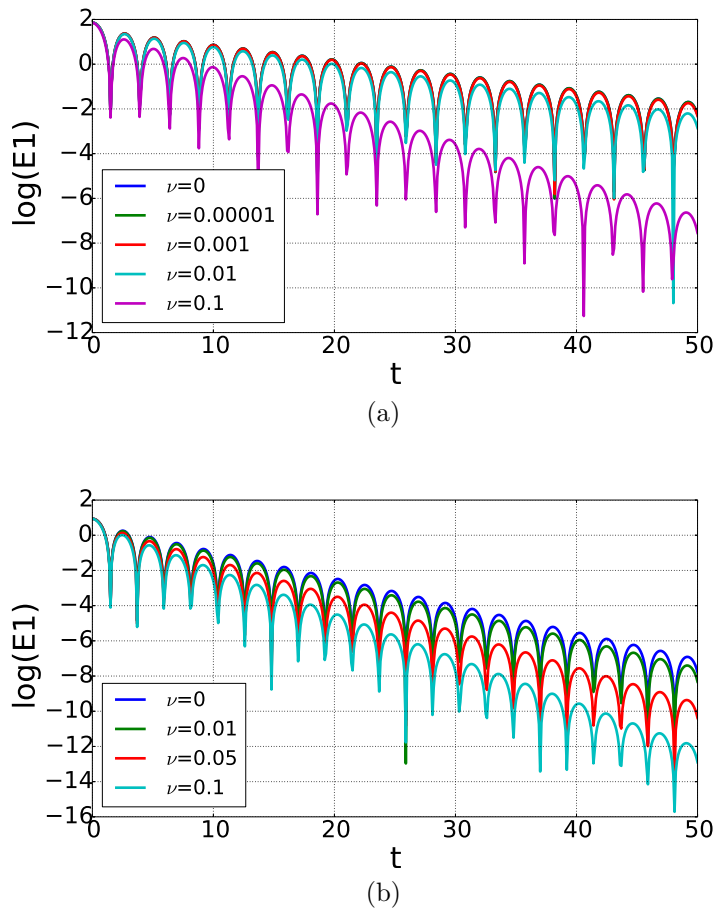


Figure 6.1: Linear Landau Damping (LLD)- Plots of logarithmic of first fundamental harmonic  $\log|E1|$  with time, when collisions are applied through Krook operator:- (a)  $k = 0.4$ ,  $\alpha_0 = 0.01$  (b)  $k = 0.5$ ,  $\alpha_0 = 0.005$ .

### 6.3.2 Non-Linear Landau Damping:- Role of Collisions

As described earlier, in collisionless plasmas, when the amplitude of perturbation becomes larger, contribution from the nonlinear terms become more significant and the behavior deviates from uniform exponential damping. This causes trapping nonlinearity which leads to form coherent structures in phase-space[10]. Electrons with velocity  $v_\phi \simeq \omega_r/k$ , resonate with the plasma wave field and energy exchange takes place between resonant particles and wave. This results in the flattening of the distribution function around  $v_\phi \simeq \omega_r/k$ . For eg.,  $k = 0.4$ , when plasma is perturbed with a nonlinear amplitude of perturbation  $\alpha_0 = 0.05$ , the velocity distribution function gets flattened near 3.21 and a corresponding phase space vortex is found at  $v_\phi = 3.21$ . This implies that there is a prominent potential well formed due to trapped particle effects. However, when the plasma

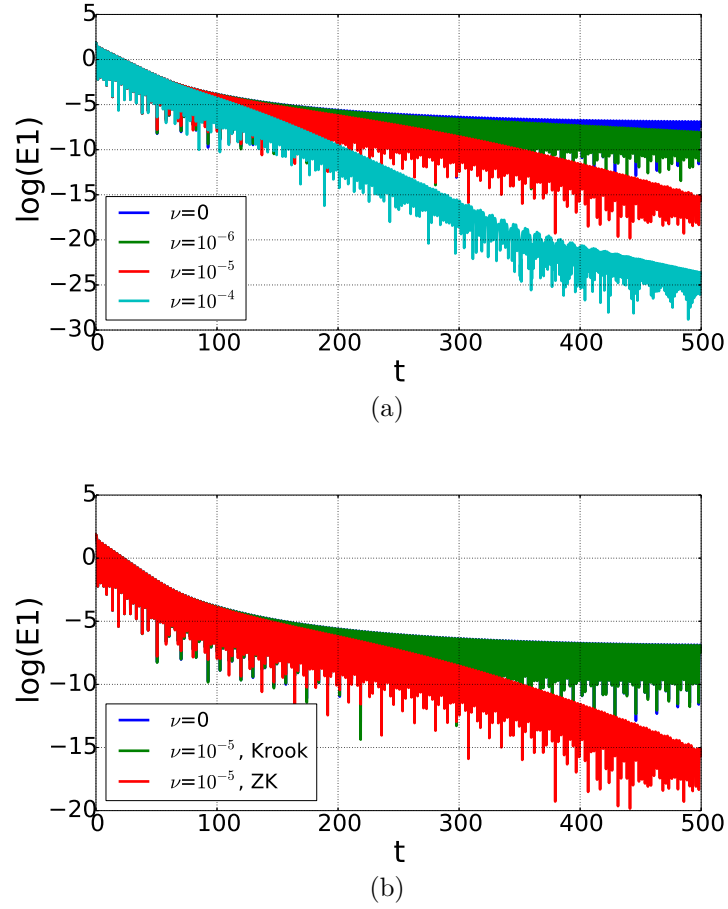


Figure 6.2: Linear Landau Damping (LLD)- Plots of  $\log|E1|$  with time for  $k = 0.4$ ,  $\alpha_0 = 0.01$  and  $\nu = 10^{-5}$ , (a) when collisions are applied through ZK operator, (b) Comparison between Krook and ZK operators.

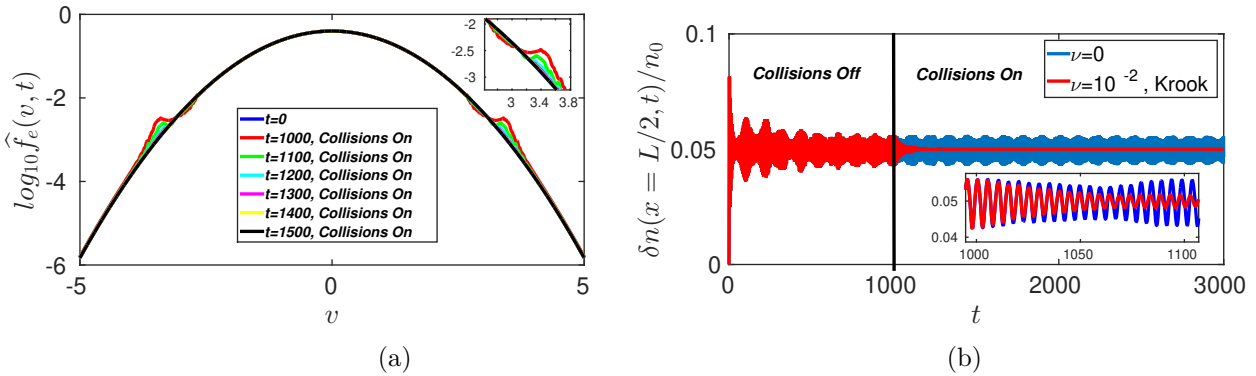


Figure 6.3: Collisional damping of PSVs, when collisions are applied through Krook operator and turned on at  $t = 1000$  for  $k = 0.4$ ,  $\alpha = 0.05$  and  $\nu = 0.01$ : (a) Plot of evolution of spatially averaged electron velocity distribution  $\widehat{f}_e(v)$ , and (b) Plot of excess density fraction  $\delta n/n_0$  evolution at  $x = L/2$  with time. The vertical black line indicated the time at which collisions are turned on i.e. at  $t = 1000$ .

is not fully collisionless, the possibility of sustainability of such potential well with trapped

Table 6.5: ZK operator for  $k = 0.4$

$\nu$	$\omega_r$	$\gamma$
0.00	1.285	-0.06612
$10^{-6}$	1.285	-0.06612
$10^{-5}$	1.285	-0.06612
$10^{-4}$	1.285	-0.06612

particles, depends on the competition between nonlinear trapping oscillations, which try to make the velocity distribution flat around the phase velocity of the structure and collisions tends to restore the Maxwellian velocity distribution.

In the following set of simulations, the initial distribution function is considered a

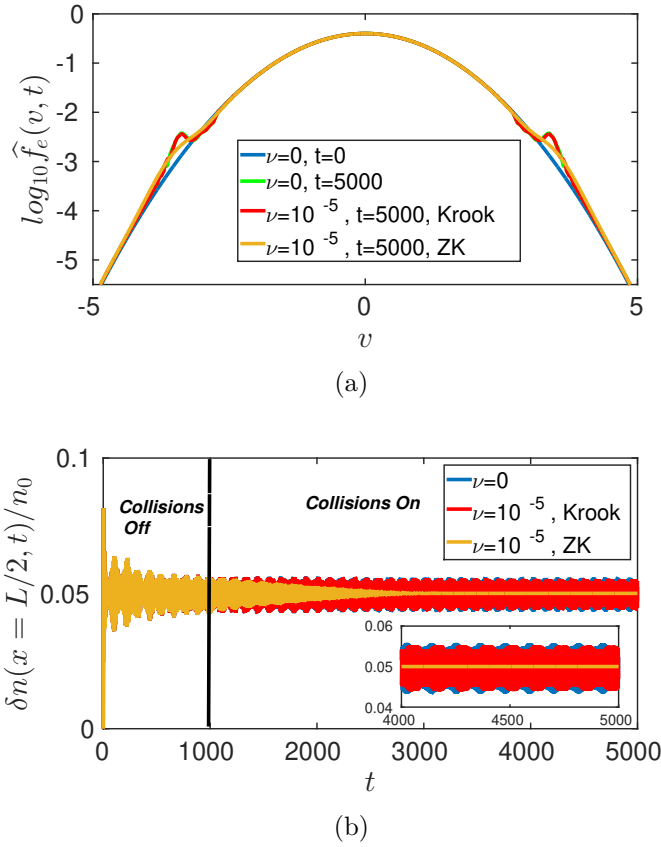


Figure 6.4: Collisional damping of PSVs, when collisions are applied through both Krook and ZK operators for  $k = 0.4$ ,  $\alpha = 0.05$  and  $\nu = 10^{-5}$  and the collisions are turned on at  $t = 1000$ : (a) Plot of evolution of spatially averaged velocity distribution  $\hat{f}(v)$ , and (b) Plot of excess density fraction evolution at  $x = L/2$  with time.

Maxwellian in velocity space, over which a perturbation in physical space with amplitude  $\alpha = 0.05$  and wave number  $k = 0.4$  is superposed, given by:-  $f_0(x, v, t = 0) = (1 + \alpha \cos(x))f_0(v)1/\sqrt{(2\pi)}\exp(-v^2/2)$ . This simulation is divided into two

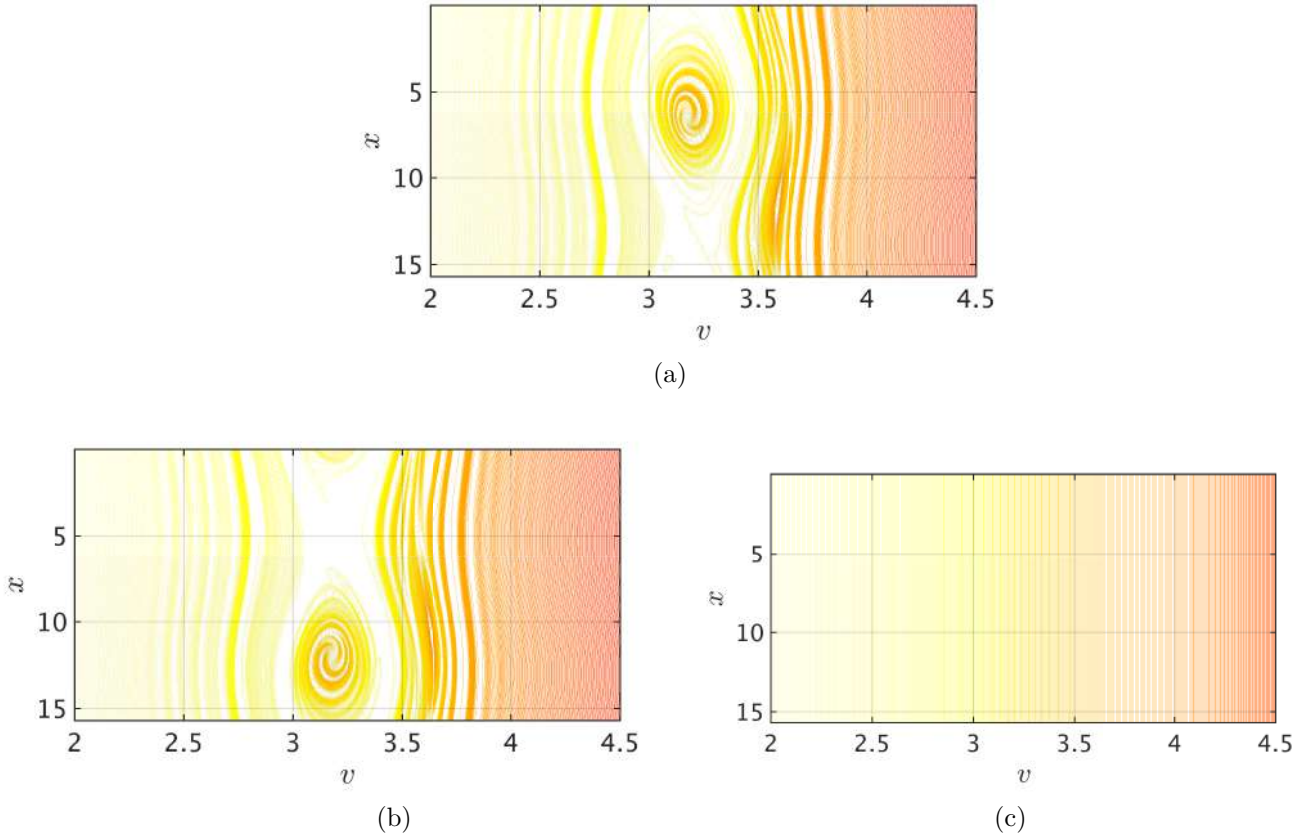


Figure 6.5: Phase space plot of  $f(x, v)$  at  $t = 5000$ , where an initial density perturbation of non-linear amplitude ( $\alpha = 0.05$ ,  $k = 0.4$ ) is applied at  $t = 0$  and the collisions are turned on at  $t = 1000$  for following cases:- (a)  $\nu = 0$ , (b)  $\nu = 10^{-5}$ , Krook operator and (c)  $\nu = 10^{-5}$ , ZK operator

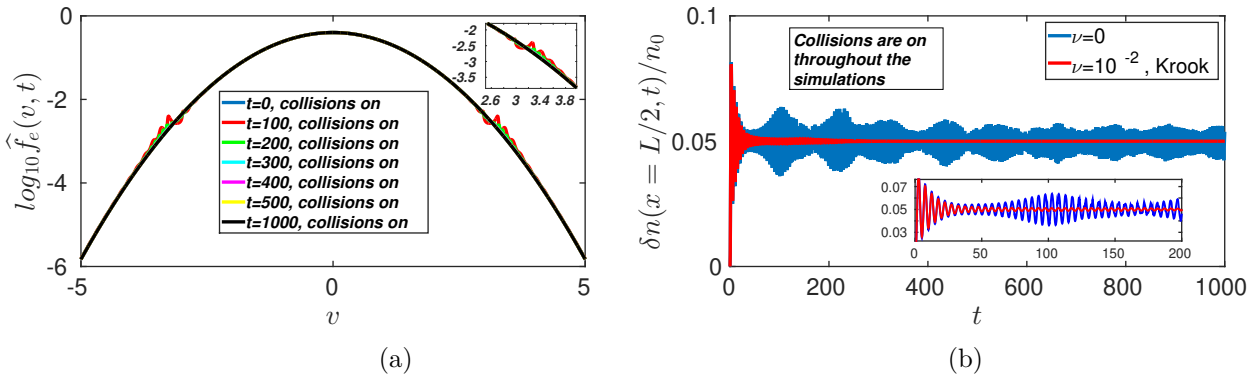


Figure 6.6: Collisional damping of PSVs, when collisions are turned on from the start (i.e. at  $t = 0$  onwards) and kept on throughout the simulation. Collisions are applied through Krook operator for  $k = 0.4$ ,  $\alpha = 0.05$  and  $\nu = 0.01$ : (a) Plot of evolution of spatially averaged electron velocity distribution  $\widehat{f}_e(v)$ , and (b) Plot of excess density fraction  $\delta n/n_0$  evolution at  $x = L/2$  with time.

steps. As a first step, an initial density perturbation is given of a non-linear amplitude in the absence of collisions, in order to form the plateau in the resonant region of the

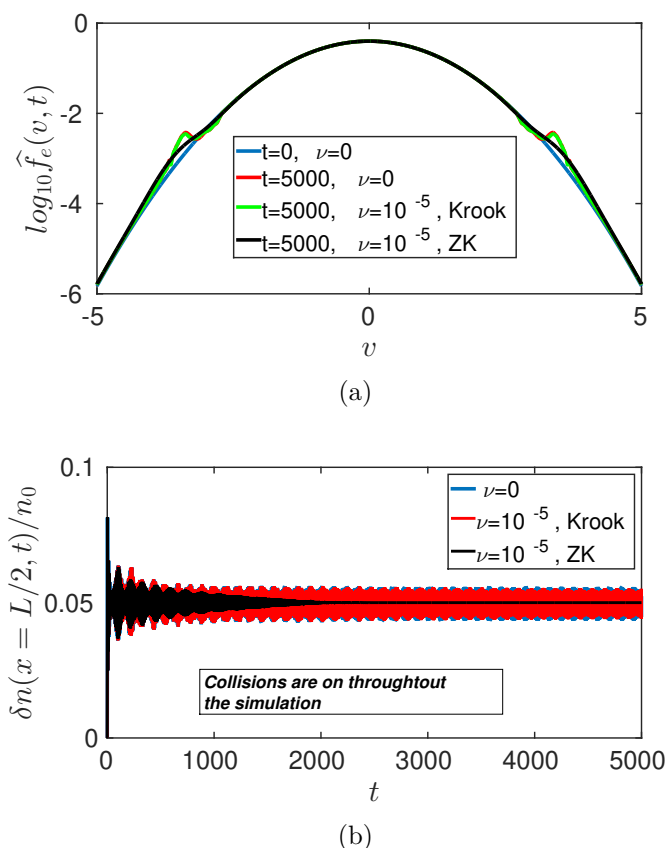


Figure 6.7: Collisional damping of PSVs, when collisions are applied from the start (i.e. at  $t = 0$  onwards) and kept on throughout the simulation. Collisions are applied using both Krook and ZK operators for  $k = 0.4$ ,  $\alpha = 0.05$  and  $\nu = 10^{-5}$ : (a) Plot of evolution of spatially averaged velocity distribution  $\hat{f}(v)$ , and (b) Plot of excess density  $\delta n/n_0$  fraction evolution at  $x = L/2$  with time.

electron distribution function, turn off Landau damping, and finally excite the phase space vortices. Once the PSV structure is formed and the electric field “rings” at a nearly constant amplitude in time [10], I dub this “ring” as “Manfredi ringing”. As a second step, collisions are turned on and the collisional damping of the amplitude of the PSV is observed, created through the initial density perturbation through collisionless nonlinear process.

In the simulations presented in this Section, collisions are included using two operators, namely: (a) Krook ( $\nu = 0.01, 10^{-5}$ ) operator, and (b) ZK ( $10^{-5}$ ) operator. In the first case, an initial density perturbation is applied to excite phase space vortices in the resonant region and let the plasma evolve till  $t = 1000$ . Then collisions are turned by applying the

one of the collision operators. Here, two different cases has been considered:- (i) for  $\nu = 0.01$  with Krook operator, and (ii) for  $\nu = 10^{-5}$  with both Krook and ZK operators. In Fig.??, the time evolution of space averaged velocity distribution function and the time evolution of excess density fraction  $\delta n/n_0$ , (as defined by  $\delta n(x, t)/n_0 = \int f(x, v, t)dv - \int f_0(v)dv$ ), at  $x = L/2$ , have been shown where the Krook operator is applied with collision frequency  $\nu = 0.01$ . In response to the initial non-linear amplitude perturbation, excess particle density starts with a maximum value. Then the system relaxes and saturates to attain a certain value of excess density fraction and remains almost the same due to formation of PSV. This can also be seen as formation of plateau in the velocity distribution function. Once the PSV is formed, as soon as the collisions are turned on at  $t = 1000$ , the width of plateau and the excess density fraction decrease and the typical vortex structure, signature of the trapping of particles in the wave potential well gradually vanishes due to detrapping of trapped particles and the velocity distribution becomes Maxwellian at  $t = 1500$ . In other words, the nonlinear plasma mode disappear for  $t > 1500$ .

In Fig.??, I report the simulations for smaller collision frequency i.e.  $\nu = 10^{-5}$  applied

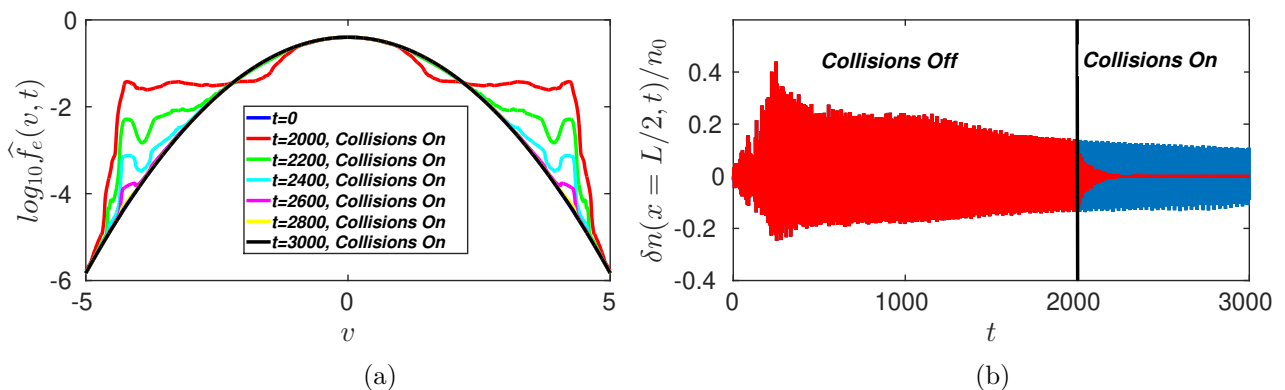


Figure 6.8: Collisional damping of Chirp driven giant PSVs, when plasma is driven with a downward frequency chirp for  $\Delta t_d = 250$  and collisions are applied through Krook and turned on at  $t = 2000$  for  $k = 0.4$ , and  $\nu = 0.01$ : (a) Plot of evolution of spatially averaged velocity distribution  $\hat{f}(v)$ , and (b) Plot of excess density fraction evolution at  $x = L/2$  with time.

using two different operators: Krook and ZK. The time evolution of space averaged distribution, in Fig.??(a), shows that when the collisions are turned on at  $t = 1000$ , with collision frequency  $\nu = 10^{-5}$ , the ZK operator is more effective than Krook operator. The

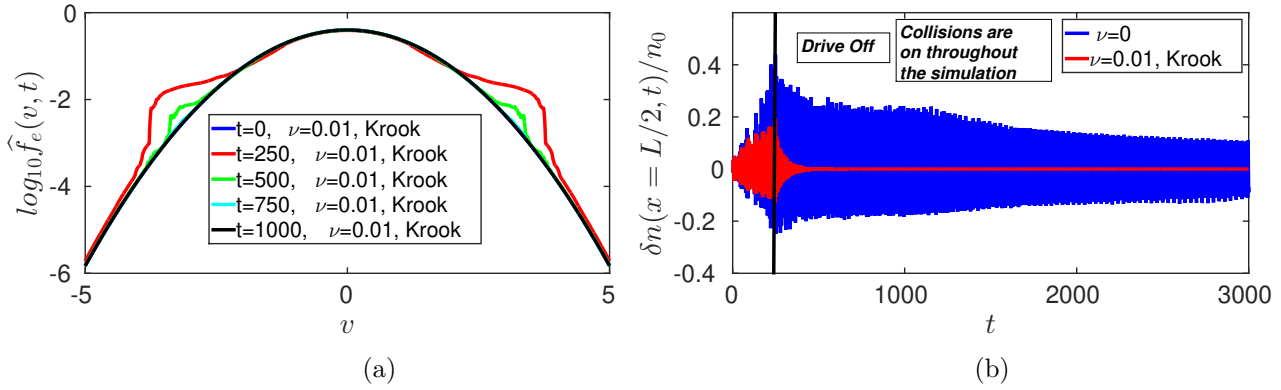


Figure 6.9: Collisional damping of Chirp driven giant PSVs, when plasma is driven with a downward frequency chirp for  $\Delta t_d = 250$  and collisions are applied from the start (i.e. at  $t = 0$  onwards) and kept on throughout the simulation. Collisions are applied through Krook for  $k = 0.4$ , and  $\nu = 0.01$ : (a) Plot of evolution of spatially averaged velocity distribution  $\hat{f}(v)$ , and (b) Plot of excess density fraction evolution at  $x = L/2$  with time.

“plateau” region remains same for both without collisions ( $\nu = 0$ ) and with Krook collisions of frequency  $\nu = 10^{-5}$ . However, for ZK operator, collisional effects are strongly visible which causes the detrapping of all trapped particles and velocity distribution function tends towards the Maxwellian.

In Fig.??, the phase-space contour plots of  $f(x, v, t)$  have been shown that were captured at  $t = 5000$  in the trapped region around the wave phase velocity for different cases:- (a)  $\nu = 0$ , (b)  $\nu = 10^{-5}$ , Krook operator, and (c)  $\nu = 10^{-5}$ , ZK operator. At  $t = 1000$ , collisions are turned on in the simulation and they start playing a crucial role in the time evolution of the system. For Krook operator, such low collisional frequency does not affect the trapped particle distribution and the PSV. However, for ZK operator, collisional effects are strongly visible in phase space, even though the value of the collision frequency is very small. At  $t = 5000$  the phase space structure, totally disappear due to a collisional phase mixing and the separatrix between trapped region and free region is no more visible in the long time limit, meaning that particles, that were trapped in the wave trough, are detrapped by the effect of diffusion in velocity. In the second case, the collisions are present from the initial time (i.e.  $t = 0$  onwards) while an initial density perturbation is applied to excite phase space vortices in the resonant region and let the plasma evolve in

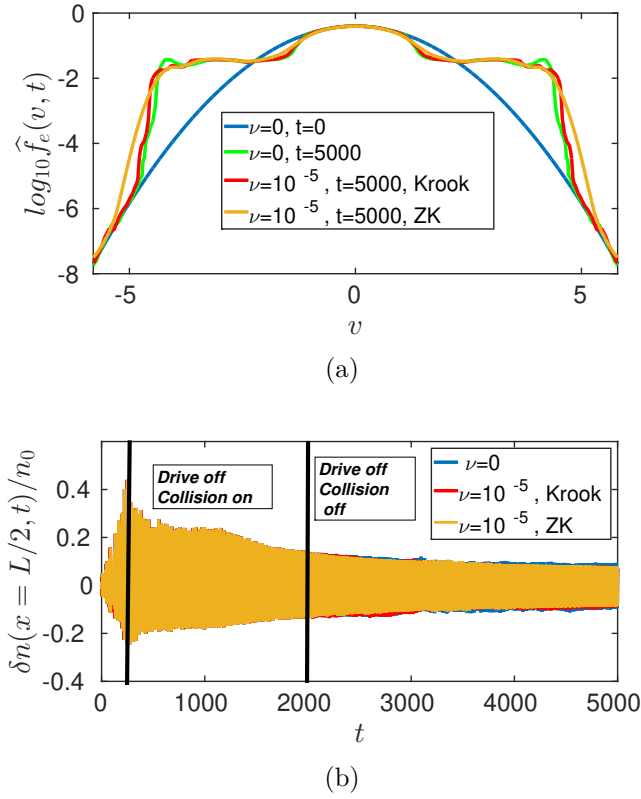


Figure 6.10: Collisional damping of Chirp driven giant PSVs, when plasma is driven with a downward frequency chirp for  $\Delta t_d = 250$  and collisions are applied through Krook and turned on at  $t = 2000$  for  $k = 0.4$ , and  $\nu = 10^{-5}$ : (a) Plot of evolution of spatially averaged velocity distribution  $\hat{f}(v)$ , and (b) Plot of excess density fraction evolution at  $x = L/2$  with time.

the presence of collisions. Here, two different cases has been considered:- (i) for  $\nu = 0.01$  with Krook operator, and (ii) for  $\nu = 10^{-5}$  with both Krook and ZK operators. In Fig.??, the time evolution of space averaged velocity distribution function and the time evolution of excess density fraction  $\delta n/n_0$ , (as defined by  $\delta n(x, t)/n_0 = \int f(x, v, t)dv - \int f_0(v)dv$ ), at  $x = L/2$ , have been shown where the Krook operator is applied with collision frequency  $\nu = 0.01$  from the initial time. In response to the initial non-linear amplitude perturbation, excess particle density starts with a maximum value. However, in the presence of collisions the excess density fraction decrease rapidly and the plasma wave disappears completely for  $t > 300$ . In fig.??, the same numerical experiment is done for both Krook and ZK operator, with collision frequency  $\nu = 10^{-5}$ , is shown. In this case results are similar to what shown in Fig.?? where the ZK operator is more effective than Krook operator. The “plateau” region forms for both cases, without collisions ( $\nu = 0$ ) and with Krook collisions of frequency  $\nu = 10^{-5}$ . However, for ZK operator, collisional effects are strongly visible

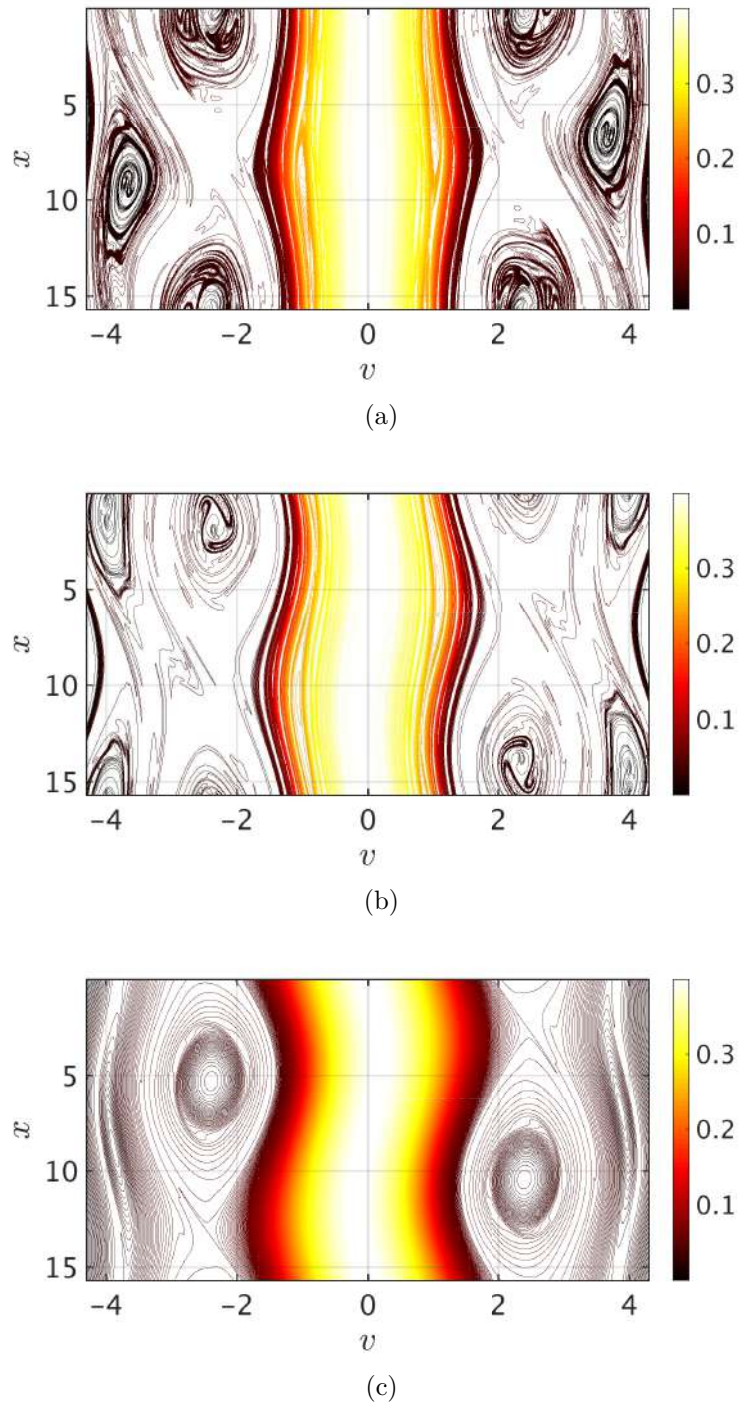


Figure 6.11: Phase space plot of  $f(x, v)$  at  $t = 5000$ , where the plasma is driven with a downward frequency chirp for  $\Delta t_d = 250$  to excite chirp driven giant PSVs for  $k = 0.4$ , and the collisions are turned on at  $t = 2000$  for following cases:- (a)  $\nu = 0$ , (b)  $\nu = 10^{-5}$ , Krook operator and (c)  $\nu = 10^{-5}$ , ZK operator

which causes the plasma wave to disappear completely and velocity distribution function tends towards the Maxwellian.

### 6.3.3 Collisional Effects On Chirp Driven PSVs

In this Section, the effect of collisions on the driven phase space vortices has been studied using Krook and ZK operators. As described earlier in Chapter[3], when a homogeneous Maxwellian plasma is driven with an time dependent external drive or chirp of an infinitesimal amplitude, it leads to steady state giant PSV, with multiple extrema due to embedded holes and clumps. These PSVs were shown to survive long after the external drive was turned off. In the present set, simulations are again divided into two steps. As a first step, the plasma is driven with a small amplitude external drive of time dependent frequency (or chirp) in the absence of collisions, in order to form the giant driven multiextrema phase space vortices. Once the PSVs are formed, the driver is turned off and the plasma is evolved further for several  $\omega_{pe}^{-1}$  times such that the electric field “rings” at a nearly constant amplitude in time. As a second step, I turn on collisions and observe the effects of collisions on these PSVs, previously created through the driving (or chirp) process.

In the simulations presented in this Section as before, collisions are modeled using two operators, namely: (a) Krook ( $\nu = 0.01, 10^{-5}$ ) operator and (b) ZK ( $10^{-5}$ ) operator. As before, two different cases has been considered here:- (i) for  $\nu = 0.01$  with Krook operator, and (ii) for  $\nu = 10^{-5}$  with both Krook and ZK operators.

For the first case, starting with a Maxwellian homogeneous plasma, driven by an external downward frequency chirp which is applied to the plasma right at  $t = 0$  for time duration  $\Delta t_d$  till  $t = t_1$  from  $\omega_{high}/\omega_2$  to  $\omega_{low}/\omega_1$ . The parameters for simulations are:-  $k = 0.4$ ,  $E_0 = 0.025$ ,  $\Delta t_d = 250$ ,  $\omega_{high} = 2$ ,  $\omega_{low} = 1$ . The chirp parameter are  $\alpha = -4 \times 10^{-3}$  and  $\beta = 2$ . In order for the transients to relax the system is evolved till  $t_2 = 2000$ . The steady state phase space vortex structure thus created is a combination of both untrapped and trapped particle dynamics during chirp. This phase space structure exhibits several interesting features, such as, large hole/ PSV structure contains peaked spikes and holes embedded in it along with a “shark”-like structure, i.e., a bunch of particles moving together within the giant phase space vortices. At  $t = 2000$ , collisions are turned on using Krook operator with collision frequency  $\nu = 0.01$  and plasma is evolved till  $t = 3000$ . In Fig.??, the time evolution of space averaged velocity distribution function and the time evolution

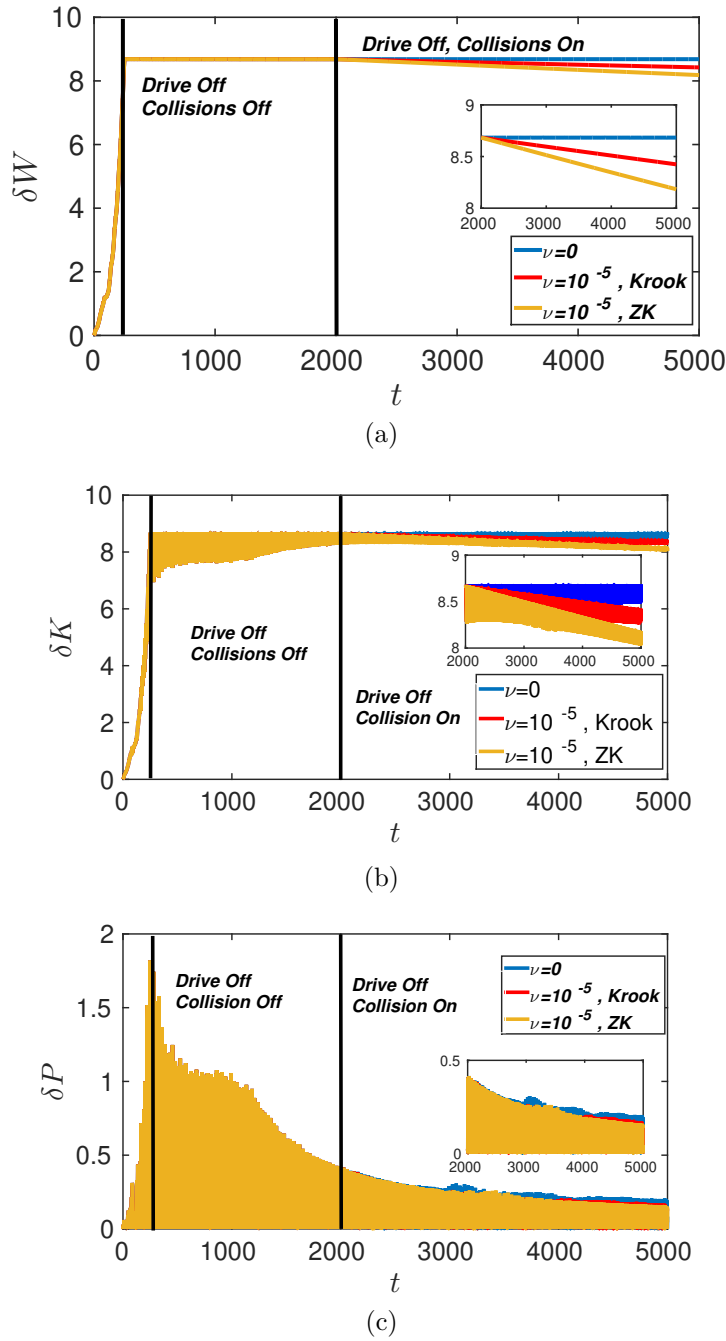


Figure 6.12: Plots of relative energy (a)  $\delta W$ , (b)  $\delta K$ , (c)  $\delta P$  with time, when plasma is driven with a downward frequency chirp from  $\omega_{high} = 2$  to  $\omega_{low} = 1$  for  $\delta t_d = 250$  and collisions are turned on at  $t = 2000$  for the following cases: (i)  $\nu = 0$ , (ii)  $\nu = 10^{-5}$ , Krook operator and (iii)  $\nu = 10^{-5}$ , ZK operator

of excess density at  $x = L/2$  have been shown where the Krook operator is applied with collision frequency  $\nu = 0.01$ . In response to the small amplitude chirp, excess particle density increases linearly in time till the drive is on. The growth of excess density fraction is arrested when the drive is turned off. Then the system relaxes and saturates to attain a

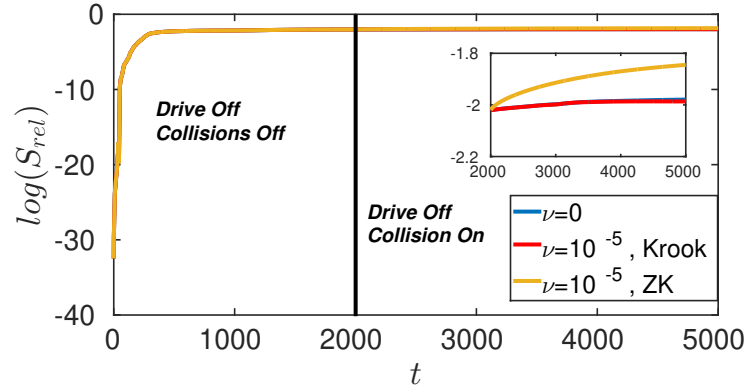


Figure 6.13: Plot of relative entropy  $S_{rel}$  with time, where plasma is driven with a downward frequency chirp from  $\omega_{high} = 2$  to  $\omega_{low} = 1$  for  $\Delta t_d = 250$  and collisions are turned on at  $t = 2000$  for the following cases: (i)  $\nu = 0$ , (ii)  $\nu = 10^{-5}$ , Krook operator and (iii)  $\nu = 10^{-5}$ , ZK operator

certain value of excess density fraction and remains almost the same till the collisions are absent. The time at which collisions are turned on in the simulation is indicated in the figure by a vertical line. Once the PSVs are formed and the steady state is obtained, the collisions are turned on at  $t = 2000$ , the width of plateau and the excess density fraction decrease and the typical vortex structure, signature of the trapping of particles in the wave potential well gradually vanishes due to detrapping of trapped particles and the velocity distribution becomes Maxwellian at  $t = 3000$ . The nonlinear plasma structure and the trapping disappears at  $t = 3000$ .

The same numerical experiment ( $\nu = 0.01$ , Krook operator) as above is performed for the case where collisions are present from the initial time (at  $t = 0$  onwards-) till the end of the simulation ( $t = 3000$ ). The initial homogeneous Maxwellian plasma is driven by an external downward frequency chirp for time duration  $\Delta t_d$  with the same simulation parameters:-  $k = 0.4$ ,  $E_0 = 0.025$ ,  $\Delta t_d = 250$ ,  $\omega_{high} = 2$ ,  $\omega_{low} = 1$ . The chirp parameter are  $\alpha = -4 \times 10^{-3}$  and  $\beta = 2$ . In Fig.??, the comparison of time evolution of space averaged velocity distribution and comparison of time evolution of excess density at  $x = L/2$  has been shown for  $\nu = 0.01$ , Krook operator, where collisions are present from the initial time. As one can observe, during the external drive time ( $0 \leq t \leq 250$ ), the collisions dominates over drive, which leads to very strong effect on the formation of chirp driven

PSVs. After the drive is turned off, the growth of excess density fraction is arrested for where the maximum value of  $\delta n/n_0$  attained by collisional case is much less than the  $\nu = 0$  case. After the drive is turned off, the collisionless system relaxes and saturates to attain a certain steady state. However, for the collisional case ( $\nu = 0.01$ ), the excess density fraction decrease rapidly and the signature of the trapping of particles in the wave potential well vanishes due to detrapping of trapped particles and the velocity distribution becomes Maxwellian. The nonlinear plasma structure and the trapping disappears completely.

In the second case, collisions are applied for smaller collision frequency  $\nu = 10^{-5}$ . In Fig.??, the effect of collisions on the time evolution of space averaged velocity distribution function is displayed for  $\nu = 10^{-5}$ . In comparison to  $\nu = 0$  case, when low frequency collisions are applied through Krook operator, such small collision frequency  $\nu = 10^{-5}$  have very little effect on the excess density fraction and small velocity scale details. However, with ZK operator, with time collisions smooth out small velocity scale distortions, yet retain large excess density fractions. It can be clearly seen in the phase space plots of  $f(x, v, t)$  (Fig.??), where the steady state structure survives long time after the drive is off for  $\nu = 0$  (here, at  $t = 5000$ ). For Krook operator with collision frequency  $\nu = 10^{-5}$ , small velocity scale distortions can still be seen at  $t = 5000$ . However, for ZK operator with collision frequency  $\nu = 10^{-5}$ , small velocity scale distortions smooth out completely, yet the separatrix between trapped region and free region is clearly visible which means large amount of particles are still trapped in the wave trough unaffected by the the effect of diffusion in velocity space.

The total energy of the system is defined as:  $W(t) = K(t) + P(t)$ , where kinetic energy is computed as  $K(t) = (1/2) \int \int v^2 f(x, v, t) dx dv$  and potential energy computed as  $P(t) = (1/2) \int E^2(x, t) dx$ . In Fig. ??, (a) the total relative energy  $\delta W = W(t) - W(0)$ , (b) the total relative kinetic energy  $\delta K = K(t) - K(0)$  and (c) the total relative potential energy  $\delta P = P(t) - P(0)$  are plotted. It is clear that as the chirp frequency is swept downwards, both relative kinetic energy and relative potential energy of the system increases which reflects the increase in untrapped and trapped particle populations, respectively. The growth of these relative energies is arrested when the drive is turned off. Then the system

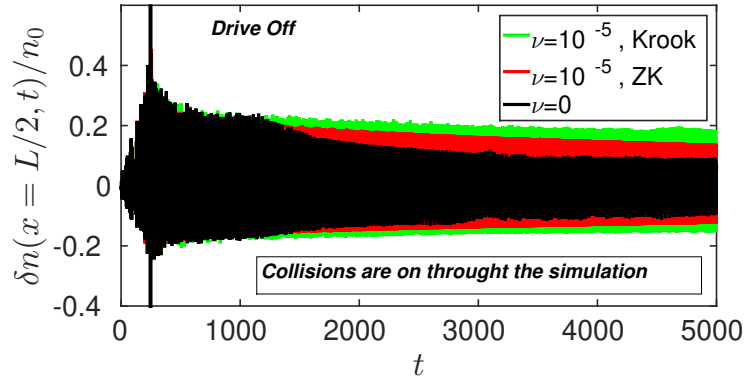


Figure 6.14: Plot of excess density fraction evolution at  $x = L/2$  with time. The plasma is driven with a downward frequency chirp for  $\Delta t_d = 250$  to excite chirp driven giant PSVs for  $k = 0.4$ , and the collisions are on from the start ( $t = 0$ ) till the end of the simulation ( $t = 5000$ ) for following cases:- (a)  $\nu = 0$ , (b)  $\nu = 10^{-5}$ , Krook operator and (c)  $\nu = 10^{-5}$ , ZK operator

relaxes and saturates to attain a certain value of  $\delta W$ ,  $\delta K$ ,  $\delta P$  and remains almost the same till the collisions are absent i.e. till  $t = 2000$ . At  $t = 2000$ , collisions are turned on, indicated in the figure by a vertical line, all three values of  $\delta W$ ,  $\delta K$  and  $\delta P$  start decreasing. As can be seen in Fig. ??, (a)  $\delta W$ ,  $\delta K$  and  $\delta P$  decrease faster for ZK operator than the Krook operator, (b) difference in decrement of  $\delta K$  for both the operators is much larger than the difference in decrement of  $\delta P$ . The decrease in  $\delta K$  indicates the decrease in the energy of untrapped region surrounding the PSVs and causes to smooth out the small velocity scale distortions. However, there is not so much difference in  $\delta P$  which indicates the presence of the large amount of trapping fraction.

The entropy of the system is given by:

$$S(t) = - \int_0^L \int_{-v_{max}}^{+v_{max}} f(x, v, t) \log f(x, v, t) dv dx \quad (6.5)$$

It is plotted as relative entropy [See Fig.(??), defined as  $S_{rel} = (S(t) - S(0))/S(0)$  with time. For a collisionless plasma  $dS/dt = 0$ . However, because of the numerical scheme, entropy does increase with time (which is a measure of finite phase space grid size effects in simulation) and then saturates. Here, the entropy is seen to grow when the drive is on but saturates as soon as the drive is turned off. Also, the simulation is extended till  $t = 2000$  in order to confirm the formation of a steady-state solution. At  $t = 2000$ , when

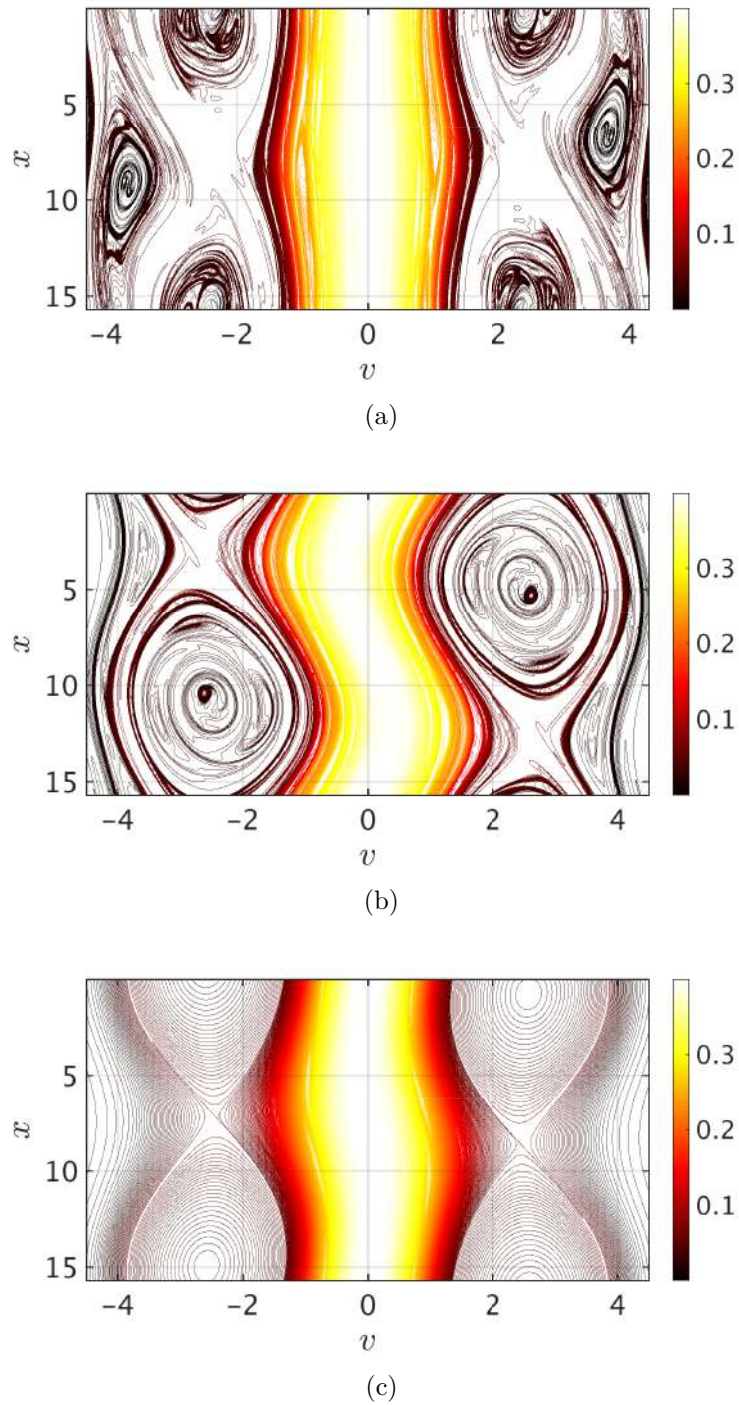


Figure 6.15: Phase space plot of  $f(x, v)$  at  $t = 5000$ , where the plasma is driven with a downward frequency chirp for  $\Delta t_d = 250$  to excite chirp driven giant PSVs for  $k = 0.4$ , and the collisions are on from the start ( $t = 0$ ) till the end of the simulation ( $t = 5000$ ) for following cases:- (a)  $\nu = 0$ , (b)  $\nu = 10^{-5}$ , Krook operator and (c)  $\nu = 10^{-5}$ , ZK operator

the collisions are turned on, the relative entropy is seen to grow again due to inclusion of weak collisions.

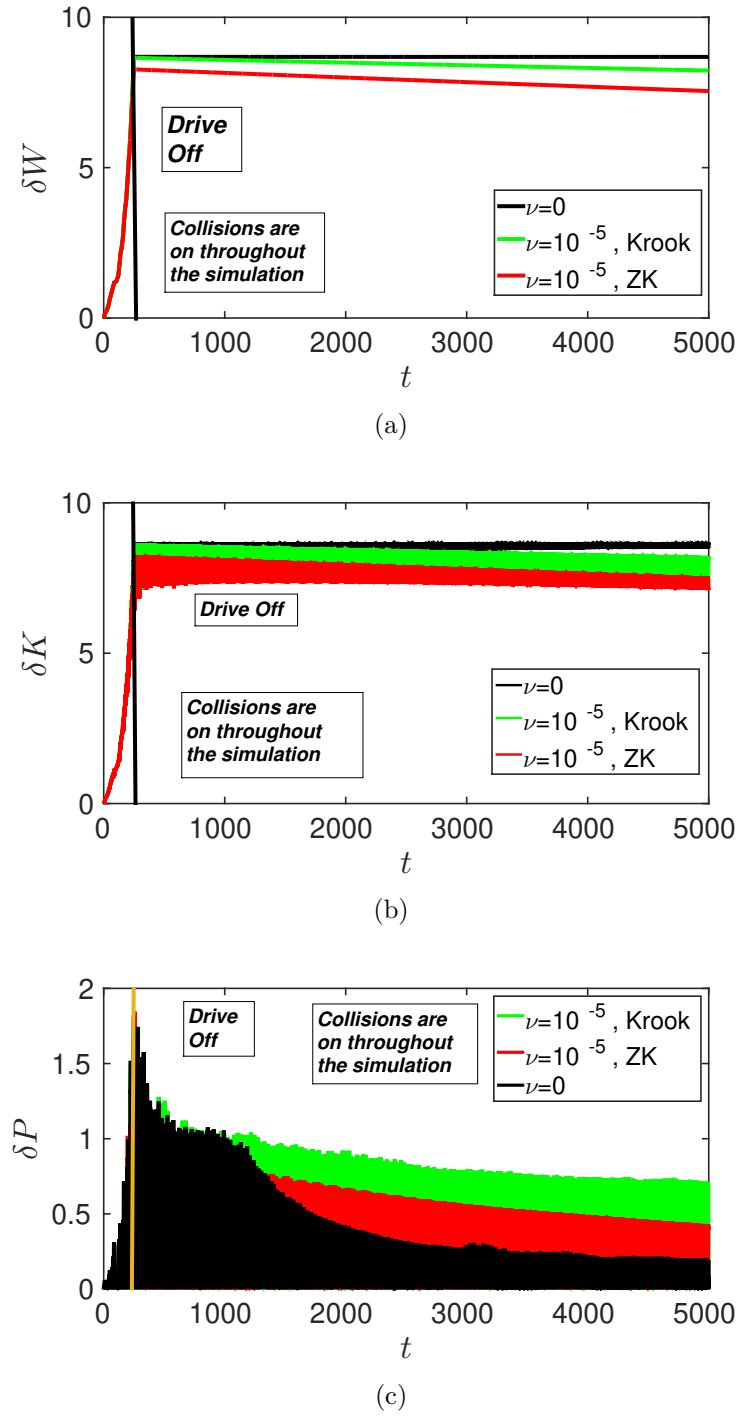
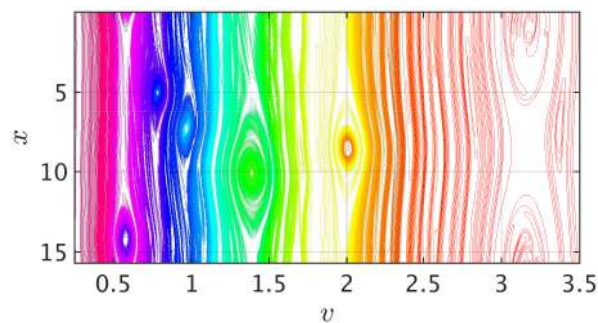
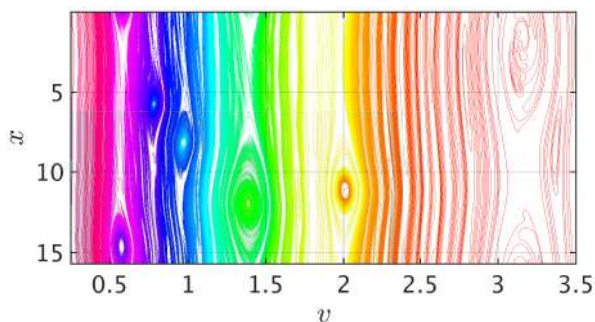


Figure 6.16: Plots of relative energy (a)  $\delta W$ , (b)  $\delta K$ , (c)  $\delta P$  with time, when plasma is driven with a downward frequency chirp from  $\omega_{high} = 2$  to  $\omega_{low} = 1$  for  $\delta t_d = 250$  and the collisions are on from the start ( $t = 0$ ) till the end of the simulation ( $t = 5000$ ), for the following cases: (i)  $\nu = 0$ , (ii)  $\nu = 10^{-5}$ , Krook operator and (iii)  $\nu = 10^{-5}$ , ZK operator

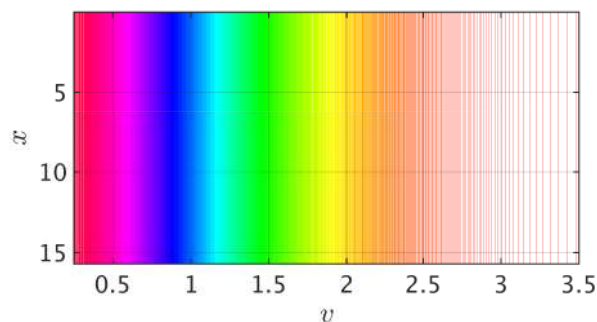
For the third case, collisions are present from the initial time (at  $t = 0$  onwards-) till the



(a)



(b)



(c)

Figure 6.17: Phase space plot of  $f(x, v)$  at  $t = 5000$ , where the plasma is driven with a downward frequency chirp for  $\Delta t_d = 250$  to excite chirp driven “honeycomb”-like PSVs for  $k = 0.4$ , and the collisions are turned on at  $t = 2000$  for following cases:- (a)  $\nu = 0$ , (b)  $\nu = 10^{-5}$ , Krook operator and (c)  $\nu = 10^{-5}$ , ZK operator.

end of the simulation ( $t = 5000$ ). The initial homogeneous Maxwellian plasma is driven by an external downward frequency chirp for time duration  $\Delta t_d$  with the same simulation parameters:-  $k = 0.4$ ,  $E_0 = 0.025$ ,  $\Delta t_d = 250$ ,  $\omega_{high} = 2$ ,  $\omega_{low} = 1$ . The chirp parameter are  $\alpha = -4 \times 10^{-3}$  and  $\beta = 2$ . In Fig.??, the comparison of time evolution of excess density at  $x = L/2$  has been shown for following cases:- (a)  $\nu = 0$ , (b)  $\nu = 10^{-5}$ , Krook operator and (c)  $\nu = 10^{-5}$ , ZK operator. During the external drive time ( $0 \leq t \leq 250$ ), the drive dominates over collisions, which leads to very little effect on the formation of steady state PSVs. After the drive is turned off, the growth of excess density fraction is arrested for all the cases, after which collisions start to play a crucial role in the saturation of the transients and the PSVs formed. Then, the system relaxes and saturates to attain a certain steady state which is different for all three cases. With both Krook and ZK operators, collisions smooth out small velocity scale distortions, yet retain large excess density fractions. However, unlike the second case [see Fig. ??(b)], where collisions were

turned on after the steady state is achieved, these operators affects the total density fraction in reverse way, where with Krook operator, maximum trapped fraction is observed to be achieved and the collision less case with the minimum excess density fraction. In our understanding, it happens due to presence of collisions during the PSV saturation time, just after the drive is tuned off.

In Fig.??, the phase space plots of  $f(x, v, t)$  are shown, where the steady state structure survives long time after the drive is off for all the  $\nu$  cases (here, at  $t = 5000$ ). For Krook operator, small velocity scale distortions can still be seen at  $t = 5000$  and for ZK operator, small velocity scale distortions smooth out completely, yet the separatrix between trapped region and free region is clearly visible which means large amount of particles are still trapped in the wave trough unaffected by the the effect of diffusion in velocity space. However, trapped fractions for both Krook and ZK operators are greater than the collisionless ( $\nu = 0$ ) case.

These can also be observed in the Fig.??, where (a) the total relative energy  $\delta W$ , (b) the total relative kinetic energy  $\delta K$  and (c) the total relative potential energy  $\delta P$  are plotted. As the chirp frequency is swept downwards, both relative kinetic energy  $\delta K$  and relative potential energy  $\delta P$  of the system increases which reflects the increase in untrapped and trapped particle populations, respectively. The growth of these relative energies is arrested when the drive is turned off. The vertical line represents the time when the drive is turned off. The maximum growth attained in all three  $\nu$  cases is different due to presence of collisions during the drive time. Then the system relaxes and saturates to attain a certain value of  $\delta W$ ,  $\delta K$ ,  $\delta P$ . As can be seen in Fig. ??, (a)  $\delta W$ ,  $\delta K$  and  $\delta P$  decrease faster for ZK operator than the Krook operator, (b) Saturation values of  $\delta W$  and  $\delta K$  are maximum for  $\nu = 0$  and minimum for ZK operator. However, unlike the second case [see Fig.??(c)] saturation value of  $\delta P$  is maximum for Krook operator and minimum for  $\nu = 0$  collisionless case. The difference in  $\delta K$  indicates the decrease in the energy of untrapped region surrounding the PSVs and causes to smooth out the small velocity scale distortions and difference in  $\delta P$  indicates the presence of the large amount of trapping fraction.

### 6.3.4 Transient Honeycomb Structures

In this Subsection, the response of the plasma is presented to the downward chirp in the smaller frequency regime in the weakly collisional medium. It has been found that in an collisionless case ( $\nu = 0$ ) the downward chirp in smaller frequency regime leads to formation of multiple phase space vortices, all appearing at different regions of phase space, which gives a “honeycomb”-like transient structure of the distribution function. Here, I report the results of the excitation of the plasma with a drive amplitude of  $E_0 = 0.025$ , with frequency swept from  $\omega_{high} = 0.8$  to  $\omega_{low} = 0.4$  with a sweep rate of  $\alpha = -1.6 \times 10^{-3}$ .

As the  $\omega(t)$  of the drive chirps down from  $\omega_{high}$  to  $\omega_{low}$  with a single mode number, the entire sub-harmonic region of phase space is seen to be driven strongly which results in an interacting, finite amplitude phase-space structures during the drive phase. The phase space portrait of the plasma as shown in Fig. ??(a) provides a convincing visualization that the phase space structures or “honeycomb” like appearance created by the drive persists till the end of the simulation i.e.  $t = 5000$ . In other two cases, weak collisions are considered, where collisions are turned on at  $t = 2000$ . It has been find out that for collision frequency  $\nu = 10^{-5}$ , Krook operator does not affect the “honeycomb” like appearance (Fig. ??(b)). However, with ZK operator, the particle trajectories start diffusing in velocity and the multiple phase space vortices, created during the driving process, totally disappear due to a collisional phase mixing, meaning that particles, that were trapped in the wave trough, are detrapped by the effect of diffusion in velocity (Fig. ??(c)).

## 6.4 Summary and Conclusions

In this Chapter, study the effect of collisions on the electrostatic phase space vortices is analyzed by means of Eulerian simulation with two different collision models. Here, a systematic study has been presented with two different collision models:- (1) Boltzmann

## CHAPTER 6. EULERIAN SIMULATIONS OF COLLISIONAL EFFECTS ON ELECTROSTATIC PHASE SPACE VORTICES

---

collision operator or Bhatnagar-Gross-Krook (Krook) operator, where the colliding particles can be treated as isolated pairs and, (2) Zakharov-Karpman (ZK) operator, where many weak collisions lead to particle diffusion in velocity space. The entire study is divided into three main components:- In the first part, the effect of collisions on linear Landau damping has been studied with both collisional operators. As can be expected, with increase in the collision frequency, damping of plasma wave also increases for both Krook and ZK operator cases. For very small collision frequency, such as  $\nu = 10^{-5}$ , both operators do not contribute to any change in the damping rate in the linear regime. However, for long time simulation, ZK operator is much more effective than Krook operator in the non-linear regime even for such small collision frequency.

In the second part, the collisional damping of Bernstein-Greene-Kruskal modes or PSV has been studied where at first step, a PSV is excited by applying an initial density perturbation of non-linear amplitude. Once the PSV structure is formed and the electric field “rings” at a nearly constant amplitude in time, the collisions are turned on, as a second step. It was found that for  $\nu = 0.01$  with Krook operator, the width of plateau and the excess density fraction start decreasing as soon as the collisions are turned on and the typical phase space vortex structure, signature of the trapping of particles in the wave potential well gradually vanishes due to detrapping of trapped particles and the velocity distribution becomes Maxwellian within next  $500\omega_{pe}^{-1}$ . However, for smaller collision frequency ( $\nu = 10^{-5}$ ), simulation with Krook operator indicates that, such low collisional frequency does not affect the trapped particle distribution but with ZK operator, phase space structure, totally disappear due to a collisional phase mixing and the separatrix between trapped region and free region is no more visible. Next, both of the above runs for an initial density perturbation of non-linear amplitude with  $\nu = 0.01$  and  $\nu = 10^{-5}$  are given where collisions are turned on from the initial time (i.e. at  $t = 0$  onwards) and kept on throughout the simulation. For  $\nu = 0.01$  case, it is found that in response to the initial non-linear amplitude perturbation, excess particle density starts with a maximum value. However, due to the presence of collisions from the start the excess density fraction decrease rapidly and the plasma wave disappears completely for  $t > 300$ .

## CHAPTER 6. EULERIAN SIMULATIONS OF COLLISIONAL EFFECTS ON ELECTROSTATIC PHASE SPACE VORTICES

---

The same numerical experiment is done for both Krook and ZK operator, with collision frequency  $\nu = 10^{-5}$ , where the ZK operator is more effective than Krook operator. The “plateau” region forms for both cases, without collisions ( $\nu = 0$ ) and with Krook collisions of frequency  $\nu = 10^{-5}$ . However, for ZK operator, collisional effects are strongly visible which causes the plasma wave to disappear completely and velocity distribution function tends towards the Maxwellian.

The last part of this Chapter concerns the study of chirp driven PSVs in the weakly collisional plasma. First, a homogeneous Maxwellian plasma is driven with a time dependent external drive or chirp of an infinitesimal amplitude, which leads to steady state giant PSV, with multiple extrema due to embedded holes and clumps/ multiple phase space vortices (“honeycomb”-like appearance, depends on the frequency range of chirp). These PSVs are shown to survive long after the external drive is turned off (i.e. till  $t = 5000$ ). Once the PSVs are formed, the driver is turned off and the plasma is evolved for further several  $\omega_{pe}^{-1}$  times and then, collisions are turned on as a second step. It has been found that for  $\nu = 0.01$  with Krook operator, the width of plateau and the excess density fraction decrease as soon as the collisions are turned on. The PSV, signature of the trapping of particles, gradually vanishes due to detrapping of trapped particles and the velocity distribution becomes Maxwellian at  $t = 3000$ . For smaller collision frequency ( $\nu = 10^{-5}$ ), three results have been found:-

- (1) In case of giant PSVs, with Krook operator, small velocity scale distortions can still be seen at the end of long time simulation along with large scale separatrix. However, with ZK operator, small velocity scale distortions smooth out completely, yet the separatrix between trapped region and free region is clearly visible which means large amount of particles are still trapped in the wave trough unaffected by the the effect of diffusion in velocity space.
- (2) In case of transient honeycomb structures, Krook operator does not affect the “honeycomb” like appearance even at the late times of simulation. However, with ZK operator, the particle trajectories start diffusing in velocity and the multiple phase space vortices, created during the driving process, totally disappear due to a collisional phase mixing,

meaning that particles, that were trapped in the wave trough, are detrapped by the effect of diffusion in velocity.

(3) The order of saturation values (increasing or decreasing) of excess density fraction  $\delta n(x, t)/n_0$  for all three cases [(a)  $\nu = 0$ , (b)  $\nu = 10^{-5}$ , Krook operator and (c)  $\nu = 10^{-5}$ , ZK operator], depends upon whether (i) collisions are turned on after the steady state is attained or, (ii) collisions are present since the initial time ( $t = 0$ ). In the first case, saturation value of  $\delta n(x, t)/n_0$  is maximum for collisionless case ( $\nu = 0$ ) and minimum for ZK operator where as in the secons case, saturation value of  $\delta n(x, t)/n_0$  is maximum for Krook operator and minimum for collisionless case ( $\nu = 0$ ). In the first case, collisions are turned on when the steady state is already attained whereas in the later case, are present since the initial time, thus also affect the saturation process of PSVs.



---

## Conclusions & Future Work

*In this Chapter, important results obtained in various Chapters of this Thesis are summarized. Also, possible extensions of the present work in various directions is discussed.*

### 7.1 Highlights

Highlights of this Thesis work is categorized below as two major parts, viz Computational Aspects and Plasma Physics Aspects respectively.

As has been discussed several times in the Thesis, nonlinear wave-particle interaction associated with several laboratory as well as astrophysical plasmas, for example energetic particles produced in fusion experiments, solar wind and magnetospheric plasmas etc. This phenomenon can excite various modes and leads to various frequency bursts over the spatial and temporal scales which results into formation of phase space vortices (PSVs). Several investigations aim to understand the features of dynamics of wave-particle interaction such as excitation of electrostatic modes and phase space structures, at ion scales and electron scales in space plasmas by analyzing both spacecraft data, solar wind observations and numerical results from kinetic or phase space simulations. In the present Thesis, an attempt

has been made to investigate of a variety of electrostatic modes and driven phase space vortices starting in an unmagnetized homogeneous plasma Periodic Boundary Conditions (basically unbounded), by performing numerical experiment with a 1D1V Vlasov-Poisson solver. I present major highlights of the Thesis as follows:-

### 7.1.1 Computational Aspects

Phenomena considered in this Thesis have been studied by upgrading the already existing 1D electrostatic Vlasov-Poisson Solver code with Piecewise Parabolic Method (VPPM-version 1.0) with various additions and important modifications [VPPM-version 2.0] such as:-

- Inclusion of an external drive.
- Inclusion of Vlasov-Yukawa (VY) system - Kinetic Ions and Boltzmann Electrons.
- Inclusion of Ion dynamics, which facilitates the study of both Kinetic Ions and Kinetic Electrons.
- Inclusion of Collisions which are modeled through one-dimensional operators of the type Bhatnagar-Gross-Krook (Krook)/Zakharov-Karpman (ZK).

### 7.1.2 Vlasov-Poisson Plasma Aspects

The Thesis work begins with the brief overview of the numerical scheme used for solving Vlasov-Poisson plasmas. Chapter 2 presents the phase space Eulerian approach for a 1D Vlasov-Poisson (VP) numerical solver that simulates 1D collisionless dynamics of plasmas and can self-consistently solve both the Vlasov and Poisson equations as well as advance the solution in time. The well known “time-splitting” method[59] coupled with the “piecewise parabolic method” (PPM)[60] advection scheme are applied to simulate the evolution of phase space distributions of both electrons and ions. All phenomena considered in this Thesis have been studied by upgrading the already existing 1D electrostatic Vlasov-Poisson

Solver code with Piecewise Parabolic Method (VPPM-version 1.0) developed at IPR [58]. This version the code has been upgraded to VPPM-version 2.0 or VPPM-2.0 by including various additions and important modifications such as (1) Inclusion of external drive, (2) Inclusion of Vlasov-Yukawa (VY) solver - Kinetic Ions and Boltzmannian Electrons, (3) Inclusion of Ion dynamics- facilitates the study of both Kinetic Ions and Kinetic Electrons, (4) Inclusion of Collisions which are modeled through one dimensional operators of the Bhatnagar-Gross-Krook (BGK)/Zakharov-Karpman (ZK) operator type etc. The benchmarking of the upgraded code with various modification has been presented in Chapter 2 and the following Chapters, wherever required.

In Chapter 3, I have studied numerically, a simple, novel and efficient way to obtain giant Phase Space Vortices (PSV) with multiple extrema in a 1D, unbounded Vlasov plasma modelled using periodic boundary conditions. A very low amplitude external drive with frequency chirping is found to drive giant structures in phase space at steady state. In the first part of chapter 3, 1D simulations have been performed to excite LAN mode which represents the damping and trapping phenomenon of plasma for initial density perturbation problems as well as work as benchmark of our solver. Then, by assuming an initially homogeneous Maxwellian distributional, plasma is driven with constant frequency  $\omega_0$  external drive. This drive creates two “seeds” flattening, one at weakly nonlinear EAW frequency and other is at LAN frequency. Both EAW and LAN are excited with this constant frequency drive which are seen to persist long after the weakly nonlinear drive is turned off. In the second part, it has been demonstrated that large steady state PSV structures can be excited when the drive frequency is swept from the start ( $t = 0$ ) for a short time period  $\Delta t_d$  from  $\omega_{high}$  to  $\omega_{low}$ . Keeping other parameters fixed, the response of the plasma on applying different chirp rates reveals that the longer the frequency is swept (i.e. slower the chirp rate), the greater is the region of flattening in velocity space. The growth of these coherent phase space structures are arrested beyond a certain chirp interval as  $\frac{\partial \langle f \rangle}{\partial v}$  attains large negative value. In general, the chirp driven phase space structures found are seen to possess multiple extremas of  $f(x, v)$  embedded within the giant hole structure. Moreover, more than one giant hole structures are squashed

together amongst separatrix like structures, each of these structures moving at a different phase velocities. The complexity of these structures are seen to increase with  $\Delta t$ . As the drive is turned off, the system is seen to relax to a phase space vortices but with multiple extrema “shark” like structures squashed between ergodic regions of separatrices. However, for small frequency regime, the external downward chirp with a single mode number  $k$  drives the entire sub-harmonic region of phase space driven strongly even for “linear-like” drive amplitudes. This results in strongly interacting transient multi-extrema phase structures in sub-harmonic region or “honey-comb-like structures”. Long after the linear drive is switched off, some of the smaller structures slowly “merging”, as it can be expected in a 2D inverse cascade process leading to a quasi-steady phase space structures.

The above said studies were for the initial velocity distributions which were Maxwellian. In Chapter 4, for a non Maxwellian plasma described by  $q$ -distribution, the nonlinear evolution of Maxwellian and  $q$ -nonextensive Maxwellian plasma has been addressed when perturbed with an external drive, of very low amplitude, which is slowly chirped downwards in frequency. From the numerical results, it is concluded that the chirp dynamics and trapping phenomenon is strongly affected by the deviations from the Maxwellian distribution. In other words, the trapping efficiency is related to the region around wave phase velocity or the velocity derivative of the initial distribution function near the resonance region. It is found that, for values of the entropy-index  $q$  less than unity, trapping decreases with decrease in  $q$  values. On the contrary, for large value of  $q$ , trapping decreases with increase in  $q$  values. This implies the trapping efficiency for a given set of parameters is maximum for Maxwellian plasma. As  $q$  increases beyond unity, the phase velocity comes closer to the velocity cutoff for the distribution which makes an upper limit for  $q$  below which we find PSVs.

Further, I have extended the studies to observe the role of ions on the phase space dynamics. The above said electrostatic waves have been studied in the background of immobile ions resulting in a “thumb curve” dispersion (for LAN and EAW waves) with kinetic electrons. In Chapter 5, the role and effect of ions on the phase space dynamics,

has been studied in two parts:-

(1) In the first part of Chapter 5, to study electrostatic waves on ion scale in the frame of Boltzmann electrons with kinetic ions has been done with Vlasov-Yukawa (VY) solver. This model results in a “teardrop” curve (for IA and IBk waves). Using 1D1V VY solver Landau damping and electrostatic waves at ion scales (IA and IBk waves) have been studied. It was found that the weak external driver of constant frequency  $\omega_0 = \omega_{IBk}$  successfully creates the trapped particle regions or weak flattening of distribution function simultaneously in IA and IBk regions for  $T_R = 0.1$ . However, for  $T_R = 0.01$  and  $T_R = 10^{-7}$ , the weak external drive creates significant trapping in IA region only. Also, formation and dynamics of chirp driven phase space vortices at ion scales have been studied for different temperature ratios, namely  $T_R = 0.1, 0.01, 10^{-7}$ . In all three cases, plasma is externally driven with a downward chirp in the IBk region. For  $T_R = 0.1$  case, the chirp affects the plasma from IA to IBk region which in turn creates multiple PSVs in between IA to IBk region. As the ion to electron temperature ratio  $T_R$  decreases, the “teardrop” curve becomes broader and the distance between IA branch and IBk branch increases. For such cases, the downward chirp excites the IA region more than the IBk region, which created giant PSV in the IA region. For very small value of  $T_R$ , for example  $T_R = 10^{-7}$ , contribution from electrons become negligible, in that case only IA region gets excited while applying the external chirp.

(2) In the second part of Chapter 5, the electron scale physics and ion scale physics have been studied by including both ion and electron scale dynamics self consistently and simultaneously in a model or symmetric framework. With this model both high frequency and low frequency solutions can be obtained simultaneously which consists of a high frequency branch (LAN/IA) and a low frequency branch(EAW/IBk). Therefore, an attempt has been made by means of numerical simulations, considering both kinetic electrons and kinetic ions on the same physics footing, wherein the Vlasov equations are integrated for both electron and ion species without any approximations in length scale or time scales. First the linearized eigenvalue equations have been solved considering weak trapping which allows us to neglect the contribution from the imaginary part of the dielectric function. The eigenvalue values thus obtained for various wavenumber are

compared with frequencies obtained from solving weakly driven fully nonlinear Vlasov-Poisson (VP) equations which facilitates weak flattening of distribution function or weak trapping. The numerical results obtained show that both electron and ion waves can be excited simultaneously in phase space. In appropriate limits, it is shown that the “thumb” and “teardrop” curves are different parts of a general symmetric dispersion relation and are recovered in appropriate limits of that dispersion relation.

In systems governed by kinetic processes, limit of low collisionality is not the same as the limit of zero collisionality. In such conditions, kinetic processes and collisionality are in competition between each other: while the first process works to produce deformations of the particle distribution function away from a Maxwellian, the latter tends to restore the Maxwellian configuration. The evolution of the plasma is, therefore, a result of complex combination of these two effects. In Chapter 6, study the effect of collisions on the electrostatic phase space vortices is analyzed by means of Eulerian simulation with two different collisional models, for the collisional damping of nonlinear plasma structures. Here, a systematic study has been presented with two different collision models:- (1) Boltzmann collision operator or Bhatnagar-Gross-Krook (BGK) operator, where the colliding particles can be treated as isolated pairs and, (2) simplified Fokker-Plank operator i.e. Zakharov-Karpman (ZK) operator, where many weak collisions lead to particle diffusion in velocity space. The entire study is divided into three main components:- (i) In the first part, the effect of collisions on linear Landau damping has been studied with both collisional operators. As can be expected, with increase in the collision frequency, damping of plasma wave also increases in both BGK and ZK operator cases. For very small collision frequency, such as  $\nu = 10^{-5}$ , none of the operators contribute to any change in the damping rate in the linear regime. However, for long time simulation, in the non-linear regime even for such small collision frequency, ZK operator is much more effective in affecting the phase space vortices than BGK operator.

(ii) In the second part, the collisional damping of Bernstein-Greene-Kruskal waves or PSV has been studied where at first step, a PSV is excited by applying an initial density

perturbation of non-linear amplitude. Once the PSV structure is formed, the collisions are turned on, as a second step. It was found that for  $\nu = 0.01$  with BGK operator, the typical phase space vortex structure, signature of the trapping of particles in the wave potential well gradually vanishes due to detrapping of trapped particles and the velocity distribution becomes Maxwellian within next  $500\omega_{pe}^{-1}$ . However, for smaller collision frequency ( $\nu = 10^{-5}$ ), simulation with BGK operator indicates that, such low collisional frequency does not affect the trapped particle distribution but with ZK operator, multiple extrema phase space structure, totally disappear due to a collisional phase mixing and the separatrix between trapped region and free region is no more visible.

(iii) The third part of this Chapter concerns the study of chirp driven PSVs in the weakly collisional plasma. Here, a homogeneous Maxwellian plasma is driven with an time dependent external drive or chirp of an infinitesimal amplitude, which leads to steady state giant PSV, with multiple extrema due to embedded holes and clumps/ multiple phase space vortices (“honeycomb”-like appearance, depends on the frequency range of chirp). Once the PSVs are formed, the driver is turned off and the plasma is evolved for further several  $\omega_{pe}^{-1}$  times and then, collisions are turned on as a second step. It has been found that for  $\nu = 0.01$  with BGK operator, the PSV, signature of the trapping of particles, gradually vanishes due to detrapping of trapped particles and the velocity distribution becomes Maxwellian at  $t = 3000$ . For smaller collision frequency ( $\nu = 10^{-5}$ ), three results have been found:-

(1) In case of giant PSVs, with BGK operator, small velocity scale distortions can still be seen at the end of long time simulation along with large scale separatrix. However, with ZK operator, small velocity scale distortions smooth out completely, yet the separatrix between trapped region and free region is clearly visible which means large amount of particles are still trapped in the wave trough unaffected by the the effect of diffusion in velocity space.

(2) In case of transient honeycomb structures, BGK operator does not affect the “honeycomb” like appearance even at the late times of simulation. However, with ZK operator, the particle trajectories start diffusing in velocity and the multiple phase space vortices, created

during the driving process, totally disappear due to a collisional phase mixing, meaning that particles, that were trapped in the wave trough, are detrapped by the effect of diffusion in velocity.

(3) The order of saturation values (increasing or decreasing) of excess density fraction  $\delta n(x, t)/n_0$  for all three cases [(a)  $\nu = 0$ , (b)  $\nu = 10^{-5}$ , BGK operator and (c)  $\nu = 10^{-5}$ , ZK operator], depends upon whether (i) collisions are turned on after the steady state is attained or, (ii) collisions are present since the initial time ( $t = 0$ ). In the first case, saturation value of  $\delta n(x, t)/n_0$  is maximum for collisionless case ( $\nu = 0$ ) and minimum for ZK operator where as in the second case, saturation value of  $\delta n(x, t)/n_0$  is maximum for BGK operator and minimum for collisionless case ( $\nu = 0$ ). In the first case, collisions are turned on when the steady state is already attained whereas in the later case, are present since the initial time, thus also affect the saturation process of PSVs.

## 7.2 Future Scope

In this Thesis, a formation and dynamics of 1D electrostatic phase space vortices has been studied, at electron as well as ion scale and in collisionless plasmas as well as in the collisional environment, using in-house developed and upgraded 1D1V Vlasov-Poisson solver (VPPM 2.0). This Thesis points out to several interesting directions for future work. These avenues of future research are enlisted under following categories.

### 7.2.1 Numerical Experiments On Vlasov Plasmas

- For various laboratory and naturally occurring plasmas, great interest lies in plasma dynamics in the background of non-uniformity or for inhomogeneous plasmas which can be used to compare different theoretical approaches to the problem. The collective oscillations of such non-magnetized, inhomogeneous plasmas (the Tonks-Dattner resonances) possess many properties that allow a precise comparison between experiment and theory [127]. In the present Thesis, the study of phase space vortices

has been performed in the background of unmagnetized, unbounded (or periodically bounded), homogeneous plasma. It would be interesting to study the formation and dynamics of such PSVs in the inhomogeneous background of ions.

- In the Thesis, the study of chirp dynamics is performed for the unmagnetized plasmas (or along the magnetic field direction). It would be very interesting to understand the effect of such chirp (which is applied along the magnetic field direction) in the radial direction or perpendicular direction to the magnetic field. Also, to understand the response of plasma when the chirp is applied across the magnetic field which usually occurs in fusion plasmas [39]. Therefore, it would be very useful to extend the code in other dimensions to include across magnetic field dynamics such as 1D2V/2D2V/3D3V electrostatic and electromagnetic models.
- In the past, the instabilities which are driven by the fast-ion population have been extensively studied in toroidal devices [128]. The nonlinear dynamics of these instabilities is essential to predict the amplitude and subsequent fast-ion transport associated with alpha particles driven instabilities which are found in the International Thermonuclear Engineering Reactor (ITER) and other burning plasmas. The frequencies of these fast ion driven instabilities often results in frequency shifting or chirp bursts. The relaxation oscillations associated with chirping bursts are also observed in the presence of small but finite collisional regimes. Therefore, the fate of driven PSVs resulting from such chirp bursts on ion scales in the presence of collisions would be an interesting problem. Therefore, in order to understand the effect of collisions on short scale, ions are also need to be included.
- In fusion plasmas, a turbulent plasma self-organizes to a global profile in which different sources like the heat source, the momentum source, the particle source, and the profile of background plasma in the presence of collisions (or sink) interact to sustain a global self-organized feedback loop. Within this loop, one can only control the sources and sinks if the confinement geometry is known. In order to enhance the predictability of such systems, the simulation with source and sink terms are desirable, where the balance conditions of particle and fluxes are need to be satisfied

[129, 130]. To study such kind of problems, various computational boundaries and simultaneous source-sink terms need to be added.

- In ignition/fusion experiments, the kinetic dynamics of low-frequency waves in multiple ion species plasma plays an essential role in inertial confinement fusion (ICF). For example, the significant energy transfer to IAWs leads to production a non-Maxwellian distribution, which may further reduce Landau damping in the multi-ion species plasmas [131]. For such physics problems, inclusion of multiple ion species is required which further needs parallelization of VPPM-2.0 by using an OPEN-MP parallelization nested within an MPI parallelization. Alternatively the codes may be parallelized on a GPU platform.
- In the present collisional model, both Krook and ZK operators are used which do not conserve either momentum or energy. However, the Krook operator does conserve the number of particles. There are other operators with better conservation properties like the Gaussian BGK model, ESBGK model, the BGK model with velocity dependent collision frequency, Dougherty collisional operator etc [125, 126]. In order to perform a qualitative comparison study using simplistic collision operators, conventional Krook and ZK operators have been used here. Quantitatively, there will be indeed some differences between the results obtained using other operators than the results obtained from Krook and ZK operators. However, I believe that there will be no difference qualitatively. To ascertain the effect of momentum and energy conserving collisions on the PSVs, it would be meaningful and beneficial to generalize the present models (Krook and ZK) so that they conserve both momentum and energy. This would be an interesting future work.
- In the present solver, to solve the advection equation a third order accurate PPM method has been used. In order to improve the accuracy of VPPM-2.0 and its future upgraded versions, more accurate and compatible to the different physics problems, advection methods are needed. Therefore, better (perhaps numerically expensive) advection schemes namely 6<sup>th</sup> order PPM Scheme [132], Discontinuous Galerkin (DG) method [104] may be looked into in the future.

- A theoretical understanding for chirp driven PSVs has not been attempted in this Thesis work. However, as shown in Appendix-B, a 1D free electron gas when confined in a periodic 1D well and subject to chirping clearly indicates a “trap-drag-drop” picture in phase space, which suggests that both untrapped and trapped electrons gain energy. In future, it will be interesting to include self-consistent electric field and generalize the model indicated in Appendix-B.





---

## Plasma Dispersion Relation:- Kinetic Electrons and Immobile Ions

In this Appendix, I describe two methods, as I understand them, to study undamped, small amplitude, single harmonic, electrostatic waves in a 1D Vlasov-Poisson plasma, both giving rise to the same plasma dispersion relation in the harmonic limit, namely the real part of the complex dispersion relation with real argument  $\omega_r$ . The first method is due to Schamel and co-workers which is based on pseudo-potential method [44, 96, 12]. In this method, they started from exact solutions of the time-independent electron Vlasov equation by using a Maxwellian based distribution which constitutes of two parts: one represents the untrapped particles and second represents the trapped fraction of particles. The second method is due to Landau [1], which I have followed in this Thesis, is based on the perturbation theory where plasma dispersion relation for real arguments is obtained by assuming local flattening of distributions and setting the imaginary part of complex dielectric function to zero. Both of these methods lead to the same dispersion relation in the harmonic limit. In the following, I will outline the major steps to see this point.

## A.1 Pseudo Potential Method

For a stationary, 1D, electrostatic waves, which are traveling with wave speed  $v_0$  in a collisionless, unperturbed, thermal plasma. The electron motion in phase space is governed by the Vlasov equation, which reads in the frame moving with  $v_0$ , i.e., in the wave frame,

$$v \frac{\partial f}{\partial x} + \Phi' \frac{\partial f}{\partial v} = 0 \quad (\text{A.1})$$

where normalized quantities have been used, based on the density, and the temperature of the unperturbed plasma in the background of immobile ions. An appropriate solution is given by the following Ansatz:[96]

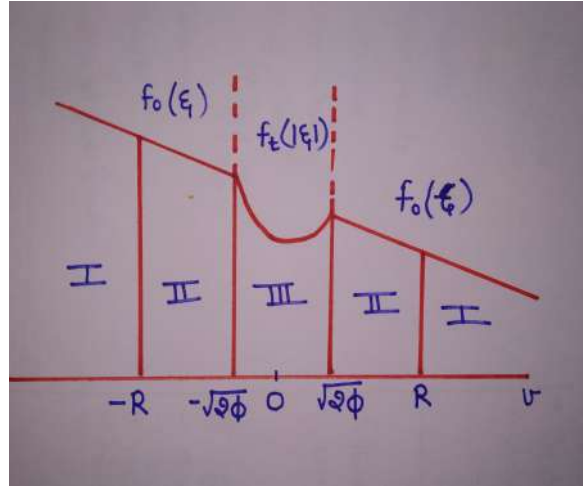


Figure A.1: The distribution function as a function of the velocity. The trapped range is denoted by III, and the range II (I) refers to untrapped resonant (nonresonant) particles.

$$f(x, v) = \begin{cases} \frac{(1+k_0^2\Psi/2)}{\sqrt{2\pi}} \exp[-\frac{1}{2}(\sqrt{2\epsilon} + v_0)^2], & \text{For } v^2 \geq 2\Phi. \\ \frac{(1+k_0^2\Psi/2)}{\sqrt{2\pi}} \exp[-\frac{1}{2}v_0^2 - \beta\epsilon], & \text{For } v^2 \leq 2\Phi. \end{cases} \quad (\text{A.2})$$

Where  $\epsilon = v^2/2 - \Phi(x)$  is the energy of a single particle,  $\Phi(x)$  the electrostatic potential, and  $v_0$  the not yet known phase velocity of the expected structure. The first part in Eq.A.2 represents the free or untrapped electrons and the second part represents the trapped electrons, where  $f(x, v)$  is continuous but its velocity derivative jumps at the seperatrix and

APPENDIX A. PLASMA DISPERSION RELATION:- KINETIC ELECTRONS  
AND IMMOBILE IONS

---

$\partial f_0/\partial v$  is singular at  $\epsilon = 0$ . Here, it is assumed that  $0 \leq \Phi(x) \leq \Psi$ , where  $\Psi$  represents the amplitude of the perturbation. Thus, the unperturbed plasma state given by  $\Psi = 0$  which is represented by a shifted Maxwellian i.e.  $f_M(v) = \frac{1}{\sqrt{2\pi}} \exp[-\frac{1}{2}(v + v_0)^2]$ . The amount of trapped particles is controlled by  $\beta$  parameter. A dip in the distribution function in the trapped particle region in phase space,  $\epsilon < 0$ , is thereby provided by negative  $\beta$ . The  $f(x, v)$  divides phase space in three regions for the electrons:

1. A free non-resonant region  $|v| > R$ .
2. A free resonant region  $\sqrt{2\Phi} \leq |v| \leq R$ .
3. A free non-resonant region  $|v| \leq \sqrt{2\Phi}$ .

where  $R$  separates free electrons that are in resonance with the wave from those that are not. Here, it is assumed that  $R \approx \sqrt{\epsilon} \ll 1$ , where  $\epsilon$  is  $O(\Psi)$ . By considering  $\xi = \sigma|v^2 - 2\Phi(x)|$ , where  $\sigma = \text{sgn}(v)$  the sign of velocity, different expansions are appropriate for the above three regions:

1. In the trapped region (tr):- ( $0 \leq |v| \leq \sqrt{2\Phi}$ ,  $|\xi|$ ,  $|v| = O(\sqrt{\epsilon})$ )

$$f_t(\xi) = f_t(0) + \xi f_t'(0) + \frac{1}{2}\xi^2 f_t''(0) + O(\xi^3)$$

$$\Rightarrow f_t(\xi) = f_t(0) + \frac{1}{2}(2\Phi - v^2) f_t''(0) + O(\xi^3)$$

due to symmetry of  $f_t$  in  $v$  space  $f_t'(0)$  vanishes.

2. In the free resonant region (frr):- ( $\sqrt{2\Phi} \leq |v| < R \approx \sqrt{\epsilon}$ ;  $|\xi|$ ,  $|v| = O(\sqrt{\epsilon})$ )

$$f_0(\xi) = f_0(0) + \xi f_0'(0) + \frac{1}{2}\xi^2 f_0''(0) + O(\xi^3)$$

$$\Rightarrow f_0(\xi) = f_0(0) + \sigma(v^2 - 2\Phi)^{1/2} f_0'(0) + \frac{1}{2}(v^2 - 2\Phi) f_0''(0) + O(\xi^3)$$

3. In the free non resonant region (fnr):- ( $|v| > R \propto \sqrt{\epsilon}$ ,  $|\xi|$ ,  $|v| \geq O(1)$ )

hence  $\frac{2\Phi}{v^2} = O(\epsilon)$  &  $\xi = v - \Phi/v + O(\epsilon^2)$

$$f_0(\xi) = f_0(v) - \Phi \frac{1}{v} \frac{\partial f_0(v)}{\partial v} + \frac{\Phi^2}{2} \left( \frac{1}{v} \frac{\partial}{\partial v} \right)^2 f_0(v) + O(\Phi^3)$$

## APPENDIX A. PLASMA DISPERSION RELATION:- KINETIC ELECTRONS AND IMMOBILE IONS

For small amplitudes,  $\Psi \ll 1$ , the electron density can be obtained by a Taylor expansion of Eq.A.2 first (as it is done above), followed by the velocity integration, given by,

$$n_e(\Phi) = \int f_e(x, v) dv = \int_{f.n.r.} f_0(\xi) dv + \int_{f.r.r.} f_0(\xi) dv + \int_{t.r.} f_t(\xi) dv \quad (\text{A.3})$$

which will end up in the following expression:-

$$n_e(\Phi) = 1 + \frac{k_0^2 \Psi}{2} - \frac{1}{2} Z'_r\left(\frac{v_0}{\sqrt{2}}\right) \Phi - \frac{4}{3} b(\beta, v_0) \Phi^{3/2} + .. \quad (\text{A.4})$$

where  $\frac{1}{2} Z'_r\left(\frac{v_0}{\sqrt{2}}\right)$  is defined by  $\frac{1}{2} Z'_r\left(\frac{v_0}{\sqrt{2}}\right) := P \int \frac{1}{v} \frac{\partial f_M(v)}{\partial v} dv$ , where  $P$  stands for principal value, and  $Z_r$  represents the real part of the complex plasma dispersion function for real arguments. In general,  $Z(\xi) = \frac{1}{\sqrt{\xi}} \int_{-\infty}^{\infty} \frac{e^{-t^2}}{t-\xi} dt$  is the Hilbert transform of a Gaussian which is related to Dawson's integral and  $Z'(\xi) = \frac{1}{\sqrt{\xi}} \int_{-\infty}^{\infty} \frac{e^{-t^2}}{(t-\xi)^2} dt$ . The trapping effects are incorporated in  $b(\beta, v_0)$  which is defined by

$$b(\beta, v_0) = \frac{1}{\sqrt{\pi}} (1 - \beta - v_0^2) \exp\left(-\frac{v_0^2}{2}\right) \quad (\text{A.5})$$

In order to get a self-consistent solution, the Poisson equation in the immobile ion limit becomes,

$$\Phi''(x) = \int f dv - 1 = n_e - 1 = -V'(\Phi) \quad (\text{A.6})$$

where  $V(\Phi)$  is the pseudo-potential (often called Sagdeev potential).

After substitution of Eq.A.4 into Eq.A.6 and a subsequent  $\Phi$ -integration we get  $V(\Phi)$  and from  $V(\Phi = \Psi) = 0$ ,

$$k_0^2 - \frac{1}{2} Z'_r\left(\frac{v_0}{\sqrt{2}}\right) - \frac{16}{15} b \Psi^{1/2} = 0, \text{ or} \quad (\text{A.7})$$

$$k_0^2 - \frac{1}{2} Z'_r\left(\frac{v_0}{\sqrt{2}}\right) = B \quad (\text{A.8})$$

This Eqn.A.8 is called the nonlinear dispersion relation since it determines  $v_0$  in terms of  $B = \frac{16}{15} b \Psi^{1/2}$  and  $k_0$ . In case of harmonic limit which corresponds to monochromatic case i.e.  $B = 0$ , Eq.A.8 becomes,

$$k_0^2 - \frac{1}{2} Z'_r\left(\frac{v_0}{\sqrt{2}}\right) = 0 \quad (\text{A.9})$$

APPENDIX A. PLASMA DISPERSION RELATION:- KINETIC ELECTRONS  
AND IMMOBILE IONS

Here,  $B$  can become zero in two cases:-(i) in infinitively small amplitude limit i.e.  $\Psi \rightarrow 0^+$  and (ii) when  $b = \frac{1}{\sqrt{\pi}}(1 - \beta - v_0^2) \exp(-\frac{v_0^2}{2}) = 0 \Rightarrow \beta = 1 - v_0^2$ , which indicates the presence of a depressed trapped particle region. In the pseudo potential method, the latter case ( $b = 0$ ) is considered. For  $B = 0$  the phase velocity of the harmonic waves lies in the range  $1.307 < v_0 < 2.13$ , from which the trapped particle parameter  $\beta$  can be deduced, which is negative for  $B = 0$  case, yielding a depressed trapped particle region and an altogether well behaved distribution. Note that  $B$  can become zero without taking the infinitesimal amplitude limit  $\Psi \rightarrow 0^+$ .

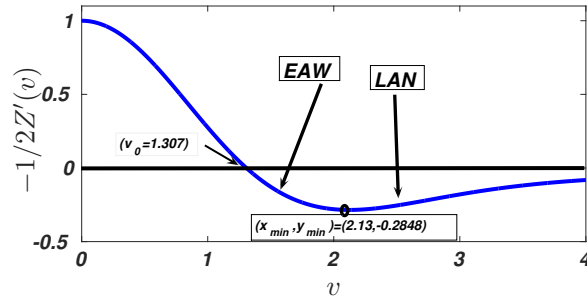


Figure A.2: The gradient of the real part of the complex plasma dispersion function  $-\frac{1}{2}Z'(v)$  is plotted for real arguments for immobile ions.

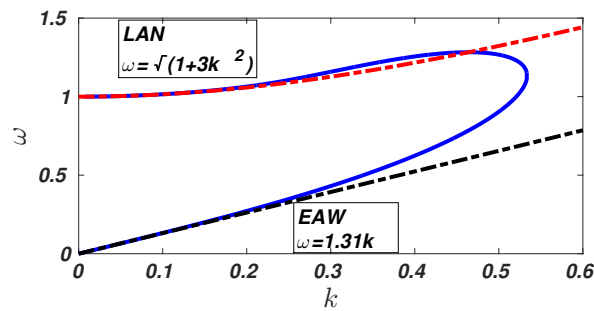


Figure A.3: Dispersion curves or “Thumb” curves for the electrostatic waves (LAN, EAW) in  $k - \omega$  plane, obtained by both Pseudo potential method as well as by assuming zero damping.

## A.2 Landau Method

In the Landau's linear perturbation method, for an unmagnetized, uniform plasma with a distribution  $f_0(v)$  and the perturbation in  $f(x, v, t)$  by  $f_1(x, v, t)$  is denoted by,

$$f(x, v, t) = f_0(v) + f_1(x, v, t) \quad (\text{A.10})$$

The first order Vlasov equation for electrons in the background of immobile ions is given by,

$$\frac{\partial f_1}{\partial t} + v \frac{\partial f_1}{\partial x} - \frac{e}{m} E_1 \frac{\partial f_0}{\partial v} = 0 \quad (\text{A.11})$$

Considering the perturbation waves are plane waves in one dimension is given by,

$$f_1 \propto e^{i(kx - \omega t)} \quad (\text{A.12})$$

Then Eqn.A.11 becomes

$$f_1 = \frac{ieE_x}{m} \frac{\partial f_0 / \partial v_x}{\omega - kv_x} \quad (\text{A.13})$$

Poisson equation gives

$$\epsilon_0 \frac{\partial E}{\partial x} = \epsilon_0 ikE_x = -en_1 = -e \int f_1 dv \quad (\text{A.14})$$

$$\rightarrow n_1 = \int f_1 dv = \frac{ieE_x}{m} \int_{-\infty}^{\infty} \frac{\partial f_0 / \partial v_x}{v_x - (\omega/k)} dv \quad (\text{A.15})$$

Since, one dimensional problem is considered here, therefore, in order to avoid any confusion, I drop the subscript  $x$ . By putting Eqn.A.15 into Eqn.A.14, I will get,

$$1 = \frac{\omega_p^2}{k^2} \int_{-\infty}^{\infty} \frac{\partial f_0 / \partial v}{v - (\omega/k)} dv \quad (\text{A.16})$$

$$1 = \frac{\omega_p^2}{k^2} \left[ P \int_{-\infty}^{\infty} \frac{\partial f_0 / \partial v}{v - (\omega/k)} dv + i\pi \frac{\partial f_0}{\partial v} \Big|_{v=\omega/k} \right] \quad (\text{A.17})$$

APPENDIX A. PLASMA DISPERSION RELATION:- KINETIC ELECTRONS  
AND IMMOBILE IONS

---

Let the equilibrium distribution  $f_0$  be one dimensional Maxwellian:

$$f_0 = \frac{n_0}{v_{th} \sqrt{2\pi}} e^{-\frac{v^2}{2v_{th}^2}}, \quad v_{th} = \sqrt{KT/m} \quad (\text{A.18})$$

Introducing the dummy variable  $s = v/\sqrt{2}v_{th}$ , it can be written as:

$$n_1 = \int f_1 dv = \frac{-ieEn_0}{kv_{th}^2 m \sqrt{2\pi}} \int_{-\infty}^{\infty} \frac{(d/ds)(e^{-s^2})}{s - \xi} ds \quad (\text{A.19})$$

where  $\xi = \omega/\sqrt{2}kv_{th}$ . Now, by defining the plasma dispersion function  $Z(\xi)$ :

$$Z(\xi) = \frac{1}{\sqrt{2\pi}} \int_{-\infty}^{\infty} \frac{e^{-s^2}}{s - \xi} ds \quad \text{Im}(\xi) > 0 \quad (\text{A.20})$$

In order to express  $n_1$  in terms of  $Z(\xi)$ , the derivative  $Z(\xi)$  is taken of with respect to  $\xi$ :

$$Z'(\xi) = \frac{1}{\sqrt{2\pi}} \int_{-\infty}^{\infty} \frac{e^{-s^2}}{(s - \xi)^2} ds \quad (\text{A.21})$$

Integration by parts yields

$$Z(\xi) = \frac{1}{\sqrt{2\pi}} \left[ \frac{-e^{-s^2}}{s - \xi} \right]_{-\infty}^{\infty} + \frac{1}{\sqrt{2\pi}} \int_{-\infty}^{\infty} \frac{e^{-s^2}}{s - \xi} ds \quad (\text{A.22})$$

The first term vanishes as it must for any well-behaved distribution function. This allows us to write density as:

$$n_1 = \frac{-ieEn_0}{kmv_{th}^2} Z'(\xi) \quad (\text{A.23})$$

Here,  $Z(\xi)$  constitutes both real and imaginary parts. Assuming a weak flattening (or trapped region) of the vanishing velocity width, i.e.  $\frac{\partial f_0}{\partial v}|_{v=\omega/k} \simeq 0$ , which allows us to neglect the contribution from the imaginary part. Therefore, Eqn.A.16 becomes,

$$k^2 = \frac{\omega_p^2}{2v_{the}^2} Z'_r(\xi) \quad (\text{A.24})$$

In electron normalized units (i.e.  $\omega/\omega_p$ ,  $k\lambda_D$ ,  $v/v_{th}$ , Eqn.A.24) becomes,

$$k^2 - \frac{1}{2} Z'_r(\xi) = 0 \quad (\text{A.25})$$

## APPENDIX A. PLASMA DISPERSION RELATION:- KINETIC ELECTRONS AND IMMOBILE IONS

---

which is exactly same as Eqn.A.9, which is obtained by Pseudo potential method in the harmonic limit.

In Fig.A.2, a plot of the function  $-\frac{1}{2}Z'_r(v)$  with  $v$  for kinetic electrons and immobile ions is displayed. The negative values of  $-\frac{1}{2}Z'_r(v)$  represents the real physical solutions. The term  $-\frac{1}{2}Z'(v)$  can be interpreted as a gradient of the real part of the complex plasma dispersion function for real arguments. In the limit of immobile ions, the function  $-\frac{1}{2}Z'(v)$  represents electron contribution, where all the negative values of this function represents the real solutions for electrostatic waves and it divides the phase velocity regions and reveals different branches of the dispersion relation. It has one zero transition (at  $v = 1.307$ ) and one minimum (at  $v = 2.13$ ) which results in two separated regions for the phase velocity[96]:-(i)  $v \leq 2.13$  (EAW), (ii)  $v \geq 2.13$  (LAN). The function is positive for  $v < 1.307$  and negative for other values of  $v$  and vanishes at infinity. In Fig.A.3, the  $\omega_r, k$  curve is displayed for the Eqn.A.9, which is also known as “Thumb-curve”. The upper branch of the “thumb curve” is the well known Langmuir branch and the lower branch of the “thumb curve” is electron acoustic branch.

From these two plots, it is evident that there are mainly two undamped roots and no undamped roots exist beyond a critical value of the wavenumber  $k$ . Moreover, this thumb curve also represents that each point in the  $k - \omega$  plane along the thumb curve corresponds to a different particle velocity distribution function. This so-called “thumb” dispersion curve is obtained by assuming the small wavenumber  $k$  and retaining only the principle part in the velocity integral of the Landau dispersion relation in my Thesis.[1]

---

## Electron Gas Model

In this Appendix, the dynamics of passage and capture into resonance of a distribution of particles driven by a chirped frequency perturbation is discussed for an electron gas in a periodically bounded plasma by excluding self-consistency. This model is inspired from the electron gas model for bounded case reported in Friedland *et.al.* [37]. As is well known, a pure electron plasma confined by a strong external B-field and an electron-ion plasma with immobile ions are nearly isomorphic [133] as far as electron dynamics is concerned.

Let me consider a 1D electron gas along the direction of B-field and subject the same to an external electric field. In [37], the electron gas was bounded along B-field and were bouncing between the end-caps. Here, in my case, I am considering the direction along the B-field to be periodic. Except for self-consistent electric field, this model is near-identical to the problem I have addressed in Chapter 3. In the following, I shall continue to use the terminology of pure electron plasma, as I am generalizing the work in [37] from bounded potential to periodic confining potential, suitable for my work.

The electron dynamics for a pure electron plasma in this model is considered to be one-dimensional (1D) and driven by a one-dimensional potential

$$\phi_d = \phi_0(z)\cos[\psi_d(t)] \quad (\text{B.1})$$

where the driving frequency  $\omega_d(t) = d\psi_d/dt = \omega_0 - \alpha t$  is linearly down chirped in time, with the chirp rate  $\alpha$ . Assuming external trapping potential of length  $L$  and initially normalized Maxwellian distribution, defined as  $f_0 = \exp(-v^2/2v_{th}^2)/\sqrt{(2\pi v_{th})}$ . The goal is to study the evolution of the electron distribution in phase space due to the chirped frequency drive, neglecting the self-electric field in this case. It is assumed that the driving amplitude is small i.e.  $[(e/m)\phi_0]^{1/2} \ll v_{th}$ .

The electron dynamics in 1D problem are governed by the following Hamiltonian:-

$$H(p, z, t) = \frac{p^2}{2m} - e\phi_0(z)\cos[\psi_d(t)], \quad 0 \leq z \leq L \quad (\text{B.2})$$

Transformation  $(p, z) \rightarrow (I, \theta)$  canonical action-angle variable such that :-  $p = \pi I/L$ ,  $z = L\Theta/\pi$  for  $0 \leq \Theta < \pi$  and  $z = L(2\pi - \theta)/\pi$  for  $\pi \leq \theta < 2\pi$  where  $\Theta = \text{mod}(\theta, 2\pi)$ .

The transformed Hamiltonian becomes:-

$$H = \frac{1}{2}\mu I^2 - \cos[\psi_d(t)] \sum_{n=1}^{\infty} [a_n \cos(n\theta) + b_n \sin(n\theta)] \quad (\text{B.3})$$

where we have expanded  $e\phi_0(z)$  in Fourier series. The frequency chirp rate  $\alpha$  is assumed to be small enough that, near a given time  $\tau$ , the dynamics can be viewed as a weak perturbation of a similar system in which the drive frequency assumes the constant value  $\omega_d(\tau)$ . Then the single resonance approximation can be considered, as long as the adjacent resonances do not overlap. For Single resonance approximation:- interaction of the electrons with the  $n^{\text{th}}$  component of the drive. Hamiltonian for  $n^{\text{th}}$  component of drive:-

$$H = \frac{1}{2}\mu I^2 - \cos[\psi_d(t)][a_n \cos(n\theta) + b_n \sin(n\theta)] \quad (\text{B.4})$$

$$H = \frac{1}{2}\mu I^2 - A_n[\cos(n\theta + \psi_d) + \cos(n\theta - \psi_d)] - B_n[\sin(n\theta + \psi_d) + \sin(n\theta - \psi_d)] \quad (\text{B.5})$$

Now, by introducing dimensionless units as following normalization:

- $t \rightarrow \Omega_{th}t, I \rightarrow I/I_{th}, \omega_d \rightarrow \omega_d/\Omega_{th},$

- $A_n \rightarrow A_n/(mv_{th}^2)$ ,  $B_n \rightarrow B_n/(mv_{th}^2)$ ,  $\alpha \rightarrow \alpha/\Omega_{th}^2$ ,
- where  $\Omega = \pi v_{th}/L$  and  $I_{th} = mLv_{th}/pi$ . Here,  $\mu$  scales out after these transformation.

The Hamiltonian yields the following evolution equation:-

$$\frac{\partial I}{\partial t} = -\frac{\partial H}{\partial \theta} \quad (\text{B.6})$$

$$-\frac{\partial H}{\partial \theta} = nA_n[\sin(n\theta + \psi_d) + \sin(n\theta - \psi_d)] + nB_n[\cos(n\theta + \psi_d) + \cos(n\theta - \psi_d)] \quad (\text{B.7})$$

$$\frac{\partial \theta}{\partial t} = \frac{\partial H}{\partial I} = I \quad (\text{B.8})$$

Let  $\Phi = n\theta - \psi_d = n\theta - \omega_d t$ , where  $\omega_d = \omega_0 - \alpha t = d\psi_d/dt$

$$\frac{d^2\Phi}{dt^2} = -n^2 A_n[\sin(n\theta + \psi_d) + \sin(n\theta - \psi_d)] + n^2 B_n(\cos(n\theta + \psi_d) + \cos(n\theta - \psi_d)) + \alpha \quad (\text{B.9})$$

Now,  $n\theta + \omega_d t = \Phi + 2\omega_d t = \Phi + 2\omega_0 t - 2\alpha t^2$ , which leads to

$$\frac{d\Phi}{dt} = nI - \omega_d = nI - \omega_0 + \alpha t \quad (\text{B.10})$$

$$\frac{d^2\Phi}{dt^2} = n\frac{dI}{dt} + \alpha \quad (\text{B.11})$$

$$\frac{d^2\Phi}{dt^2} + n^2 A_n[\sin(\Phi + 2\omega_0 t - 2\alpha t^2) + \sin(\Phi)] - n^2 B_n(\cos(\Phi + 2\omega_0 t - 2\alpha t^2) + \cos(\Phi)) - \alpha = 0 \quad (\text{B.12})$$

$$\frac{d^2\Phi}{dt^2} + \frac{dV_{eff}}{d\Phi} = 0 \quad (\text{B.13})$$

This is an autonomous dynamical problem, describing the motion of a quasi particle in an effective, time independent, tilted potential.

$$V_{eff} = -n^2 A_n[\cos(\Phi + 2\omega_0 t - 2\alpha t^2) + \cos(\Phi)] - n^2 B_n(\sin(\Phi + 2\omega_0 t - 2\alpha t^2) + \sin(\Phi)) - \alpha \Phi \quad (\text{B.14})$$

For Phase space, consider  $\Phi = x \rightarrow d\Phi/dt = v$

$$\frac{dv}{dt} = \frac{d^2\Phi}{dt^2} \quad (\text{B.15})$$

$$\frac{dv}{dt} \frac{d\Phi}{dt} = \frac{1}{v} (-n^2 A_n [\sin(\Phi + 2\omega_0 t - 2\alpha t^2) + \sin(\Phi)] + n^2 B_n (\cos(\Phi + 2\omega_0 t - 2\alpha t^2) + \cos(\Phi)) + \alpha) \quad (\text{B.16})$$

Now, from Eqn.B.16,

$$\int v dv = \int (-n^2 A_n [\sin(\Phi + 2\omega_0 t - 2\alpha t^2) + \sin(\Phi)] + n^2 B_n (\cos(\Phi + 2\omega_0 t - 2\alpha t^2) + \cos(\Phi)) + \alpha) d\Phi \quad (\text{B.17})$$

$$v^2 = 2[n^2 A_n (\cos(\Phi + 2\omega_0 t) + \cos(\Phi)) + n^2 B_n (\sin(\Phi + 2\omega_0 t) + \sin(\Phi)) + 2\alpha\Phi + 2C] \quad (\text{B.18})$$

where  $C$  is a integration constant. At  $t = 0$ , Eqn.B.18 becomes,

$$v^2 = 2[2n^2 A_n \cos(\Phi) + 2n^2 B_n \sin(\Phi) + 2\alpha\Phi + 2C] \quad (\text{B.19})$$

Let  $n^2 A_n = n^2 B_n = V_n$ , then

$$v^2 = 4[V_n \cos(\Phi) + V_n \sin(\Phi) + \alpha\Phi + C] \quad (\text{B.20})$$

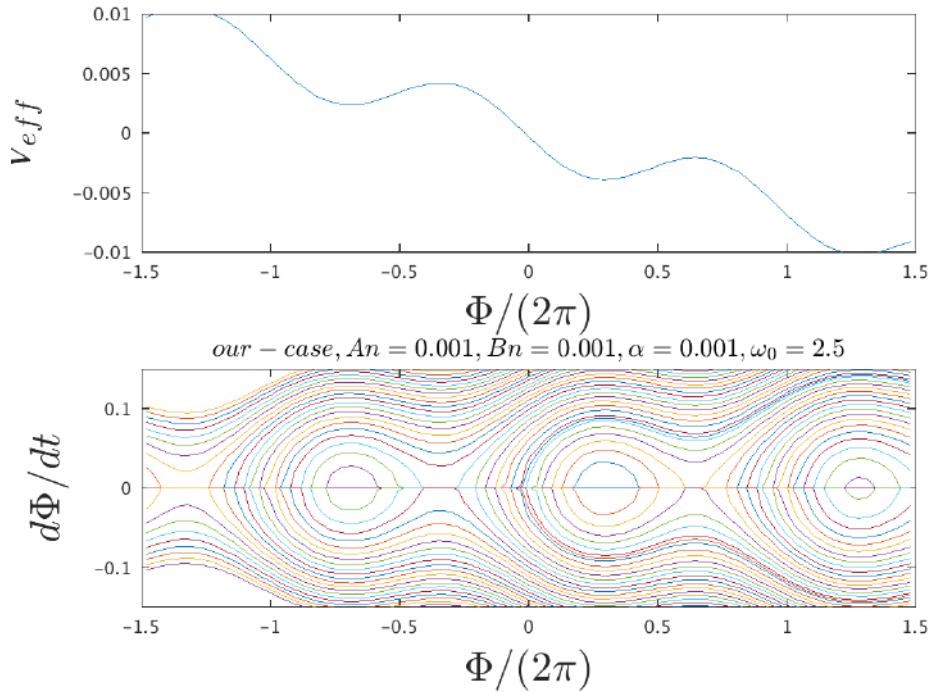


Figure B.1: The effective potential  $V_{eff}$  and the corresponding trajectories in  $(d\Phi/dt, \Phi)$  space indicating potential wells and trapped trajectories in phase space exist in this case.

In Fig.B.1, the effective potential ( $V_{eff}$ ) and the corresponding phase space trajectories are shown. The phase space diagram indicates that even for a small amplitude perturbation ( $A_n = B_n = 0.001$ ) with chirp rate  $\alpha = 10^{-3}$ , the effective potential has potential wells which divide the phase space into trapped and untrapped regions. The chirp dynamics can be considered to be made up of several single resonance cases where during the drive period, it creates trapped and untrapped regions by increasing both Kinetic energy and potential energy of the system for  $\omega_D\tau$ . This study has been attempted to introduce the simplistic case for the chirp dynamics via single resonance method without self-consistency. Depending on the range of frequency chirp, I believe that this model, when self consistent electric field is included, will help understand the formation of multiple PSVs (“honeycomb”). Similarly when resonances overlap, the same model should render multiextrema PSVs (“shark”). In order to understand the phase dynamics in the presence of external chirp and self consistent electric field, more work needs to be performed.



---

---

## References

- [1] LD Landau and IM Khalatnikov. *On the theory of superconductivity, Collected Papers of LD Landau* (ed. D. Ter Haar) Pergamon. 1965.
- [2] Thomas O’Neil. “Collisionless Damping of Nonlinear Plasma Oscillations”. In: *The Physics of Fluids* 8.12 (1965), pp. 2255–2262.
- [3] Ira B Bernstein, John M Greene, and Martin D Kruskal. “Exact nonlinear plasma oscillations”. In: *Physical Review* 108.3 (1957), p. 546.
- [4] M Temerin et al. “Observations of double layers and solitary waves in the auroral plasma”. In: *Physical Review Letters* 48.17 (1982), p. 1175.
- [5] Jason R Franz, Paul M Kintner, and Jolene S Pickett. “POLAR observations of coherent electric field structures”. In: *Geophysical research letters* 25.8 (1998), pp. 1277–1280.
- [6] Anne Mangeney et al. “WIND observations of coherent electrostatic waves in the solar wind”. In: *Annales Geophysicae*. Vol. 17. 3. Springer. 1999, pp. 307–320.
- [7] Jens-Peter Lynov et al. “Observations of solitary structures in a magnetized, plasma loaded waveguide”. In: *Physica Scripta* 20.3-4 (1979), p. 328.
- [8] K Saeki et al. “Formation and coalescence of electron solitary holes”. In: *Physical Review Letters* 42.8 (1979), p. 501.

- [9] J R Danielson, F Anderegg, and C F Driscoll. “Measurement of Landau damping and the evolution to a BGK equilibrium”. In: *Physical review letters* 92.24 (2004), p. 245003.
- [10] Giovanni Manfredi. “Long-time behavior of nonlinear Landau damping”. In: *Physical review letters* 79.15 (1997), p. 2815.
- [11] H. Schamel. “Stationary solitary, snoidal and sinusoidal ion acoustic waves”. In: *Plasma Physics* 14.10 (1972), p. 905.
- [12] H. Schamel. “Particle trapping: A key requisite of structure formation and stability of Vlasov-Poisson plasmas”. In: *Physics of Plasmas* 22.4 (2015), p. 042301.
- [13] H. Schamel. “Stability of electron vortex structures in phase space”. In: *Physical Review Letters* 48.7 (1982), p. 481.
- [14] S.D. Bale et al. “Measurement of the electric fluctuation spectrum of magnetohydrodynamic turbulence”. In: *Physical Review Letters* 94.21 (2005), p. 215002.
- [15] Fouad Sahraoui et al. “Evidence of a cascade and dissipation of solar-wind turbulence at the electron gyroscale”. In: *Physical review letters* 102.23 (2009), p. 231102.
- [16] S Peter Gary and Robert L Tokar. “The electron-acoustic mode”. In: *The Physics of fluids* 28.8 (1985), pp. 2439–2441.
- [17] Francesco Valentini et al. “Undamped electrostatic plasma waves”. In: *Physics of Plasmas* 19.9 (2012), p. 092103.
- [18] Francesco Valentini et al. “Excitation of nonlinear electrostatic waves with phase velocity close to the ion-thermal speed”. In: *Plasma Physics and Controlled Fusion* 53.10 (2011), p. 105017.

- 
- [19] Francesco Valentini et al. “New ion-wave path in the energy cascade”. In: *Physical review letters* 106.16 (2011), p. 165002.
- [20] F Valentini, Francesco Califano, and P Veltri. “Two-dimensional kinetic turbulence in the solar wind”. In: *Physical review letters* 104.20 (2010), p. 205002.
- [21] Pallavi Trivedi and Rajaraman Ganesh. “Chirp-driven giant phase space vortices”. In: *Physics of Plasmas* 23.6 (2016), p. 062112.
- [22] Pallavi Trivedi and Rajaraman Ganesh. “Driven phase space vortices in plasmas with nonextensive velocity distribution”. In: *Physics of Plasmas* 24.3 (2017), p. 032107.
- [23] Pallavi Trivedi and Rajaraman Ganesh. “Symmetry in electron and ion dispersion in 1D Vlasov-Poisson plasma”. In: *Physics of Plasmas* 25.11 (2018), p. 112102.
- [24] DA Gurnett et al. “Parametric interaction and spatial collapse of beam-driven Langmuir waves in the solar wind”. In: *Journal of Geophysical Research: Space Physics* 86.A10 (1981), pp. 8833–8841.
- [25] I Silin, R Sydora, and K Sauer. “Electron beam-plasma interaction: Linear theory and Vlasov-Poisson simulations”. In: *Physics of plasmas* 14.1 (2007), p. 012106.
- [26] Pierre Henri et al. “Vlasov-Poisson simulations of electrostatic parametric instability for localized Langmuir wave packets in the solar wind”. In: *Journal of Geophysical Research: Space Physics* 115.A6 (2010).
- [27] Donald A Gurnett and Roger R Anderson. “Plasma wave electric fields in the solar wind: Initial results from Helios 1”. In: *Journal of Geophysical Research* 82.4 (1977), pp. 632–650.
- [28] Donald A Gurnett and Louis A Frank. “Ion acoustic waves in the solar wind”. In: *Journal of Geophysical Research: Space Physics* 83.A1 (1978), pp. 58–74.

- [29] DA Gurnett et al. “Ion acoustic waves and related plasma observations in the solar wind”. In: *Journal of Geophysical Research: Space Physics* 84.A5 (1979), pp. 2029–2038.
- [30] James Paul Holloway and JJ Dorning. “Undamped plasma waves”. In: *Physical Review A* 44.6 (1991), p. 3856.
- [31] IH Hutchinson. “Electron holes in phase space: What they are and why they matter”. In: *Physics of Plasmas* 24.5 (2017), p. 055601.
- [32] DS Montgomery et al. “Observation of stimulated electron-acoustic-wave scattering”. In: *Physical review letters* 87.15 (2001), p. 155001.
- [33] Francesco Valentini, Thomas M O’Neil, and Daniel HE Dubin. “Excitation of nonlinear electron acoustic waves”. In: *Physics of plasmas* 13.5 (2006), p. 052303.
- [34] F Valentini et al. “A hybrid-Vlasov model based on the current advance method for the simulation of collisionless magnetized plasma”. In: *Journal of Computational Physics* 225.1 (2007), pp. 753–770.
- [35] F Valentini et al. “Response to “Comment on Undamped electrostatic plasma waves”[Phys. Plasmas 20, 034701 (2013)]”. In: *Physics of Plasmas* 20.3 (2013), p. 034701.
- [36] William Bertsche, J Fajans, and L Friedland. “Direct Excitation of High-Amplitude Chirped Bucket-BGK Modes”. In: *AIP Conference Proceedings*. Vol. 692. 1. AIP. 2003, pp. 22–29.
- [37] L Friedland et al. “Driven phase space holes and synchronized Bernstein, Greene, and Kruskal modes”. In: *Physics of plasmas* 11.9 (2004), pp. 4305–4317.
- [38] F Peinetti et al. “Numerical studies of driven, chirped Bernstein, Greene, and Kruskal modes”. In: *Physics of plasmas* 12.6 (2005), p. 062112.

- 
- [39] HL Berk, MS Pekker, and BN Breizman. *Nonlinear theory of kinetic instabilities near threshold*. Tech. rep. Texas Univ., Austin, TX (United States). Inst. for Fusion Studies, 1997.
- [40] B.N. Breizman et al. “Critical nonlinear phenomena for kinetic instabilities near threshold”. In: *Physics of Plasmas* 4.5 (1997), pp. 1559–1568.
- [41] D Yu Eremin and H.L. Berk. “Frequency sweeping of phase space structures”. In: *Physics of Plasmas* 9.3 (2002), pp. 772–785.
- [42] Francois Anderegg et al. “Electron acoustic waves in pure ion plasmas”. In: *Physics of Plasmas* 16.5 (2009), p. 055705.
- [43] H S Zhang, Z Lin, I Holod, et al. “Nonlinear frequency oscillation of Alfvén eigenmodes in fusion plasmas”. In: *Physical review letters* 109.2 (2012), p. 025001.
- [44] H Schamel. “Hole equilibria in Vlasov–Poisson systems: a challenge to wave theories of ideal plasmas”. In: *Physics of Plasmas* 7.12 (2000), pp. 4831–4844.
- [45] A R Plastino and A Plastino. “Tsallis Entropy and Jaynes information theory formalism”. In: *Brazilian Journal of Physics* 29.1 (1999), pp. 50–60.
- [46] R Silva Jr, A R Plastino, and J A S Lima. “A Maxwellian path to the  $q$ -nonextensive velocity distribution function”. In: *Physics Letters A* 249.5-6 (1998), pp. 401–408.
- [47] Constantino Tsallis. “Possible generalization of Boltzmann-Gibbs statistics”. In: *Journal of statistical physics* 52.1-2 (1988), pp. 479–487.
- [48] J T Gosling et al. “Interplanetary ions during an energetic storm particle event: The distribution function from solar wind thermal energies to 1.6 MeV”. In: *Journal of Geophysical Research: Space Physics* 86.A2 (1981), pp. 547–554.

- [49] J M Liu et al. “Measurements of inverse bremsstrahlung absorption and non-Maxwellian electron velocity distributions”. In: *Physical review letters* 72.17 (1994), p. 2717.
- [50] A Lavagno et al. “Non-extensive thermostistical approach of the peculiar velocity function of galaxy clusters”. In: *arXiv preprint astro-ph/9607147* (1996).
- [51] G Kaniadakis, A Lavagno, and P Quarati. “Generalized statistics and solar neutrinos”. In: *Physics Letters B* 369.3-4 (1996), pp. 308–312.
- [52] Hamid Reza Pakzad. “Effect of q-nonextensive electrons on electron acoustic solitons”. In: *Physica Scripta* 83.1 (2011), p. 015505.
- [53] V Munoz. “A nonextensive statistics approach for Langmuir waves in relativistic plasmas”. In: *Nonlinear Processes in Geophysics* 13.2 (2006), pp. 237–241.
- [54] Mouloud Tribeche and Lyes Djebarni. “Electron-acoustic solitary waves in a nonextensive plasma”. In: *Physics of Plasmas* 17.12 (2010), p. 124502.
- [55] AS Bains, Mouloud Tribeche, and TS Gill. “Modulational instability of ion-acoustic waves in a plasma with aq-nonextensive electron velocity distribution”. In: *Physics of Plasmas* 18.2 (2011), p. 022108.
- [56] JAS Lima, R Silva Jr, and Janilo Santos. “Plasma oscillations and nonextensive statistics”. In: *Physical Review E* 61.3 (2000), p. 3260.
- [57] Francesco Valentini. “Nonlinear Landau damping in nonextensive statistics”. In: *Physics of plasmas* 12.7 (2005), p. 072106.
- [58] M Raghunathan and R Ganesh. “Nonlinear Landau damping and formation of Bernstein-Greene-Kruskal structures for plasmas with q-nonextensive velocity distributions”. In: *Physics of Plasmas* 20.3 (2013), p. 032106.

- 
- [59] Chio-Zong Cheng and Georg Knorr. “The integration of the Vlasov equation in configuration space”. In: *Journal of Computational Physics* 22.3 (1976), pp. 330–351.
- [60] Phillip Colella and Paul R Woodward. “The piecewise parabolic method (PPM) for gas-dynamical simulations”. In: *Journal of computational physics* 54.1 (1984), pp. 174–201.
- [61] Prabhu Lal Bhatnagar, Eugene P Gross, and Max Krook. “A model for collision processes in gases. I. Small amplitude processes in charged and neutral one-component systems”. In: *Physical review* 94.3 (1954), p. 511.
- [62] VE Zakharov and VI Karpman. “On the nonlinear theory of the damping of plasma waves”. In: *Soviet Journal of Experimental and Theoretical Physics* 16 (1963), p. 351.
- [63] Francis Filbet and Lorenzo Pareschi. “A numerical method for the accurate solution of the Fokker-Planck-Landau equation in the nonhomogeneous case”. In: *Journal of Computational Physics* 179.1 (2002), pp. 1–26.
- [64] Roald Z Sagdeev. “The 1976 Oppenheimer lectures: Critical problems in plasma astrophysics. II. Singular layers and reconnection”. In: *Reviews of Modern Physics* 51.1 (1979), p. 11.
- [65] B. Eliasson and P. K. Shukla. “Formation and dynamics of coherent structures involving phase-space vortices in plasmas”. In: *Physics reports* 422.6 (2006), pp. 225–290.
- [66] K Saeki et al. “Formation and coalescence of electron solitary holes”. In: *Physical Review Letters* 42.8 (1979), p. 501.
- [67] G Petraconi and Homero S Maciel. “Formation of electrostatic double-layers and electron-holes in a low pressure mercury plasma column”. In: *Journal of Physics D: Applied Physics* 36.22 (2003), p. 2798.

## REFERENCES

---

- [68] HL Pecseli, RJ Armstrong, and J Trulsen. “Experimental observations of ion phase-space vortices”. In: *Physics Letters A* 81.7 (1981), pp. 386–390.
- [69] HL Pecseli, J Trulsen, and RJ Armstrong. “Formation of ion phase-space vortexes”. In: *Physica Scripta* 29.3 (1984), p. 241.
- [70] Hans L Pecseli. “Ion phase-space vortices and their relation to small amplitude double-layers”. In: *Laser and Particle Beams* 5.2 (1987), pp. 211–217.
- [71] Y Nakamura, H Bailung, and PK Shukla. “Observation of ion-acoustic shocks in a dusty plasma”. In: *Physical review letters* 83.8 (1999), p. 1602.
- [72] C Franck et al. “Dynamics of periodic ion holes in a forced beam–plasma experiment”. In: *Physics of Plasmas* 8.10 (2001), pp. 4271–4274.
- [73] AA Kabantsev et al. “Trapped particles and asymmetry-induced transport”. In: *Physics of Plasmas* 10.5 (2003), pp. 1628–1635.
- [74] J Dombeck et al. “Observed trends in auroral zone ion mode solitary wave structure characteristics using data from Polar”. In: *Journal of Geophysical Research: Space Physics* 106.A9 (2001), pp. 19013–19021.
- [75] CA Cattell et al. “Polar observations of solitary waves at the Earth’s magnetopause”. In: *Geophysical research letters* 29.5 (2002), pp. 9–1.
- [76] JP McFadden et al. “Ion and electron characteristics in auroral density cavities associated with ion beams: No evidence for cold ionospheric plasma”. In: *Journal of Geophysical Research: Space Physics* 104.A7 (1999), pp. 14671–14682.
- [77] JP McFadden et al. “FAST observations of ion solitary waves”. In: *Journal of Geophysical Research: Space Physics* 108.A4 (2003).
- [78] H. Matsumoto et al. “Electrostatic solitary waves (ESW) in the magnetotail: BEN wave forms observed by GEOTAIL”. In: *Geophysical Research Letters* 21.25 (1994), pp. 2915–2918.

- 
- [79] M.P. Gryaznevich et al. “Recent experiments on Alfvén eigenmodes in MAST”. In: *Nuclear Fusion* 48.8 (2008), p. 084003.
- [80] M. K. Lilley, B. N. Breizman, and S. E. Sharapov. “Effect of dynamical friction on nonlinear energetic particle modes”. In: *Physics of Plasmas* 17.9 (2010), p. 092305.
- [81] TD Arber and RGL Vann. “A critical comparison of Eulerian-grid-based Vlasov solvers”. In: *Journal of computational physics* 180.1 (2002), pp. 339–357.
- [82] Francis Filbet, Eric Sonnendrucker, and Pierre Bertrand. “Conservative numerical schemes for the Vlasov equation”. In: *Journal of Computational Physics* 172.1 (2001), pp. 166–187.
- [83] Richard B Horne and Mervyn P Freeman. “A new code for electrostatic simulation by numerical integration of the Vlasov and Ampere equations using MacCormack’s method”. In: *Journal of Computational Physics* 171.1 (2001), pp. 182–200.
- [84] John P Boyd. *Chebyshev and Fourier spectral methods*. Courier Corporation, 2001.
- [85] TF Russell et al. “Stability analysis and switching criteria for adaptive implicit methods based on the CFL condition”. In: *SPE Symposium on Reservoir Simulation*. Society of Petroleum Engineers. 1989.
- [86] Matteo Frigo and Steven G Johnson. “The design and implementation of FFTW3”. In: *Proceedings of the IEEE* 93.2 (2005), pp. 216–231.
- [87] Kendall E Atkinson. *An introduction to numerical analysis*. John Wiley & Sons, 2008.
- [88] Andrew Lenard and Ira B Bernstein. “Plasma oscillations with diffusion in velocity space”. In: *Physical Review* 112.5 (1958), p. 1456.

- [89] Zhenning Cai, Ruo Li, and Yanli Wang. “Solving Vlasov Equations Using NR xx Method”. In: *SIAM Journal on Scientific Computing* 35.6 (2013), A2807–A2831.
- [90] H. Schamel. “Theory of electron holes”. In: *Physica Scripta* 20.3-4 (1979), p. 336.
- [91] S.B. Bujarbarua and H. Schamel. “Theory of finite-amplitude electron and ion holes”. In: *Journal of Plasma Physics* 25.3 (1981), pp. 515–529.
- [92] H. Schamel and S. Bujarbarua. “Analytical double layers”. In: *The Physics of Fluids* 26.1 (1983), pp. 190–193.
- [93] H. Schamel. “Electron holes, ion holes and double layers: Electrostatic phase space structures in theory and experiment”. In: *Physics reports* 140.3 (1986), pp. 161–191.
- [94] A. Luque and H. Schamel. “Electrostatic trapping as a key to the dynamics of plasmas, fluids and other collective systems”. In: *Physics reports* 415.5-6 (2005), pp. 261–359.
- [95] A. Luque et al. “Kinetic electrostatic structures in current-carrying pair plasmas”. In: *Plasma physics and controlled fusion* 48.4 (2006), p. L57.
- [96] H. Schamel. “Cnoidal electron hole propagation: Trapping, the forgotten nonlinearity in plasma and fluid dynamics”. In: *Physics of Plasmas* 19.2 (2012), p. 020501.
- [97] BB Kadomtsev and OP Pogutse. “Trapped particles in toroidal magnetic systems”. In: *Nuclear Fusion* 11.1 (1971), p. 67.
- [98] FS Mozer et al. “The dc and ac electric field, plasma density, plasma temperature, and field-aligned current experiments on the S3-3 satellite”. In: *Journal of Geophysical Research: Space Physics* 84.A10 (1979), pp. 5875–5884.

- 
- [99] Bedros Afeyan et al. “Kinetic electrostatic electron nonlinear (KEEN) waves and their interactions driven by the ponderomotive force of crossing laser beams”. In: *arXiv preprint arXiv:1210.8105* (2012).
- [100] MR Feix, P Bertrand, and A Ghizzo. “Eulerian codes for the Vlasov equation”. In: *Series on Advances in Mathematics for Applied Sciences* 22 (1994), pp. 45–81.
- [101] CG Chakrabarti and Kajal De. “Boltzmann-Gibbs entropy: axiomatic characterization and application”. In: *International Journal of Mathematics and Mathematical Sciences* 23.4 (2000), pp. 243–251.
- [102] Nicholas A Krall and Alvin W Trivelpiece. “Principles of plasma physics”. In: *American Journal of Physics* 41.12 (1973), pp. 1380–1381.
- [103] Hui Xu et al. “Effects of ion motion on linear Landau damping”. In: *Physics of Plasmas* 24.2 (2017), p. 022101.
- [104] JP Dougherty. “Model Fokker-Planck equation for a plasma and its solution”. In: *The Physics of Fluids* 7.11 (1964), pp. 1788–1799.
- [105] Lyman Spitzer Jr and Richard Härm. “Transport phenomena in a completely ionized gas”. In: *Physical Review* 89.5 (1953), p. 977.
- [106] SI Braginskii. “Transport phenomena in a completely ionized two-temperature plasma”. In: *Sov. Phys. JETP* 6.33 (1958), pp. 358–369.
- [107] SI Braginskii. “Transport processes in a plasma”. In: *Reviews of plasma physics* 1 (1965).
- [108] Radu Balescu. “Transport processes in plasmas”. In: (1988).
- [109] Zuoyang Chang and JD Callen. “Unified fluid/kinetic description of plasma microinstabilities. Part I: Basic equations in a sheared slab geometry”. In: *Physics of Fluids B: Plasma Physics* 4.5 (1992), pp. 1167–1181.

## REFERENCES

---

- [110] ED Held et al. “Conductive electron heat flow along magnetic field lines”. In: *Physics of Plasmas* 8.4 (2001), pp. 1171–1179.
- [111] ED Held. “Unified form for parallel ion viscous stress in magnetized plasmas”. In: *Physics of Plasmas* 10.12 (2003), pp. 4708–4715.
- [112] Marshall N Rosenbluth, William M MacDonald, and David L Judd. “Fokker-Planck equation for an inverse-square force”. In: *Physical Review* 107.1 (1957), p. 1.
- [113] SP Hirshman and DJ Sigmar. “Approximate Fokker-Planck collision operator for transport theory applications”. In: *The Physics of Fluids* 19.10 (1976), pp. 1532–1540.
- [114] JP Wang and James Donald Callen. “Fluid/kinetic hybrid moment description of plasmas via a Chapman-Enskog-like approach”. In: *Physics of Fluids B: Plasma Physics* 4.5 (1992), pp. 1139–1151.
- [115] MW Anderson and TM O’Neil. “Eigenfunctions and eigenvalues of the Dougherty collision operator”. In: *Physics of plasmas* 14.5 (2007), p. 052103.
- [116] Fred L Hinton. “Simulating Coulomb collisions in a magnetized plasma”. In: *Physics of Plasmas* 15.4 (2008), p. 042501.
- [117] P Helander, LG Eriksson, and F Andersson. “Runaway acceleration during magnetic reconnection in tokamaks”. In: *Plasma Physics and Controlled Fusion* 44.12B (2002), B247.
- [118] E. Marsch and H. Goldstein. “The effects of Coulomb collisions on solar wind ion velocity distributions”. In: *Journal of Geophysical Research: Space Physics* 88.A12 (1983), pp. 9933–9940.
- [119] S Peter Gary. “Kinetic theory of current and density drift instabilities with weak charged-neutral collisions”. In: *Journal of Geophysical Research: Space Physics* 89.A1 (1984), pp. 179–186.

- 
- [120] AA Batishcheva et al. “A kinetic model of transient effects in tokamak edge plasmas”. In: *Physics of Plasmas* 3.5 (1996), pp. 1634–1639.
- [121] Thomas M O’Neil. “Effect of Coulomb collisions and microturbulence on the plasma wave echo”. In: *The physics of fluids* 11.11 (1968), pp. 2420–2425.
- [122] Oreste Pezzi et al. “Eulerian simulations of collisional effects on electrostatic plasma waves”. In: *Physics of Plasmas* 20.9 (2013), p. 092111.
- [123] Oreste Pezzi et al. “Erratum:“Eulerian simulations of collisional effects on electrostatic plasma waves”[Phys. Plasmas 20, 092111 (2013)]”. In: *Physics of Plasmas* 21.1 (2014), p. 092111.
- [124] Luc Mieussens and Henning Struchtrup. “Numerical comparison of Bhatnagar-Gross-Krook models with proper Prandtl number”. In: *Physics of Fluids* 16.8 (2004), pp. 2797–2813.
- [125] Henning Struchtrup. “The BGK-model with velocity-dependent collision frequency”. In: *Continuum Mechanics and Thermodynamics* 9.1 (1997), pp. 23–31.
- [126] Pierre Andries et al. “The Gaussian-BGK model of Boltzmann equation with small Prandtl number”. In: *European Journal of Mechanics-B/Fluids* 19.6 (2000), pp. 813–830.
- [127] G Dorman. “Theoretical models for resonance oscillations of inhomogeneous plasmas”. In: *Journal of Plasma Physics* 3.3 (1969), pp. 387–410.
- [128] W W Heidbrink et al. “Weak effect of ion cyclotron acceleration on rapidly chirping beam-driven instabilities in the National Spherical Torus Experiment”. In: *Plasma Physics and Controlled Fusion* 48.9 (2006), pp. 1347–1372.
- [129] Y. Idomura et al. “Study of ion turbulent transport and profile formations using global gyrokinetic full-fVlasov simulation”. In: *Nuclear Fusion* 49.6 (2009), p. 065029.

## REFERENCES

---

- [130] S. Ku, C.S. Chang, and P.H. Diamond. “Full-f gyrokinetic particle simulation of centrally heated global ITG turbulence from magnetic axis to edge pedestal top in a realistic tokamak geometry”. In: *Nuclear Fusion* 49.11 (2009), p. 115021.
- [131] T. Chapman et al. “Kinetic Theory and Vlasov Simulation of Nonlinear Ion-Acoustic Waves in Multi-Ion Species Plasmas”. In: *Phys. Rev. Lett.* 110 (19 2013), p. 195004.
- [132] James Kent et al. “Determining the effective resolution of advection schemes. Part II: Numerical testing”. In: *Journal of Computational Physics* 278 (2014), pp. 497 –508.
- [133] Ronald Davidson. *Methods in nonlinear plasma theory*. Elsevier, 2012.